C—H Bond Activation in Transition Metal Species from a Computational Perspective

David Balcells, Eric Clot, and Odile Eisenstein*

Institut Charles Gerhardt, Université Montpellier 2, CNRS 5253, cc 1501, Place Eugène Bataillon, 34000 Montpellier, France

Received September 16, 2009

Contents

* To whom correspondence should be addressed. E-mail: odile.eisenstein@univ-montp2.fr.

1. Introduction

Alkanes constitute the cheapest and most abundant feedstock for organic chemicals. However, the redistribution of C—C and C—H bonds in hydrocarbons into more sophisticated value-added architectures is a highly difficult task. The bonds to be broken are thermodynamically strong and kinetically inert. Therefore, hydrocarbons are mainly used as fuels, and the energy content of the bonds is dispensed as heat. Consequently, the efficient and selective activation of C—H bonds, the elementary building block of hydrocarbons, constitutes an interesting alternative with potentially a huge economic impact.

Homogeneous catalysis mediated by transition metal complexes is one of the most efficient ways to achieve both high activity and control of the selectivity in C—H activation. The Shilov system[1] is an early example of an alkane oxidation catalyst that long remained an isolated case of metal-catalyzed C—H activation. It was generally thought that the hydrido-alkyl, product of the C—H activation, was too unstable to be observed. With the work of Bergman[2] and Jones[3] on the intermolecular C—H activation of aromatic and aliphatic C—H bonds by Cp*ML (Cp* = η^5-C_5Me_5; M = Rh, L = PMe_3; M = Ir, L = CO, PMe_3), it proved possible to isolate the C—H oxidative addition products. This paved the way to intense activity and resulted in the publication of many reviews on stoichiometric[4–11] and catalytic[12–21] C—H activation. The large body of experimental results allowed us to gain a better understanding of the C—H activation process. Even though C—H activation is to be contrasted with alkane functionalization involving replacement of C—H hydrogen by a functional group X, the latter often proceeds through C—H bond activation when catalyzed by transition metal species. Depending on the nature of the metal M and the ligand set L_n in the active L_nM species, different situations are encountered, and the C—H activation processes are classified according to four main different mechanisms (Figure 1).

Oxidative addition is the most common mechanism by which a C—H bond cleaves and a M—C bond and a M—H bond are formed. It is well accepted that this mechanism

10.1021/cr900315k
Published on Web 01/12/2010

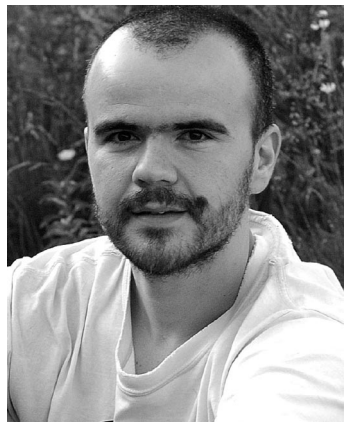

David Balcells was born in Sant Martí de Tous (Catalonia, Spain) in 1978. In 2001, he received the Bachelor of Science degree in Chemistry at the Universitat Autònoma de Barcelona. From 2001 to 2006, he worked on a Ph.D. project under the guidance of Prof. Feliu Maseras, firstly at the Universitat Autònoma de Barcelona (2001−2003) and afterwards at the Institute of Chemical Research of Catalonia (2004−2006). His Ph.D. focused on the application of computational chemistry to the study of the asymmetric synthesis of chiral sulfoxides. In 2006, he obtained the Ph.D. degree in chemistry. In 2007, he obtained a Sanofi-Aventis postdoctoral fellowship for 3 years in the group of Prof. Odile Eisenstein, where he worked in the study of green synthetic methods and C—H activation processes from a computational perspective. He has earned a Juan de la Cierva position for 3 years in the group of Prof. Agustí Lledós, where he will work on the theoretical study of metal-catalyzed water oxidation.

Eric Clot was born in 1967 in Marseilles, south of France. After graduating from the Ecole Normale Supérieure de Lyon, he obtained the Agrégation de Chimie. After a Ph.D. with Odile Eisenstein and Claude Leforestier in 1995 on the dynamics of metal polyhydrides, he entered the CNRS in 1996. He has been promoted to Research Director in 2007. He conducts his research in the group headed by Odile Eisenstein in Montpellier. He also lectures at Ecole Polytechnique, Palaiseau. His research interest focuses on the computational study of the reactivity of transition metal complexes, with specific interest in the activation of inert bonds and applications to organic reactions. His research is conducted in close collaboration with many experimentalists throughout the world. He is especially happy when they share his keen interest in rugby, a sport for which he is a coach in Ecole de Rugby du Pic Saint Loup.

starts by coordination of the C—H bond to the metal vacant site (Figure 1). This mechanism is typical for electron-rich, low-valent complexes of the late transition metals (Re, Fe, Ru, Os, Ir, Pt) for which the higher oxidation state of the metal in the product and the necessary change in geometry upon formation of the two new bonds are not energetically penalizing. For early transition metals (groups 3 and 4, lanthanides and actinides) with d^0 electronic configuration, an oxidative process is not possible, and the preferred mechanism is σ-bond metathesis involving usually an alkyl

Odile Eisenstein was born in 1949 in Boulogne-Billancourt, near Paris. After a Ph.D. in 1977 with Nguyen Trong Anh and Lionel Salem at University of Paris-Sud, Orsay, she joined the CNRS. She was research associate with Jack Dunitz at the ETH, Zurich, and with Roald Hoffmann at Cornell. She was assistant professor at University of Michigan at Ann Arbor. She became Research Director and head of the group of Theoretical Chemistry in Orsay in 1986. She moved to Université Montpellier 2 in 1996 where she is still. She has been invited professor in several universities such as University of York (U.K.), Indiana University, which gave her an honorary degree, and UC Berkeley, where she was Miller Professor. She has received several awards including the Lebel award from the SFC, the Langevin award from the French Academy of Science, the Silver Medal of the CNRS, the Frankland RSC award, and the ACS Organometallics award. She has a keen interest in scientific journals and has been on the board of NJC for many years. She is Chevalier de la Légion d'Honneur. She is a member of the International Academy of Quantum Molecular Science (IAQMS).

or a hydride complex (Figure 1). The essential aspect of the σ-bond metathesis mechanism is the concerted formation (M—C and C′—H) and breaking (M—C′ and C—H) of bonds at the transition state. A reactivity formally equivalent to σ-bond metathesis is observed for late- or post-transition metals (Pd^{2+}, Pt^{2+} or Pt^{4+}, Hg^{2+}), usually in a strongly polar medium. The putative intermediate is formed by electrophilic attack of the metal. In the product, the hydrogen atom of the substrate has been formally substituted by the metal center acting only as a Lewis acid, hence the classification as electrophilic substitution. Finally, the C—H bond can add across an unsaturated M—X bond in a 1,2 addition (Figure 1). This mechanism resembles σ-bond metathesis except that the newly formed X—H bond does not lead to release of XH because the M—X σ-bond is still present in the product. The functional groups X leading to such reactivity are generally amido and alkylidene complexes of early to middle transition metals, but alkoxy and alkylidyne complexes have also been shown to activate C—H bonds.

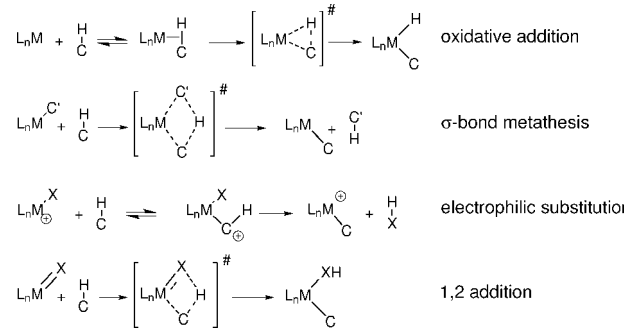

Figure 1. Schematic representation of the different mechanisms for C—H activation.

From a conceptual point of view, despite seemingly large differences among the various mechanisms, there are three different fundamental aspects to consider in C—H activation:

- How is the C—H bond brought into the proximity of the metal?
- How is the C—H bond cleaved in the metal coordination sphere?
- What is the thermodynamic stability of the organometallic product featuring the new M—C bond?

A better understanding of the factors affecting the three fundamental aspects mentioned above is useful to design more efficient systems to promote *selective* C—H activation. Rationalization of the reactivity observed is usually based on qualitative concepts such as steric bulk, electronic influence of the ligands, acidity of the C—H bond to be broken, etc. These are valuable tools to build a qualitative picture, but they lack the required quantitative aspects to effectively delineate the subtle influences of the ligand set, the metal, and the substituents on the reactants.

Computational studies of the structure and reactivity of organometallic complexes have now proven to be an essential tool in homogeneous catalysis.[22–26] A wealth of comparative studies has now established density functional theory (DFT) as a reliable method to study organometallic reactivity.[27,28] Since the seminal review by Niu and Hall,[23] the majority of the computational studies published in the field have used DFT methods and in particular the hybrid B3LYP approach. Together with the increase in computing power, this has allowed us to model systems closer to the actual experimental situation.

One essential asset of computational studies is that they give access to information difficult, if not impossible, to obtain directly from experiment. One key piece of information for the studies of reaction mechanisms, which is not available by any other method, is the characterization of the transition state (TS) on the potential energy surface (PES). The energy of the transition state allows the evaluation of an energy barrier ($\Delta E^{\ddagger}$ or $\Delta H^{\ddagger}$) or an activation barrier ($\Delta G^{\ddagger}$), which can be compared with experimental values from kinetic studies, when available.[29] The electronic structure of the TS allows characterization in more detail of the mechanism of the reaction in terms of bonds that are broken and made. The reactants and products connected by a given TS are also easy to obtain from calculations giving access to the thermodynamics of the reaction. Calculations are also useful to locate intermediates, which may be too unstable to be observed, and to suggest modifications to the experimental systems to favor or disfavor the intermediate. Calculations have thus contributed to the discovery of new pathways for C—H activation.

Emphasis is often put on the C—H bond-breaking step in a multistep process because it is assumed to be the most difficult transformation due to the inertness of the C—H bond. However, studying the C—H activation step thoroughly is not enough to get insight into *catalytic selective C—H functionalization*. Computing the energy profile for the entire catalytic cycle is a daunting task but it leads to a better understanding of the relative activation barriers for the individual steps. It also allows us to tackle the essential aspect of selectivity by comparing catalytic cycles leading to different isomers. Computation of the full energy profile also gives access to the rate-determining step for the transformation of interest and enables us, in principle, to propose alterations of the catalyst and experimental conditions to improve activity and selectivity.

The purpose of this review is to describe the computational work that has addressed C—H activation by transition metal complexes since the reviews by Hall, Dedieu, Frenking, and their respective co-workers published in 2000 in the *Chemical Reviews* special issue "Computational Transition Metal Chemistry" edited by Davidson.[23–25] The focus of the present review is on homogeneous C—H activation of alkanes and arenes with particular emphasis on selectivity issues in activation and functionalization. More specifically, calculations of C—H activation on bare metals are not considered. These calculations have been essential in order to unravel the basic electronic features of the C—H cleavage process and have allowed extensive benchmarking of the computational methods.[30,31] However, most of the complexes active in C—H activation and functionalization are surrounded by ligands, and the latter have a critical influence on the outcome of the reaction. Moreover, given the size of the systems considered in the calculations, the majority of the studies have been carried out within the framework of DFT. Therefore, we will not describe any methodological issues because our main interest is on the chemical concepts obtained from the calculations. When necessary, methodology issues will be mentioned for specific cases. A review including description of computational works on C—H activation by surface organometallic complexes has just appeared.[32]

The first part of the review (section 2) addresses the computational characterization of the mechanisms for C—H activation shown in Figure 1. The description follows the usual partitioning between the various mechanisms,[33] oxidative addition, σ-bond metathesis, 1,2 addition, but the calculations show that such a distinction is often difficult to make and that many intermediate situations exist (section 2.4). In the context of selective C—H oxidation, it is also interesting to mention radical processes, particularly important in biological and biomimetic reactions (section 2.5).[34] This latter transformation has been well studied computationally because it offers challenges both in the definition of the model system and in the choice of the computational methodology.

In the second part (section 3), the emphasis is put on selectivity issues. Because the C—H bond is a poor Lewis base, different strategies have been designed to achieve selective activation. Substituents on the reactant may influence the thermodynamics of the C—H activation, thus affording a means to control the site of reaction. A substituent can also be used as a directing group to trigger the metal toward a specific position as in the Murai reaction.[35] More generally, the metal fragment can be designed such as to bring the target C—H bond close to the metal by molecular recognition.[36] Finally, selectivity can also be induced by an external partner such as an added base as in the concerted metalation−deprotonation (CMD) mechanism proposed by Fagnou,[37] or the ambiphilic metal−ligand activation (AMLA) proposed by Davies and Macgregor.[38]

The third part (section 4) describes the computational studies of catalytic cycles for C—H functionalization processes. Despite intensive efforts, only a few examples of transformations based on C—H activation have been shown to work under catalytic conditions. We focus here on the three different classes, which have led to extensive computational works. At the beginning of the 1980s, Crabtree

developed iridium-based catalysts that showed activity in alkane dehydrogenation.[39] Introduction of PCP pincer type ligands improved the catalytic performance as illustrated by Goldman, Jensen, and Kaska[19,40,41] and led to alkane metathesis by tandem alkane dehydrogenation and olefin metathesis.[42] In terms of C—C bond formation based on C—H activation, a significant breakthrough by Murai and Kakiuchi occurred in 1993 with the Ru-catalyzed selective hydroarylation of olefins ortho to the carbonyl group on aromatic ketones.[35] The transformation was later shown by Gunnoe and Periana to work without using an orienting group.[43,44] Also important to C—C bond formation processes is the catalytic borylation of alkanes developed by Hartwig because the alkyl-boranes are important reagents in various organic reactions.[45,46] The cases where only the C—H activation step of a catalytic cycle has been studied computationally are described in different parts of the review.

In the fourth part (section 5), the computational studies on alkane oxidation by transition metal complexes are considered. Historically, the Pt-catalyzed formation of methanol from methane described by Shilov long remained as the sole example of catalytic homogeneous C—H alkane oxidation.[47] Nevertheless, the use of a stoichiometric amount of oxidant (usually Pt(IV)) limits the practical use of this catalytic system. The situation was dramatically improved in the 1990s by Periana with the Hg- or Pt-catalyzed formation of methyl bisulfate from methanol in hot sulfuric acid.[48,49] In the field of alkane oxidation, MO and MDX (X=H, O, OH, M, R) species have been shown to promote C—H activation, mostly through a radical pathway based on the rebound mechanism. These processes offer selectivity different from the one observed in Shilov-type chemistry. The focus here is limited to non-heme systems because other contributions in this issue address the computational studies on cytochrome P450.[50,51]

2. Mechanisms of C—H Bond Activation

The breaking of a σ(C—H) bond in the coordination sphere of a transition metal complex results generally from two synergic transfers of electron density: σ-donation from the bonding σ(C—H) molecular orbital (MO) into a symmetry-adapted vacant orbital on L_nM and π-backdonation from an occupied d_π MO on L_nM into the antibonding σ^*(C—H) MO. Both factors concur to weaken the σ(C—H) bond leading eventually to bond cleavage. However, a vacant site needs to be created on the metal to allow coordination of the σ bond. The experimental observation of a σ-complex is challenging because the interaction between the metal and the C—H bond is usually weak.[52–56] Computationally, such intermediates are often encountered prior to the C—H cleavage step. The backdonation from the metal is usually effective from a nonbonding d_π MO on L_nM, but in principle, any high-lying occupied MO could be involved in electron transfer into σ^*(C—H) if symmetry allows. The various mechanisms for C—H activation thus depend on the actual nature and magnitude of the two contributions to the transfer of electron density: σ-donation from σ(C—H) and π-backdonation into σ^*(C—H).

2.1. Oxidative Addition

The main characteristics of the oxidative addition mechanism are the concerted breaking of C—H and formation of M—C and M—H in the TS, the formal increase by 2 units of the oxidation state of the metal, and the change of geometry of the complex to accommodate the two new σ bonds. Efficient C—H activation through the oxidative addition mechanism results from the interplay between the various requirements and depends naturally on the electronic configuration of the metal in the fragment L_nM. The computational studies on C—H activation by d^{10} Pd and Pt complexes, where oxidative addition is prevalent, have been reviewed by Dedieu up to 2000.[25] Sakaki and Tilset have updated the literature to 2005 with no significant changes in the fundamental aspects of C—H activation by d^{10} transition metal fragments.[26,57] The C—H activation by d^{10} metal complexes will not be reviewed further in the present contribution.

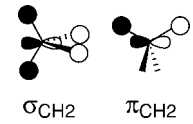

Figure 2. Schematic representation of the σ_{CH_2} and π_{CH_2} MOs for alkanes.

2.1.1. d^8 Configuration

The first systems in which the hydrido-alkyl complex (product of intermolecular C—H activation) has been directly observed have the general formula Cp*ML (M = Rh, Ir; L = PMe_3, CO).[3,6] These 16-electron d^8 unsaturated fragments are generated *in situ* thermally or photochemically from coordinatively saturated 18-electron precursors through reductive elimination of H_2 (or RH) or ligand dissociation. In alkane or benzene solution, they immediately react with the solvent to yield the oxidative addition product Cp*M(L)(R)(H). Following the publication of the work of Bergman and Jones, several computational studies have examined C—H activation by CpML,[58–65] and they are described in detail in the review by Niu and Hall.[23] Recently, Xavier et al. have studied at the MP4(SDQ)//MP2 level the C—H activation of methane promoted by (η^5-phospholyl)$Rh(CO)_2$ and compared it with $CpRh(CO)_2$.[66]

The work by Su and Chu on the reaction between $CpM(PH_3)$ (M = Rh, Ir) and propane is the first attempt to address computationally the important aspect of selectivity in C—H activation.[67] Alkanes are very poor Lewis bases, and the only MOs available for σ-donation are σ_{CH_2} and π_{CH_2} (Figure 2).

Six different structures (**1**—**6**) describe the various ways that the metal fragment $CpM(PH_3)$ interacts with the primary and secondary C—H bonds (Figure 3). The six different situations yielded local extrema structures on the PES, although only three are regular transition states with only one negative eigenvalue of the Hessian matrix. For the other cases, two or three negative eigenvalues are obtained, the largest one (in absolute value) being associated with C—H cleavage and the others corresponding to rotational motion of the groups attached to the carbon atom. Table 1 collects the energies of the various extrema relative to separated $CpM(PH_3)$ and propane. Note that for Rh, no first-order TS could be located at the secondary position; **1** corresponds to a second-order TS with $\nu = 906i$ cm^{-1} for C—H cleavage, and $\nu' = 78.7i$ cm^{-1} for rotation of the *sec*-propyl fragment.

For both Rh and Ir, C—H activation is kinetically preferred at the primary position by 2.1 kcal mol^{-1} (Rh) and 1.65 kcal mol^{-1} (Ir). Selectivity is larger for Rh in agreement with experimental observations. The structures **1**—**3** correspond

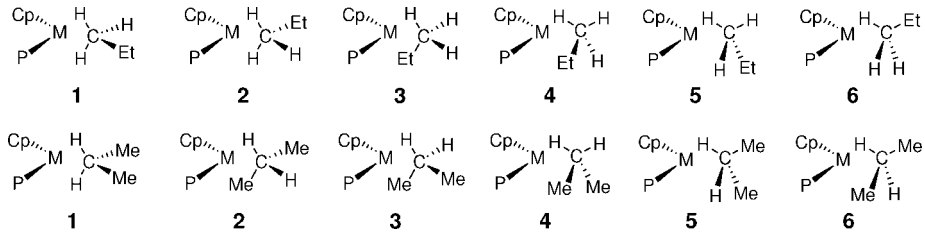

Figure 3. Geometries of interaction between $CpM(PH_3)$ and primary (top) or secondary (bottom) carbon atom of propane.

Table 1. Energy (kcal mol^{-1}) Relative to Separated Reactants of the Extrema Structures Corresponding to the Various Geometries of Attacks (Number of Negative Eigenvalues in the Hessian in Parentheses)[a]

	1	2	3	4	5	6	M[σ(CH)]	M(H)(C)
Rh 1°	−0.92 (2)	−1.97 (1)	1.21 (2)	0.68 (3)	0.85 (3)	−0.05 (3)	−10.9	−15.6
Rh 2°	0.13 (2)	2.40 (3)	2.61 (2)	4.40 (2)	2.85 (2)	2.64 (3)		
Ir 1°	−4.47 (2)	−5.78 (1)	−1.04 (3)	−2.39 (2)	−2.88 (3)	−4.31 (3)	−6.56	−34.6
Ir 2°	−4.13 (1)	−0.69 (2)	−0.38 (2)	0.59 (3)	−2.01 (3)	−1.32 (3)	−6.07	−31.7

[a] The σ-complexes and hydrido-alkyl products are connected through the first-order TS. M 1° and M 2° correspond to a reaction occuring at the primary and secondary carbon, respectively.

to situations where a σ_{CH_2}-type MO is used for σ-donation, while the structures **4**−**6** use a π_{CH_2}-type MO. Table 1 shows that sterics at the C—H bond to be activated play a crucial role. Structure **3**, featuring Et or Me close to the metal, is significantly less stable than **1** and **2**. Structures **4**−**6** all lie at higher energy than **1** and **2**, but the difference between these two sets of structures is larger for Rh than for Ir. There is also an influence of the nature of the metal. Metals with less diffuse orbitals (Rh) increase the preference for a σ_{CH_2}-type mode of interaction with the least sterically encumbered position of the alkane. The metal with more diffuse orbitals (Ir) is less selective both for the geometry of interaction (σ_{CH_2} or π_{CH_2}) and for the position of activation (primary or secondary).

The negative values of the energy of the first-order TS indicate that a molecular precursor was located on the PES. Three σ-complexes (σ-Rh1, σ-Ir1, σ-Ir2) were optimized, and their energies are given in Table 1 relative to separated reactants. The energies of the products of the reaction, $CpM(PH_3)(H)(C_3H_7)$, are also given in Table 1. The stability of the σ-complexes is not strong enough to compensate for the loss of entropy (mostly translational entropy) associated with a change of molecularity upon formation of the complexes. For rhodium, the absence of a σ-complex at the secondary position is in agreement with greater preference for activation at the primary position. For iridium, the energy difference between the two σ-complexes is only 0.5 kcal mol^{-1}, in favor of σ-Ir1, a value lower than the energy difference between the two corresponding TSs. The selectivity for activation at the primary position is thus only partially present in the precursor complex.

The main difference between Rh and Ir lies in the thermodynamics of the reaction. In both cases, the oxidative addition is exothermic with respect to the σ-complexes but only by 4.70 kcal mol^{-1} for Rh and by 28.04 and 25.63 kcal mol^{-1} for Ir, because bonds are stronger to third than to second row metals. Consequently, oxidative addition at Ir is not reversible, and there is no possibility to equilibrate the various products through formation of the σ-complex by C—H reductive elimination. The energy difference between the two TSs thus determines the product ratio, and the calculated value of 1.65 kcal mol^{-1} corresponds to a 1.9:1 ratio at room temperature between activation at the primary and secondary positions. In contrast, for Rh the oxidative addition is not exothermic enough to prevent equilibration through the σ-complexes. Consequently, the product resulting from reaction at the primary carbon can be obtained, in agreement with the experimental observations.

Another important aspect of selectivity is the competition between C—H bonds in different substrates. Thus, although the C—H bond is stronger in benzene than in methane (and in other alkanes), aromatic C—H activation is usually preferred over aliphatic C—H activation both kinetically and thermodynamically (see section 3.1). This competition was addressed computationally by Bi and co-workers with B3LYP calculations of the C—H activation of benzene and methane by $CpRh(PMe_3)(H)_2$.[68] The reductive elimination of H_2 from the dihydride is computed to be endergonic by $\Delta G = 26.7$ kcal mol^{-1}. The σ-(C—H) adduct of methane is less stable than separated $CpRh(PMe_3)$ and CH_4 by 5.2 kcal mol^{-1} on the Gibbs free energy surface but more stable by 5.2 kcal mol^{-1} on the enthalpy surface. The difference of ca. 10 kcal mol^{-1} is mostly due to the loss of translational entropy upon formation of the adduct. Stronger coordination of benzene ($\Delta H = -15.7$ kcal mol^{-1}) leads to an η^2-adduct more stable than separated reactants by $\Delta G = -2.6$ kcal mol^{-1}. This η^2-(C═C) adduct evolves to a σ-(C—H) complex of benzene less stable by $\Delta G = 5.7$ kcal mol^{-1} through an activation barrier of $\Delta G^{\ddagger} = 6.7$ kcal mol^{-1}. Thus, the σ-(C—H) adduct of benzene is 2 kcal mol^{-1} more stable than the σ-(C—H) adduct of methane on the Gibbs free energy surface. This introduces a kinetic bias toward aromatic C—H activation that is reinforced in the TS for C—H cleavage by the significantly lower activation barrier, $\Delta G^{\ddagger}$, of 3.8 kcal mol^{-1} for benzene compared with that for methane ($\Delta G^{\ddagger} =$ 7.4 kcal mol^{-1}). The essential difference between the two TSs is the value of the Rh···C distance (2.23 Å, methane; 2.12 Å, benzene) leading to a late TS in the case of benzene. The stronger Rh—Ph bond relative to the Rh—CH_3 bond contributes to lower the transition state for the addition to benzene. The same argument accounts for the larger exergonicity of the reaction with $\Delta G = -7$ and $\Delta G = -9.9$ kcal mol^{-1} for methane and benzene, respectively. The energy diagram in Figure 4 schematically illustrates the energetics associated with the competitive reaction of methane and benzene with $CpRh(PMe_3)(H)_2$. Only the TS for C—H cleavage and the oxidative addition products are shown. It indicates that heating $CpRh(PMe_3)(R)(H)$ (R = alkyl) in benzene solution results in irreversible formation of the phenyl hydride product.

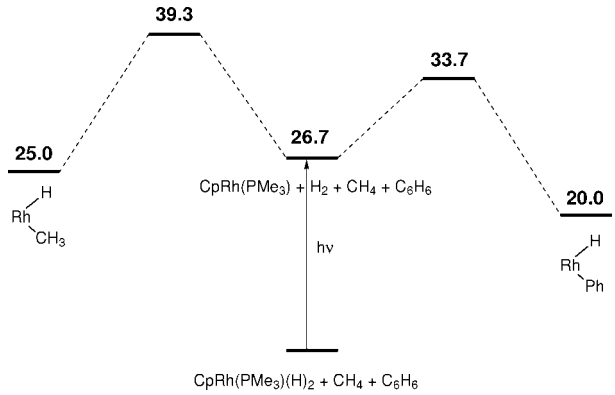

Figure 4. Calculated Gibbs free energy (kcal mol^{-1}) diagram of the competitive reaction of CH_4 and C_6H_6 with $CpRh(PMe_3)(H)_2$.

Thermodynamics is not always the leading factor in deciding the outcome of the transformation. Reaction of $Cp^*Rh(PMe_3)(H)(Ph)$ with 1,4-$C_6H_4F_2$ yields exclusively the C—H oxidative addition product $Cp^*Rh(PMe_3)(H)(C_6H_3F_2)$ featuring an *ortho*-F; no C—F activation product is observed.[69] B3LYP calculations by Bosque et al. on $CpRh(PH_3)$ reacting with 1,4-difluorobenzene highlighted the larger thermodynamic stability of the C—F activation product.[70] However, from the η^2-(C═C) coordinated fluorobenzene, the energy barrier for C—H cleavage is 9.4 kcal mol^{-1}, while it amounts to a high 34.3 kcal mol^{-1} for cleaving C—F. There is thus a strong kinetic bias toward C—H activation even though the corresponding product is 2.7 kcal mol^{-1} higher in energy than the product of C—F activation. Moreover, coordination of the fluorobenzene to the Rh fragment also favors C—H activation since the coordination of the nonsubstituted CH═CH bond is preferred over coordination of the CH═CHF bond. This shows that C—H activation is preferred because it starts from a more stable initial adduct and it is associated with a lower energy barrier. A detailed analysis of the interactions at the transition states in the case of simpler systems suggests that the oxidative addition at C—F is disfavored because of the protective effects of the fluorine lone pairs.[71] Further studies on the competition between C—H and C—F activations within the same molecular systems, which will not be discussed further, have shown that different mechanisms may be operative.[72–74]

A further example of interplay between coordination and activation is given by thermolysis of $Cp^*Ir(PMe_3)(C_6H_{11})(H)$ in cyclohexane, which generates $Cp^*Ir(PMe_3)$, which reacts *in situ* with $H_2C═CH_2$ to form $Cp^*Ir(PMe_3)(CH═CH_2)(H)$ and $Cp^*Ir(PMe_3)(H_2C═CH_2)$ in a 2:1 ratio.[75] While $Cp^*Ir(PMe_3)(CH═CH_2)(H)$ is stable under the thermolytic conditions of its formation, at higher temperatures it is converted cleanly to $Cp^*Ir(PMe_3)(H_2C═CH_2)$. B3LYP calculations on $CpIr(PH_3)(CH_3)(H)$ reacting with ethylene were performed by Harvey et al.[76] In agreement with experiment, the η^2-ethylene complex is computed to be more stable than the vinyl hydride product by 10.6 kcal mol^{-1}. However, calculations on a singlet spin state surface failed to explain all the experimental observations. Calculations on the triplet spin state surface and characterization of the minimum energy crossing point (MECP)[77,78] show that reductive elimination from singlet $CpIr(PH_3)(H)(CH_3)$ yields triplet $CpIr(PH_3)$ and CH_4 directly. The weak van der Waals adduct between ethylene and the triplet 16-electron fragment is the key intermediate in the reaction. The interchange of the available ethylene C—H bonds in this adduct accounts for the observed kinetic isotope effects. Partitioning between alkene π-complexation and C—H bond activation may also occur from this common intermediate.

Two-state reactivity of methane with $CpM(PH_3)$ (M = Co, Rh, Ir) was studied at the B3LYP level by Poli et al.[79] For $CpM(PH_3)$, the triplet state is always more stable than the singlet (33.3 kcal mol^{-1}, Co; 6.2 kcal mol^{-1}, Rh; 8.4 kcal mol^{-1}, Ir). The interaction of methane with the triplet state of $CpM(PH_3)$ is repulsive, while it is attractive with the singlet state. Consequently, the two surfaces cross for M = Rh or Ir, and the MECP presents a long M···C distance (3.067 Å, Rh; 3.350 Å, Ir). For M = Co, the distance is short (2.312 Å), similar to that for the σ-complex on the singlet surface (2.387 Å). Thus, from singlet $CpCo(PH_3)(\sigma$-$CH_4)$, two pathways are possible: (i) C—H oxidative addition on the singlet surface with $\Delta E^{\ddagger} = 7.8$ kcal mol^{-1} and $\Delta E = -1.7$ kcal mol^{-1}; (ii) dissociation of methane on the triplet surface with $\Delta E^{\ddagger} = 0.9$ kcal mol^{-1} and $\Delta E = -24.9$ kcal mol^{-1}. This explains why C—H oxidative addition has not been observed experimentally with $CpCo(PR_3)$. For Rh, the two pathways are competitive with $\Delta E^{\ddagger} = 8.6$ kcal mol^{-1} for C—H oxidative addition and $\Delta E^{\ddagger} = 4.5$ kcal mol^{-1} for CH_4 dissociation. However, the oxidative addition product is 5.4 kcal mol^{-1} more stable than separated CH_4 and triplet $CpRh(PH_3)$. C—H oxidative addition is thus possible with Rh, but the alkyl hydride product is very reactive and may easily evolve through reductive elimination. Finally, for M = Ir, no σ-complex could be located, and the oxidative addition product is 30.9 kcal mol^{-1} more stable than separated CH_4 and triplet $CpIr(PH_3)$, rendering reductive elimination difficult.

The preceding studies point to a general picture for C—H oxidative addition by group 9 metal complexes proceeding in three consecutive steps: (1) creation of a vacant site by photolysis or thermolysis to generate a 16-electron d^8 coordinatively unsaturated fragment; (2) coordination of the alkane or the arene to the vacant site to generate an intermediate σ- or π-complex (with isomerization from π(C═C) to σ(C—H) coordination in the case of arenes); (3) cleavage of the C—H bond to yield the oxidative addition product.

This sequence of events was observed experimentally on the time-resolved difference IR spectra of $CpRh(CO)_2$ in *n*-pentane and *n*-hexane following UV excitation.[80] At early times (10 ps), the monocarbonyl alkane solvate $CpRh(CO)(RH)$ is observed, as well as the parent $CpRh(CO)_2$ compound. There is a decrease in the absorption of the alkane-solvated intermediate on a 2.5 ns time scale with the concomitant formation of the oxidative addition product $CpRh(CO)$-$(H)(R)$. The ultrafast dynamics of $CpRh(CO)_2$ in cyclohexane was studied by Asbury et al., and the results showed exclusive formation of the σ-adduct of cyclohexane.[81] There was no evidence for the formation of the oxidative addition product or for Cp ring slippage. This result is in agreement with the known preference of bond activation toward primary C—H sites with Rh.

The isoelectronic system $Tp^*Rh(CO)_2$ (Tp^* = HB(3,5-dimethyl-pyrazolyl)$_3$) has been shown to activate C—H bonds, and the dynamics of the process has been followed on the femtosecond time scale.[80,82] Photochemically induced dissociation of CO occurs in less than 100 fs, followed by coordination of the alkane in a few picoseconds to yield the solvated intermediate (κ^3-Tp*)Rh(CO)(RH). Within 200 ps, $\kappa^3 \rightarrow \kappa^2$ isomerization of the Tp* ligand forms the square-

planar d^8 ML_4 σ-complex of the alkane, (κ^2-Tp*)Rh(CO)(RH). The activation energy for the isomerization is estimated to be 4.2 kcal mol^{-1}. Disappearance of (κ^2-Tp*)Rh(CO)(RH) follows first-order kinetics with characteristic time τ of 110 and 290 ns for activation of pentane and cyclohexane, respectively. The alkyl hydride κ^2-intermediate (κ^2-Tp*)Rh(CO)(R)(H) evolves rapidly to the product (κ^3-Tp*)Rh(CO)(R)(H). Similar results are obtained for hexane vs cyclohexane showing a faster formation of the product in the linear alkane compared with the cyclic counterpart. From the values of τ, the activation energy for C—H cleavage is between 6 and 7.8 kcal mol^{-1} for primary alkanes and amounts to 8.4 kcal mol^{-1} for cyclic hydrocarbons.

DFT calculations by Zarić and Hall located two intermediates for CH_4 reacting with TpRh(CO) (Tp = $HB(C_3H_3N_2)_3$).[83] A very weak η^1-CH_4 adduct (Rh···C = 3.538 Å, Rh—H—C = 177.6°, $\Delta E = -1.7$ kcal mol^{-1}) of (κ^3-Tp)Rh(CO) was identified as the first intermediate seen experimentally. Dissociation of one Tp arm allowed for stronger η^2-coordination of methane (Rh···C = 2.45 Å, Rh—H—C = 104.6°, $\Delta E = -2.4$ kcal mol^{-1}). This complex was identified as the second intermediate seen after 200 ps. The calculated difference in ν(CO) vibrational frequencies for the two intermediates, 22 cm^{-1}, is in good agreement with the value observed experimentally, 18 cm^{-1}.

Recent time-resolved infrared (TRIR) experiments combined with DFT calculations by George et al. on (Tp′)Rh(CO)$_2$(Tp′ = HB(4-^{t}Bu-3,5-Me-pyrazolyl)$_3$) reacting with *n*-heptane, *n*-decane, and cyclohexane afforded new insight into the mechanism for C—H oxidative addition.[84] Experimentally, species (κ^3-Tp′)Rh(CO)(RH) and (κ^2-Tp′)Rh(CO)(RH) are shown to be in equilibrium and concentrations of both decrease simultaneously upon formation of (κ^3-Tp′)Rh(CO)(R)(H). B3LYP calculations on (Tp*)Rh(CO) reacting with C_2H_6 showed that (κ^3-Tp*)Rh(CO)(RH) is an η^1-adduct of C_2H_6 with the fragment (κ^3-Tp*)Rh(CO) in a triplet spin state. The corresponding η^1-adduct of C_2H_6 with the metal fragment in the singlet spin state lies higher in energy and evolves easily ($\Delta H^{\ddagger} = 0.9$ kcal mol^{-1}) into the η^2 (C—H)-adduct with (κ^2-Tp*)Rh(CO) featuring a decoordinated pyrazolyl ring. The discrepancy between the experimental (4.2 kcal mol^{-1}) and calculated (0.9 kcal mol^{-1}) values for the transformation (κ^3-Tp*)Rh(CO)(RH) → (κ^2-Tp*)Rh(CO)(RH) could be lifted by considering the MECP between the singlet and triplet spin-state surfaces for the η^1-adduct of C_2H_6. Acknowledging the known tendency of B3LYP to overestimate the stability of high spin state, a value close to the experimental one is obtained. Calculations also showed that C—H oxidative addition in (κ^2-Tp*)Rh(CO)(RH) to generate (κ^2-Tp*)(Rh)(CO)(H)(C_2H_5) is not on the reaction pathway for this C—H activation process ($\Delta H^{\ddagger} = 13$ kcal mol^{-1}). The ML_4 square planar complex (κ^2-Tp*)Rh(CO)(RH) is very close in energy (0.3 kcal mol^{-1}) to a distorted ML_5 intermediate best described as a square-based pyramid with a long apical Rh···N bond (2.90 Å). This ML_5 complex features a $\kappa^{2.5}$-coordination of the Tp* ligand and leads to the lowest TS for C—H cleavage with an energy barrier $\Delta H^{\ddagger}$ = 8.4 kcal mol^{-1} in good agreement with experiment. Because ($\kappa^{2.5}$-Tp*)Rh(CO)(RH) both lies on the pathway between (κ^3-Tp*)Rh(CO)(RH) and (κ^2-Tp*)Rh(CO)(RH) and is the active species in C—H cleavage, it explains the concomitant decrease in (κ^3-Tp*)Rh(CO)(RH) and (κ^2-Tp*)Rh(CO)(RH) upon formation of (κ^3-Tp*)Rh(CO)(R)(H).

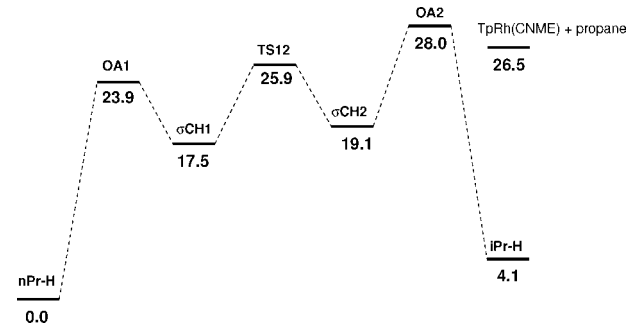

Figure 5. Energy (kcal mol^{-1}) diagram of the reaction of propane with TpRh(CNMe) showing formation of the activation product at the primary carbon (**nPr-H**) in preference to secondary carbon (**iPr-H**).

Interestingly, the X-ray structure for (Tp′)Rh(CO)$_2$ has been determined and features this intermediate $\kappa^{2.5}$-bonding mode of Tp.[84] The computed ν(CO) frequency of ($\kappa^{2.5}$-Tp*)Rh(CO)(C_2H_6) is nearly identical to the one obtained for the dicarbonyl starting material, thus rendering experimental observation of ($\kappa^{2.5}$-Tp*)Rh(CO)(RH) difficult.

A similar $\kappa^{2.5}$-coordination mode of Tp had been proposed independently by Clot et al. slightly earlier in a DFT study of the dynamic properties of propane coordinated to TpRh(CNMe).[85] This followed the experimental studies by Jones of the C—H oxidative addition of alkanes and arenes to (Tp*)Rh($CNCH_2CMe_3$) generated *in situ*.[86,87] Reaction with propane yielded exclusively activation at the primary position, and independent synthesis of (Tp*)Rh($CNCH_2CMe_3$)(^{i}Pr)(H) resulted in conversion to (Tp*)Rh($CNCH_2CMe_3$)(Pr)(H) without dissociation of the alkanes as confirmed by labeling studies. The B3PW91 calculations showed that at long distance the alkane interacts with Rh in an η^1-geometry and that for Rh···C between 3.0 and 3.5 Å one arm of the Tp ligand starts to dissociate to allow η^2-coordination of the alkane in a square-planar geometry. The Rh···N distance of ca. 3 Å and the geometry of the pyrazolyl ring are similar to those observed later by Hall. Two σ-complexes, σ**CH1** and σ**CH2**, corresponding to coordination of the primary and secondary positions, are located, and the latter is less stable by 1.6 kcal mol^{-1}. Both complexes feature coordination of a σ(C—H) bond with H *trans* to the long Rh···N bond. A transition state geometry, **TS12**, where Rh interacts with primary and secondary C—H bonds lies 8.4 kcal mol^{-1} above σ**CH1** and is associated with the migration from one σ-complex to the other. From σ**CH1**, the TS for oxidative addition, **OA1**, is 6.4 kcal mol^{-1} higher in energy, whereas the energy barrier at the secondary position, through **OA2**, is 8.9 kcal mol^{-1} higher than σ**CH2**. The oxidative addition product at the secondary position, **iPr-H**, is 4.1 kcal mol^{-1} less stable than that at the primary position, **nPr-H**. The energy diagram of Figure 5 summarizes the results. When propane reacts with TpRh(CNMe), the two σ-complexes are likely to form. However, C—H oxidative addition in σ**CH2** is less facile than that in σ**CH1**, and the energy barrier for isomerization from σ**CH2** to σ**CH1** is lower than oxidative addition at σ**CH2**. Moreover, **TS12** lies at lower energy than separated TpRh(CNMe) and propane thus explaining the labeling studies. This type of chain-walking mechanism may be general and could explain selective activation at the primary position independently of the initial interaction of the alkane C—H bonds with the metal. However, chain walking is influenced by the nature

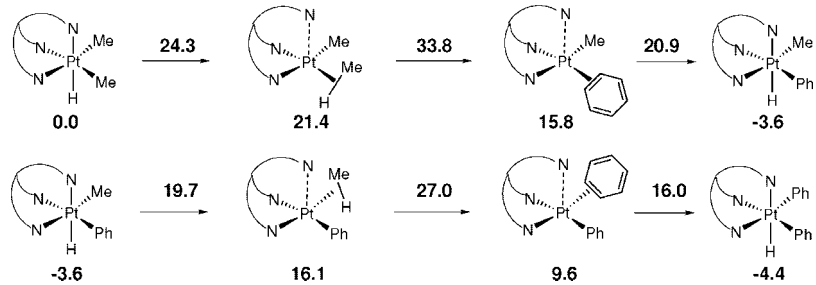

Figure 6. Sequence of transformations in the reaction of $TpPt(Me)_2(H)$ with benzene. The enthalpy (kcal mol^{-1}) of the intermediates and TSs (above the arrow) is given relative to the separated reactants.

of the spectator ligands and is thus disfavored in presence of poorly electron-donating ligand such as trifluoroacetate.[88]

In the related Pt-complex $TpPtMe(H)_2$, Keinan observed H/D scrambling of the methyl group but no methane loss when the complex is heated in CD_3OD at 55 °C.[89] The mPW1k calculations by Martin yielded a sequence of events similar to that shown in Figure 5. Formation of the σ-complex $TpPt(H)(\eta^2\text{-}CH_4)$ from TpPt(H) and CH_4 proceeds through a TS featuring an η^2-(C—H) interaction (Pt···C = 3.16 Å, Pt···H = 2.288 Å) lying at $\Delta G^{\ddagger} = 5.9$ kcal mol^{-1} above separated reactants. The σ-complex is 6 kcal mol^{-1} more stable than separated reactants on the Gibbs free energy surface. It features the characteristic intermediate coordination mode of the Tp ligand already observed in the other studies with a long Pt···N contact (3.067 Å) *trans* to the coordinated H atom. From this intermediate, two pathways are described: scrambling of the coordinated hydrogen with $\Delta G^{\ddagger} = 3$ kcal mol^{-1} and C—H oxidative addition with $\Delta G^{\ddagger} = 6.6$ kcal mol^{-1} and $\Delta G = -19.1$ kcal mol^{-1}. When the principle of microreversibility is applied, the σ-methane complex formed from C—H reductive coupling in $TpPt(Me)(H)_2$ has a higher activation barrier to surmount to dissociate than to revert to the Pt(IV) complex ($\Delta\Delta G^{\ddagger} = 5.3$ kcal mol^{-1}). The reactivity of Tp complexes is thus strongly influenced by the ability of the ligand to change coordination mode.

Jensen et al. reported the reductive elimination of methane and oxidative addition of C_6D_6 to form $Tp^*Pt(C_6D_5)_2(D)$ from $Tp^*Pt(Me)_2(H)$.[90] From kinetic studies, the values of the activation energies for methane reductive elimination (35 kcal mol^{-1}) and H/D scrambling (26 kcal mol^{-1}) allowed estimation of the stability of the σ-methane complex as 9 kcal mol^{-1}. Vastine et al. computed the reaction mechanism of the transformation $TpPt(Me)_2(H) + 2C_6H_6 \rightarrow TpPt(Ph)_2(H) + 2CH_4$ with different density functionals and basis sets.[91] The B3LYP enthalpy profile is shown in Figure 6 and features the characteristic steps already encountered in C—H activation with related Tp complexes. The calculated $\Delta H^{\ddagger}$ of 33.8 kcal mol^{-1} for methane dissociation compares well with the experimental value of the activation energy and is thus identified as the rate-determining step. The TS for C—H reductive coupling computed at $\Delta H^{\ddagger} = 24.3$ kcal mol^{-1} is compared with the experimental activation parameters for H/D scrambling since site exchange within the σ-complex is usually considered easier than C—H oxidative addition. The overall energy profile clearly illustrates the thermodynamic driving force associated with the formation of the strong Pt—Ph bond at the expense of the weaker Pt—Me one. For benzene, η^2-(C═C) coordination is preferred over η^2-(C—H), and the σ-(C_6H_5—H) complex is only marginally more stable than the corresponding TS for C—H oxidative addition. Finally, substitution of Me for Ph lowers both the energy barrier for C—H reductive coupling (23.3 vs 24.3 kcal mol^{-1}) and the energy barrier for methane dissociation (30.6 vs 33.8 kcal mol^{-1}).

Figure 7. C—H activation by diamine and diimine cationic Pt complexes.

In another example, reaction of $(tmeda)Pt(Me)_2$ with $[H(NC_5F_5)_n][BArf]$ in NC_5F_5 at 0 °C gives $[(tmeda)Pt(Me)(NC_5F_5)][BArf]$ (tmeda = *N*, *N*, *N*′, *N*′—tetramethylethylenediamine, BArf=B(3,S-C_6H_3 $(CF_3)_2)_2$). The latter complex is converted at 85 °C in the presence of benzene to the phenyl analog, while under 30 atm of $^{13}CH_4$, the complex $[(tmeda)Pt(^{13}CH_3)(NC_5F_5)[BArf]$ is formed.[92] Related to the work of Holtcamp et al., the controlled protonolysis of $(N^f\text{-}N^f)Pt(Me)_2$ ($N^f\text{-}N^f$ = ArN═CMe—CMe═NAr, Ar = 3,5-$(CF_3)C_6H_3$) with $HBF_4 \cdot Et_2O$ in wet CH_2Cl_2 gives $[(N^f\text{-}N^f)Pt(Me)(H_2O)][BF_4]$.[93] The aqua complex, when dissolved in CF_3CH_2OH (TFE), effects the activation of methane and benzene C—H bonds under very mild conditions.[93,94] These reactions can be described as the result of C—H activation by the unsaturated d^8 fragment (N-N)$Pt(Me)^+$ (Figure 7).

Calculations by Heiberg et al. on the reaction of $(NH_2CH_2CH_2NH_2)Pt(Me)^+$ with CH_4 at the BP86 level located a σ-complex with an energy of −21.9 kcal mol^{-1} relative to separated reactants.[95] The oxidative addition from this σ-complex is very easy ($\Delta E^{\ddagger} = 3.6$ kcal mol^{-1}) but not favored thermodynamically ($\Delta E = 1.6$ kcal mol^{-1}). In an attempt to model the influence of the solvent NC_5F_5, calculations have been carried out with NF_2H. The latter coordinates only weakly to the σ-complex and to the TS for C—H activation but occupies the vacant site in the product of C—H activation. The significant stabilization of the latter makes the reaction exothermic by 14.8 kcal mol^{-1} from the σ-complex. The role of NF_2H is here similar to that of the arm of the Tp ligand: partial or total decoordination allows the formation of a stable σ-complex and after C—H cleavage, recoordination provides stabilization to the product of oxidative addition.

The reaction between $(N^f\text{-}N^f)Pt(Me)(H_2O)$ and CH_4 was investigated by DFT calculations using a model system with HN═CH—CH═NH (N-N) as the diimine ligand.[93] Coordination of methane to (N-N)$Pt(Me)^+$ is downhill by 23.7 kcal mol^{-1}, but water or TFE coordination is preferred (37.8 and 35.4 kcal mol^{-1}, respectively). However, the coordination of methane to Pt with H_2O or TFE interacting with the diimine backbone is only slightly uphill from the H_2O and TFE complexes (6.9 and 5.3 kcal mol^{-1}, respectively). C—H oxidative addition from (N-N)$Pt(Me)(\eta^2\text{-}CH_4)^+$ is computed with an energy barrier of 7.9 kcal mol^{-1}, and the product is

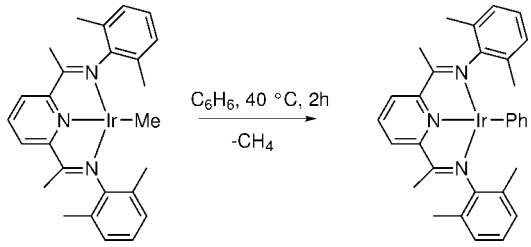

Figure 8. C—H activation by neutral Ir(I)—methyl complex.

5.5 kcal mol^{-1} less stable than the σ-complex. The energy barrier is reduced to 6.2 kcal mol^{-1} when the σ-complex with water interacting with the diimine is considered. Interestingly, at the TS, the water has shifted from the diimine ligand to the Pt center with a Pt···O distance of 2.84 Å, a value similar to the Pt···N contacts observed in C—H activation by Tp complexes. Coordination of water to Pt while passing through the TS stabilizes the product of C—H activation, and the reaction is exothermic by 8.1 kcal mol^{-1}.

The reaction shown in Figure 7 could formally be the result of a σ-bond metathesis process (see section 2.2). Gropen and co-workers have considered this possibility in their study of diamine and diimine Pt—Me complexes.[93,95] In both cases, the TS for σ-bond metathesis has a planar structure with H migrating between the two carbon atoms while featuring a short Pt···H distance (C···H = 1.62 Å, Pt···H = 1.55 Å, diamine; C···H = 1.56 Å, Pt···H = 1.59 Å, diimine). In the case of the diamine ligand, the σ-bond metathesis TS is 5.8 kcal mol^{-1} above the oxidative addition TS, whereas it is 2.6 kcal mol^{-1} higher for the diimine case. The energy difference between the two transition states increases to 4.8 kcal mol^{-1} when the water, present in the experimental conditions, is introduced in the model of the reaction. In the σ-bond metathesis pathway, the extra ligand (water) has no influence and the metal—diimine bonds are maintained, while in the oxidative TS, the water is shifted toward the Pt center and effectively stabilizes the octahedral geometry of the d^6 product. The need to stabilize the d^6 product in an octahedral environment appears to be a key factor for the oxidative addition to d^8 metal systems. It accounts for the role of solvent or additional ligand in the case of oxidative addition to a d^8 ML$_3$ complex.

Calculations on the activation of methane by oxidative addition and σ-bond metathesis have been carried out for (N-N)M(Me) (M = Pd$^+$, Pt$^+$, Rh, Ir).[96] The pathway through oxidative addition is favored except for Pd$^+$. In each case, the oxidative addition is preceded by the formation of a σ-complex. The nature of the preferred pathway depends on the nature of the ligand as illustrated by a computational study (B3LYP) by Li and co-workers on (N′-N′)Pt(Ph)$^+$ (N′-N′ = Ar′N=CMe—CMe=NAr′, Ar′ = 2,6-(Me)$_2$C$_6$H$_3$) reacting with benzene.[97] The energy barrier for σ-bond metathesis is 14.7 kcal mol^{-1}, while it is 20.5 kcal mol^{-1} for the oxidative addition. So, unlike methane C—H activation, the σ-bond metathesis pathway is predicted to take place predominantly in this arene C—H activation.

Diimine pyridine ligands provide a nice platform for C—H activation processes as illustrated by the transformation shown in Figure 8 reported by Nückel and Burger.[98] BP86 calculations on the actual experimental system indicate that the reaction proceeds through a Ph—H oxidative addition/Me—H reductive elimination sequence of steps. No transition state for a σ-bond metathesis pathway could be located on the PES. Bending of the methyl group away from the molecular plane has a crucial impact on the ease of the C—H activation. Deformation of the complex to reach the geometry presenting frontier orbitals adapted to C—H activation is facilitated by CF_3 substituents on the pyridine ring rendering the latter more π-accepting toward Ir.

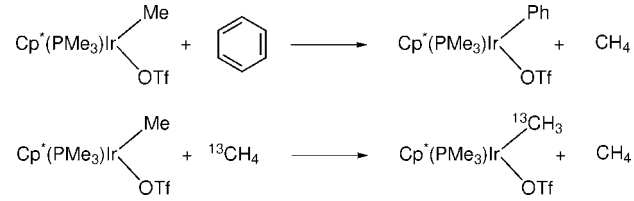

Figure 9. C—H activation by Ir(III) complex.

2.1.2. d^6 Configuration

After the initial discovery by Bergman of intermolecular C—H activation by the d^8 Cp*Ir(PMe$_3$) fragment, more than 10 years elapsed until a related d^6 fragment proved active in C—H activation. In 1993, the Ir(III) complex Cp*Ir(PMe$_3$)(Me)(OTf) was shown to undergo mild and selective reaction with C—H bonds in arenes and alkanes (Figure 9).[99]

The C—H activation has been shown to proceed after dissociation of the triflate;[100] thus the active species is d^6 Cp*Ir(PMe$_3$)(Me)$^+$. Electrospray ionization tandem mass spectrometry, in conjunction with solution-phase experiments and *ab initio* calculations, indicated that an intermediate of the reaction in the gas phase is Cp*Ir(η^2-CH$_2$PMe$_2$)$^+$. This intermediate results from intramolecular C—H activation of PMe$_3$.[101] However, studies in solution on Cp*Ir(η^2-CH$_2$PMe$_2$)(OTf) showed that the cyclometalated complex is not an intermediate in the reaction shown in Figure 9, even though it reacts faster with C—H bonds than Cp*Ir(PMe$_3$)(Me)(OTf).[102]

For the reaction with CH$_4$ shown in Figure 9, there are again two possible pathways: σ-bond metathesis and oxidative addition/reductive elimination. Both pathways are also feasible, in principle, for the cyclometalated complex. B3LYP calculations by Strout et al. on CpIr(PH$_3$)(CH$_3$)$^+$ reacting with methane yielded an oxidative addition TS at 11.5 kcal mol^{-1} above the σ-complex, the stability of which with respect to separated reactants is −1.0 kcal mol^{-1}.[103] The Ir(V) intermediate CpIr(PH$_3$)(CH$_3$)$_2$(H)$^+$ lies at 4.4 kcal mol^{-1} above the σ-complex and would subsequently evolve to the product upon C—H reductive elimination. Despite an intensive search, no TS for a metathesis pathway could be located on the PES. In a later study, Niu and Hall considered the reaction of methane with CpIr(PMe$_3$)(Me)$^+$.[104] The oxidative addition/reductive elimination pathway was not significantly altered by the substitution of PMe$_3$ for PH$_3$ ($\Delta E^\ddagger$ = 13.0 kcal mol^{-1} and ΔE = 5.2 kcal mol^{-1}, PMe$_3$; $\Delta E^\ddagger$ = 11.5 kcal mol^{-1} and ΔE = 4.4 kcal mol^{-1}, PH$_3$). The intramolecular C—H activation to form CpIr(η^2-CH$_2$PMe$_2$)(CH$_3$)(H)$^+$ was shown to be more difficult ($\Delta E^\ddagger$ = 26.5 kcal mol^{-1} and ΔE = 14.7 kcal mol^{-1}). Interestingly, the energy of the separated intermediate CpIr(η^2-CH$_2$PMe$_2$)$^+$ and methane is higher than the Ir(V) cyclometalated intermediate (ΔE = −5.9 kcal mol^{-1}), and methane C—H activation is easier for the cyclometalated intermediate ($\Delta E^\ddagger$ = 5.2 kcal mol^{-1}), in agreement with the experimental observations. These calculations confirm that the cyclometalated complex is not an intermediate in the reaction. Here again, despite a careful search, no TS for a σ-bond metathesis pathway could be found for either the inter- or the intramolecular cases.

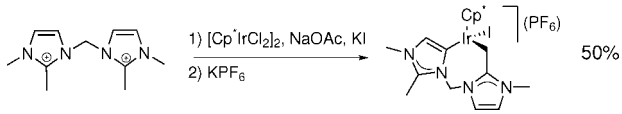

Figure 10. Formation of mixed normal/abnormal bis-NHC−Ir complex by C−H activation.

A comparison between C−H activation of cyclopropane by $Cp(Ir)(PH_3)(CH_3)^+$ and $CpIr(PH_3)$ was carried out by Webster and Hall at the B3LYP level.[105] In the case of $CpIr(PH_3)(CH_3)^+$, the mechanism is a sequence of cyclopropane oxidative addition/methane reductive elimination that leads to *endo* and *exo* cyclopropyl complexes of similar energy. These complexes transform to η^3-allyl isomers after formation of an $Ir(CH_2)(CH{=}CH_2)$ intermediate through C−C oxidative addition. The rate-determining step is the C−H cleavage of cyclopropane with $\Delta E^{\ddagger} = 13.1$ kcal mol^{-1}. In the case of the reaction with $CpIr(PH_3)$, a σ-complex of cyclopropane with a stability of −7.5 kcal mol^{-1} could be located, and the TS for C−H cleavage is only 0.1 kcal mol^{-1} above the σ-complex. From the same σ-complex, a TS for C−C cleavage to form an iridacyclobutane could be located with $\Delta E^{\ddagger} = 2.8$ kcal mol^{-1}. The product of C−C activation, which is the thermodynamic product, is computed to be 15.8 kcal mol^{-1} more stable than the hydrido-cyclopropyl product.

C−H activation by Ir(III) complexes proceeds through an Ir(V) intermediate that is expected to be less stable. Thus any factor leading to stabilization of the Ir(V) intermediate should ease C−H activation. Webster and Hall have addressed the computational design of stable Ir(V) complexes.[106] The reaction (η^x-L)L′Ir^{III}R + R′H → (η^x-L)L′Ir^{V}RR′H (η^x-L = Cp, Tp, and carborane; L′ = PR_3, CR_3^-, SiR_3^-, and SnR_3^-; R′ = alkyl, CR_3, H) has been studied at the DFT level. Finding a ligand set that allows "trapping" of an Ir(V) intermediate has proven difficult. Improved stability of an Ir(V) intermediate is obtained in the reaction of methane with $Cp^*Ir(PMe_3)(H)^+$. When neutral complexes, obtained by substitution of PR_3 with silyl or stannyl, are considered, the Ir(V) intermediate and the Ir(III) precursor have similar energies ($\Delta E < 0$ but $\Delta G > 0$).

In an attempt to form abnormal bis-N-heterocyclic carbene (NHC) complexes from C2-methylated bis-imidazolium salts, Viciano et al. observed an interesting competition between C−H activation at sp^2 and sp^3 carbon atoms (Figure 10).[107] B3PW91 calculations indicated that the first C−H activation by Cp^*IrI_2 is easier at the sp^3 than at the sp^2 position ($\Delta E^{\ddagger}$ = 31.6 vs 34.1 kcal mol^{-1}, respectively). The second C−H activation is an intramolecular process at the d^6 Ir(III) complex $Cp^*Ir(CH_2\text{-}R)(I)$. C−H activation of the methyl group of the second imidazolium ring has an energy barrier of 24.6 kcal mol^{-1} thus showing the ability of the ligands on Ir to modulate the energetics of the C−H cleavage by making the metal center more electrophilic. However, the TS for C−H activation at the sp^2 position of the second imidazolium to give the observed product is favored by 7.1 kcal mol^{-1} as a result of prior coordination of the C4=C5 π bond. The calculations have thus highlighted the sequence responsible for formation of the mixed ligand: intermolecular sp^3 C−H activation first, followed by intramolecular sp^2 C−H activation. The role of the base AcO^- is to deprotonate the Ir center after each C−H oxidative addition step, thus providing a thermodynamic driving force for the reaction.

A comparative study of methane C−H activation by $TpRe(CO)_2$ and $CpRe(CO)_2$ was carried out by Bergman et al. at the B3LYP level in order to understand why oxidative addition is observed with CpRe and not with TpRe.[108] The σ-complexes were computed to have similar stability with respect to separated reactants (−6.3 kcal mol^{-1}, Tp; −8.7 kcal mol^{-1}, Cp), but the TS for C−H activation with $CpRe(CO)_2$ is 9.1 kcal mol^{-1} more stable than the TS for C−H activation with $TpRe(CO)_2$. Consequently the reaction is exothermic for $CpRe(CO)_2$ (−7.9 kcal mol^{-1}) and endothermic for $TpRe(CO)_2$ (+6.4 kcal mol^{-1}), in good agreement with the experimental observations. The different behavior is ascribed to the steric influence of the Tp ligand that disfavors the seven-coordinated geometry of the oxidative addition product.

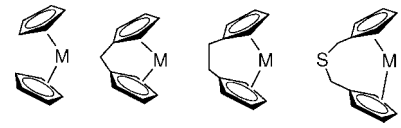

Figure 11. Systems computed in the study by Su and Chu.[122]

Clot et al. studied the mechanism of arene C−H activation by $CpRe(CO)_2$ at the B3PW91 level.[109] As expected, the π-benzene adduct is more stable than the σ-adduct (4.3 kcal mol^{-1}), and the latter is a precursor for the C−H cleavage step, which gives a *cis* isomer ($\Delta E^{\ddagger} = 9.1$ kcal mol^{-1} and $\Delta E = 6$ kcal mol^{-1}). This *cis* isomer subsequently evolves exothermically ($\Delta E = -4.9$ kcal mol^{-1}) to the *trans* isomer with an energy barrier of 24 kcal mol^{-1}. The rate-determining step in this transformation is not the C−H activation but an isomerization process of the oxidative addition product. The *trans* isomer is computed to be less stable than the π-benzene adduct by 5.3 kcal mol^{-1}, in agreement with the experimental observations where no activation is seen for benzene.[110] Legzdins et al. have studied the intermolecular activation of hydrocarbon C−H bonds by $Cp^*W(NO)(PMe_3)$.[111] The role of fluoro substituents on the C−H activation in arenes will be further discussed in section 3.1.

2.1.3. d^4 Configuration

The d^4 fragment Cp_2W, which can be formed by solution photolysis of $Cp_2W(H)_2$ or $Cp_2W(CO)$, has been shown to activate C−H bonds.[112–116] NMR studies of methane elimination from $Cp_2W(Me)(H)$ provided insight into the process of reductive elimination and hence of its microscopic reverse oxidative addition.[117,118] Other metallocene complexes have been studied ($Cp^*_2W(Me)(H)$[119] and $Me_2CCp_2W(Me)(H)$[120]), and they all show significant differences in their thermal stability. The non-ansa methyl−hydride complexes decompose over the range 40−100 °C, producing methane, while the ansa-bridged compound is thermally stable up to 120 °C.

Several computational studies have addressed the mechanism of methane elimination from group 6 metallocene methyl−hydride complexes.[121–125] Su and Chu carried out B3LYP calculations on various metallocenes (Figure 11, M = Mo, W).[122] They computed the singlet and triplet spin states for the d^4 metallocene fragments, but the oxidative addition of methane was considered only on the singlet surface. The oxidative addition is composed of two steps: methane coordination to form a σ-complex and C−H oxidative cleavage. The latter step is computed to be more facile for the structure with parallel Cp rings than for the bent geometry of the ansa system. This is due to the larger stability of the σ-complex with the ansa-metallocene based on the shapes of its frontier orbitals. The singlet−triplet gap, which is smaller for Cp_2W than ansa-Cp_2W (5.2 kcal mol^{-1}

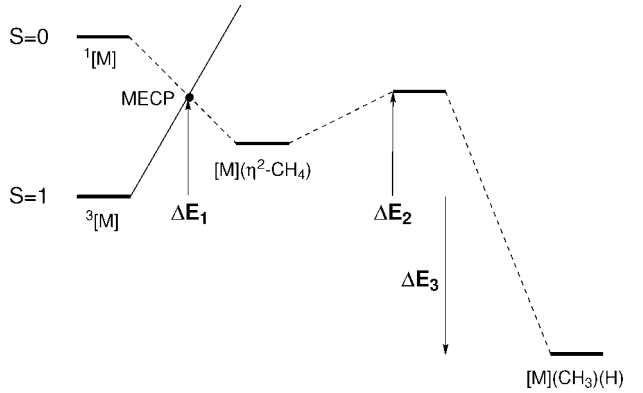

Figure 12. Schematic representation of the mechanism for methane oxidative addition to triplet group 4 metallocenes.

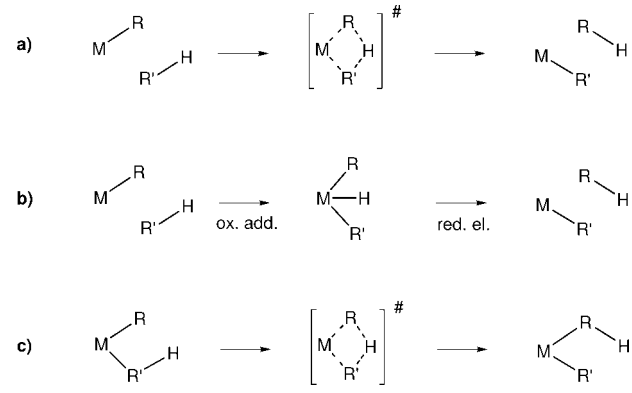

Figure 13. Various mechanisms for formal σ-bond metathesis.

vs 18.9 kcal mol^{-1} with triplet more stable as shown experimentally by Perutz[126,127]), is shown to determine the relative rate of reactions, following a rationale in terms of configuration mixing.[128]

DFT calculations were also performed by Green et al. on Cp_2M, H_2CCp_2M, and Cp^*_2M (M = Mo, W) reacting with methane.[121,123] The d^4 metallocenes have a triplet ground state, but the C—H coordination and cleavage occur on the singlet surface. To rationalize the chemistry of these systems, it is important to determine how the singlet and triplet surfaces cross. Therefore, the minimum energy crossing point (MECP) was determined for Cp_2M (M = Mo, W), and the PES for methane activation on the singlet surface was also calculated (Figure 12).

Table 2 collects the values of the energies ΔE_i (kcal mol^{-1}, $i = 1-3$ see Figure 12). From these values, it is clear that the rate-determining step is crossing the MECP for the ansa-W complexes and the C—H cleavage for the other complexes. The energy barrier is significantly lower for the ansa-W complexes, in agreement with the expected greater reactivity. The small energy gap between the singlet and triplet H_2CCp_2W complex is a result of the constraint imposed by the tether and is at the origin of the greater reactivity. The triplet, which prefers the two cyclopentadienyl rings to be parallel, is destabilized in the ansa complex and is thus more reactive. Any photogenerated ansa-Cp_2W fragment immediately reacts with any C—H bond present in the solution. This explains the experimental observations that an ansa-methyl hydride W complex is stable even at 120 °C. The energy barriers for reductive elimination are in good agreement with the available values for $Cp_2W(CH_3)(H)$[117,118] and $Cp^*_2W(CH_3)(H)$.[119] For $Cp_2W(\eta^2\text{-}CH_4)$, the energy barrier for H exchange is lower than that for reinsertion, while it is of the same order for $Cp^*_2W(\eta^2\text{-}CH_4)$, explaining the H/D scrambling observed experimentally.

The preceding study was completed by a characterization of the mechanism for methane oxidative addition to H_2SiCp_2M and $Me_2SiCp^*_2M$ (M = Mo, W) by Harvey et al.[125] Here again, the relative energy of the MECP and the TS for oxidative cleavage is the crucial factor. Experimentally, it was shown by Churchill et al. that methane reductive elimination from $Me_2SiCp^*_2M(Me)(H)$ is characterized by an inverse primary kinetic isotope effect for M = W but a normal one for M = Mo.[129] For M = Mo, the C—H coupling step is rate-determining (Table 2), and thus KIE is normal. For M = W, the situation is reversed with methane dissociation through the MECP being now the rate-determining step (Table 2). Thus the experimental KIE is an equilibrium isotope effect, and the inverse value reflects the tendency for deuterium to occupy the sites associated with high vibrational frequencies (η^2-(C—H) vs M—H). However, kinetic isotope effects are not always straightforward to analyze, and Parkin has shown how transition from a normal to an inverse behavior could be obtained by changing the temperature.[130,131]

2.2. σ-Bond Metathesis

σ-Bond metathesis is a one-step reaction by which two σ bonds are broken and two new σ bonds are formed in a concerted manner without change of the metal oxidation state (Figure 13a). A recent review describes the current understanding for this reaction.[132] This mechanism has been proposed for early and late transition metal complexes. However, in the case of the late transition metal complexes, where the metal can have various oxidation states, the same transformation can be formally achieved either by σ-bond metathesis or by successive oxidative addition and reductive elimination (Figure 13b). Preference for either of these mechanisms has been the topic of a number of theoretical studies, which will be presented in section 2.4. In this section, we focus on the case of early d^0 transition metal complexes for which a change in the oxidation state of the metal is not energetically accessible. Activation of C—H bond by σ-bond metathesis is prevalent in the case of groups 3 and 4 metal complexes, as well as with lanthanide and actinide complexes. Hydrogen transfer between ligands (Figure 13c), which involves a transition state analogous to that of classical σ-bond metathesis, is also achieved without modification of the oxidation state at the metal, and some representative cases will be presented.

Computational studies have focused on metallocene complexes, which have been found to be very useful as catalysts

Table 2. Energies (kcal mol^{-1}) in the Process of Methane C—H Activation by Various d^4 Metallocenes[a]

	Cp_2Mo	Cp_2W	Cp^*_2W	H_2CCp_2W	$Me_2SiCp^*_2Mo$	$Me_2SiCp^*_2W$
ΔE_1	21.8	17.8	25.0	6.5	11.1	11.8
ΔE_2	28.2	18.0	25.8	3.4	15.4	9.4
ΔE_3	9.8	−11.0	−24.4	−29.2	−4.0	−21.6

[a] See Figure 12 for definition of energies.

for olefin polymerization and have considerable potential for aliphatic and alicyclic C—H bond activation.[133,134] The mechanistic aspects of the C—H activation have also been studied in relation to the Ziegler—Natta polymerization process notably by Bercaw and co-workers.[135,136] We will not review the computational works related to polymerization. However, we cite a key computational study on C—H activation in relation to chain termination for the interested reader.[137]

One of the most emblematic reactions involving C—H activation with early transition metal complexes has been the activation of methane by $(C_5Me_5)_2LuCH_3$ for which the degenerate reaction of exchange of methyl groups has been proven by isotope labeling.[138,139] The C—H bond activation is also a key step in the reaction of CH_3X with metallocene cerium complexes.[140,141] The competition between C—H and C—X bond activation in fluorarenes by the same cerium complexes has been studied.[142,143] Competition between C—H and C—X (X = Cl) has been observed in Ti(IV) complexes, and the mechanism of this reaction has also attracted the interest of computational chemists.[144,145] The catalytic hydromethylation of olefins by a metallocene of scandium is an example of methane functionalization.[146,147]

The key structural and electronic features of the transition state for σ-bond metathesis were established in the study of the H for H exchange reaction between a metal hydride complex and H_2. The earlier studies, which included a generalized valence bond (GVB) analysis of the reaction,[148,149] were followed by DFT calculations by Ziegler[150] and by Maron and Eisenstein,[151] carried out for reactions with Sc, Y, and lanthanide complexes. Earlier calculations have used chloride ligand to represent the cyclopentadienyl ligand. In the more recent studies, C_5H_5 and C_5Me_5 have been used in the models, and various levels of calculations have been tested for C_5Me_5.[152,153] For the calculations of lanthanide elements, large core pseudorelativistic effective core potentials have been used. This methodology, which puts the inner 4f electrons in the core, has been validated by comparison with calculations using small core pseudorelativistic effective core potentials.[154]

The transition state for H for H exchange between the M—H bond of X_2MH and H_2 has a kite-shaped geometry with the metal and the three hydrogen atoms lying in a plane bisecting the X—M—X angle. This applies to any model used to represent the metallocene (X = Cl or Cp) and for any group 3 or lanthanide metal. In principle, the reaction starts by the coordination of the substrate to the electron-deficient metal center. However, the stability of the adduct relative to separated components is weak due in particular to the absence of back-donation from the metal to the empty orbitals of the substrate. Its stability, in the case of H_2 and Cp_2ScH, is less than 4 kcal mol^{-1}.[150] No equivalent adduct was found in the case of Cp_2LnH.[151] Adducts of CH_4 are also found to be weak even though the bonding energy of CH_4 depends on the model used for the metal fragment. The presence of a stable adduct between the electron-deficient complex and the reagent (H_2, CH_4) is thus not an important feature in the σ-bond metathesis reaction in the case of d^0 metal fragment and will not be discussed further.

The geometrical features of the transition state deserve further comments. In a study of the reaction of Cp_2ScH with H_2, Ziegler et al. mention the presence of a short contact between the metal and the β-H.[150] They also state that the Sc—H bond lengths at the transition state for the H for H exchange are only slightly longer than a normal Sc—H bond length. These facts account for the low energy barrier. In a study of the reaction of Cp_2LnH with H_2, Maron and Eisenstein obtained similar geometrical results.[151] The energy barriers are low and similar for all Ln(III) metals. The Ln—H bonds at the transition state are just slightly longer than the Ln—H bond in Cp_2LnH. The authors also note that the H—H—H angle is around 156° for any Ln(III) element, which leads to a shorter M—H distance for the β- than for the α-hydrogen (Figure 14). For instance, in the case of Cp_2LaH, the La—H distance for the α-hydrogen is 2.276 Å, while it is 2.262 Å for the β-hydrogen and it is 2.142 Å in Cp_2LaH. The large H—H—H angle at the transition state suggests that the three hydrogen atoms have accumulated a negative charge, localized on the hydrogens near the metal, and take the geometry of a H_3^- moiety, in interaction with the metal fragment; this fact is supported by a charge analysis.[155] Therefore, these authors consider that the reaction is best viewed as a proton transfer between two hydrides in the stabilizing field of a positively charged metal center. The positive charges at both the metal and the migrating H exclude any interaction between them, despite the short internuclear M···H distance.

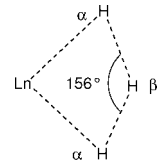

Figure 14. Transition state for σ-bond metathesis.[151]

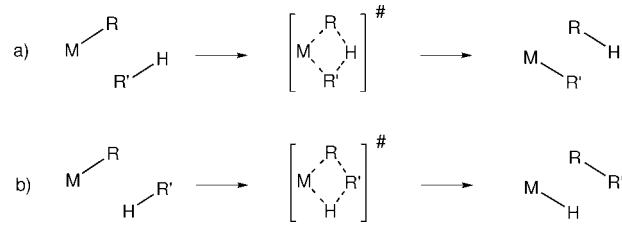

Figure 15. Different regiochemistry in σ-bond metathesis.

The transition state for σ-bond metathesis between the M—C bond of Cp_2M—R and the C—H bond of R′—H has similar geometrical features as described above: the four-membered ring has a kite-shaped geometry and the metal, the carbon of R bonded to M, and the activated C—H bond lie in a plane, bisecting the Cp—M—Cp angle. Two transition states, corresponding to two different reactions, are in principle possible. One reaction corresponds to an R for R′ exchange, and the hydrogen atom occupies the β-position at the transition state (Figure 15a). The other reaction forms R—R′ and M—H, and R′ occupies the β-position at the transition state (Figure 15b).

These two reactions are found to have dramatically different energy barriers in the case where R′ is an alkyl group. Only the reaction with the hydrogen atom at the β-position at the transition state (Figure 15a) is calculated to have accessible energy barriers. If R′ = H, the reaction is calculated to be exothermic for the formation of the metal hydride. In other words, the metal hydride does not activate the C—H bond of an alkane, while the metal—alkyl bond is hydrogenolyzed by H_2 in agreement with experiment. These results have been found for either Cp_2ScH[150] and Cp_2LnH complexes.[156–158] The energy barrier of the reaction shown in Figure 15a varies between 5 and 19 kcal mol^{-1} depending

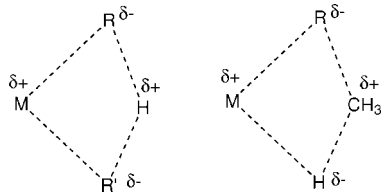

Figure 16. Charge distribution at the transition state for σ-bond metathesis.

on the model used for the ligand (lower for Cl than for Cp) and the nature of the metal. In contrast, the reaction of Figure 15b has an energy barrier in the range of 37.5 kcal mol^{-1} relative to the adduct between Cl_2ScCH_3 and CH_4.[159] For the reaction of H for H exchange between Cp_2LnH and CH_4 (CH_3 at the β position), the activation barrier has been calculated to be around 70 kcal mol^{-1} for any Ln(III) complexes.[157] The rationale for the very different barriers of these two reactions has been discussed notably by Maron and Eisenstein. Following the analysis for the reaction of Cp_2MH with H_2, the transition state for the reaction of Figure 15a can be viewed as a proton transfer between two negatively charged R and R′ alkyl groups (Figure 16). This is supported by the structure of the transition state: for instance, in the reaction of Cp_2LaCH_3 with CH_4, the C—H—C angle is equal to 180°.

The charge distribution is similar when the alkyl, such as Me, is at the β-position. The positively charged alkyl group is thus interacting with two negatively charged groups (H and R). The result is that the $[H(CH_3)R]^-$ ensemble has an electronic structure similar to that of CH_5^-, which is not a favorable situation. To support this interpretation, calculations show that replacing C by Si at the β-position yields considerably lower barriers.[160] This is in agreement with the commonly accepted idea of the ability of Si to become hypervalent as in SiH_5^-. The accessibility of a σ-bond metathesis reaction with a silyl group and not with the methyl group at the β-position is central to the understanding of the reactions between alkyl and aryl silanes with Cp^*_2Sm derivatives.[161,162] The discrimination between paths with H or alkyl at the β-position has been used to rationalize the H for D exchange on Zr—H supported by silica.[163]

It has been shown by experiment that the rate of the reaction of $Cp^*_2M—CH_3$ with CH_4 decreases in the order Y > Lu > Sc. This comparison was studied with DFT calculations by Cramer[164] and by Maron and Eisenstein.[158] The two groups of authors have compared the influence of Cp vs Cp* on the reactivity trends and have found that introducing Cp* is necessary for reproducing the experimental observations. Maron and Eisenstein mention that it is necessary to consider the charges developed on the four centers at the transition state in order to understand the reactivity better. Cramer et al. have also studied the reactions that take place in competition with the bimolecular methyl exchange (Figure 17). They have shown that the unimolecular methane ejection via formation of a tuck-in complex competes with the bimolecular methyl exchange reaction for Sc but not for Y and Lu. The greater propensity for Sc to form the tuck-in complex is related to the shorter metal—ligand distances observed for this metal atom. The calculated enthalpy for C—H activation of methane is 24.1 kcal mol^{-1} via the bimolecular process, which is significantly higher than the experimental value of 11.6 kcal mol^{-1}. The enthalpy of activation is lowered to 19.2 kcal mol^{-1} by including the tunneling contribution.

This latter study was extended to the reaction of methane with Cp^*_2MR (M = Sc, Lu; R = Me, $CH_2C(CH_3)_3$), with the aim of understanding the influence of the R group on the metathesis reaction.[165] With the mPW1K density functional, the bimolecular reaction is calculated to dominate but the unimolecular reaction, proceeding through the tuck-in complex, becomes increasingly competitive for bulky alkyl groups and for metals with small ionic radius. The quantum-mechanical tunneling is predicted to increase the overall reaction rates by 1−3 orders of magnitude over the temperature range 284−323 K. This study was repeated for ansa-(bis(η^5-2-indenyl)methane)MR complexes (M = Sc, Y, Lu; R = CH_3,$CH_2C(CH_3)_3$).[166] It was shown that the presence of an ansa bridge disfavors the unimolecular reaction via the tuck-in complex and favors the bimolecular reaction.

The full path for hydromethylation of propene, where several σ-bond metathesis processes are in competition, was studied for metallocene complexes of scandium and lutetium (Figure 18).[167,168] The formation of secondary products, notably resulting from various C—H activations, was studied in addition to the main pathway. Vinylic and allylic C—H activation of propene are competitive with the main path and are responsible for the formation of the secondary products. These reactions, although releasing isobutane, destroy the catalyst since no regeneration from C—H activation of methane is possible. The elementary steps responsible for

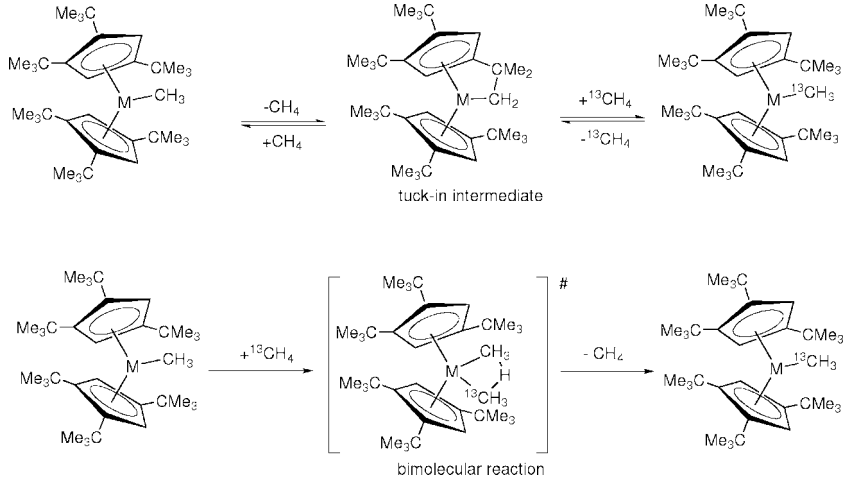

Figure 17. Competition between intramolecular (top, unimolecular methane dissociation) and intermolecular (bottom, bimolecular methyl group exchange) σ-bond metathesis reactions.

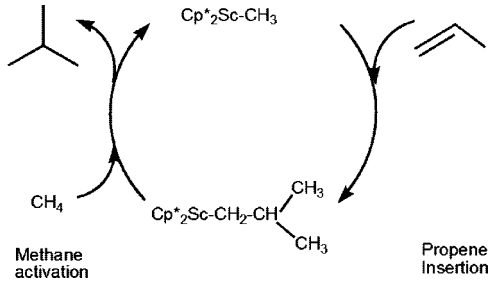

Figure 18. Postulated mechanism for the hydromethylation of propene.

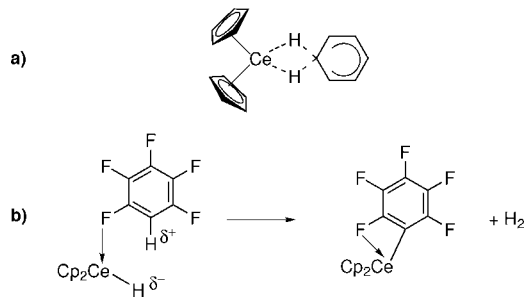

Figure 19. Reactions between Cp_2CeH and arenes: (a) transition state that could not be located; (b) pathway for formation of $Cp_2Ce(C_6F_5)$ from Cp_2CeH and C_6F_5H.

the disappearance of the catalyst have lower energy barriers in the case of lutetium, which excludes the Lu complex as an efficient catalyst. A similar study was carried out for the reaction of propene and isobutene with ansa-$H_2Si(C_5H_4)_2ScCH_3$, a model for ansa-$Me_2Si(C_5Me_4)_2ScCH_3$.[168] It has been concluded that the hydromethylation is more efficient for isobutene than for propene, in agreement with experiment. In particular, the vinylic C—H activation has an accessible energy barrier and produces intermediates like $Me_2Si(C_5Me_4)_2Sc(CH{=}(CH_3)_2)$.

Monomeric Cp'_2CeH ($Cp' = 1,2,3\text{-}(Me_3C)_3(C_5H_2)$) reacts with C_6F_5H to form Cp'_2CeF and H_2, via an intermediate, $Cp'_2Ce(C_6F_5)$, which was isolated.[142] DFT(B3PW91) calculations of the reaction of C_6F_5H with Cp_2CeH to form $Cp_2Ce(C_6F_5)$ and H_2 were carried out. A transition state with the phenyl group at the β-position was searched for (Figure 19a). Despite considerable effort, no such transition state could be located. The proposed pathway starts by the coordination of C_6H_5F to the empty coordination site of Cp_2CeH by way of the fluorine ortho to the C—H bond (Figure 19b). In this adduct, the arene lies in the plane bisecting the Cp_2Ce angle. This geometry brings the positively charged H of C_6F_5H close to the hydride. The activation barrier to form $Cp_2Ce(C_6F_5)$, which is an observed intermediate, and H_2 from the adduct $Cp_2Ce(C_6F_5H)H$ is 10.2 kcal mol^{-1}. The results obtained in this study show that the reactivity pattern found for alkanes is also applicable to arenes. Thus, a transition state of σ-bond metathesis with a carbon at the β-site is in general energetically unfavorable.

The reaction of $Cp^*(^tBu_3P{=}N)TiH^+$ and C_6H_5X (X = H, Cl, Br) leads to different products depending on the pressure of H_2 used in the experiment (Figure 20).[144] At low pressure of H_2, the release of H_2, through *ortho*-C—H activation and the formation of the β-halophenyl cation $Cp^*(^tBu_3P{=}N)Ti(2\text{-}X\text{-}C_6H_4)^+$ has been observed. This halophenyl complex evolves further. At higher pressure of H_2, an H for X exchange is observed with release of benzene. Calculations were carried out with DFT(TPSS) method.[145] The pathway

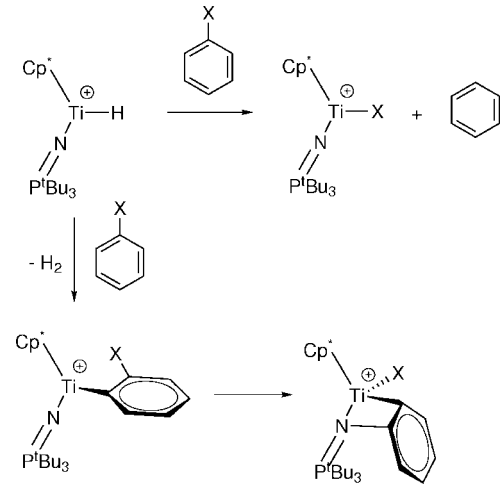

Figure 20. Products of the reaction of $Cp^*(^tBu_3P{=}N)TiH^+$ and halobenzene.

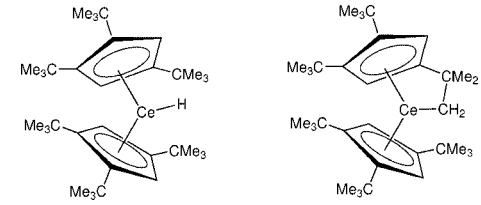

Figure 21. Cp'_2CeH and associated metallacycle.

for the ortho-metalation of the halobenzene is found to be similar to that described for Cp_2LaH and C_6F_5H.[142] However, for the H for X exchange, a direct σ-bond metathesis pathway with a kite-shaped transition state has been located with an enthalpy of activation of 20.1 kcal mol^{-1} above the halophenyl complex (X = Cl). The authors also mention that using B3LYP and B3PW91 methods, they also located a kite-shaped transition state for the H for F exchange between Cp_2LaH and C_6F_6 ($\Delta H^{\ddagger}$ ca. 6 kcal mol^{-1}, $\Delta G^{\ddagger}$ ca. 9 kcal mol^{-1}), in contrast to the results published previously.[142,169]

We have described earlier the reasons why the kite-shaped transition state of σ-bond metathesis with an alkyl group at the β-position has a high energy. A way to lower the energy of the transition state is to replace C with Si. Another way is to substitute the H atoms on the alkyl group by electron-withdrawing atoms. This proposal was tested by calculating the energy profile for the H for F exchange in the reaction of Cp_2LnH with CF_4. Although the energy barrier is significantly lower than that associated with CH_4, it is still too high for the reaction to be feasible.[170] This was confirmed by Andersen by the absence of any reaction between Cp'_2CeH ($Cp' = 1,2,4\text{-}(Me_3C)_3(C_5H_2)$) (Figure 21) and CF_4. However, CH_3F, CH_2F_2, and CHF_3 react with Cp'_2CeH. In all cases, Cp'_2CeF is formed as well as CH_4, but the rate decreases in the order $CH_3F < CH_2F_2 \ll CHF_3$.[140]

The DFT calculations, carried out with Cp_2CeH as a model for Cp'_2CeH, show that the σ-bond metathesis has high activation barriers for all fluoromethane derivatives ($\Delta G^{\ddagger}$ = 31.1 kcal mol^{-1}, CH_3F; $\Delta G^{\ddagger}$ = 33.2 kcal mol^{-1}, CH_2F_2; $\Delta G^{\ddagger}$ = 41.1 kcal mol^{-1}, CHF_3). The preferred pathway is found to be a two-step pathway (Figure 22). In the case of the reaction with CH_3F, the first step is a proton transfer to form $Cp_2Ce(CH_2F)$ and H_2. In this intermediate, the CH_2F group is dihapto-bonded to the metal center. This intermediate further evolves by inserting CH_2 into H_2 to form CH_4. As CH_2 inserts into H_2, the C—F bond is cleaved, and the final

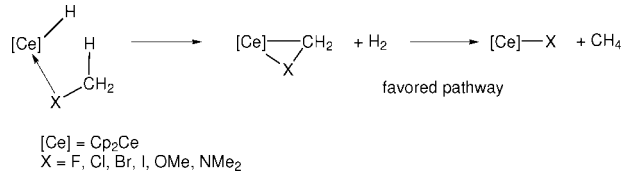

Figure 22. Two-step pathway for the reaction of Cp_2CeH with CH_3X.

products Cp_2CeF and CH_4 are formed. The proton transfer has a lower barrier than the following step, which involves the C—F cleavage, is rate-determining. The reaction pathways are calculated to be similar for the CH_2F_2 and CHF_3 substrates, which yield the Cp_2CeCHF_2 and Cp_2CeCF_3 intermediates, respectively. While the activation barrier of the proton transfer step does not vary much with the number of fluorines and stays low in all cases ($\Delta G^{\ddagger} < 18$ kcal mol^{-1}), the activation barrier of the transfer of the carbene into H_2, which increases in the order $CH_2 < CHF < CF_2$, determines the overall rate of the reaction. Repetition of the sequence allows defluorination of the haloalkane. Experimental support for this two-step mechanism comes from the characterization of several products resulting from the insertion of CH_2 into C—H bonds, as well as addition of CH_2 into various traps.

This two-step pathway, which is best viewed as a carbenoid pathway, was generalized through a combined experimental and theoretical study of the H for X exchange in the reaction of CH_3X (X = F, Cl, Br, I, OMe, and NMe_2) with Cp'_2CeH and the associated metallacycle (Figure 22).[141] It was shown that the reactions fall into three distinct classes: (i) class a (X = Cl, Br, and I) rapidly forms Cp'_2CeX and CH_4 without formation of identifiable intermediates in the ^{1}H NMR spectra, (ii) class b (X = OMe) proceeds rapidly to $Cp'_2Ce(\eta^2\text{-}CH_2OMe)$ and H_2, which is sufficiently stable to be isolated and characterized, and then to Cp'_2CeOMe and CH_4, and (iii) class c (X = NMe_2) does not result in formation of Cp'_2CeNMe_2, but deuterium labeling experiments show that H for D exchange occurs in NMe_3. The DFT calculations show that H for X exchange via one-step synchronous σ-bond metathesis is associated with the highest activation barrier in all cases. The preferred pathway is a two-step pathway, in which the first step, with a low activation barrier, is an α-C—H activation, i.e., a proton transfer, that forms $Cp_2Ce(\eta^2\text{-}CH_2X)$ and H_2, followed by trapping of CH_2 by H_2, which proceeds with a higher activation barrier, its height defining the classification as either a, b, or c. The free energy profiles show that the free energy barrier of the proton transfer is similar for all X (between 13.9 kcal mol^{-1} for X = OMe and 18 kcal mol^{-1} for X = I). However, the values do not follow the experimental gas-phase proton dissociation enthalpies for CH_3X. Thus, the activation barrier is not just determined by the acidity of the α-C—H bond, even though the relative acidity is the primary reason for the higher activation energy when H_2 and CH_4 are compared,[171] and the identity of X plays a role in determining the barrier. While these reactions are formally H for X exchange, they do not occur by means of the one-step σ-bond metathesis but by a two-step mechanism initiated by a C—H activation process. At the origin of this preference are the low barrier associated with the C—H bond activation and the high barrier associated with a σ-bond metathesis transition state with a carbon at the β-position.

A very recent study of the amine-catalyzed benzene C—H bond activation in $Cp^*_2ZrMe^+$ olefin polymerization catalysts has highlighted a new pathway for the deactivation route in aromatic solvent.[172] The external base NMe_3 deprotonates the coordinated benzene molecule and protonates the methyl group, thus yielding formally a metathesis reaction. This two-step pathway was shown by DFT calculations to be preferred over the one-step direct σ-bond metathesis pathway.

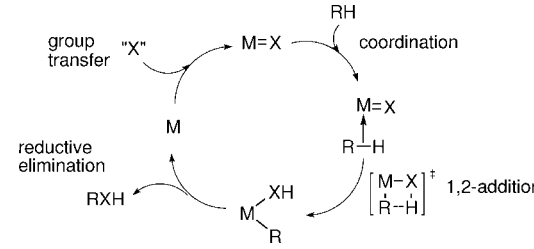

Figure 23. Hypothetical catalytic cycle for hydrocarbon heterofunctionalization through C—H 1,2-addition across M=X.

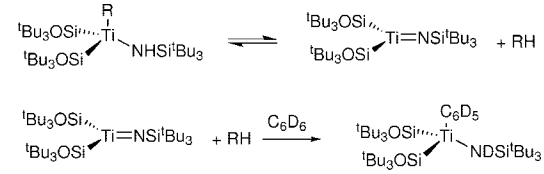

Figure 24. C—H activation by $(silox)_2(^tBu_3SiNH)TiR$ through 1,2-addition.

2.3. 1,2 Addition

2.3.1. Early Transition Metals

When a ligand with π-bonding capability (alkylidene, alkylidyne, amide, imide, alkoxide, aryloxide) is coordinated to an early transition metal, the unsaturation at the metal center is stabilized through π-donation from the ligand. The M=X functionality (X = CR_2, CR, NR_2, NR, OR) adds to a C—H bond in a $[2_\sigma + 2_\pi]$-type reaction (Figure 23). The 1,2-addition product M(XH)(R) could lead to a heterofunctionalized hydrocarbon upon reductive elimination. If the regeneration of the M=X group could be made catalytic, this would constitute a major advance. A key step in such a putative catalytic cycle is net 1,2-addition of a C—H bond across a metal—oxygen or metal—nitrogen bond. The C—H cleavage in itself is only one of the several steps that need to be achieved. As in the case of oxidative addition reactions, a vacant site on the metal should be created for the C—H bond to coordinate and engage in an interaction with M=X.

A combined experimental and computational study by Wolczanski, Cundari, and co-workers on $(silox)_2(^tBu_3SiNH)TiR$ (silox = $^tBu_3SiO$; R = Me, Et, CH_2Ph, $CH{=}CH_2$, ^{t}Bu, ^{n}Bu, Ph, H, ^{c}Pr, ^{c}Pe) illustrates the basic aspects of the 1,2-addition.[173–175] Thermolysis of $(silox)_2(^tBu_3SiNH)TiR$ in benzene-d_6 produces RH and $(silox)_2(^tBu_3SiND)Ti(C_6D_5)$, consistent with the mechanism shown in Figure 24. Activation parameters for RH elimination were determined for R = Me and ^{c}Pe. They indicate significant bond-breaking ($\Delta H^{\ddagger}$ ca. 20 kcal mol^{-1}) occurring within a constrained, unimolecular transition state ($\Delta S^{\ddagger}$ ca. −12 cal K^{-1} mol^{-1}), supporting a planar geometry for R—Ti—N—H in the TS. Large primary kinetic isotope effects were observed for 1,2-C—H elimination in agreement with a four-center TS with a relatively linear R···H···N geometry featuring similar amounts of N—H bond breaking and C—H bond-making.[173]

Ab-initio calculations (MP2//RHF) were performed on the model system $(HO)_2Ti{=}NR'$ reacting with RH (R = Me,

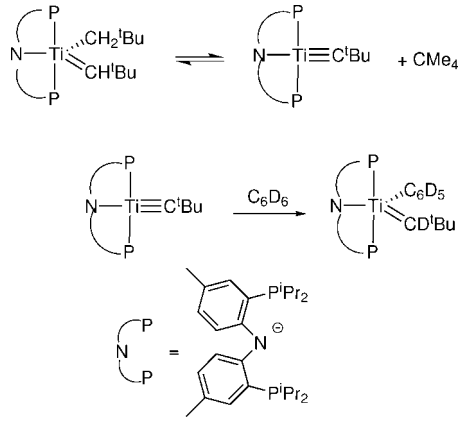

Figure 25. C—H activation by (PNP)Ti(≡CR).

Et, CH=CH$_2$, ^{c}Pr, Cy, Ph, or CH$_2$Ph and R′ = H; R = Me, ^{c}Pr, or Cy and R′ = SiH$_3$; R = Me and R′ = SiMe$_3$).[175] Increasing the size of the R′ group results in a more polarized Ti$^{\delta+}$—N$^{\delta-}$ bond and a more stable σ-adduct between Ti and RH. The structure and the energetics of the substrate/Ti-imido interaction is considered to be the main factor that determines the selectivity between activation of the various C—H bonds in RH. Molecular mechanics calculations on the various adducts between (silox)$_2$Ti(NSi^{t}Bu$_3$) and isopentane are in agreement with primary C—H bond preferentially coordinated versus secondary and then tertiary C—H bonds.

Sakaki et al. studied in detail the reaction of (Me$_3$SiO)$_2$Ti(=NSiMe$_3$) with methane.[176] DFT, MP2 to MP4(SDQ), and CCSD(T) calculations were carried out. The B3LYP binding energy of methane is −4.5 kcal mol^{-1}, and from this σ-adduct, the kinetic and thermodynamic parameters for C—H activation are $\Delta E^{\ddagger}$ = 14.6 kcal mol^{-1} and ΔE = −18.2 kcal mol^{-1}. Formation of the σ-complex is associated with a diminution of the electron population on CH$_3$ and H concomitant with an increase of the Ti electron population, indicative of a ligand to metal charge transfer (electrophilic attack). The passage through the transition state is accompanied by a significant increase of electron population on CH$_3$ and a significant decrease of electron population on H, which suggests that the C—H cleavage is heterolytic. These population changes are due to electron transfers from populated σ(C—H) to vacant Ti d_{z^2} MOs and from populated d_π—p_π(Ti=N) to vacant σ*(CH) MOs. An energy density analysis of the potential energy surface by Nakai et al. confirmed that Ti, N, C, and H are the active sites in the system.[177]

Mindiola, Baik, and co-workers studied intermolecular C—H bond activation promoted by a titanium—alkylidyne complex.[178,179] The reactive Ti≡CR functionality is generated from a titanium alkyl alkylidene through α-H migration (Figure 25). Experimentally, the α-migration is shown to be the rate-determining step. This is confirmed by DFT calculations, which show that the TS for α-migration is 27.8 kcal mol^{-1} above the reactant, whereas the TS for 1,2-addition of benzene is 21.0 kcal mol^{-1} above the same reference. Although the reactive Ti—alkylidyne intermediate is only 4.6 kcal mol^{-1} less stable than the reactant, its energy prevents any direct experimental observation. The overall reaction is computed to be exothermic by 11.8 kcal mol^{-1}.[178]

Coordination of the C—H bond to the Ti—alkylidyne complex is not selective, as σ-adducts of CMe$_4$ and C$_6$H$_6$ are computed to have similar energies. However, there is a clear distinction between C(sp^3)—H and C(sp^2)—H bond cleavage in these σ-adducts. The former is 6.9 kcal mol^{-1} more difficult than the latter ($\Delta G^{\ddagger}$ = 12 kcal mol^{-1}, CMe$_4$; $\Delta G^{\ddagger}$ = 5.1 kcal mol^{-1}, C$_6$H$_6$). Charge analysis again showed a build-up of negative charge on C and a build-up of positive charge on H in the TS for 1,2-addition, in agreement with an heterolytic cleavage of the C—H bond. Concomitantly, the Ti≡C bond polarity Ti$^{\delta+}$—C$^{\delta-}$ increases in the TS. Experimentally, for the reaction of the Ti—alkylidyne complex with C—H bonds, it was shown that C—H cleavage is the rate-determining step for C(sp^3)—H, whereas C—H bond coordination is rate-determining for C(sp^2)—H.

OsCl$_3$(C—CH=CPh$_2$)(PPh$_3$)$_2$ is reduced to the indenyl complex {(η^5-C$_9$H$_6$(Ph)}OsCl(PPh$_3$)$_2$ by Zn in the presence of PPh$_3$.[180] An unusual metallanaphthalyne complex is isolated as an intermediate during this reaction. DFT calculations on the model complex OsCl(PH$_3$)$_2$(C—CH=CHPh) show that the transformation is initiated by an aryl C—H oxidative addition at the osmium center, even though a carbyne functionality is present and could have been involved in a 1,2 addition.

Legzdins has studied in detail the thermal activation of hydrocarbon C—H bonds by Cp*M(NO)(CHR) complexes of molybdenum and tungsten, and some significant results are represented in Figure 26.[181] Poli and Smith have carried out B3LYP calculations on CpM(NO)(CH$_2$) (M = Mo, W) reacting with CH$_4$.[182] They located σ-complexes on the PES and showed that the C—H cleavage is more difficult for Mo than for W, as shown by the higher energy barriers ($\Delta E^{\ddagger}$ = 14.3 kcal mol^{-1}, Mo; $\Delta E^{\ddagger}$ = 7.8 kcal mol^{-1}, W) and the smaller exothermicity (ΔE = −24.9 kcal mol^{-1}, Mo; ΔE = −35.7 kcal mol^{-1}, W). The lower stability of the dimethyl Mo complex is in agreement with the milder conditions used experimentally (20 °C, 30 h, Mo; 70 °C, 40 h, W) to generate the active alkylidene complex (Figure 26).

A combined experimental and theoretical study of the reaction mechanism was carried out by Legzdins et al. on the tungsten complex.[183] The KIE values were inconsistent with rate-determining C—H bond activation by the M=C linkage and indicated that coordination of the substrate to the metal center is the discriminating factor in alkane and arene intermolecular competitions. B3LYP calculations on CpW(NO)(CH$_2$) reacting with toluene probed this competition through characterization of the extrema along C(sp^3)—H and C(sp^2)—H activation. The π—arene complexes (two orientations with respect to Cp) are computed to be ca. 10 kcal mol^{-1} more stable than the σ(C—H) adduct of the methyl group of toluene. This energy difference is also found in the TS for 1,2-addition and in the products, thus leading to a selective activation at the aromatic positions over the aliphatic ones. For the aromatic positions, the TSs for C—H cleavage are of similar energies for para and meta positions, while that at the ortho position is 4.5 kcal mol^{-1} higher. This is also in agreement with the relative amounts observed experimentally (ortho, 1%; meta, 47%; para, 33%).

The reactions of CH$_4$ with CpW(NO)(CH$_2$), Cp*W(NO)(CH$_2$), and the isoelectronic CpW(CO)(CH$_2$)$^-$ were computed at the B3LYP level by Fan and Hall.[184] The main purpose of this work was to test whether an oxidative addition/reductive elimination pathway was possible as an alternative to the 1,2-addition. The d^2 electronic configuration in the W—alkylidene reactive species allows, in principle, for a C—H activation through oxidative addition, contrary to the situation with d^0 Ti complexes. Even though, the hydrido-alkyl intermediate CpW(NO)(H)(CH$_3$)(CH$_2$),

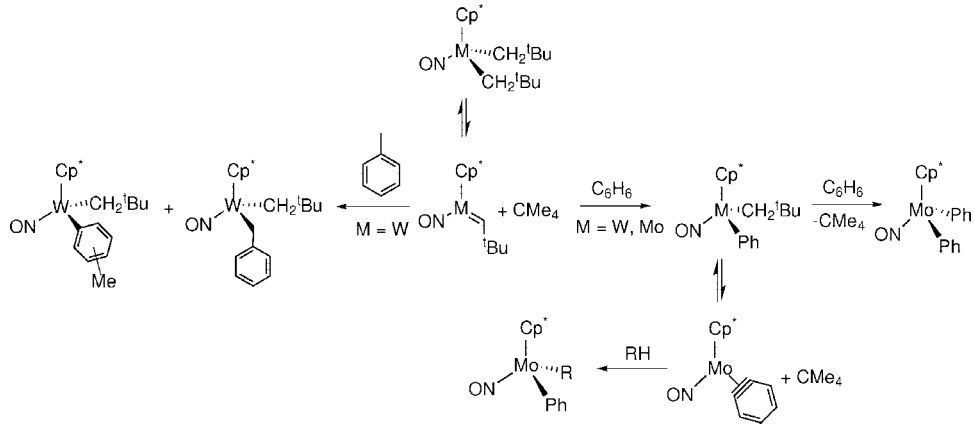

Figure 26. Reactivity of Cp*M(NO)(CH_2'Bu)$_2$ toward C—H bonds.

Cp*W(NO)(H)(CH_3)(CH_2), and CpW(CO)(H)(CH_3)(CH_2)$^-$ could be located on the PES, only in the case of the anionic carbonyl complex was a TS for oxidative addition from a σ(CH_4) adduct located. In that case, the oxidative addition/reductive elimination pathway is slightly preferred over the 1,2-addition. For the nitrosyl complexes, the high energy of the oxidative addition intermediate with respect to the TS for 1,2-addition and the absence of a TS for oxidative C—H cleavage leave the 1,2-addition as the sole mechanism. The authors pointed out that the 1,2-addition is strongly assisted by the metal as illustrated by the short W···H contact in the TS (ca. 1.8 Å). The preference for 1,2-addition with nitrosyl is ascribed to the greater π-acidity of this ligand in comparison to CO.

In the case of Cp*Mo(NO)(CH_2CMe_3)$_2$, reaction in benzene at room temperature yielded a mixture of Cp*Mo(NO)(CH_2CMe_3)(Ph) and Cp*Mo(NO)(Ph)$_2$ in a sequential manner.[185] The mixed product Cp*Mo(NO)(CH_2CMe_3)(Ph) can transform into two different intermediates upon α-migration, Cp*Mo(NO)($CHCMe_3$) and Cp*Mo(NO)(η^2-C_6H_4), which have been trapped by pyridine.[186] B3LYP calculations have been carried out to locate the extrema along the pathway for CpMo(NO)(CH_2R)(Ph) reacting with benzene (R = H, CMe_3).[186] α-H migration to form the benzyne adduct is significantly more difficult than that to form the alkylidene Mo(CHR). However, the energy difference between the two TSs is significantly influenced by the nature of R ($\Delta\Delta E^{\ddagger}$ = 4.1 kcal mol^{-1}, R = H; $\Delta\Delta E^{\ddagger}$ = 10.8 kcal mol^{-1}, R = CMe_3) because the TS for α-migration toward the alkyl is stabilized upon changing R from H to CMe_3. In this process, a M—C bond is broken, and this is easier for a secondary carbon (CH_2CMe_3) than for a primary carbon (CH_3), thus showing the importance of representing the experimental system properly in the computational models. From the π—arene complex CpMo(NO)(CHR)(η^2-C_6H_6), the C—H 1,2-addition is computed to be more difficult ($\Delta E^{\ddagger}$ = 12.7 kcal mol^{-1}, R = H; $\Delta E^{\ddagger}$ = 11.5 kcal mol^{-1}, R = CMe_3) than the C—H activation from the benzyne complex CpMo(NO)(η^2-C_6H_4)(η^2-C_6H_6) ($\Delta E^{\ddagger}$ = 7.5 kcal mol^{-1}). In all cases, the distance between the migrating proton and the Mo center in the TS is significantly shorter than the sum of the van der Waals radii (Mo···H = 1.856 Å, R = H; Mo···H = 1.814 Å, R = CMe_3; Mo···H = 1.856 Å, benzyne). This suggests some metal participation in the process.

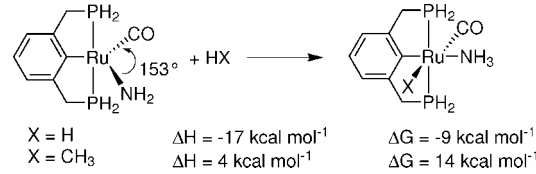

Figure 27. Reactivity of (PCP′)Ru(CO)(NH_2) toward H—H and C—H bonds.

2.3.2. Late Transition Metals

New synthetic strategies have now made possible the isolation and study of a variety of monomeric late metal alkoxide, aryloxide, and amide complexes.[187] The M—X complexes typically exhibit nucleophilic reactivity, and even deprotonate relatively weak acids. The five-coordinate parent amido complex (PCP)Ru(CO)(NH_2) (PCP = 2,6-($CH_2P(CMe_3)_2)_2C_6H_3$) reacts with phenylacetylene to yield the Ru(II) acetylide complex (PCP)Ru(CO)(C≡CPh) and ammonia.[188] The same complex also activates H—H to yield ammonia and the hydride (PCP)Ru(CO)(H). B3LYP calculations have been carried out by Cundari et al. on the reaction of (PCP′)Ru(CO)(NH_2) (PCP′ = 2,6-($CH_2PH_2)C_6H_3$) with H_2 and CH_4 (Figure 27).[188] Only thermodynamic aspects were evaluated, and the computed values for the reaction with H_2 are in agreement with the experimental observations. For the hypothetical C—H activation of methane, the calculations indicate that the reaction is both endothermic and endoergic. This unfavorable thermodynamics of transformation has been ascribed to a large and unfavorable change in Ru—N bond dissociation energy upon conversion from Ru—amido to Ru—amine (ΔBDE = 40 kcal mol^{-1}). Forming N—H and Ru—C bonds at the expense of the strong C—H bond only results in a gain of 30 kcal mol^{-1}, not enough to compensate the weakening of the Ru—N bond. In the reaction with H_2, the Ru—H bond, which is ca. 25 kcal mol^{-1} stronger than the Ru—CH_3 bond, renders the transformation both exothermic and exoergic.

This ML_5 d^6 complex with a square-based pyramidal geometry could potentially have been a good candidate to promote C—H activation through 1,2-addition. There is no need to create a vacant site because the system is coordinatively unsaturated. Moreover, the d^6 configuration in this geometry prevents π-donation from N, so that the lone pair on nitrogen is fully available to abstract a proton. However, the product of the reaction is too unstable to lead to any C—H activation.

Evidence for the net addition of arene C—H bonds across a Ru(II)—OH bond was disclosed by Gunnoe, Cundari, and

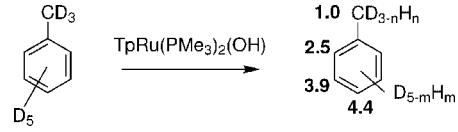

Figure 28. Selectivity in H/D exchange in toluene catalyzed by $TpRu(PMe_3)_2(OH)$.

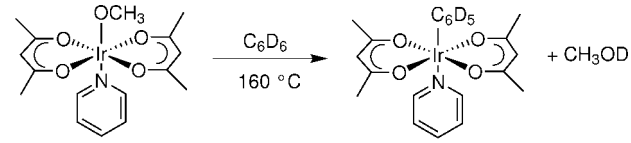

Figure 29. Reactivity of Ir−methoxo complex toward C−H bond.

co-workers.[189,190] Heating the complex $TpRu(PMe_3)_2(OH)$ in C_6D_6 at 80 °C results in H for D exchange at the hydroxide ligand to produce $TpRu(PMe_3)_2(OD)$. The complex $TpRu(PMe_3)_2(OH)$ catalyzes H/D exchange between H_2O and C_6D_6. Aliphatic C−H bonds are also activated as illustrated by the results of the reaction with deuterated toluene (Figure 28).[191] However, the exchange occurs selectively at the aromatic positions and, in particular, at the para and meta sites. B3LYP calculations on the model $(Tab)Ru(PH_3)_2(OH)$ (Tab = $HB(N{=}NH)_3^-$) showed that the reaction proceeds through initial loss of phosphine followed by benzene π-coordination. From this precursor, the C−H activation step is a 1,2-addition across the Ru−O bond to yield a phenyl−water complex ($\Delta G^{\ddagger} = 17.6$ kcal mol^{-1} and $\Delta G = -13.3$ kcal mol^{-1}). However, due to the endoergic character of benzene coordination ($\Delta G = 14$ kcal mol^{-1}), the overall transformation $(Tab)Ru(PH_3)_2(OH) + C_6H_6 \rightarrow (Tab)Ru(PH_3)(H_2O)(Ph) + PH_3$ is also endoergic ($\Delta G = 18.4$ kcal mol^{-1}) and would not lead to any observable Ru(Ph) derivative. However, H for D exchange is still possible as observed experimentally. Interestingly, the phenyl complex $(Tab)Ru(PH_3)_2(Ph)$ also lies at higher energy ($\Delta G = 9.1$ kcal mol^{-1}), thus avoiding any deactivation pathway in the catalytic H/D exchange process.

The H for D exchange is also observed with the anilido complex $TpRu(PMe_3)_2(NHPh)$, whereas for the methyl complex $TpRu(PMe_3)_2(Me)$, H for D exchange is preferentially observed at the Tp 4-positions.[191] B3LYP calculations on $(Tab)Ru(PH_3)(Me)(\eta^2\text{-}C_6H_6)$ yielding $(Tab)Ru(PH_3)(\eta^2\text{-}CH_4)(Ph)$ gave $\Delta G^{\ddagger} = 21.2$ kcal mol^{-1} for the C−H cleavage step, while it is 17.6 kcal mol^{-1} with the hydroxide complex $(Tab)Ru(PH_3)(OH)(\eta^2\text{-}C_6H_6)$. This lower activation barrier is due to the basic properties of the OH ligand thus stabilizing the transfer of the hydrogen as a proton. In the case of the activation by the methyl group in $(Tab)Ru(PH_3)(Me)(\eta^2\text{-}C_6H_6)$, the activated C−H bond needs to be closer to the metal (Ru···C = 2.35 Å, Ru···H = 2.02 Å, OH; Ru···C = 2.23 Å, Ru···H = 1.72 Å, Me), and the C−H bond breaking occurs later on the PES (C···H = 1.39 Å, OH; C···H = 1.49 Å, Me).[191]

For $TpRu(PMe_3)_2X$ (X = amido, hydroxo), the 1,2-addition of a C−H bond across Ru−X potentially offers a way to achieve catalytic heterofunctionalization of alkanes or arenes. Gunnoe, Cundari, and co-workers have studied computationally the C−H activation of benzene by $[(Tab)M(PH_3)_2)X]^q$ (X = OH, NH_2; $q = -1$ to $+2$; M = Tc(I), Re(I), Ru(II), Co(III), Ir(III), Ni(IV), Pt(IV)).[192] The C−H activation process is best described as a metal-mediated proton transfer in which the metal center and the X ligand function as an activating electrophile and intramolecular base, respectively. The atoms in molecules (AIM) analysis of the TS for C−H cleavage yielded a picture in agreement with the above characteristics, as bond critical points were only found along the wedges of the kite-shaped four-membered ring.

Three criteria have been considered to quantify the efficacy of (Tab)M complexes toward C−H activation and their potential use as catalysts: (1) generation of the active species (dissociation of the phosphine ligand); (2) hydrogen transfer barrier; (3) thermoneutrality of the hydrogen transfer. A good catalyst is likely to be associated with easy generation of the active species and facile H-transfer, while not generating a too-stable (or too-unstable) product for subsequent functionalization to occur. The complex $(Tab)Co(PH_3)_2(OH)^+$ is thus predicted to be the most promising for further catalyst investigation with phosphine dissociation associated with $\Delta G = 8$ kcal mol^{-1} and C−H cleavage with $\Delta G^{\ddagger} = 21.2$ kcal mol^{-1} and $\Delta G = 2$ kcal mol^{-1}.

Concomitantly with the studies carried out by Gunnoe and Cundari, Periana and Goddard developed the C−H activation chemistry with an iridium−methoxy complex (Figure 29).[193] The pyridine methoxy complex catalyzes the H for D exchange between mixtures of C_6H_6 and D_2O at 160 °C. All experimental evidence (kinetic studies, KIE evaluation) points to the rate-determining step being benzene coordination followed by fast C−H cleavage. B3LYP calculations on the hydroxo−pyridine complex confirmed the experimental observations.[194] Generation of the active species with the hydroxo *cis* to the vacant site is achieved in two steps: dissociation of pyridine ($\Delta G = 32.8$ kcal mol^{-1}) and isomerization of the chelating ligands ($\Delta G^{\ddagger} = 10.1$ kcal mol^{-1}) amounting in total to an activation barrier of 42.9 kcal mol^{-1}. The activation barrier for C−H cleavage is $\Delta G^{\ddagger} = 7.7$ kcal mol^{-1} and the associated TS is 5 kcal mol^{-1} lower than that for the ligand isomerization. The overall transformation from the hydroxo−pyridine iridium complex to the phenyl−pyridine product is exoergic by -6.8 kcal mol^{-1}, which stands in marked contrast with the Ru complex studied by Gunnoe and Cundari, where a similar transformation is computed to be endoergic by 9.1 kcal mol^{-1}.

Oxgaard et al. have further analyzed the 1,2-addition across the Ir−OMe bond by computing the localized orbital using the Pipek−Mezey methodology.[195] They showed that one lone pair on oxygen forms the O−H bond, while the orbital on O involved in Ir−O bonding is converted into the lone pair on HOMe used to coordinate to Ir. The electrophilic metal activates the C−H bond by generating a positively charged hydrogen, which is subsequently abstracted by a basic site on a vicinal ligand (OMe here). Such a transformation was shown by the authors to be different from classical σ-bond metathesis, and they have coined the name internal electrophilic substitution (IES).

2.4. Beyond Classical Descriptions

C−H activation processes are generally divided in two extreme mechanisms: oxidative addition and σ-bond metathesis. As illustrated in section 2.1, oxidative addition consists of two steps: coordination of the σ(C−H) bond after generation of a vacant site and actual cleavage of the C−H bond (Figure 1). This transformation is most commonly observed for low-valent electron-rich metals with d^8 configuration that allow easy access to an oxidized d^6 configuration accommodating two extra ligands.

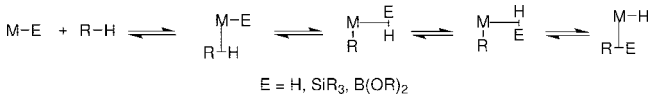

Figure 30. Various intermediates involved along a σ-CAM process.

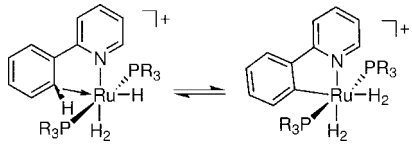

Figure 31. C—H activation as a σ-CAM process between agostic-hydride and bis-dihydrogen ruthenium complexes.

When no d electrons are available on the metal, an oxidative transformation is not possible and the C—H activation proceeds through a σ-bond metathesis pathway as described in section 2.2 (Figure 1). Essential to such a transformation are the absence of an intermediate and the concerted R—H/M—R′ bond-breaking and R′—H/M—R bond-making processes.

For transition metal fragments with d^4 to d^8 configurations, a σ-bond metathesis transformation is in principle possible, with the additional potential formation of a stable σ-adduct before and after the actual metathesis (Figure 30). Perutz and Sabo-Etienne have coined the term σ-CAM for such a transformation where metathesis is assisted by formation of stable σ-complexes (CAM = complex assisted metathesis).[196] It is usually a multistep process, and one important aspect of the σ-CAM mechanism is that the oxidation state of the metal center remains constant throughout all the steps. This allows design of catalytic cycles at constant oxidation state, as shown by Perutz and Sabo-Etienne for H for D exchange, hydrogenation, and borylation of alkanes.[196] In particular, rotation of the σ-bond in the σ-complexes (a situation not possible with classical σ-bond metathesis) opens isomerization pathways leading eventually to functionalization (Figure 30).

One early example of a σ-CAM transformation characterized computationally is the C—H activation in a phenyl—pyridine (ph-py) ruthenium hydride (Figure 31).[197] B3PW91 calculations on $Ru(PH_3)_2(H)(H_2)(ph\text{-}py)^+$ located the agostic complex featuring coordination of the phenyl *ortho*-C—H bond, the bis-dihydrogen product, which is less stable by 6.8 kcal mol^{-1}, and the TS for C—H activation ($\Delta E^{\ddagger}$ = 25.0 kcal mol^{-1}). Based on the geometrical parameters, the TS was classified as a Ru(IV) species. The complexes involved in the transformation always comprise two coordinated σ-bonds (C—H and H—H bonds in the reactant and two H—H bonds in the product). Reorganization among these σ-complexes through metathesis allows the system to adapt to the stereoelectronic requirements of the ligands (*trans* influence): hydride *trans* to σ(C—H) in the reactant and H_2 *trans* to aryl in the product.

The ruthenium complex $TpRu(PPh_3)(CH_3CN)H$ catalyzes the H for D exchange between CH_4 and deuterated organic solvents (benzene, THF, Et_2O).[198] The reaction mechanism was studied computationally by Lin et al. at the B3LYP level with the model $TpRu(PH_3)(CH_3CN)H$ reacting with C_6H_6, CH_4, and CH_3CH_2OEt.[198] H for D exchanges between CH_4 and C_6H_6 and between CH_4 and Et_2O were considered as indicated in the catalytic cycle shown in Figure 32.

The transformations **7** → **8**, **8** → **9**, **10** → **11**, and **11** → **12** are σ-CAM processes, and rotation of the HD ligand affords H for D exchange between R—D and CH_4. The

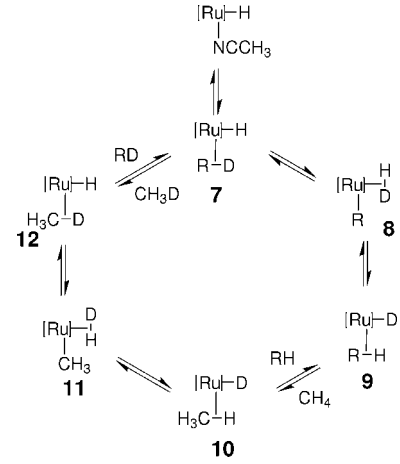

Figure 32. Catalytic cycle for H for D exchange in the reaction of R—D and CH_4 with [Ru](H)(CH_3CN) ([Ru] = $TpRu(PH_3)$; R = C_6H_5, CH_3, CH_2CH_2OEt).

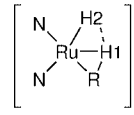

	R = Ph	R = CH_2CH_2OEt	R = Me
R...H1	1.641	1.622	1.609
H1...H2	1.525	1.582	1.585
Ru...R	2.157	2.224	2.228
Ru...H1	1.578	1.580	1.573
Ru...H2	1.614	1.609	1.614

Figure 33. Selected bond distances (Å) for the TS of C—H activation in the reaction of R—H with $TpRu(PH_3)(H)$. Only the atoms in the equatorial plane are shown.

rotation of H_2 in $TpRu(PH_3)(R)(\eta^2\text{-}H_2)$ is computed to be very easy ($\Delta G^{\ddagger}$ = 1.9 kcal mol^{-1}, R = Ph; $\Delta G^{\ddagger}$ = 3.8 kcal mol^{-1}, R = CH_2CH_2OEt; $\Delta G^{\ddagger}$ = 2.3 kcal mol^{-1}, R = CH_3). From the σ-complexes, the activation barriers for C—H activation are computed to be between 7 and 12.4 kcal mol^{-1} ($\Delta G^{\ddagger}$ = 7.0 kcal mol^{-1}, Ph; $\Delta G^{\ddagger}$ = 11.9 kcal mol^{-1}, CH_2CH_2OEt; $\Delta G^{\ddagger}$ = 12.4 kcal mol^{-1}, Me), and the Ru(R)(η^2-H_2) product is always less stable than the Ru(η^2-RH)(H) reactant (ΔG = 0.8 kcal mol^{-1}, Ph; ΔG = 5.8 kcal mol^{-1}, CH_2CH_2OEt; ΔG = 7.2 kcal mol^{-1}, Me). The most intriguing aspect of this transformation is the geometry of the TS for H-transfer between R and H, featuring a pentagonal—bipyramidal geometry with the transferring hydrogen within bonding distance to Ru (Figure 33). The geometry of the transition state is in agreement with a description of the latter as a Ru(IV) complex, hence the name oxidatively added transition state (OATS) proposed by the authors to describe the transformation.

The close contact between the transferring hydrogen and the metal makes this reaction very similar to a two-step oxidative addition/reductive elimination where the oxidized species would be an intermediate. Lin et al. have studied computationally the competition between the two pathways for $Tp(PH_3)M(R)$ reacting with methane (R = H and CH_3; M = Fe, Ru, Os).[199] When R = H, the oxidized species $Tp(PH_3)M(H)_2(CH_3)$ is a TS for H migration for M = Fe or Ru, while it is an intermediate for M = Os. The situation is almost identical for R = CH_3 with $Tp(PH_3)Fe(H)(CH_3)_2$ as a TS for H-transfer and $Tp(PH_3)Os(H)(CH_3)_2$ as an intermediate. The only difference is observed for M = Ru where a very shallow minimum is found for $Tp(PH_3)Ru(H)(CH_3)_2$, but the intermediate lies at an energy close to that of the TS for C—H oxidative addition. This shows that the one-step and two-step mechanisms are not mutually exclusive. Any factor stabilizing the higher oxidation state may turn a one-step into a two-step process. This is the case when going down the Fe group. Ancillary ligands may also play a role

(R = H vs R = CH_3 for M = Ru). For instance, changing Tp for Cp and computing the H-transfer for $CpRu(PH_3)R$ (R = H or CH_3) shows that the C—H activation is a two-step process with a Ru(IV) intermediate.

In the context of hydroarylation catalysis (see section 4.2 for further details and references), Oxgaard et al. have studied the C—H activation of benzene by *cis*-$(acac)_2Ir(CH_2CH_2Ph)$ and $TpRu(CO)(CH_2CH_2Ph)$.[200,201] These complexes result from the ethylene insertion into the M—Ph bond. The H-transfer from benzene to M—CH_2CH_2Ph constitutes the last step of the catalytic cycle, regenerating the active species (see section 4.2). In the case of the iridium complex, the activation barrier for the C—H cleavage from the π-coordinated benzene is computed to be $\Delta G^{\ddagger}$ = 12.9 kcal mol^{-1}, and the resulting σ(C—H) adduct of ethylbenzene is isoenergetic with the benzene complex (ΔG = −0.2 kcal mol^{-1}). Based on the geometry of the TS (Ir···C = 2.27 Å, Ir···Ph = 2.09 Å, Ir···H = 1.58 Å, C···H = 1.69 Å, Ph···H = 1.99 Å), the C—H activation is described as a one-step H-transfer with an Ir(V) transition state. The authors called this process oxidative hydrogen migration (OHM).[200] Transition states of similar nature had already been mentioned in the literature by Clot,[197] Lin and Eisenstein,[199] and Hall.[184]

The transition state for the hydrogen migration from benzene to CH_2CH_2Ph in $TpRu(CO)(CH_2CH_2Ph)(\eta^2\text{-}C_6H_6)$ ressembles that for *cis*-$(acac)_2Ir(CH_2CH_2Ph)$ described previously (Ru···C = 2.27 Å, Ru···Ph = 2.17 Å, Ru···H = 1.61 Å).[201] This TS is described as a Ru(IV) structure with an essentially fully formed Ru—H bond and partially formed Ru—C and Ru—Ph bonds as judged by the vibrational frequencies (Ru—H = 2110 cm^{-1}, Ru—C = 479 cm^{-1}, and Ru—Ph = 1033 cm^{-1}). Because oxidation to Ru(IV) is generally more difficult than oxidation to Ir(V), the energy barrier is computed to be larger for Ru ($\Delta H^{\ddagger}$ = 12.0 kcal mol^{-1}, Ir; $\Delta H^{\ddagger}$ = 18.0 kcal mol^{-1}, Ru).

Bercaw showed that σ-bond metathesis of para-substituted benzene is insensitive to the electron-withdrawing or electron-donating property of the para-substituent.[136] DeYonker et al. addressed the influence of para-substituent in the activation of C_6H_5X (X = Br, Cl, CN, F, H, NH_2, NO_2, OMe) by $TpRu(L)(CH_3)$ (L = PMe_3, CO).[202] The computed Ru···H distances at the TS for H-migration from the para position of C_6H_5X to CH_3 fall in the range 1.608−1.677 Å (L = CO) and 1.592−1.620 Å(L = PMe_3), thus classifying the TS as a Ru(IV) hydride. A linear Hammett correlation is calculated with a positive ρ value of 2.6 for L = CO and 3.2 for L = PMe_3. Electron-withdrawing para-substituents lower the energy of the transition state. An opposite effect on the energy would have been obtained had the reaction been an electrophilic aromatic substitution. The picture evolving from the present study is that coordination of the substrate to TpRu(L)R promotes C—H bond activation by intramolecular proton transfer.

The correlation between the acidity of the C—H bond to be broken and the energy barrier for C—H cleavage was probed by B3LYP calculations on $TpRu(PMe_3)(CH_3)$ reacting with various substrates ($MeNO_2$, acetone, CH_3CN, C_6H_{12}, THF).[203] The values for the C—H cleavage step (after C—H coordination to Ru) indicate that the more acidic C—H bonds of $MeNO_2$, CH_3CN, and acetone are associated with lower $\Delta H^{\ddagger}$ values (7.2, 9.8, and 14.8 kcal mol^{-1}, respectively) than the less acidic C—H bonds of cyclohexane and THF (21.5 and 17.2 kcal mol^{-1}).

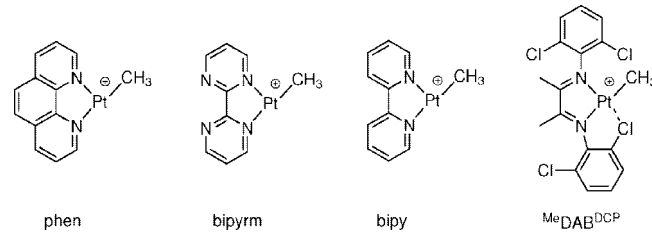

Figure 34. Ligands L considered in the reaction of $(L)Pt(CH_3)^+$ with benzene.

Thermal C—H activation of benzene with cationic platinum−methyl complexes was studied in the gas phase by Schwarz et al. (Figure 34).[204] The exchange process $(L)Pt(CH_3)^+ + C_6H_6 \rightarrow (L)Pt(C_6H_5)^+ + CH_4$ with the ligands L shown in Figure 34 was effective only for L = phen, bipyrm, and bipy, because with L = $^{Me}DAB^{DCP}$ chlorine blocks the coordination site for benzene. For the cases where methane was produced, labeling experiments showed that the C—H activation of benzene prior to methane elimination is reversible. DFT calculations were carried out for the reaction of $(bipy)Pt(CH_3)^+$ with C_6H_6, and two different pathways were tested. Oxidative addition of benzene would lead to a ML_5 $(bipy)Pt(CH_3)(C_6H_5)(H)^+$ intermediate, which would achieve the exchange upon C—H reductive elimination of H and CH_3. Another possibility is to achieve the exchange in one step from the coordinated benzene complex through a σ-CAM process. With the B3LYP functional, the transition states forming the methane adduct along both pathways are computed at a higher energy than the separated product $(bipy)Pt(C_6H_5)^+ + CH_4$. This is not in agreement with the experimental results where reversible C—H activation for benzene was observed. Computation of the two pathways with the mPW1K functional correctly positioned the two TSs below the exit channel. Moreover, the σ-CAM mechanism is favored over the oxidative addition/reductive elimination by 4.1 kcal mol^{-1}. Other functionals were tested and mPW1PW91 and M05-2X yielded correct energies in agreement with the H for D exchange studies. The situation was, however, less clear-cut for the preferred pathway. mPW1PW91 favors σ-CAM, and the two pathways are comparable with M05-2X.

A recent experimental and computational study by Bercaw et al. probed the competition between C—H bond activation of benzene and olefin insertion in a (monomethyl)palladium β-diketiminate complex.[205] The σ-CAM transition state was computed (B3LYP) to be 9.6 kcal mol^{-1} lower than the TS for C—H oxidative addition of benzene.

The differentiation between the various pathways for C—H activation is often made by inspection of the geometry of the transition state. A short M···H contact between the metal and the migrating hydrogen is taken as an indication of M···H bonding interaction. Hall et al. have recently proposed to use AIM analysis[206] to characterize the bonding paths within the TS for C—H activation.[207,208] Seven different molecular graphs were considered for the various possible degrees of connectivity in a four-membered ring geometry (Figure 35).[208] Graph **13** is typical of a σ-bond metathesis TS where the transferring hydrogen presents bond critical points with the two ligands between which it is exchanged. The latter are still connected to the metal and the four-centered TS features a ring critical point. For the TS of the reaction of CH_4 with Cp_2ScCH_3, which is the prototypal σ-bond metathesis reaction, graph **13** is obtained. Graph **19** is typical of the intermediate obtained in the reaction between

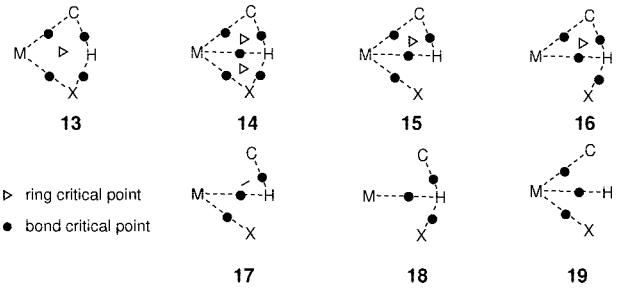

Figure 35. Various molecular graphs obtained with AIM analysis of some C—H activation transition states or intermediates.

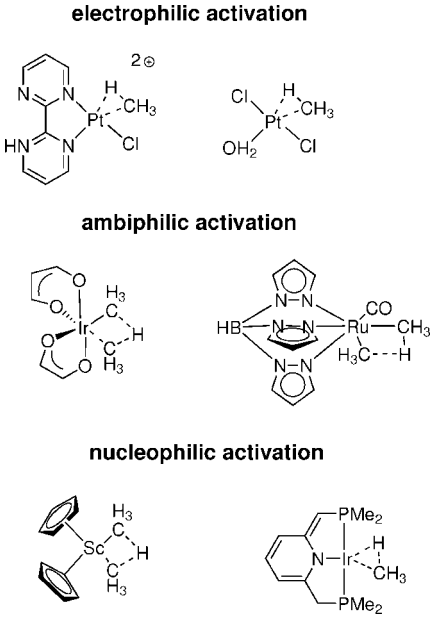

Figure 36. The three classes of regime for C—H activation as deduced from ALMO-EDA analysis of the TS.

$CpIr(PH_3)(CH_3)^+$ and CH_4. This oxidative addition intermediate presents the bond critical points between the metal and each of the three ligands. No interaction between the ligands is observed in the AIM analysis. Interestingly, whereas initially the names of the various mechanisms were proposed essentially because a close contact was obtained between M and H, Hall et al. made a connection between specific graphs and mechanisms.[207] Thus graph **14** was attributed to metal-assisted σ-bond metathesis (MAσBM) as proposed by Hall,[184,209] graph **15** was attributed to OATS or σ-CAM, graph **17** was described as a TS for oxidative addition, while finally graph **19** corresponds either to an OHM TS or to an oxidative addition intermediate. Graphs **16** and **18** were not given any specific names.

Very recently, Ess et al. have performed B3LYP calculations of the transition states for various C—H activation processes (Figure 36).[210] They have used Head-Gordon absolutely localized molecular energy decomposition analysis (ALMO-EDA)[211] to partition interaction energies between the metal/ligand and CH_4 fragments in the TS geometries. Charge transfer contributions from the metal to CH_4 (E_{ct1}) and from CH_4 to the metal fragment (E_{ct2}) were evaluated. Depending on the relative magnitude of the two contributions, three different regimes of C—H activation are proposed: electrophilic ($E_{ct2} > E_{ct1}$), ambiphilic ($E_{ct1} \simeq E_{ct2}$), and nucleophilic ($E_{ct2} < E_{ct1}$). See Figure 36 for particular examples of systems for each category.

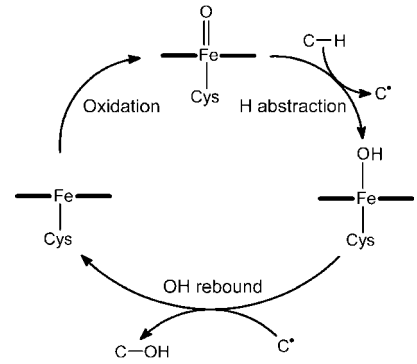

Figure 37. The rebound mechanism postulated for C—H oxidation by cytochrome P450.

2.5. Rebound Mechanism

The oxidation of hydrocarbon compounds by metal—oxo complexes[212–214] is one of the most relevant reactions in the field of C—H activation. In nature, several enzymes are capable of oxidizing hydrocarbons with very low reactivities under mild conditions in a catalytic fashion.[215] For instance, methane, the most inert alkane, is oxidized to methanol by methane monooxygenase.[216,217] In addition, more complex substrates are oxidized in a selective manner, as in the oxidation of camphor by cytochrome P450.[218]

The mechanism of this reaction, known as the oxygen rebound mechanism (Figure 37), was postulated by Groves.[34,219] This mechanism involves three steps: (1) oxidation of the catalyst to generate a high-valent metal-oxo intermediate, (2) H abstraction from the substrate by the oxo group, leading to a metal-hydroxo species and a carbon radical, and (3) OH rebound, in which the hydroxo ligand is transferred to the radical yielding the reaction product and recovering the catalyst. In most cases, the selectivity of the reaction is controlled by the relative stability of the carbon radicals. In saturated substrates, tertiary positions are preferentially oxidized over secondary positions. In unsaturated substrates, vinylic and benzylic positions are preferentially oxidized over saturated positions. Nevertheless, these simple rules can fail in enzymatic systems in which the protein environment surrounding the active site orientates the substrate, promoting the reaction in an unexpected less reactive position. This approach has recently been implemented with success in synthetic manganese catalysts, which promote selective C—H oxidation by molecular recognition.[220]

Since the rebound mechanism was proposed for cytochrome P450 more than 25 years ago, considerable details on the nature of each reaction step and active species have been unveiled by experimental studies.[221–223] This knowledge has been complemented by theoretical studies,[224,225] in some cases carried out in collaboration with experimental groups. The simple picture of Figure 37 is now known to be much more complex, with parallel reaction pathways that may involve different active species in different spin states. It has also been argued that the carbon radical may be trapped by the metal before the OH rebound step. In addition, the radical nature of the reaction has been debated. Some studies suggested that the cleavage of the C—H bond may be heterolytic, thus involving hydride transfer and the formation of a carbocation intermediate. The theoretical studies on cytochrome P450 are reviewed by other authors of this special issue, and they are thus not mentioned here.[50,51] Nevertheless, the non-heme iron biomimetics of cytochrome P450[226,227] are reviewed here.

The unique feature of the rebound mechanism is that it does not involve a direct interaction between the metal and the substrate. The cleavage of the C—H bond is promoted by an oxygen center bound to the metal. Therefore, the metal plays an indirect role by activating the oxygen ligand that oxidizes the substrate. In most cases, the metal induces radical electrophilic character in the oxygen reactive center, which promotes a nucleophilic attack of the C—H bond. On the other hand, if the carbon radical generated by H abstraction binds to the metal, the reaction can be formally regarded as a 1,2-addition.

The oxygen rebound mechanism is nowadays accepted not only for cytochrome P450 but for many other enzymes, like methane monooxygenase[216,217] and lipoxygenase.[228–230] In addition, the rebound mechanism has been also postulated for inorganic reagents like permanganate and the Fenton's reagent,[231] as well as for many biomimetic systems. Due to this diversity, it is now accepted that the nature of the oxidant intermediate is not limited only to metal-oxo species but can also be metal-hydroxo, metal-peroxo, metal-hydroperoxo, bimetallic μ-oxo, and metal-alkoxo species.

Theoretical chemists reacted to this diversification by extending their investigations beyond cytochrome P450 to other chemical systems of high interest. The theoretical study of these systems is challenging due to several issues. The proper description of the reactivity of the metal core of the catalyst may require the consideration of several electronic states of different spin. In some cases, these states have strong multireference character, which makes the application of the most commonly used computational methods, like DFT,[232] challenging. In addition, some catalysts contain two or more high-spin metal atoms, which are magnetically coupled. In the enzymatic systems, a proper modeling of the reactive center is crucial, and in some cases, QM/MM methods[233] must be used to include the influence of the protein environment. Despite these difficulties, computational studies have been successfully used to clarify some key points, like the electronic nature of the active species, the effect of the axial ligand trans to the reactive group, the influence of the pH on the reactivity, the thermodynamic and kinetic parameters of the elementary steps, the influence of the environment, and the kinetic isotope and tunneling effects.

3. Chemically Induced Selectivity

3.1. Thermodynamic Properties: Bond Energy Enthalpies Determination

Bond enthalpies are very important quantities to know because they provide key information on the thermodynamic feasibility of a reaction. Reaction enthalpies can be estimated as a sum of bond enthalpy contributions from bonds that are formed and broken. This information is particularly vital for organometallic catalysis where organic molecules are manipulated by transition metal fragments and bonds are cleaved and formed between the metal fragment and organic groups. As mentioned by Landis,[234] Shilov's groundbreaking work in the activation of hydrocarbons was motivated by the assumption that metal−carbon and metal−hydrogen bond enthalpies are reasonably similar.[235] It is also important to acknowledge that rational design of hydroamination catalysts resulted from the knowledge of the relative M—N and M—C bond enthalpies.[236]

In contrast to the large body of information accumulated for organic molecules, experimental studies of transition metal complexes are rare. Furthermore, bonding is often well localized between two atoms in main group chemistry, and thus bond enthalpies are moderately sensitive to substituents; "typical values" can thus be extracted. The situation is quite different for transition metal complexes. Determination of the absolute values of ligand−metal bond enthalpies in polyatomic transition metal complexes is exceptionally difficult and can be achieved only when demanding criteria are met.[237–239] In addition, the influence of ancillary ligands on metal−ligand bond enthalpies is unclear but often important, so that the transferability of bond enthalpies between species is questionable. An approach that has been very useful is the determination of relative bond enthalpies in place of absolute values. This gives often the desired information since many reactions consist of interchanges of ligands. Even in this case, assumptions are needed. For instance, if entropic factors and solvent effects are assumed to be constant, bond enthalpies for M—X bonds may be estimated relative to a standard. Bryndza and co-workers were probably the first to notice that a series of relative M—X bond enthalpies correlates with H—X bond enthalpies.[240] Their studies included a large variety of X groups, which were bonded to the metal via C, O, or N, and M was either an early transition metal like Sc and Th or a late transition metal like Ru, Ir, and Pt.

This very useful discovery was followed by several studies where the same type of correlation was examined focusing on either a given metal fragment or a limited choice of X groups. Two studies focused on hydrocarbyl groups. Through elaborate procedures employing kinetic and equilibrium studies, it was possible to obtain a bond energy correlation where the experimental values of the M—C bond enthalpies relative to a reference value were plotted against the H—C experimental bond dissociation enthalpies. These studies were carried out for the case of the Rh—C bond of $Rh(H)(R)(Tp^*)(CNCH_2CMe_3)$ (R = hydrocarbyl, and Tp* = HB(3,5-dimethylpyrazolyl)$_3$) by Jones and co-workers[241,242] and for the Ti—C bond of $Ti(R)(silox)_2(NHSi^tBu_3)$ (silox = OSi^tBu_3, R = various alkyl or aryl groups) by Wolczanski and co-workers.[173,243] Another experimental study concerned the correlations between Ni—N and Ni—O bond enthalpies and the corresponding H—N and H—O bonds.[244,245] Experimental correlations were also determined for cyclopentadienyl complexes of Zr and Hf with a wide variety of ligands including hydride, hydrocarbyl, alkoxide, amide, and halide.[246] The scarce experimental information available was complemented by several computational studies. Here again, the contrast between organic and organometallic chemistry is impressive. Computational study of bond dissociation enthalpies in main group molecules is a well-documented field. The size and nature of the organic molecules that have been considered have permitted the use of highly elaborate methods, and accurate bond enthalpies values have been obtained.[247–252] The size and nature of transition metal complexes made the accurate calculation of M—X bond enthalpy more difficult. *Ab initio* calculations were used notably by Goddard, Siegbahn, and Bauschlicher to calculate M—H and M—R bond energies in naked systems, that is, with no other ligand than H or R. DFT methods were required for larger complexes containing ligands, and some of the shortcomings of these methods have been discussed.[250,253,254] However these methods were used with success for the study of relative bond energies in a large variety of complexes.

The relative M—H and M—CH_3 bond energies for a variety of naked and CO-coordinated metal complexes, $M(CO)_5R$ (M = Mn, Tc, Re) and $M(CO)_4R$ (M = Co, Rh, Ir), were studied, and periodical trends were discussed.[255] Further studies included other carbon-based ligands[256] and cyclopentadienyl complexes.[257] It was, for instance, established that the M—CH_3 bond is considerably weaker than the M—H bond for late to middle transition metal as a result of repulsive interaction between occupied orbitals on the methyl and metal fragments.

Isomeric alkyl complexes of early and late transition metals were studied by Harvey.[258] The alkyl R groups cover a large range from primary to tertiary groups. It was shown that primary alkyl complexes are usually more stable than secondary or tertiary ones due to electronic effects. The metal−carbon bond is often substantially ionic in nature with a large negative charge on the alkyl group and the stability of carbanions decreases from primary to tertiary groups. For related reasons, electron-withdrawing substituents at the β-position increase the stability of the complexes. The steric effects, which are often invoked, are shown to play only a minor role.

A systematic study of metal−ligand bond enthalpies for saturated transition metal complexes that encompasses the entire d-block of the periodic table with a wide assortment of ligands has been carried out.[234] To minimize the steric effects, all ancillary ligands were set as hydrides, so the calculations of the M—L bond enthalpy by DFT and also wave-based methods such as CCSD(T) have been carried out on H_nM—R (R = H, non-hydrocarbyl, substituted hydrocarbyl, etc). This study shows that large variations in metal−ligand bond enthalpies across a row undermine the utility of intrinsic bond enthalpies. However M—H and M—CH_3 bond enthalpies increase down a period in accord with experimental values. The relation between relative H_nM—R bond enthalpies and the corresponding H—R bond enthalpy was considered for individual metals. The best fit is obtained when R is restricted to a family of groups such as hydrocarbyl. The slope of the correlation line between calculated H—C and M—C bond enthalpies, $\mathscr{R}^{M-C/H-C}$, computed for individual metals, varies between 1.2 and 1.9 over the periodic table with larger values obtained for early metals. The large values for early metals coincide with metal−carbon polarization. It is, however, not possible to describe the large variation in the metal−carbon enthalpies by Pauling's formula.

A study of the $\mathscr{R}^{M-C/H-C}$ bond energy correlations was carried out using computational models that represent closely experimental systems for which the correlation was experimentally studied.[259] The correlations $\mathscr{R}^{M-C/H-C}$ of the bond enthalpies, established for Rh and Ti complexes by Jones and Wolczanski, respectively, were reproduced with high accuracy. With DFT(B3PW91) calculations, Rh(H)(R)-(Tp)(CNMe) to model Rh(H)(R)(Tp*)($CNCH_2CMe_3$), and including all R groups that have been used in the experimental studies, a correlation was obtained for which the slope of the linear fit is 1.23, which agrees very well with the experimental value of 1.22. A similar study was carried out for the titanium complexes family studied experimentally by Wolczanski. In this case, the full experimental system, $Ti(R)(silox)_2(NHSi^tBu_3)$, was included in the model. The calculated $\mathscr{R}^{M-C/H-C}$ ratio of 1.08 agrees very well with the experimental value of 1.12. It was concluded that while absolute bond enthalpies are reproduced within 5% for H—C bonds, the very limited data for absolute M—C bond enthalpies do not allow an accurate comparison between experiment and theory. In contrast, computational evaluation of H—C and M—C relative bond enthalpies allows the prediction of trends and changes in relative bond enthalpy with substituents.

The same sets of molecules were calculated with the BP86 method and analyzed with the energy decomposition method (EDA) to determine the steric contribution to the bond energy.[260] The results are similar to those presented by Clot.[259] The slope is slightly different (1.10 and 0.96 for Rh and Ti, respectively) and slightly away from the experimental values. The steric effects are found to be important within the set Me, Et, Pe, ^{i}Pr and ^{t}Bu.

The experimental observation that M—C bond energies increase more rapidly with changes in the substituents than H—C bond energies has considerable consequences on the selectivity of the activation of the H—C bond. Wick and Jones summed it up as follows: "The ground state energy differences between alkyl and aryl hydride complexes of rhodium dominate the reactivity. The difference in M—C bond strengths is larger than the corresponding difference in C—H bond strengths giving rise to a strong thermodynamic preference for cleaving strong C—H bonds."[242] The experimental measurements of Jones and Wolczanski show that the M—C bond strength increases about 10−20% faster than the H—C bond one. Computations were thus used to determine whether higher increases in the M—C bond energy could be obtained.[261,262] The fluoroarenes H—$C_6F_nH_{5-n}$ (n = 0−5) were selected because fluorine has a strong influence on the nearby H—C bond energies. For instance, computations show that in C_6H_5F, the weakest C—H bond is at the meta position, the para C—H bond is 0.9 kcal mol^{-1} stronger, and the ortho C—H is 2.5 kcal mol^{-1} stronger. Similarly, the C—H bond dissociation energy of C_6F_5H, 114.1 kcal mol^{-1}, is 4.1 kcal mol^{-1} higher than that of benzene. The selected systems for the DFT(B3PW91) studies are shown in Figure 38. They are models for complexes that are known to be able to activate C—H bonds or able to form aryl complexes. They include metals having formal electron counts varying from d^0 to d^8, and they also represent a wide variety of coordination spheres including M(η^5-$C_5H_5)_2$(H)(Ar_F), M(η^5-$C_5H_5)_2$(H)$_2$(Ar_F), M(η^5-C_5H_5)(H)(Ar_F)L_2, M(η^5-C_5H_5)(H)(Ar_F)L and M(H)(Ar_F)L_2.

Figure 39 gives the results for RhCp(PH_3)(H)(Ar_F). The variations in the M—C bond dissociation energies relative to that of M—phenyl (ΔD(Rh—C)$_{rel}$) are plotted versus the corresponding C—H bond dissociation energies for the fluorinated benzenes (ΔD(H—C)$_{rel}$). A linear correlation appears with a slope $\mathscr{R}^{M-C/H-C}$ of 2.43 ± 0.11 (r^2 = 0.981). Remarkably, the role of the fluorine substituent strongly depends on its position on the benzene ring, since the 20 values form themselves into three subsets corresponding to zero ortho F (the lowest values for ΔD(Rh—C)$_{rel}$), to one ortho F, and two ortho F substituents (the highest values for ΔD(Rh—C)$_{rel}$).

A very similar pattern was obtained for all metal fragments shown in Figure 38 with $\mathscr{R}^{M-C/H-C}$ varying between 1.9 and 3 (Figure 40). As already noted by Landis, the values of $\mathscr{R}^{M-C/H-C}$ do not appear to follow any clear pattern with the nature of the metal center. The highest values of $\mathscr{R}^{M-C/H-C}$ have been found for $ZrCp_2$(H)(Ar_F) and for Ni(dhpe)(H)(Ar_F). However, some pattern appears with the ligands: increasing the

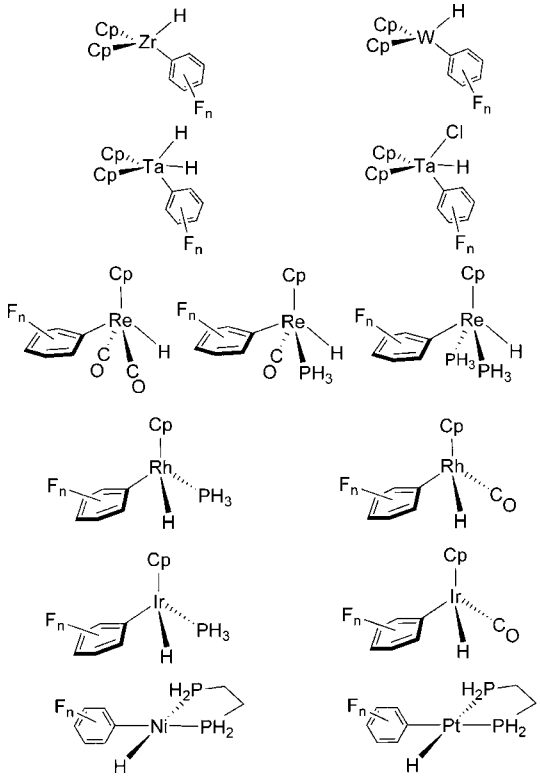

Figure 38. Metal−Ar_F ($n = 0, 5$) for which the correlation factor $\mathscr{R}^{M-C/H-C}$ was calculated.[262]

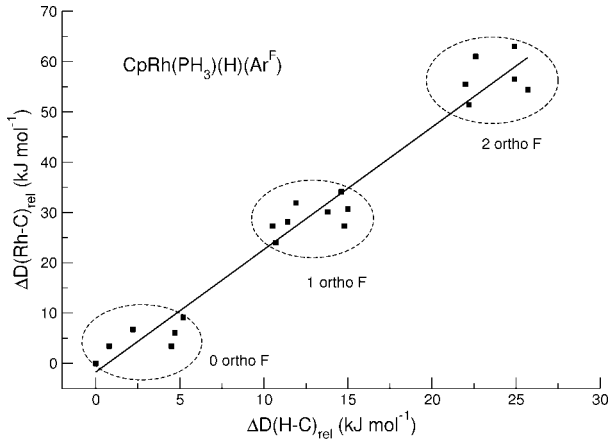

Figure 39. Correlation between the Rh−C bond dissociation energies of Rh(η^5-C_5H_5)(H)(Ar_F)(PH_3) and the H−C bond dissociation energies of fluorobenzenes. The zero corresponds to the values for H−Ph and Rh−Ph bond energies.

electron density at the metal by increasing the donating ability of one ligand (Cl vs H or CO vs PH_3) results in an increase of $\mathscr{R}^{M-C/H-C}$.

Interpreting the correlations has met difficulties similar to those mentioned by Landis. The best results were obtained by correlating $\Delta D(M-C)_{rel}$ with the total negative charge of the aryl ring, q_{aryl}, although q_{aryl} is more influenced by meta and para F than $\Delta D(M-C)_{rel}$. Thus, although the Pauling model for bonding provides a qualitative framework for interpreting the results, other factors play a role. The large influence of ortho fluorine was attributed to the delocalization of the σ lone pair of the phenyl anion into the adjacent empty σ^*(C−F) orbitals. The large value of $\mathscr{R}^{M-C/H-C}$ computed for fluoroarene was experimentally confirmed in the case of Tp*Rh(CNneopentyl)(Ar_F)H with

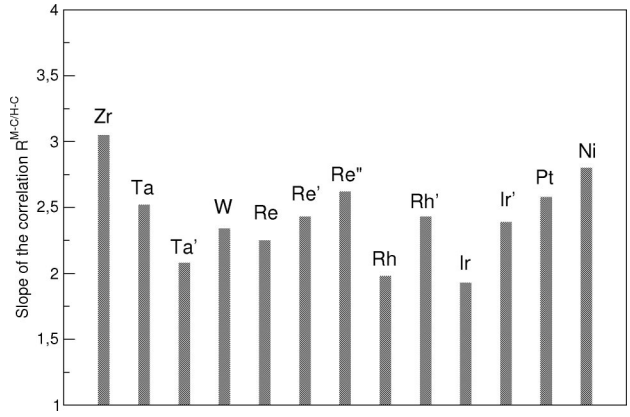

Figure 40. $\mathscr{R}^{M-C/H-C}$ for Zr = $ZrCp_2(H)(Ar_F)$, Ta = $TaCp_2(H)_2(Ar_F)$, Ta′ = $TaCp_2Cl(H)(Ar_F)$, W = $WCp_2(H)(Ar_F)$, Re = $ReCp(CO)_2(H)(Ar_F)$, Re′ = $ReCp(CO)(PH_3)(H)(Ar_F)$, Re″ = $ReCp(PH_3)_2(H)(Ar_F)$, Rh = $RhCp(CO)(H)(Ar_F)$, Rh′ = $RhCp(PH_3)(H)(Ar_F)$, Ir = $IrCp(CO)(H)(Ar_F)$, Ir′ = $IrCp(PH_3)(H)(Ar_F)$, Pt = Pt(dhpe)(H)(Ar_F), and Ni = Ni(dhpe)(H)(Ar_F).

a very good agreement between the experimental and calculated values for $\mathscr{R}^{M-C/H-C}$ of 2.14 and 2.0, respectively.[263]

The influence of F-substitution on the kinetics of reaction was studied in the case of the reaction of $CpRe(CO)_2$ with fluoarenes.[109] In this reaction, the rate-limiting step is the isomerization from the *cis* isomer, which is the product for the C−H activation, to the thermodynamic *trans* product. The energy barriers of this isomerization were found to correlate with the Re−C bond dissociation energies. Increasing the number of fluorines, notably at the ortho position, lowers the energy barriers. In this reaction, thermodynamic and kinetic aspects favor cleavage of the strongest C−H bond. The relation between kinetics and thermodynamics was also studied for the intramolecular C−X bond activation in $Ru(NHC)(PH_3)_2(CO)$, where NHC = 1-(C_6H_4-2X)imidazol-2-ylidene and X = H, CH_3, F, OH, NH_2, OCH_3, or CF_3.[264] The computed exothermicity of C(aryl)−X activation follows the trend X = NH_2 < CH_3 < H < OH ≃ OCH_3 < CF_3 < F, while the energy barriers vary as X = H < F < OH ≃ OCH_3 < CF_3 < NH_2 < CH_3. Both series reflect the promotion of C(aryl)−X activation by the formation of stronger bond in the product.

3.2. Chelation-Assisted C−H Activation

3.2.1. ortho-C−H Activation

Even though C−H bonds do not form very stable σ-adducts with transition metals, coordination of the bond that will break is a compulsory event prior to actual cleavage. Thermodynamics of the M−C bond formed favors aromatic C−H activation over an aliphatic C−H one, and in the latter the primary carbon reacts preferentially over the secondary and tertiary positions. However, within a substituted aromatic molecule, little selectivity is generally observed between the various C−H bonds and usually steric arguments are used to rationalize the results obtained. In the case of fluorinated aromatics, activation of the C−H bonds maximizing the number of ortho F atoms is strongly favored thermodynamically (see section 3.1).

One major breakthrough in the field of aromatic C−H functionalization has been achieved by Murai with olefin insertion into a C−H bond ortho to a carbonyl group in aromatic ketones (Figure 41).[16,18] The reaction is generally

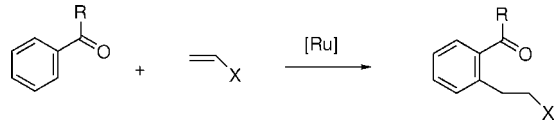

Figure 41. Ru-catalyzed olefin insertion into the ortho C—H bond of an aromatic ketone. [Ru] = $RuH_2(CO)(PPh_3)_3$.

performed in refluxing toluene with $RuH_2(CO)(PPh_3)_3$ as a catalyst precursor. The active species is thought to be a Ru(0) complex, $Ru(CO)(PPh_3)_3$ or $Ru(CO)(PPh_3)_2$, and the C—C coupling has been shown experimentally to be the rate-determining step.

B3LYP calculations have been performed by Morokuma on benzaldehyde and $Ru(CO)(PH_3)_2$ as models for the experimental system.[265] O-coordination to Ru of the aldehyde is preferred over π-coordination of the arene by 11.9 kcal mol^{-1}. This coordination of the orientating group yields an agostic complex, which opens easy access to the selective activation of the ortho C—H bond of benzaldehyde. A transition state associated with this coordination has been located with $\Delta E^{\ddagger} = 3.3$ kcal mol^{-1}. From the agostic intermediate, the C—H cleavage is very easy ($\Delta E^{\ddagger} = 2.8$ kcal mol^{-1}) and the product is 11.1 kcal mol^{-1} more stable than the agostic precursor. It is interesting to note that in the process of *ortho*-C—H activation with coordination of the carbonyl group, the most difficult step of the C—H activation is not C—H cleavage but the formation of the agostic. The crucial role played by the coordination of the orientating group is illustrated by the calculations of the *ortho*-C—H cleavage from the π—arene complex, without any participation of the carbonyl group. The energy barrier is computed to be $\Delta E^{\ddagger} = 20.1$ kcal mol^{-1}. C—H activation at the meta and para positions, for which no coordination of the remote carbonyl group is possible, are calculated to be easier ($\Delta E^{\ddagger} = 18.0$ kcal mol^{-1}, meta; $\Delta E^{\ddagger} = 17.8$ kcal mol^{-1}, para). For the C—H activation at the ortho position, there is an energy difference of 29.4 kcal mol^{-1} between the two transition states for C—H cleavage (with and without coordination), thus showing the essential role played by the orientating group in achieving selectivity.

Chaudret and Sabo-Etienne have shown that ethylene insertion into the *ortho*-C—H bond of acetophenone catalyzed by $Ru(H)_2(H_2)_2(PCy_3)_2$ is effected at room temperature (20 °C).[266] Products of *ortho*-C—H activation of acetophenone and phenyl-pyridine were isolated, but in the case of phenyl-pyridine, no ethylene insertion was observed (Figure 42). Protonation of the phenyl-pyridine orthometalated species yielded a σ(C—H) adduct, considered to be an intermediate in the Murai reaction.[197] B3PW91 calculations by Clot showed that the C—H activation from this σ(C—H) adduct to yield a bis-H_2 intermediate is best described as a σ-CAM process through a TS structure with a short Ru···H contact (see section 2.4).[197] The H_2 ligand *trans* to the Ru—C bond is labile and can be substituted by another L ligand, in particular the solvent used in the synthesis (THF). The influence of the nature of L on the energetics of the σ-CAM process has been tested computationally.[267] When no ligand is present *trans* to the forming Ru···C bond, there is nearly no energy barrier for the C—H cleavage ($\Delta E^{\ddagger} = 0.1$ kcal mol^{-1}). If the ligand *trans* to σ(C—H) is Me_2O, as a model for the experimental solvent THF, the energy barrier is still very low ($\Delta E^{\ddagger} = 1.5$ kcal mol^{-1}). Interestingly, when the *cis*-hydride, receiving the migrating H atom in the σ-CAM process, is positioned *trans* to the σ(C—H) bond and thus a vacant site is *cis* to the bond to cleave, the energy barrier increases to a high value of $\Delta E^{\ddagger} = 29.4$ kcal mol^{-1}. This can be attributed to the destabilization introduced by putting two strong σ-donor ligands in trans geometry (hydride and forming Ru—C), but it also shows that the C—H cleavage is eased by the *cis*-hydride.

ortho-C—H activation of aromatic ketones was also observed by Esteruelas.[268,269] Treatment of $OsH_6(P^iPr_3)_2$ with acetophenone and 2-fluoroacetophenone in toluene under reflux affords the osmium trihydride complexes resulting from *ortho*-C—H activation (Figure 43).[268] Similar *ortho*-C—H activation was obtained when the starting complex was a dehydrogenated phosphine stannyl complex (Figure 43).[269] In the latter, deuterium labeling experiments suggest that the *ortho*-C—H activation takes place from $OsH(SnPh_2Cl)(P^iPr_3)_2$. The reaction pathway for the formation of this intermediate has been evaluated by DFT calculations.[269] The studies by Chaudret and Esteruelas show that, contrary to the case studied by Murai, Ru(II) and Os(II) complexes can be active species in *ortho*-C—H activation. The results with 2-fluoroacetophenone indicate that the stabilization induced by coordination of the orientating group to selectively promote *ortho*-C—H activation is larger than the stabilization induced by activating a C—H bond ortho to a fluorine atom.

The *ortho*-fluorine effect (see section 3.1) has been explained in terms of increase of the ionic component of the M—C bond through inductive effect of the *ortho*-F atom. Milstein has extended this influence to other σ-attracting groups such as Cl, Br, and OMe. Selective *ortho*-C—H

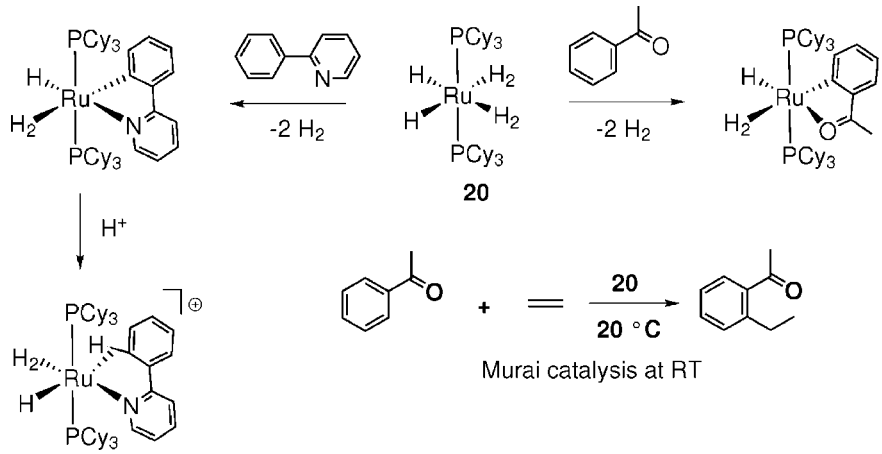

Figure 42. *ortho*-C—H activation reactivity observed between $Ru(H)_2(H_2)_2(PCy_3)_2$ and acetophenone or phenyl-pyridine.

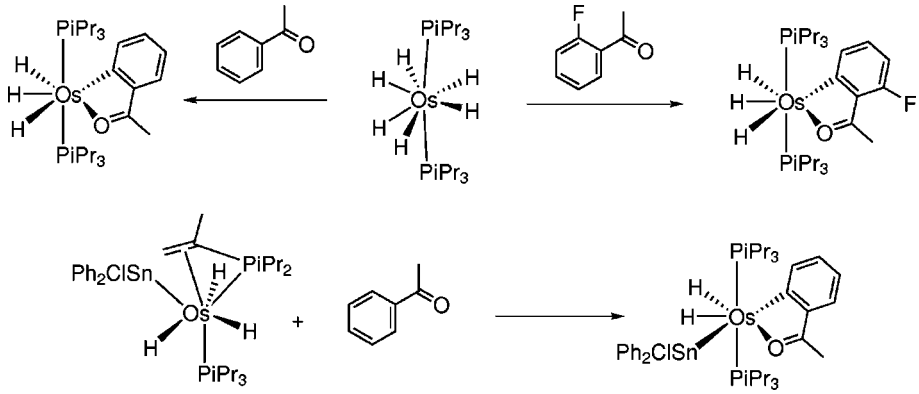

Figure 43. *ortho*-C—H activation promoted by osmium polyhydride complexes.

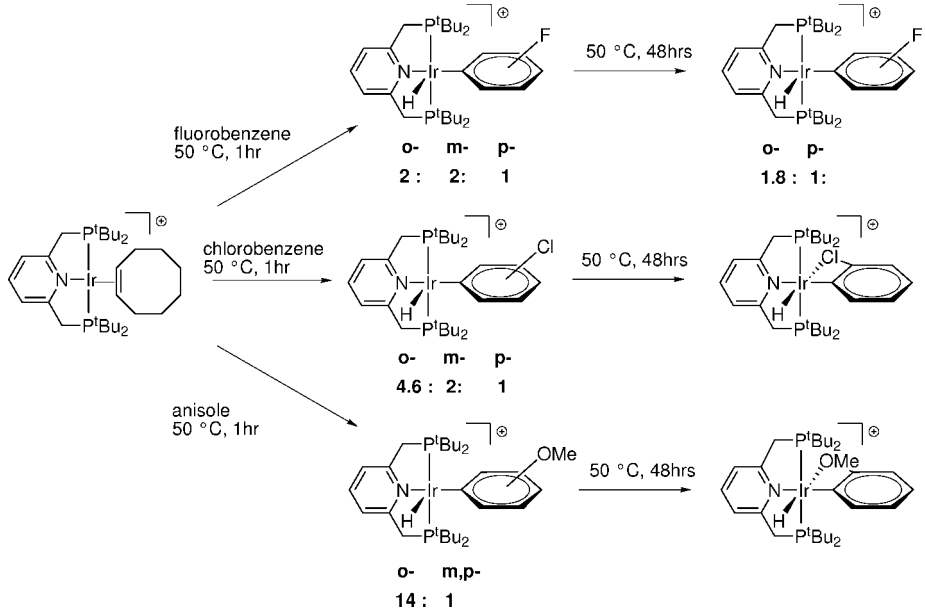

Figure 44. Selective *ortho*-C—H activation of haloarenes by an Ir(I) system.

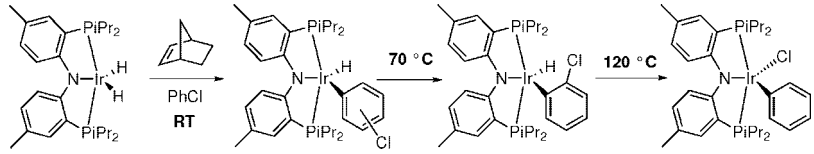

Figure 45. Kinetic C—H and thermodynamic C—Cl oxidative additions with Ir(I)—PNP pincer complex.

activation of haloarenes and anisole was observed with an Ir(I) complex (Figure 44).[270,271] The product is always a mixture of activation at the ortho, para, and meta positions, with *ortho*-C—H activation yielding the major kinetic product. Upon prolonged heating at 50 °C, the *ortho*-C—H activation species is recovered as the sole thermodynamic product (para activation is still observed with fluorobenzene). X-ray structures for the product of chlorobenzene and anisole *ortho*-C—H activation present short Ir···X distances (Ir···Cl = 2.816 Å, Ir···OMe = 2.76 Å). The observed selectivity is a result of coordination of the heteroatom to the metal center, which kinetically directs the metal to the *ortho*-C—H bond and stabilizes the resulting complex thermodynamically. DFT(mPW91) calculations were carried out on the model system $(PNP)Ir(coe)^+$ (PNP = 2,6-bis(dimethylphosphinomethyl)pyridine, coe = cyclooctene) and chlorobenzene or anisole.[271] The C—H activation is effected from the 14-electron intermediate, $(PNP)Ir^+$, whose formation upon coe dissociation is the rate-determining step for the entire process. Calculations have identified various η^2-(C=C) and η^2-(C—H) adducts of C_6H_5X (X = Cl, OMe) to the iridium center and the transition states interconverting these adducts. The preferred pathway consists of η^1-coordination of the heteroatom, followed by isomerization to the ortho η^2-(C—H) complex, thus leading to selective activation. After C—H cleavage, coordination of X in the remaining vacant site is shown to bring 6—10 kcal mol^{-1} extra stabilization, thus reinforcing the thermodynamic stability of the *ortho*-C—H activation product.

Differences in reactivity were observed by Ozerov with another PNP—iridium complex (Figure 45).[272] The reaction between the iridium dihydride and norbornene in C_6H_5Cl produced a mixture of four C—H oxidative addition products (two regioisomers for activation at the meta positions, one for activation at ortho and para) and a small fraction of the C—Cl oxidative addition product. Thermolysis at 70 °C did not change the amount of the C—Cl oxidative addition product but converted all the C—H activation products into the *ortho*-C—H activation isomer as proven by X-ray crystallography (Ir···Cl = 2.96 Å). Finally, thermolysis

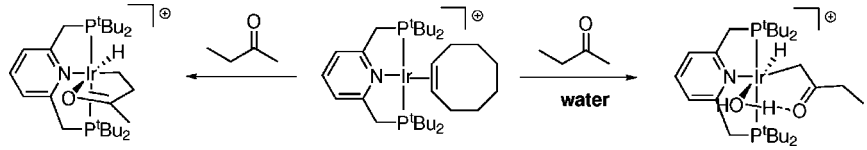

Figure 46. Competition between α- and β-(C—H) activation in the reaction of 2-butanone with Ir.

above 100 °C converted the C—H activation product into the C—Cl activation isomer, thus indicating that the latter is the thermodynamic product for this system. Similar behavior was observed with bromobenzene.

The competition between C—H and C—Cl activation in chlorobenzene by (PNP′)M (PNP′ = bis(*Z*-2-(dimethylphosphino)vinylamino); M = Ir, Rh) as a model for the experimental system was explored with B3LYP calculations by Wu and Hall.[273,274] In the present system, no Cl-coordination to Ir is involved to selectively activate the *ortho*-C—H bond. Five different products of C—H activation of chlorobenzene were located on the PES depending on the relative position of the hydride and the chlorine atom (two ortho, two meta, and one para isomers). The C—H cleavage is shown to proceed from a π—arene complex, and despite the lower stability of the π-adduct at the C(1)═C(2) position (with respect to π-adduct at other positions on the ring), the *ortho*-C—H activation product with Ir···Cl interaction is ca. 7 kcal mol^{-1} more stable than the four other C—H activation products. In the case of the (PNP)Ir$^+$ system studied by Milstein and Martin, the product of C—Cl activation was computed to be 9.5 kcal mol^{-1} less stable than the product of *ortho*-C—H activation.[271] In the (PNP′)Ir neutral system, the product of C—Cl activation is 22.5 kcal mol^{-1} more stable than the product of *ortho*-C—H activation. The TS for direct C—Cl oxidative addition from an η^1-Cl complex is 7.4 kcal mol^{-1} higher in energy than the TS for C—H oxidative addition of the *ortho*-C—H bond. The thermodynamic product (PNP′)IrCl(C_6H_5) is obtained from the *ortho*-C—H activation kinetic product through C—Cl oxidative addition forming a benzyne intermediate. The works of Ozerov and Hall indicate that coordination of the orientating group before the C—H cleavage step is not mandatory to obtain selective activation at the ortho position. However, the stability of the *ortho*-activated product is significantly enhanced by coordination of the orientating group after C—H cleavage. This has been shown experimentally by Goldman with the reaction of nitrobenzene with (PCP)IrH_2 (PCP = κ^3-C_6H_3−2,6-($CH_2P^tBu_2$)$_2$) in the presence of norbornene.[275] The experimental results are best explained if C—H activation is effected prior to O-coordination of the nitro group. Moreover, as the kinetic selectivity is quantitative for the meta and para C—H bonds, the *ortho*-C—H bond activation is kinetically hindered rather than assisted by proximity of the coordinating group.

The same authors studied the reaction of nitromethane with (PCP)Ir yielding the bidentate O,O-ligated nitromethanate complex (PCP)Ir(H)(κ^2-O,O-NO_2CH_2).[276] PBE calculations by Krogh-Jespersen showed that C—H activation is assisted by chelation of one oxygen atom and yields (PCP)Ir(H)(κ^2-O,C-NO_2CH_2) as a kinetic intermediate, which rearranges to the observed product.[276]

Selective sp^3 C—H activation of ketones at the β-position was observed by Milstein with (PNP)Ir$^+$ (Figure 46).[277] Activation at the α-position was observed only when water was present. DFT calculations on the actual experimental system were carried out at the COSMO-PBE0 level. The rate-determining step, deciding for the outcome of the reaction, was shown to be the isomerization from the O-coordinated ketone to the η^2-(C—H) adduct prior to C—H cleavage. Because of the steric bulk imparted by the phosphine substituents, the O-coordinated complex with the methyl group of 2-butanone toward Ir is 5 kcal mol^{-1} more stable than with the ethyl group toward Ir. As the former leads to α-activation and the latter to β-activation, the observed product (β-activation) is favored because of destabilization of the ground state. After C—H activation, coordination of the carbonyl further stabilizes the system toward activation at the β-position (five-membered ring) but destabilizes the product of α-activation (four-membered ring). However, upon coordination of water, the product of α-activation is almost isoenergetic with the product of β-activation through creation of a six-membered ring exhibiting a hydrogen bond between the water and the ketone group of the substituted alkyl ligand.

The thermal reaction of Tp*Ir(C_6H_5)$_2$(N_2) with 2-ethylphenol produces the hydride alkylidene as the main product (Figure 47).[278] The hydride alkene isomer that derives from β- as opposed to α-hydride elimination in the last C—H activation step amounts to only 5% of the total reaction product. Lewis bases like NCMe induce a stereospecific 1,2 hydrogen shift (Figure 47). ONIOM(BHandH:UFF) calculations of the various intermediates shown in Figure 47 are in agreement with the experimental observations. The hydride alkylidene complex is 1.8 kcal mol^{-1} more stable than the hydride—alkene.

Reaction of Tp*Ir(C_6H_5)$_2$(N_2) with anisole generates an heteroatom-stabilized hydride carbene (Figure 47).[279,280] DFT(BHanH) calculations on the actual experimental system were carried out to determine the sequence in the three consecutive C—H activations, that is, C(sp^2)—H before or after C(sp^3)—H. Initial interaction between iridium and anisole is by way of O-coordination. Forming the σ(C—H) adduct with either the *ortho*-C(sp^2)—H or with one methyl C(sp^3)—H bond does not introduce a particular energetic bias (ΔE = 10.1 and 9.6 kcal mol^{-1} from the O-coordinated isomer for C(sp^3) and C(sp^2), respectively). In both cases, the C—H cleavage is effected through a σ-CAM transformation generating a benzene complex, and the energy difference between the sp^2 and sp^3 C—H activation TS is only 0.5 kcal mol^{-1}. Substitution of the coordinated benzene by the C—H bond yet to be activated is endothermic by less than 1 kcal mol^{-1}. A second σ-CAM process leads to the C—H activation of the other type of bond, and in both cases, the TS for the second C—H activation is at a lower energy than for the first one by ca. 5 kcal mol^{-1}. Dissociation of benzene generates a vacant site cis to the Ir—CH_2 group, thus affording the observed hydrido alkylidene product after α-C—H activation. From the initial O-coordinated anisole, the reaction is exothermic by 2.8 kcal mol^{-1}, and no particular sequence (sp^2 and sp^3 vs sp^3 and sp^2) is preferred.

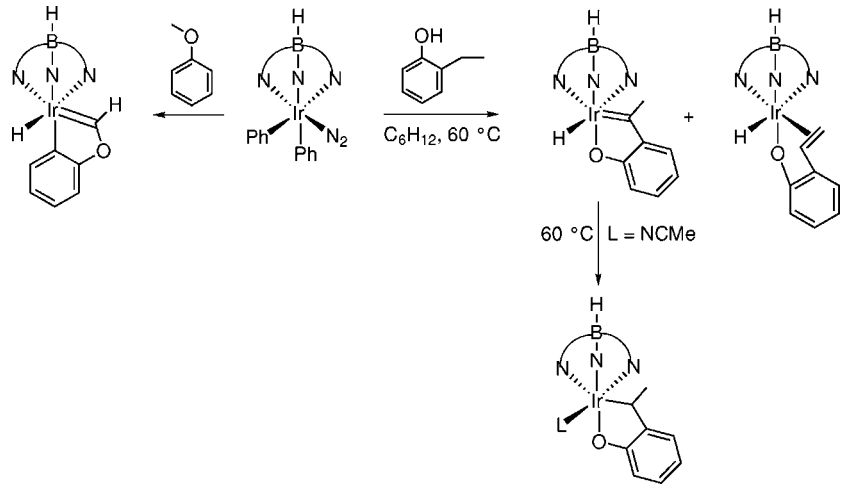

Figure 47. Hydride alkylidene and hydride alkene Ir isomeric complexes formed from C—H activation of 2-ethylphenol.

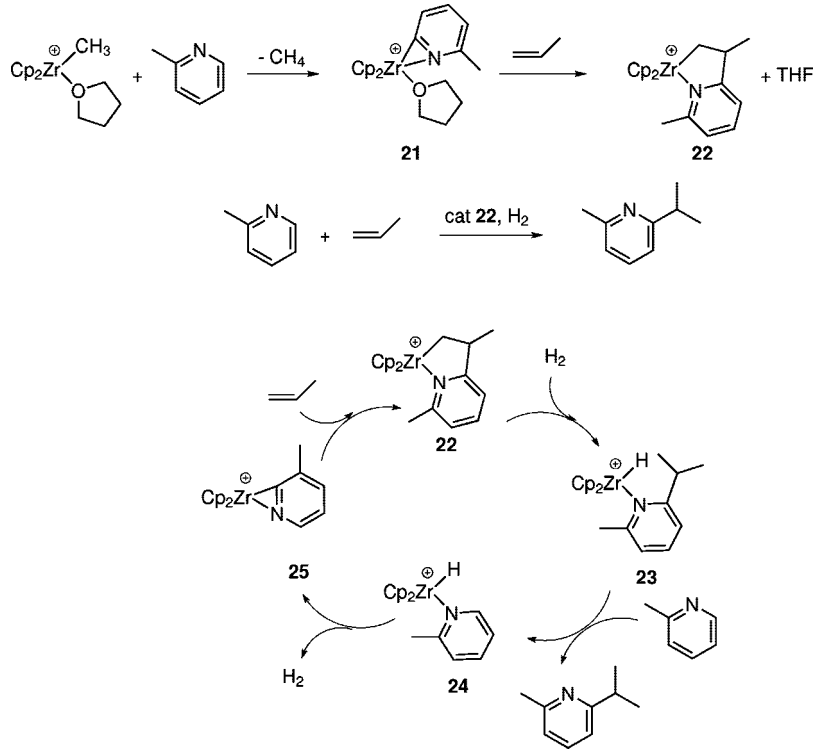

Figure 48. Zirconium-catalyzed coupling of propene and α-picoline.

3.2.2. C—H Activation in N-Heterocycles

Predictable methods for heterocycle elaboration are critical to the synthesis of pharmaceuticals. The ring heteroatom of an N-heterocycle can promote activation of an adjacent C—H bond by coordination to the metal center.[20] The first example of a direct catalytic coupling between a heterocycle and an olefin was reported by Jordan and Taylor in 1989 (Figure 48).[281]

The catalytic cycle proposed by Jordan (Figure 48) was studied computationally (B3LYP) by Lin et al.[282] The last step of the catalytic cycle is the regeneration of the η^2-picolyl complex from the $Cp_2Zr(H)$(α-picoline) complex. This transformation (**24** → **25** in Figure 48) is a typical σ-bond metathesis with $\Delta G^{\ddagger} = 19.3$ kcal mol^{-1} and $\Delta G = 5.4$ kcal mol^{-1}. The σ-bond metathesis process involving a C—H bond of the methyl group is computed to be more difficult ($\Delta G^{\ddagger} = 21.6$ kcal mol^{-1}) and less favored thermodynamically ($\Delta G = 7.4$ kcal mol^{-1}). However, the difference is not very large and C—H activation of the methyl group is possible, as illustrated by deuterium incorporation when D_2 is used. The observation of only one product is due to the relative energies of the transition states for propene insertion. The reaction at the orthometalated carbon in **25** is favored by $\Delta\Delta G^{\ddagger} = 16.2$ kcal mol^{-1} over the insertion of propene at the Zr—CH_2 bond in **22**.

Hydrogenolysis of the Zr—C bond in **22** (Figure 48) is also a σ-bond metathesis, and the reaction is computed to be the rate-determining step with $\Delta G^{\ddagger} = 25.3$ kcal mol^{-1} and $\Delta G = -5.4$ kcal mol^{-1}. Substitution of the functionalized α-picoline by a new α-picoline and C—H activation regenerate the active species. This two-step process could have been achieved in one-step through a direct σ-bond metathesis between α-picoline and the Zr—C bond of **22**. Transition state structures for the one-step process (with and without explicit N-coordination of the incoming α-picoline) were located, but their energies were very high ($\Delta G^{\ddagger} = 48.8$

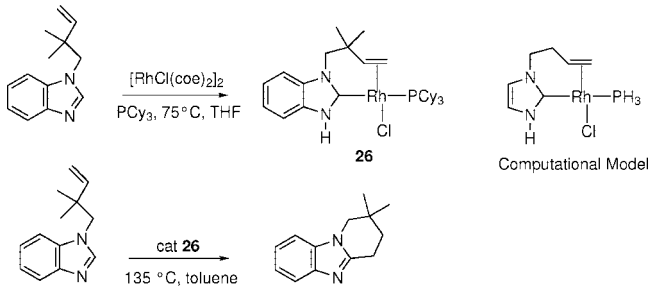

Figure 49. Catalytic C—H activation of a substituted benzimidazole.

and 41.7 kcal mol^{-1}, respectively). The easier pathway mediated by H_2 is due to the nondirectional nature of the 1s orbital on H involved in the metathesis reaction, thus lowering the energy of the corresponding TS (see section 2.2).

The thorium alkyl complex Cp*$_2$Th(Me)$_2$ and α-picoline react to give preferentially C(sp^3)—H bond activation in the presence of a more reactive C(sp^2)—H bond, while the analogous uranium complex Cp*$_2$ U(Me)$_2$ reacts with only the *ortho*-C—H bond of α-picoline.[283,284] B3LYP calculations were carried out on the competition between C(sp^2)—H and C(sp^3)—H activation in α-picoline mediated by Cp$_2$An(Me)$_2$(An = Th, U).[285] The reaction begins with the formation of a weakly bound N-adduct of α-picoline. This is followed by a σ-bond metathesis of either the *ortho*-C—H bond or one methyl C—H bond with one of the two methyl ligands. Activation at the sp^2 position is thermodynamically favored for the two actinide metals. The relative activation energies between C(sp^2)—H and C(sp^3)—H bond activation differ slightly between Th ($\Delta E^{\ddagger}$(sp^2) > $\Delta E^{\ddagger}$(sp^3)) and U ($\Delta E^{\ddagger}$(sp^2) < $\Delta E^{\ddagger}$(sp^3)). This is in agreement with the experimental observations where sp^2 activation is the thermodynamic product for both metals, while sp^3 activation is the kinetic product in the case of Th.

Metal-mediated C—H bond activation reactions have become important methods for the formation of carbon−carbon bonds. Ellman and Bergman have proposed Rh(I)-catalyzed cyclization of aromatic and heterocyclic compounds through C—H activation followed by intramolecular coupling to an alkene (Figure 49).[286,287]

The currently accepted mechanism for this type of cyclization is to start with aromatic C—H activation to form an intermediate Rh−hydride complex. Insertion of the alkene into the Rh—H bond is followed by C—C reductive elimination to yield the cyclic product. In the present case, Elmann and Bergman showed that a substantially different mechanism is operative. N-heterocyclic carbene (NHC) complex **26** was shown to be a critical intermediate. This NHC complex presents the same catalytic activity as [RhCl(coe)$_2$]$_2$/PCy$_3$, the catalyst normally used, thus implying that the NHC complex is the resting state of the catalyst. DFT(B3LYP) calculations were conducted on a model system (see Figure 49) to estimate the energetics along the cyclization pathway from the NHC intermediate.[286]

Even though the catalysis is performed at 135 °C to overcome the high barrier associated with alkene insertion, the formation of the NHC resting state via C—H activation is achieved under much milder conditions (THF, 75 °C). A detailed investigation of the mechanism of the NHC-complex formation was carried out on 3-methyl-3,4-dihydroquinazoline and the catalyst system [RhCl(coe)$_2$]$_2$/PCy$_3$ (Figure 50).[287] The N-coordinated intermediate **29** was shown to be a precursor of the NHC complex and the calculated structure for this complex (PH$_3$ instead of PCy$_3$) identified a short Rh···H contact (2.7 Å) defined as "pre-agostic".[288] The C2-deuterated substrate reacted with the usual Rh(I)/PCy$_3$ mixture to produce a N-deuterated NHC complex with 88% isotope incorporation at N1, thus indicating that the C2—H bond of the reactant is the primary source of N1—H in the NHC complex. A double-labeling crossover experiment proved that the C2—H to N1—H transformation is intramolecular.

The intramolecular pathway for the C—H activation was characterized computationally (B3LYP) with Rh(PMe$_3$)$_2$Cl as a model of the catalyst and 3-methyl-3,4-dihydropyrimidine as a model of the reactant. The high-energy process is the isomerization of the system from the N-coordinated complex (observed experimentally) to a σ(C—H) complex of the C2—H bond. The N-coordination thus selects the C—H bond to be cleaved. Migration of Rh affords a different, yet isoenergetic, σ(C2—H) complex from which C—H cleavage is easily achieved and yields a hydride intermediate. This intermediate presents the required syn geometry to form the N—H bond of the NHC complex. The proposed mechanism is in agreement with the experimental observations and the calculated activation parameters ($\Delta G^{\ddagger}$ = 28.3 kcal mol^{-1}, $\Delta H^{\ddagger}$ = 24.0 kcal mol^{-1}, and $\Delta S^{\ddagger}$ = −14.5 cal K^{-1} mol^{-1}) are in excellent agreement with the experimental values ($\Delta G^{\ddagger}$ = 29.1 kcal mol^{-1}, $\Delta H^{\ddagger}$ = 26.0 kcal mol^{-1}, and $\Delta S^{\ddagger}$ = −10.3 cal K^{-1} mol^{-1}).

In a series of papers, Esteruelas and co-workers have studied C(sp^3)—H activation in substituted pyridines promoted by osmium complexes (Figure 51).[289–293] DFT(B3LYP) calculations by Lledós on OsH$_6$(PMe$_3$)$_2$ estimated the energy cost of H_2 elimination to form OsH$_4$(PMe$_3$)$_2$ at 29.3 kcal mol^{-1}.[289] N-coordination of 8-methylquinoline and 2-(dimethylamino)pyridine stabilized the osmium tetrahydride by 9.4 and 13.2 kcal mol^{-1}, respectively. For the C—H activation to proceed, a vacant site is necessary. This is achieved by H_2 dissociation to generate an osmium dihydride featuring an agostic methyl. From this agostic intermediate, C—H activation is energetically easy ($\Delta E^{\ddagger}$ = 3.1 kcal mol^{-1}, 8-methylquinoline; $\Delta E^{\ddagger}$ = 0.4 kcal mol^{-1}, 2-(dimethylamino)pyridine) and the process is a classical oxidative addition. The osmium tetrahydride product is more stable than the N adducts (ΔE = −2.8 kcal mol^{-1}, **31**; ΔE = −4 kcal mol^{-1}, **32**).

The DFT calculations identified the products of the protonation of **31** and **32** as bis-dihydrogen complexes.[289] These bis-H_2 complexes lose H_2 and evolve through H-migration to the hydrido-dihydrogen osmium complexes with an agostic methyl interaction (see Figure 51). The process

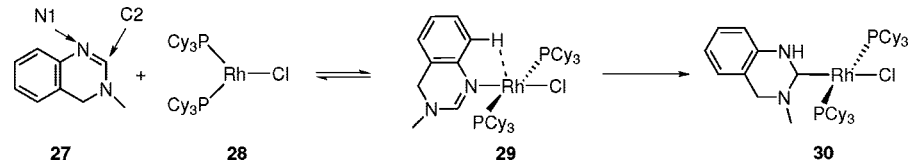

Figure 50. Mechanism of carbene formation via C—H activation.

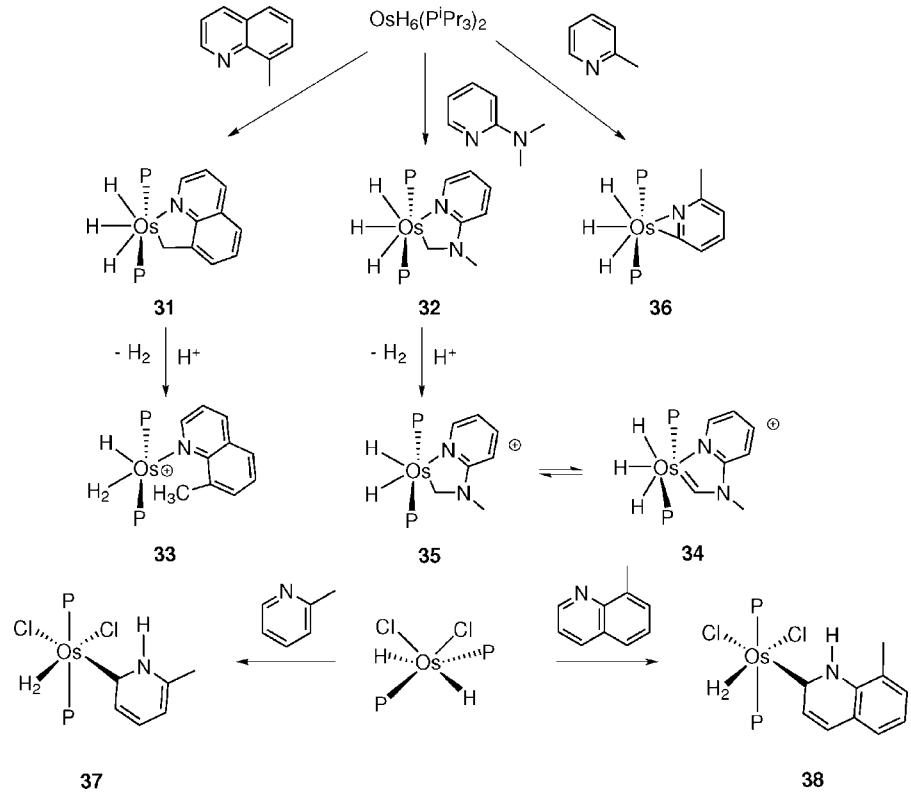

Figure 51. Reactivity observed with osmium polyhydrides and various N-heterocycles (P = P^iPr_3).

is a σ-CAM transformation, and it is easier for 8-methylquinoline than for 2-(dimethylamino)pyridine ($\Delta E^{\ddagger} = 13.3$ kcal mol^{-1} and $\Delta E^{\ddagger} = 16.9$ kcal mol^{-1}, respectively). In the case of 8-methylquinoline, the product of the H-migration is 3.8 kcal mol^{-1} more stable than the bis-dihydrogen complex and corresponds to the observed product **33**. For 2-(dimethylamino)pyridine, the product of H-migration is less stable than the bis-dihydrogen complex by 2.5 kcal mol^{-1}. One dihydrogen ligand can easily dissociate, and the remaining H_2 undergoes an oxidative addition process to yield the osmium dihydride **35** with an α-agostic interaction of the Os-CH_2 group. From this intermediate, oxidative addition yields easily the product **34** observed experimentally ($\Delta E^{\ddagger} = 9.7$ kcal mol^{-1} and $\Delta E = -3.9$ kcal mol^{-1}). Experimentally, upon protonation, **32** is transformed in a carbene complex **34** as the result of double C—H activation.

The mechanism of NH-tautomerization of α-picoline and quinoline on osmium has been studied computationally (Figure 51).[290–292] N-coordination to $OsH_2Cl_2(PMe_3)_2$, followed by hydride transfer from osmium to nitrogen to generate an η^2-(C═N) pyridinium complex is associated with a high activation barrier ($\Delta G^{\ddagger} = 48.9$ kcal mol^{-1}, α-picoline; $\Delta G^{\ddagger} = 39.3$ kcal mol^{-1}, quinoline). An intermolecular hydrogen transfer between $OsH_2Cl_2(PMe_3)_2$ and α-picoline or quinoline without N-coordination presents a lower barrier ($\Delta G^{\ddagger} = 23.6$ kcal mol^{-1}, α-picoline; $\Delta G^{\ddagger} = 23.9$ kcal mol^{-1}, quinoline). C═N η^2-coordination of the pyridinium formed opens a pathway for C—H activation at the α-position. In the case of α-picoline, the rate-determining step is the C—H activation, while it is the H-transfer from Os to N in the case of quinoline. The η^2-(C═N) pyridinium complex isomerizes to an η^2-(C_α—H) complex where the C—H bond is aligned with the P—Os—P vector. It is thus perpendicular to the equatorial plane where the two chloride ligands and the hydride are situated. A σ-CAM process is thus not possible even if the product obtained (**37** and **38**) would have suggested it. C—H cleavage is effected through an oxidative addition process generating a seven-coordinated osmium(IV) dihydride complex with a reduced P—Os—P angle (ca. 130°). This complex isomerizes to the Os(II) dihydrogen product (**37** or **38**) observed experimentally, and the trans geometry for the phosphine ligands is recovered. Overall the NH tautomerization leading to the osmium dihydrogen carbene complex is computed to be significantly exoergic ($\Delta G = -13.6$ kcal mol^{-1}, α-picoline; $\Delta G = -15.9$ kcal mol^{-1}, quinoline).

A recent study has revealed that the aromatic positions of pyridine, 3-methylpyridine, and 4-methylpyridine can be sequentially deuterated in the presence of $OsH_4(P^iPr_3)_2$ by catalytic H for D exchange with benzene-d_6.[293] The deuteration rates of the pyridine C—H bonds depend on their position in the heterocycles. B3PW91 calculations were carried out on $OsH_4(PMe_3)_2$ and pyridine or 4-methylpyridine to explain the selectivities observed experimentally. As expected, the C—H activation is composed of two steps: coordination of the C—H bond and actual cleavage. For pyridine, the stability of the η^2-(C—H) complexes varies as position 2,6 < position 4 < position 3,5. The relative order for the C—H cleavage step is position 3,5 > position 2,6 > position 4. A combination of both factors yields the para position as the preferred site of deuteration as observed experimentally. As a methyl group impedes coordination of the adjacent C—H bonds, the methyl substituent has a marked negative effect on the deuteration of its adjacent positions.

Double geminal C—H activation and reversible α-elimination in 2-(dimethylamino)pyridine Ir(III) complexes has been observed by Crabtree et al. (Figure 52).[294] DFT(B3PW91) calculations have been carried out on $IrH_2(PH_3)_2^+$ and 2-(dimethylamino)pyridine to elucidate the factors responsible for the smooth transformation observed in Figure 52. The substitution of two acetone ligands by N-coordinated pyridine and agostic amino-methyl group is only slightly

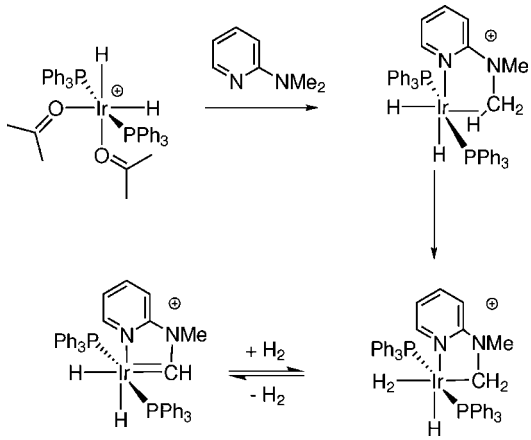

Figure 52. Double geminal C—H activation in 2-(dimethylamino)-pyridine Ir(III) complex.

endoergic ($\Delta G = 3.1$ kcal mol^{-1}). From the agostic complex, C—H cleavage is easy ($\Delta G^{\ddagger} = 10.1$ kcal mol^{-1}) and gives an iridium dihydrogen hydride complex ($\Delta G = -1$ kcal mol^{-1}). Contrary to the chemistry observed by Esteruelas with neutral osmium, the present cationic iridium promotes C—H activation through a σ-CAM transformation. The TS structure is an Ir(V) trihydride, but two hydrides couple in the product to create an H_2 ligand *trans* to the newly formed Ir—C bond. This reorganization of the nature of the ligands favors a smooth transformation. Subsequent dissociation of H_2 generates a vacant site that is needed for the second C—H activation. However, the vacant site is *trans* to the bond to activate and isomerization to a *cis*-phosphine geometry affords easy α-elimination ($\Delta G^{\ddagger} = 2.1$ kcal mol^{-1} and $\Delta G = -9.7$ kcal mol^{-1}). The *cis*-phosphine carbene complex then converts to the *trans*-phosphine product observed experimentally.

3.2.3. C—H Activation in Ancillary Ligands

Coordination of an orientating group promotes selective C—H activation in the vicinity of the group as illustrated by the Murai reaction[35] and the propene insertion in α-picoline proposed by Jordan.[281] In these reactions, the substrate is preconditioned by appropriate chemical substitution to react at a given position. This approach can also be used in ligand design to build new architectures that may lead to more efficient catalytic systems. In this respect, PCP pincer complexes have shown great potential because they are usually very stable at the high temperature required for some catalytic reactions.[295] N-heterocyclic carbenes (NHC) stabilized by bulky groups have also been shown to be very good ligands to build efficient catalysts.[296] Coordination of the stable free NHC is a common synthetic procedure, but, in some cases, C—H activation of the imidazolium has been shown to be an alternative. Moreover, the bulky groups usually present on the nitrogen atom may be engaged in intramolecular C—H activation processes with the metal.

Reaction of the ligand 1,3-bis(di-*tert*-butyl(phosphino)-methyl)benzene (**39**) with the $[Rh(CO)]^+$ fragment in THF resulted in clean formation of the bis-chelated complex (**40**), which contains an η^2-(C—H) bond (Figure 53).[297] The coordination of the C—H bond increases its acidity as illustrated by the easy formation of the PCP pincer complex **41** upon exposure to NEt_3 or collidine. B3LYP calculations on a model of **40** (Me instead of ^{t}Bu on phosphorus) revealed that the ring bond lengths in the agostic complex are affected only weakly, relative to those of the free ligand. Protonation of the free ligand to yield a Wheland type structure resulted in significantly larger changes in bond distances within the aromatic ring, with clear bond alternation as expected. Thus, a strong agostic interaction between a metal center and an aromatic compound followed by deprotonation can be considered as an alternative to electrophilic aromatic substitution.

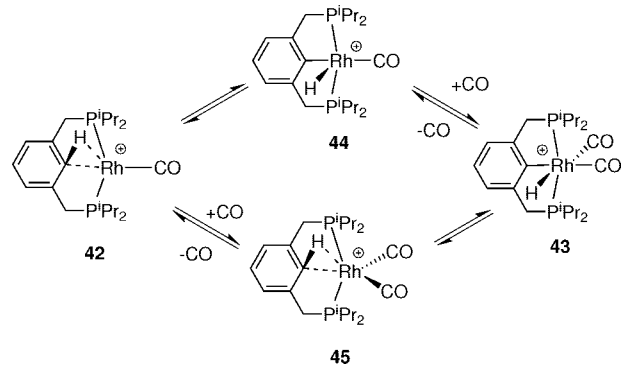

Figure 54. Unexpected role of CO in C—H oxidative addition by a cationic Rh(I) complex.

Milstein and Martin evidenced an unexpected role of carbon monoxide in C—H oxidative addition by a similar cationic Rh(I) complex. (Figure 54).[298] In the present system, the C—H oxidative addition is promoted by addition of the π-acceptor ligand CO, which is contrary to expectation for an oxidative addition favored by electron-rich metal centers. Two pathways are proposed for the transformation differing in the order for the two necessary steps, CO coordination and C—H activation, to convert the agostic complex to the hydrido aryl isomer (Figure 54). DFT(PBE0) calculations were carried out to elucidate which of the two mechanisms is preferred. C—H oxidative addition in **42** to generate the hydrido aryl intermediate **44** is associated with an activation barrier $\Delta G^{\ddagger} = 11.1$ kcal mol^{-1} and is endoergic ($\Delta G = 7.8$ kcal mol^{-1}). Coordination of CO leads to **43**, which is more stable than **42** ($\Delta G = -1.6$ kcal mol^{-1}). Coordination of CO to the agostic complex **42** leads to the agostic dicarbonyl complex **45**, which is 1.2 kcal mol^{-1} more stable than **42**. Quite surprisingly, the C—H activation in **45** has a lower barrier than that in **42** ($\Delta G^{\ddagger} = 9$ kcal mol^{-1}), and therefore the TS for C—H activation in **45** lies at 3.3 kcal mol^{-1} below that for C—H activation in **42**. Thus, while the first CO ligand inhibits C—H activation by locking the system with an agostic interaction, the coordination of the second CO ligand facilitates C—H activation.

The influence of the strength of the agostic interaction on the competition between aromatic and aliphatic C—H activa-

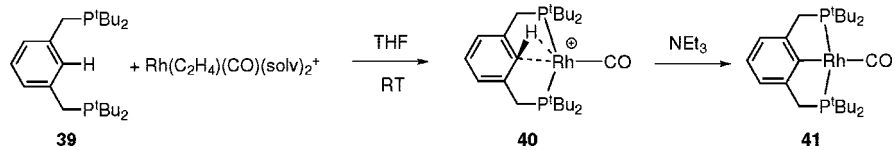

Figure 53. Formation of η^2-(C—H) agostic rhodium arene complexes and their deprotonation.

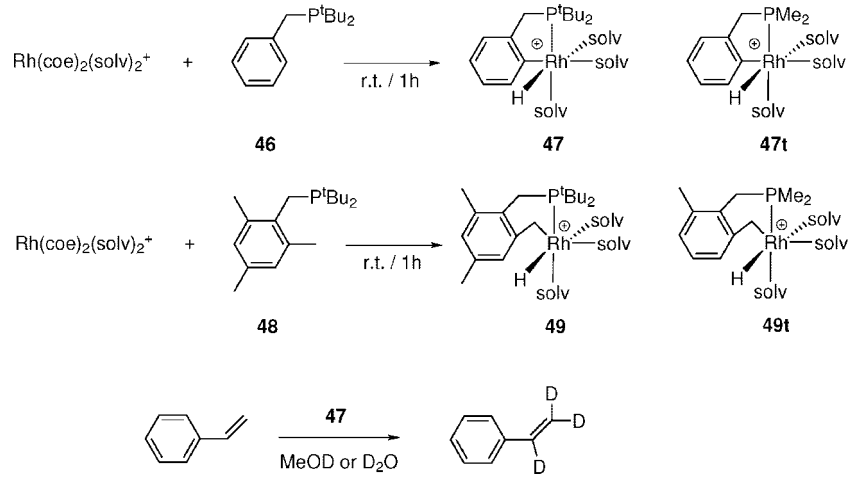

Figure 55. Aromatic vs aliphatic C—H bond activation by Rh(I) as a function of agostic interactions.

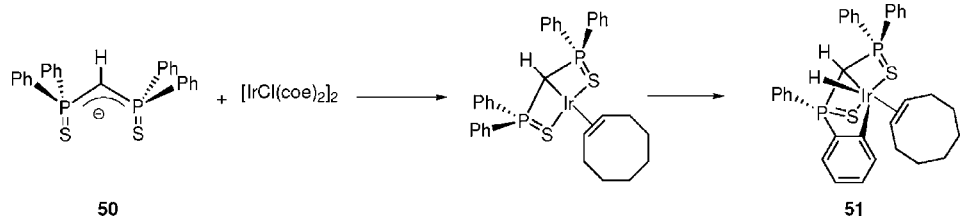

Figure 56. Intramolecular C—H activation in a strained SCS Ir pincer complex.

tion has been studied by Milstein and Martin in the reaction of PC ligands with a cationic Rh(I) complex (Figure 55).[299] The aryl-PC type ligand **46** yields the C—H activated complex **47**. The latter undergoes reversible C—H activation and H for D exchange into the hydride and aryl *ortho*-C—H with D_2O and MeOD. This complex also promotes catalytic H for D exchange into the vinylic C—H bond of olefin. The benzyl-PC ligand **48** yields the C—H activated complex **49**, which is very different from **47**.[300] In addition, **49** is not active in H/D exchange with ROD and in catalytic H for D exchange with olefin. DFT(mPW1k) calculations of the mechanism for C—H activation and H exchange were carried out on the model systems **47t** and **49t** shown in Figure 55. The main difference between the aliphatic system and its aromatic counterpart is in the activation barriers for the reductive elimination process from the Rh(III)—hydride to the Rh(I)—(η^2-(C—H)) agostic complex ($\Delta G^{\ddagger}$ = 12.7 kcal mol^{-1}, aliphatic system; $\Delta G^{\ddagger}$ = 4.5 kcal mol^{-1}, aromatic system). A comparison of the geometries of the aliphatic and aromatic agostic complexes, together with Wiberg bond indices, indicates that the agostic interaction is stronger in the aromatic case. Moreover, in the aromatic case, the agostic interaction essentially develops with the carbon and the protonic character of the hydrogen slightly increases, whereas in the aliphatic case, the agostic interaction is essentially with the hydrogen atom and the hydridic character of the latter increases. Thus, the aromatic PC system demonstrates both nucleophilic (oxidative addition) and electrophilic (H for D exchange) type of C—H activation, whereas the aliphatic PC system shows only nucleophilic C—H activation by oxidative addition.

Reaction of the bis(diphenyl(phosphino)sulfide)methanide anion with $[Ir(coe)_2Cl]_2$ affords a hydrido complex (Figure 56).[301] A DFT(B3PW91) study of the mechanism of formation of **51** was carried out on a model system where all the phenyl groups but one are replaced by hydrogen atoms and the coe ligand is modeled by ethylene. The rate-determining step is the decoordination of the sulfide to allow coordination of one *ortho*-C—H bond of the phenyl group ($\Delta H^{\ddagger}$ = 22.3 kcal mol^{-1}). From this agostic complex, C—H activation is easy and exothermic ($\Delta H^{\ddagger}$ = 12.6 kcal mol^{-1} and ΔH = −4.8 kcal mol^{-1}) and coordination of the sulfide group yields the product. DFT calculations suggest that only a very weak energy barrier is needed to promote the formation of the Ir(III) hydrido complex **51** through intramolecular oxidative addition of a C—H bond of one pendant aromatic ring. A similar reactivity with a Ru(II) complex has been studied experimentally and computationally.[302]

The simplest synthetic procedure to form an NHC complex uses free NHC as a reagent. The substituents on the nitrogen atoms are usually large enough to stabilize the carbene. One of the often used ligands is 1,3-dimesitylimidazol-2-ylidene (IMes). However, the mesityl group may be engaged in intramolecular C—C and C—H bond activation as shown by Whittlesey (Figure 57).[303,304] $Ru(IMes)(PPh_3)_2(CO)(H)_2$ (**52**) reacts with alkenes at room temperature to give the product of intramolecular C—H activation **54**. The C—H activation is effected from the Ru(0) intermediate **53** after hydrogen abstraction by the alkene. The reaction is reversible and addition of H_2 to **54** regenerates **52**. The same complex **52** can also be induced to undergo an alternative intramolecular C—C activation. Heating **52** at 80 °C with excess IMes results in substitution of PPh_3 by IMes to generate the dihydride **55**. Further heating at 110 °C yields **56**, the product of C(sp^2)—C(sp^3) activation, with release of methane and substitution of IMes by PPh_3. The formation of **56** is irreversible.

ONIOM(BP86:HF) calculations estimated the energy barriers from the various Ru(0) complexes of PPh_3 and IMes either tri- or tetracoordinated. The energy barriers for C—H activation from these complexes are small enough to observe C—H activation at room temperature. However, the energy barriers are significantly lower for the tricoordinated complexes than for the tetracoordinated systems. In contrast, the

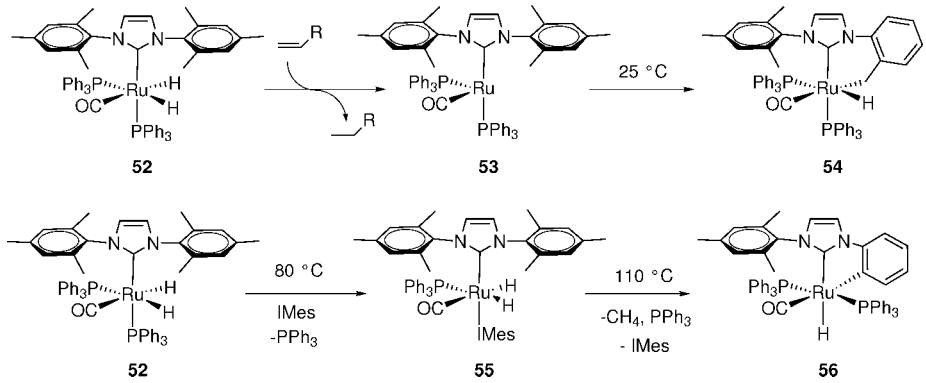

Figure 57. C—C and C—H bond activation reactions in N-heterocyclic carbene complexes of ruthenium.

energy barriers for C—C cleavage are significantly larger and heating is required to overcome the hurdle. The introduction of a second IMes ligand does not promote C—C cleavage. It serves to stabilize the unsaturated $Ru(CO)(IMes)_2$ intermediate and thus makes a reactive intermediate accessible. In this system, C—H activation is always preferred kinetically, but this reaction is reversible and upon prolonged heating, and with excess of IMes, the product of C—C activation accumulates. Recently, a B3LYP mechanistic study has been carried out to explore the structural and energetic features leading to the decomposition pathways of a Grubbs second-generation catalyst.[305] The theoretical results strongly suggest that the deactivation pathway initiates with a C—H activation process.

Because NHC ligands have often been presented as alternatives to phosphines and are considered to render the metal center more electron-rich, oxidative addition processes are expected to be easier upon substitution of phosphine by NHC. To test this hypothesis, Macgregor has studied computationally (BP86) the C—H activation of methane by $Ru(CO)(PH_3)_n(IR)_{3-n}$ ($n = 1-3$; for R = H, IR = (1,3-imidazol-2-ylidene); for R = Me, IR = (1,3-dimethylimidazol-2-ylidene)).[306] The energy barriers are all computed to be ca. 18 kcal mol^{-1}, and the reaction is approximately thermoneutral. Interestingly, the energy barrier increases upon substitution of PH_3 by IH or IMe, even though computations confirm that introducing NHC ligands renders the metal more electron-rich. A fragment analysis reveals that increasing the electron density at Ru destabilizes the occupied d_π levels, thus increasing the Lewis basicity of the metal. However, a more important effect is a reduction in Lewis acidity, and this factor lies behind the similar reaction energetics computed for analogous PH_3 or IH-containing species.

Base-assisted generation of NHC from imidazolium salts is another common strategy for synthesizing NHC complexes when the nitrogen substituents do not afford enough stabilization to the free carbene.[307] A combined experimental and computational study of C—H oxidative addition of bisimidazolium salts to iridium complexes has been carried out by Peris and Lledós (Figure 58).[308] The first metalation affords Ir(I) complexes, and the calculations could not differentiate between the two possible pathways, deprotonation of the imidazolium by the base and coordination or C—H oxidative addition to Ir and deprotonation of the cationic Ir-hydride by the base. The second Ir—C bond is formed through C—H oxidative addition as illustrated by the product observed with the short methylene linker (Figure 58). Calculations confirm that for the second metalation, C—H oxidative addition is the preferred pathway over the direct deprotonation of the imidazolium followed by coordination. Because of the geometric constraints imposed by the coe ligand and the already formed M—C bond, three different geometries are possible for the interaction of the second C—H bond to cleave with the metal center. Two out of the three geometries lead to an isomer with cis H and Cl in the product of C—H activation, whereas in the remaining one H and Cl are trans. From these cis isomers, H—Cl reductive elimination yields the square planar complexes observed with the longer linkers.

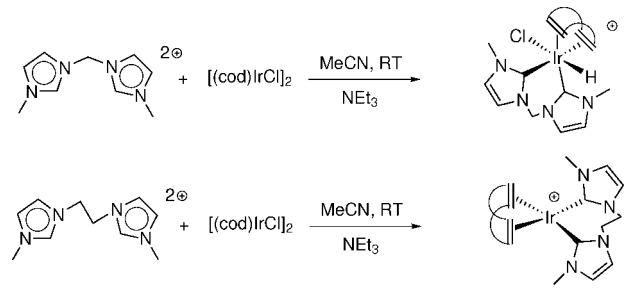

Figure 58. Formation of chelate NHC complexes through C—H activation.

In the case of the short C1 linker, the C—H cleavages forming the trans and cis isomer (with respect to the positions of H and Cl) have similar energy barriers, and the more stable trans product is obtained under thermodynamic control. For the longer C3 case, the C—H activation leading to the trans isomer is effected through a TS lying 3 kcal mol^{-1} higher in energy than the one yielding the cis isomer. The latter is thus formed kinetically and readily eliminates HCl to form the observed square planar bis(NHC)—Ir(I) species. A unified mechanism can apply to the formation of bis(NHC)—Ir(III)—H and bis(NHC)—Ir(I) complexes, based on the oxidative addition of the imidazolium C—H bonds to the metal. The weak base can play the role of an HCl reductive elimination inductor, rather than a deprotonating agent.

In a study of the formation of NHC complexes through C—H activation of imidazolium salts, Crabtree observed a striking influence of the counteranion A^- that switches the ligand binding from C2 to C5 (Figure 59).[309,310] With R = Me and $A^- = Br^-$, the expected product of metalation at the C2 position (**58**) is obtained as the major product (91:9). With $A^- = BF_4^-$ as the counteranion and R = Me, a 45:55 mixture of both isomers (C5 isomer, **59**, major product) is obtained. Increasing the bulk at nitrogen (R = ^{i}Pr) slightly lowers the amount of the C2 product (84:16) in the case of Br and triggers the system toward exclusive formation of the C5 product (**59**) in the case of BF_4^-.

ONIOM(B3PW91:UFF) calculations have shown that bonding at C2 is thermodynamically preferred for the naked

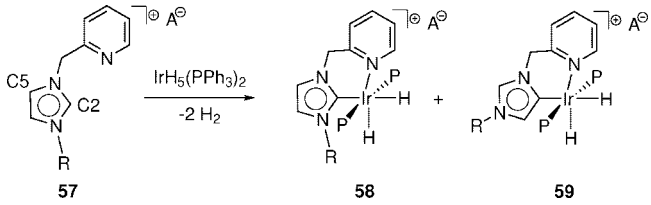

Figure 59. Counterion effects on the geometry of metalation of imidazolium salts to iridium. P stands for PPh_3.

cation ($\Delta E = 10.1$ kcal mol^{-1}).[310] Calculations of the ion-pair structure[311] identified the location of the anion−cation contact at the backbone of the pyridine−NHC ligand. This brings extra stabilization by creating H-bonding interactions between the anion and the ligand. Due to the greater acidity of the C2−H bond, the H-bonds are stronger for isomer **59**, and the energy difference between **58** and **59** almost cancels ($\Delta E = 1.6$ kcal mol^{-1}, BF_4^-; $\Delta E = 3.8$ kcal mol^{-1}, Br^-).

The computational study of the reaction pathways leading to the C2- and C5-carbene isomers was carried out on a model system consisting of $IrH_3(PMe_3)_2$ and the *N*,*N*′-dimethylimidazolium cation in the presence of Br^- or BF_4^-.[310] The anion-induced selectivity was shown to originate from different anion participation in the TS for C−H activation. With Br^-, a strong H-bond develops with the acidic proton at C2, and this interaction is maintained in the TS during the cleavage of C2−H. The anion follows the hydrogen atom that is transferred as a proton. The transformation is a σ-CAM process as the initial η^2-(C−H) bond in interaction with Br is converted in an η^2-(H−H) bond still in interaction with Br^-. The larger BF_4^- anion, involved in a network of H-bonds, is not able to stabilize such a σ-CAM transformation, and oxidative addition at the C5 position is computed to be preferred. The reason for the change of mechanism is the very strong donor character of the C5-carbene, which favors attainment of Ir(V) versus the highly protonic character of the C2−H of an imidazolium salt that favors the heterolytic C−H path. This relatively rare case of an anion-dependent selectivity change is therefore explained by a relatively rare coincidence of several criteria.

In a very recent study, Whittlesey and Macgregor have shown that a base selectively deprotonates the alkyl C−H bond geminal to an agostic interaction.[312] With *N*,*N*′-dimethylimidazol-2-ylidene as a base, calculations (BP86) indicated that the abstraction of the nonagostic proton has an energy barrier of $\Delta E^{\ddagger} = 12.7$ kcal mol^{-1}. In contrast, reaction profiles for the approach of the external base toward the agostic hydrogen did not lead to deprotonation. The base remains a spectator, and C−H oxidative addition is associated with an energy barrier of $\Delta E^{\ddagger} = 19.6$ kcal mol^{-1}, leading to an unstable Ru(IV) intermediate ($\Delta E = 18.9$ kcal mol^{-1}). This Ru(IV) intermediate is deprotonated by the base ($\Delta E^{\ddagger} = 3.6$ kcal mol^{-1}) to yield the final product. This computational study indicates that the base-induced cleavage of a nonagostic C−H bond is possible despite the perception that the latter should be less acidic than the agostic C−H bond.

DFT(BP86) calculations have been carried out on the cycloplatination reaction of *cis*-[$Pt(Me)_2$(dmso)($P(o\text{-tol})_3$] leading to the C,P-cyclometalated compound with liberation of methane.[313] The reaction was shown to proceed in four steps: (i) dissociation of dmso, (ii) intramolecular C−H activation of a methyl group on the $P(o\text{-tol})_3$ ligand, (iii) reductive elimination of methane to give the σ-complex, and (iv) fast reassociation of the dmso ligand.

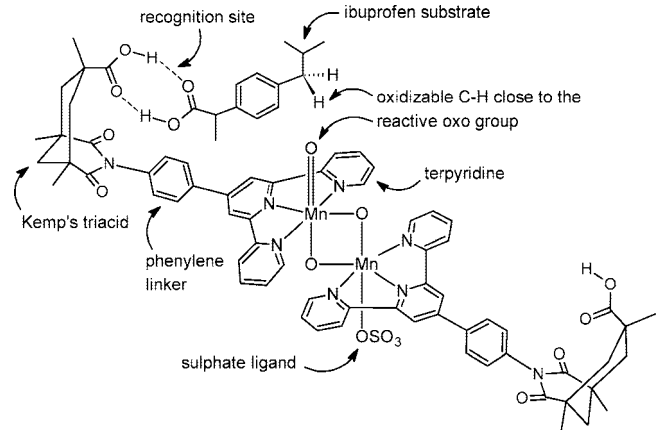

Figure 60. Catalytically selective C−H oxidation of ibuprofen by molecular recognition.

The competition between carbene and olefin products of C−H activation within the PCP ligand ^{t}Bu$_2$PNHC$_3$H$_4$-NHP^{t}Bu$_2$ on ruthenium via competing α- and β-H elimination was studied experimentally and computationally by Gusev.[314] Double intramolecular C−H activation of a pendant group of a PNP pincer ligand (^{t}Bu$_2$PCH$_2$SiMe$_2$)$_2$N) to yield an alkylidene ruthenium complex was studied experimentally and computationally by Caulton.[315,316]

3.3. C−H Activation under Molecular Recognition

High selectivities are often achieved in enzymatic reactions thanks to molecular recognition. In this strategy, a functional group of the substrate binds to the recognition site of the enzyme by means of weak noncovalent interactions, like π-stacking or H-bonds. This prevents the reaction on the functional group and orientates a specific fragment of the substrate toward the reactive center, thus promoting the reaction in a selective manner. Very recently, this approach was successfully implemented in an artificial catalytic system by Brudvig and Crabtree[36,220,317] The active catalytic species, [(terpy′)(O)Mn(μ-O)$_2$Mn(SO$_4$)(terpy′)]$^+$, is a mixed-valence dinuclear manganese complex with two bridging oxo ligands (Figure 60). Each metal center is bound to a functionalized terpyridine ligand, and one apical position is occupied by an oxo ligand whereas the other is occupied by a sulfate ligand. The reactivity of this complex was theoretically studied by Eisenstein et al.[318] considering the oxidation of toluene to benzyl alcohol as model reaction. The calculations showed that the substrate is oxidized by the apical oxo group of the catalyst in its ground state, which is an antiferromagnetic doublet.[319] The reaction follows the classical rebound mechanism, as in the mononuclear manganese systems studied by the same authors (*vide infra*).[320–322]

The C−H oxidation of ibuprofen involves both benzylic positions, and a mixture of two products is thus obtained. Nevertheless, when the reaction is catalyzed by [(terpy′)(O)-Mn(μ-O)$_2$Mn(SO$_4$)(terpy′)]$^+$ only the isobutyl group is oxidized. The terpy′ ligand is a terpyridine functionalized with a phenyl ring, used as linker, and a Kemp's triacid, used as recognition site. The origin of selectivity was explained by postulating the molecular recognition model represented in Figure 60.[220] The carboxylic group of ibuprofen is recognized by the catalyst, which prevents the oxidation of the $-CH(CH_3)COOH$ fragment. The other substituent of the phenyl ring, $-CH_2CH(CH_3)_2$, is brought into the reactive site, thus undergoing selective C−H

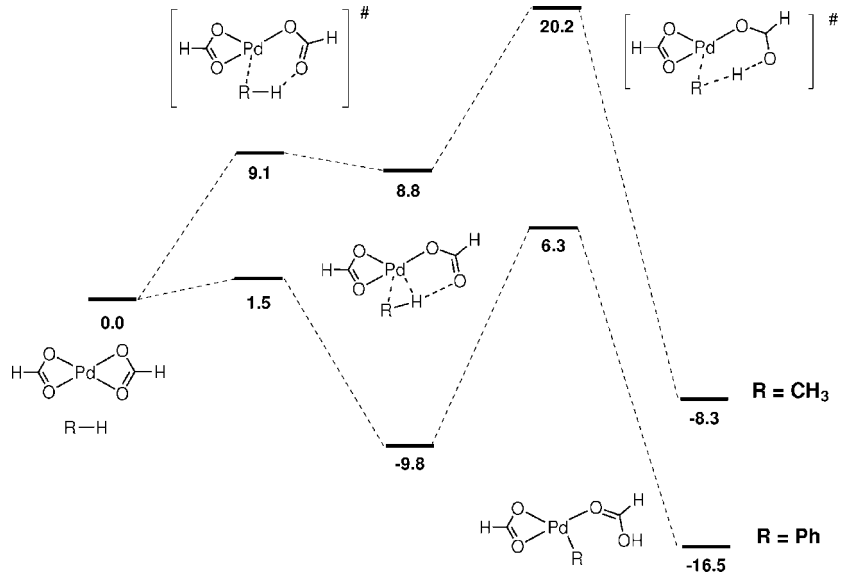

Figure 61. Energy diagram (kcal mol^{-1}) associated with the C—H bond activation of R—H by Pd(κ^2-$O_2CH)_2$ for R = C_6H_5, CH_3.

oxidation. This model was theoretically confirmed.[318] The calculations showed that the substrate is recognized by a double H-bond, which is maintained through the whole reaction pathway. The substrate does not fit perfectly into the pocket open between the recognition and reactive sites, but the system is flexible enough to promote the reaction and preserve the double H-bond. The reaction without molecular recognition, which would be nonselective, is not observed due to the energy penalty of ~15 kcal mol^{-1} associated with the loss of the double H-bond. This study also revealed that the catalyst may bind to two molecules of substrate simultaneously. One molecule reacts with the oxo group, whereas the other blocks the approach of unrecognized molecules of substrate to the reactive site, which will diminish the selectivity of the reaction. This model also explained the inhibition of the catalyst by *tert*-butyl benzoic acid found experimentally.[317]

3.4. Base-Assisted C—H Activation

The Fujiwara reaction represents an early example of C—H functionalization of aromatic compounds through C—H bond activation.[15] In this reaction, the catalyst is $Pd(OAc)_2$, and the coordinated acetate is considered to play an active role in the C—H bond cleavage process. A very recent review by Macgregor and Davies addresses specifically the description of the mechanism of C—H activation at late transition metal systems.[38] An early computational study of C—H bond activation of benzene and methane by M(κ^2-$O_2CH)_2$ (M = Pd, Pt) has been carried out by Sakaki.[323] In this work, a comparison between benzene and methane C—H activation by $M(PH_3)_2$ has also been conducted. For benzene and methane activation by M(κ^2-$O_2CH)_2$, the reaction proceeds in two steps (Figure 61). The η^2-coordination of the C—H bond requires partial decoordination of one formate ligand. In the intermediate species, the coordinated C—H bond presents a short contact between the hydrogen and the oxygen atom of the formate that is not bonded to M. In the case of M = Pd, the distances are 1.958 and 2.141 Å for benzene and methane, respectively. As the acidity of the C—H bond increases upon coordination to the electrophilic metal center, these relatively short distances are indicative of extra stabilization. Accordingly, the energy of the intermediate relative to the separated reactants is computed (MP4SDQ) to be −9.8 kcal mol^{-1} for M = Pd and benzene and 8.8 kcal mol^{-1} for M = Pd and methane. From this intermediate, the C—H cleavage is effected through proton transfer from C to O, and the energy barrier is low ($\Delta E^{\ddagger}$ = 16.1 kcal mol^{-1}, M = Pd, benzene; $\Delta E^{\ddagger}$ = 11.4 kcal mol^{-1}, M = Pd, methane). At the TS for H-transfer, the Pd···H contact is long showing that there is no Pd(IV) character in this step.

It is interesting to compare these results with those obtained for C—H activation by $Pd(PH_3)_2$. In this case, the energy barriers for C—H oxidative addition of benzene and methane are 26.5 kcal mol^{-1} and 34.7 kcal mol^{-1}, respectively. The C—H activation mediated by Pd(II)−formate is thus significantly easier than the C—H oxidative addition at Pd(0)−phosphine. Another particular aspect of the reaction with $Pd(O_2CH)_2$ is that the oxidation state of the metal is constant throughout the transformation, whereas with $Pd(PR_3)_2$ the activation product is a Pd(II) complex. The reaction is computed to be exothermic for Pd(κ^2-$O_2CH)_2$ (−16.5 kcal mol^{-1}, benzene; −8.3 kcal mol^{-1}, methane), and endothermic for $Pd(PH_3)_2$ (22.1 kcal mol^{-1}, benzene; 31.5 kcal mol^{-1}, methane). The determining factor for the favorable thermodynamics of the C—H activation by $Pd(O_2CH)_2$ is the creation of a strong OH bond in the formate ligand. Analysis of the electron distribution indicates that the C—H bond activation by M(κ^2-$O_2CH)_2$ is heterolytic, while in the case of $M(PH_3)_2$, the activation is homolytic.

Acetate-assisted C—H activation is also a potential alternative in cyclometalation reactions as illustrated in the works by Davies and Macgregor.[324–327] The various pathways (oxidative addition, 1,2-addition, and proton transfer to acetate) for cyclometalation of dimethylbenzylamine (DMBA-H) with $Pd(OAc)_2$ were characterized by BP86 calculations (Figure 62).[324] In the acetate-assisted C—H activation, the rate-determining step is not C—H cleavage but formation of the agostic intermediate. After coordination of the NMe_2 group of DMBA-H to Pd, substitution of one coordinated acetate oxygen atom with one *ortho*-C—H bond within DMBA-H is associated with an energy barrier of $\Delta E^{\ddagger}$ = 13.0 kcal mol^{-1}. The agostic intermediate presents a short H···O contact of 2.04 Å, and the proton transfer to O is almost barrierless ($\Delta E^{\ddagger}$ = 0.1 kcal mol^{-1}). In comparison, the TS

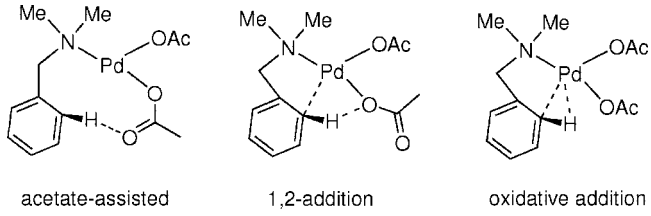

Figure 62. Possible transition states for C—H activation of DMBA-H by $Pd(OAc)_2$.

for the 1,2-addition across the Pd—O bond and the TS for oxidative addition have significantly larger energy barriers (34.3 and 25.7 kcal mol^{-1}, respectively). The acetate-assisted C—H activation is thus clearly preferred. After C—H cleavage, the protonated acetate rotates and transfers the hydrogen to the other acetate, creating a hydrogen bond stabilizing the product. It also allows adaption of the electronic influence of the ligands to the new bonding situation. The strong σ-donor aryl ligand is trans to the weak ligand that constitutes the acetic acid bonded by way of the oxygen of the C=O bond. A similar mechanism was reported by Lledós for the selective cyclopalladation of R_3P—NCH_2aryl iminophosphoranes with $Pd(OAc)_2$.[328,329]

Davies and Macgregor also reported DFT calculations showing that intramolecular hydrogen bonding to acetate can provide a low-energy pathway to C—H activation with iridium (Figure 63).[325,326] For the acetate-assisted C—H activation, no agostic intermediate was located, and the TS structure presents a geometry similar to that observed for the Pd-agostic intermediate (C—H = 1.11 Å, H···O = 2.15 Å).[324] The energy barrier of 16 kcal mol^{-1} is similar to that obtained with Pd (13 kcal mol^{-1}). The cyclometalation is slightly exothermic ($\Delta E = -2.4$ kcal mol^{-1}). Whereas the CpIr fragment is usually associated with C—H activation via oxidative addition, in the present case the oxidative addition TS has a high energy ($\Delta E^{\ddagger} = 30.7$ kcal mol^{-1}). Even though the 1,2-addition, via a four-membered ring in the TS, has a lower energy barrier ($\Delta E^{\ddagger} = 14.0$ kcal mol^{-1}), it starts from a κ^1-acetate isomer that is 8.8 kcal mol^{-1} less stable than the κ^2-acetate ground state. Consequently, the TS for the 1,2-addition is 6.8 kcal mol^{-1} above that assisted by acetate, via a six-membered ring (Figure 63). Ligands such as κ^2-OAc can provide both strong basic character and, via arm dissociation, a geometrically convenient route for intramolecular H-transfer.

DFT(BP86) calculations have been employed to study the role of chelating base, RCO_2^- (R = Me, Ph, CCl_3, CF_3, OH, Ph) in the cyclometalation reaction of DMBA-H with CpIr.[326] In contrast to the results of the previous study,[325] these new calculations identified a two-step pathway for the acetate-assisted C—H activation similar to that observed with $Pd(OAc)_2$.[324] The formation of the agostic intermediate with dissociation of one acetate arm has an energy barrier of $\Delta E^{\ddagger} = 13.4$ kcal mol^{-1}. In contrast to the case of Pd, the interaction of the agostic C—H bond is with the oxygen atom coordinated to Ir and not the one that has dissociated. This would tend to indicate that a 1,2-addition pathway is preferred but the corresponding TS is 11 kcal mol^{-1} above the agostic intermediate. The TS for H-transfer to the noncoordinated oxygen via a six-membered ring is computed to be only 0.9 kcal mol^{-1} less stable than the agostic intermediate. The two-step process involving initial κ^2—κ^1 displacement of the base, followed by facile C—H cleavage, was found for $PhCOO^-$ and CCl_3COO^-, while with $HCOO^-$ and CF_3COO^-, no agostic intermediate was located. The calculations show that C—H activation is controlled by the energy of the κ^2—κ^1 isomerization of the base, so higher energy barriers are computed with more strongly coordinating bases $RCOO^-$ ($\Delta E^{\ddagger} = 13.4$ kcal mol^{-1}, R = Me; $\Delta E^{\ddagger} = 14.6$ kcal mol^{-1}, R = Ph; $\Delta E^{\ddagger} = 9.5$ kcal mol^{-1}, R = CCl_3). The proton transfer from the agostic intermediate has a low energy barrier that is rather insensitive to the actual basicity of $RCOO^-$ ($\Delta E^{\ddagger} = 0.9$ kcal mol^{-1}, $pK_a = 4.8$, R = Me; $\Delta E^{\ddagger} = 0.9$ kcal mol^{-1}, $pK_a = 4.3$, R = Ph; $\Delta E^{\ddagger} = 1.3$ kcal mol^{-1}, $pK_a = 0.65$, R = CCl_3). The basicity of the free base is shown to be significantly attenuated by binding to the metal

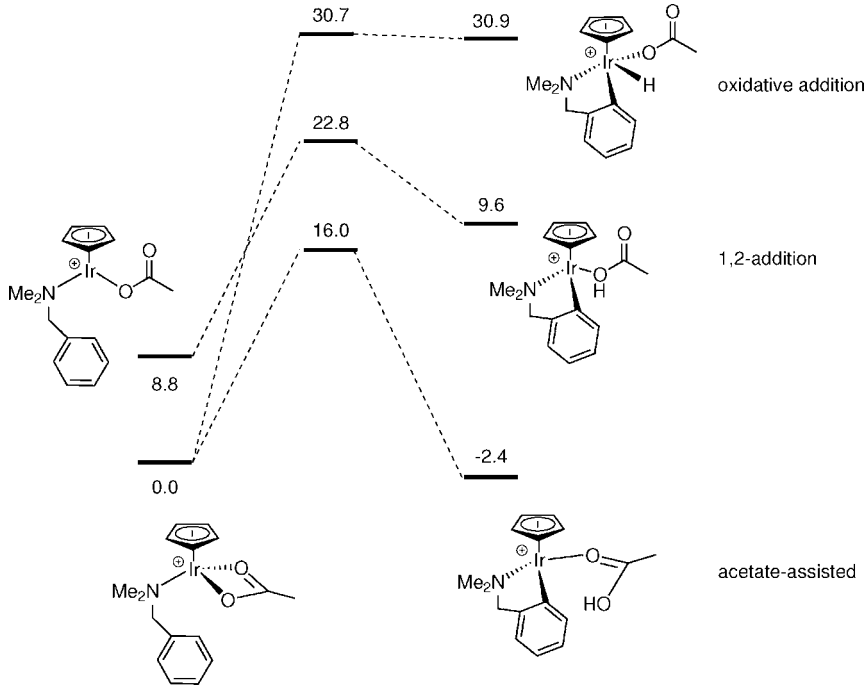

Figure 63. Computed reaction profiles (kcal mol^{-1}) for C—H activation in $CpIr(DMBA\text{-}H)(OAc)^+$. The product of C—H oxidative addition (top right) is computed to lie 0.4 kcal mol^{-1} below the associated TS prior to the inclusion of ZPE corrections.

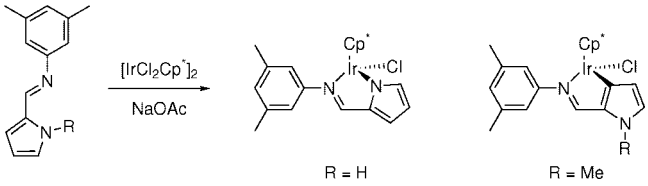

Figure 64. N—H versus C—H activation of a pyrrole imine at iridium.

Figure 65. Pd-catalyzed intramolecular arylation.

center. The counterdirecting effects of coordination strength and basicity mean that the overall energy associated with C—H activation in these species is remarkably insensitive to the nature of the intramolecular base employed.

The $(IrCl_2Cp^*)_2$/NaOAc system can activate the N—H bond of a pyrole imine at the expense of a C—H bond (Figure 64).[327] However, with the N-methylated ligand, C—H activation occurs. The competition between N—H and C—H activation by $CpIr(\kappa^2\text{-}O_2CMe)^+$ on the model substrate $HN{=}CHCNC_4H_4$ was studied by DFT(BP86) calculations. Two isomers of the precursor complex $CpIr(HN{=}CHCNC_4H_4)(\kappa^2\text{-}OAc)^+$ were located with different orientations of the pyrole ring, thus creating N—H···O or C—H···O interactions. The former situation is more stable than the latter by 2.6 kcal mol^{-1}. In both cases, the TS for X—H cleavage is associated with $\kappa^2-\kappa^1$ isomerization of acetate, and the H-transfer is easier from X = N than from X = C ($\Delta E^{\ddagger}$ = 14.2 kcal mol^{-1}, X = N; $\Delta E^{\ddagger}$ = 19.6 kcal mol^{-1}, X = C). Thermodynamics is also in favor of N—H activation (ΔE = −0.3 kcal mol^{-1}, X = N; ΔE = 1.2 kcal mol^{-1}, X = C). It is perhaps surprising that the barrier to C—H activation is only 5.4 kcal mol^{-1} larger than that for N—H activation. This reflects the synergetic nature of acetate-assisted X—H activation, where both X—H···O H-bonding and X—H···M agostic interactions reinforce each other to facilitate the bond activation process. The effect of the acetic acid as a solvent to assist the cyclometalation of amino-imine in palladium complexes has been studied computationally by Aullón and co-workers.[330]

The mechanism of acetate-assisted C—H bond activation by $(acac\text{-}O,O)_2Ir(OAc)$ was studied computationally by Goddard.[331] Interaction energies for benzene and methane C—H bond activation were evaluated using the ALMO-EDA method. The TS for acetate-assisted deprotonation via a six-membered ring has a significantly lower activation barrier than the TS for 1,2-addition across the Ir—O bond via a four-membered TS ($\Delta G^{\ddagger}$ = 25.4 kcal mol^{-1}, six-membered ring, $\Delta G^{\ddagger}$ = 44.7 kcal mol^{-1}, four-membered ring, benzene; $\Delta G^{\ddagger}$ = 30.2 kcal mol^{-1}, six-membered ring, $\Delta G^{\ddagger}$ = 49.5 kcal mol^{-1}, four-membered ring, methane). Ambiphilic bonding character in these transition states is the result of an electrophilic iridium metal interacting strongly with the incoming methyl or aryl group along with a nearly equivalent amount of covalent bonding resulting from deprotonation by acetate.

In the studies by Davies and Macgregor, the C—H bond to activate is brought into close proximity to the acetate group by coordination of the NMe_2 group of DMBA-H. This favorable situation can be achieved in intramolecular arylation reactions catalyzed by palladium. Generally, the catalyst system is composed of a source of Pd(0), a bulky phosphine ligand, and a base (Figure 65). C—X (X = halogen) oxidative addition on Pd(0) anchors the substrate on the metal and generates a situation adapted for further C—H activation.

Echavarren and Maseras have studied the proton-abstraction mechanism in the palladium catalyzed intramolecular arylation with a combined experimental and theoretical approach (Figure 66).[332–334] Similar regioisomeric ratios (1.1−2.4:1) favoring reaction at the substituted aryl ring were obtained, independently of the electronic nature of the R group (electron-releasing or electron-withdrawing), thus ruling out an S_EAr process for the cyclization. In fact, the experimental results would be better explained by a mechanism where the hydrogen from the phenyl is transferred as a proton in the step deciding the selectivity. B3LYP calculations on the model system $PdBr(PH_3)(o\text{-}(CH_2Ph)Ph)$ estimated the activation barrier for *ortho*-C—H oxidative addition to Pd at 43.3 kcal mol^{-1}. This originates from the instability of a Pd(IV) intermediate and the too low basicity of bromide to abstract the proton on the phenyl ring. Substitution of Br^- by HCO_3^-, a model for the base used experimentally (CO_3^{2-}), allowed the location of a TS for proton abstraction assisted by bicarbonate. The activation barrier for the C—H cleavage drops to 23.5 kcal mol^{-1}, an acceptable value for a reaction at 100−135 °C. Introducing three fluorine atoms on the phenyl ring results in an even lower activation barrier (13.2 kcal mol^{-1}), thus confirming the experimental observation that electron-withdrawing substituents accelerate the reaction.

An intermolecular pathway, where the base HCO_3^- abstracts the proton without prior coordination of the base to Pd or substitution of bromide, was also probed by the calculations.[334] The activation barrier was found to be lower than that in the intramolecular pathway for the phenyl case (17.4 versus 23.5 kcal mol^{-1}). In the case of the fluorinated phenyl ring, the intermolecular pathway is computed to be slightly more difficult than the intramolecular reaction (14.4 versus 13.2 kcal mol^{-1}). Both intermolecular and intramolecular pathways can be operative, and the preference for one over the other may depend on the substrate.

For instance, the palladium-catalyzed intramolacular arylation of aryl-bromide can be carried out in the presence of a bidentate phosphine under mild conditions.[334] DFT(B3LYP) calculations of the TS for the intermolecular proton abstraction were carried out on model systems for the monodentate and bidentate phosphine complexes (Figure 67). The activation barriers are of similar magnitude ($\Delta G^{\ddagger}$ = 17.2 kcal mol^{-1}, **60**; $\Delta G^{\ddagger}$ = 16.1 kcal mol^{-1}, **60-F**; $\Delta G^{\ddagger}$ = 20.1 kcal mol^{-1}, **61**; $\Delta G^{\ddagger}$ = 18.9 kcal mol^{-1}, **61-F**) and indicate that the fluorinated ring is preferentially activated (ratio ca. 4:1).

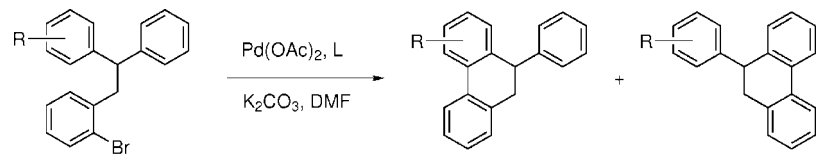

Figure 66. Pd-catalyzed intramolecular arylation with substituted aryl groups.

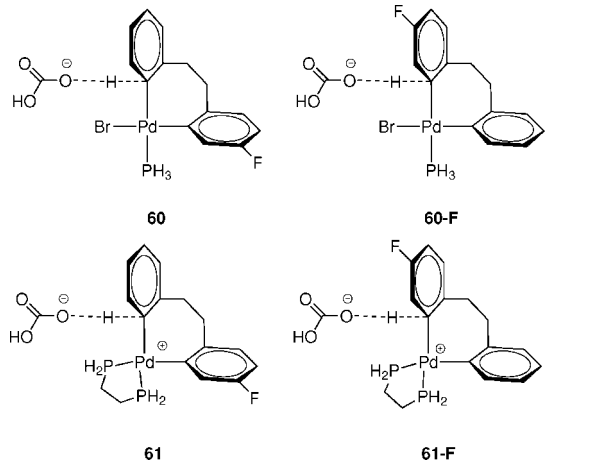

Figure 67. Models of the monodentate and bidentate phosphine complexes used in the calculations for the study of the competition between intermolecular base-assisted C—H activation reactions.

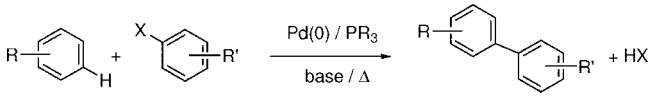

Figure 68. General reaction for catalytic direct arylation.

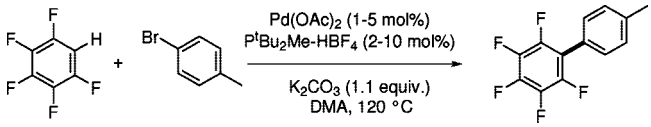

Figure 69. Catalytic intermolecular direct arylation of pentafluorobenzene.

These ratios are in qualitatively good agreement with the ratios observed experimentally (ca. 1.7:1).[333]

Palladium-catalyzed direct arylation of simple arenes (Figure 68) in synthesis of biaryl molecules is a very interesting alternative to classical cross-coupling strategies where aryl organometallic precursors must be prepared beforehand and are sometimes difficult to synthesize or unstable.[335] With direct arylation, the two reacting partners are not part of the same molecule. The C—X oxidative addition does not anchor the other reacting site and has thus no influence on the interaction of the C—H bond with the metal.

Fagnou and Woo have carried out a combined experimental and computational study of the reaction of pentafluorobenzene with parabromotoluene (Figure 69).[336] The catalyst system is assumed to be a monophosphine−Pd(0) complex, and the first reaction is considered to be C—Br oxidative addition to generate the intermediate $Pd(PR_3)(4\text{-}MeC_6H_4)(Br)$. In the B3LYP calculations, this intermediate has been modeled by $Pd(PH_3)(Ph)(Br)$, and six different mechanisms for the C—H activation of C_6F_5H have been considered (Figure 70).

For mechanism A, no oxidative addition Pd(IV) product ($Pd(PH_3)(Ph)(C_6F_5)(Br)(H)$) could be located on the PES, and for mechanism B, no adduct corresponding to an electrophilic attack of Pd on C_6F_5H could be located. Therefore, these two mechanisms are deemed not to be operative. All attempts to locate a TS for intermolecular proton abstraction from a weak adduct of C_6F_5H to $Pd(PH_3)(Ph)(Br)$ as in mechanism C3 failed, because the bicarbonate anion was found to always bind to the Pd center before abstracting the proton. For the mechanism C1, no TS could be located either because it was shown that the reverse reaction is barrierless. The energy of the reaction $Pd(PH_3)(Ph)(Br)(C_6F_5H) \rightarrow Pd(PH_3)(Ph)(Br)(C_6F_5) + HBr$ is taken as an estimate of the activation barrier along this mechanism. Finally, two mechanisms where C—H cleavage is assisted by coordination of acetate (C2 and C4) have led to the characterization of a proper TS structure on the PES. The main difference between the two mechanisms is the nature of the active species and the calculations indicate that the energy barrier is $\Delta E^{\ddagger} = 9.9$ kcal mol^{-1} for C1 and $\Delta E^{\ddagger} = 13.3$ kcal mol^{-1} for C4. Given the high temperature used for the reaction, no preference can be attributed to a particular mechanism.

However, competition experiments were performed between various fluoroarenes, and the results were compared with the calculations on the same systems. The C—C coupling occurs selectively at the position maximizing the number of *ortho*-F's, which has been attributed to the increased acidity of the C—H bond at this position. The agreement between experimental and computational ratios of regioisomers is much better for mechanism C2 than for mechanism C4. Fagnou has coined the name concerted metalation deprotonation (CMD) for this mechanism where the hydrogen is abstracted by the coordinated base simultaneously as the M—C bond is formed.

The characteristics of the CMD mechanism have been analyzed through calculations of C—H activation in a broad range of aromatic substrates.[37] The calculations show that activation barriers for C—H activation critically depend on the position of the C—H bond in the ring. To elucidate the origin of this effect, an activation strain analysis was performed (Figure 71). The E_{dist} term reflects the energy needed to distort both reactants to the geometry of the TS. For the palladium complex, the energy range spanned is rather narrow (from 15.4 to 20.4 kcal mol^{-1}). In contrast, for the aromatic substrate, the variation is large (from 29.3 to 50.1 kcal mol^{-1}). Thus the reactivity of the various C—H bonds cannot be explained solely with Brönsted acidity arguments. The E_{int} term reflects the stabilization introduced by the simultaneous Pd···C and O···H interactions in the TS and varies between −32.2 and −58.0 kcal mol^{-1}. Further studies are nevertheless needed to better understand the factors controlling E_{dist} and E_{int} and establish predictive rules for the optimization of palladium-catalyzed biaryl synthesis.

The CMD mechanism was shown to be operative in the direct arylation of arene C—H bonds in phenyl-pyridine by a NHC−Ru(II) complex.[337] DFT calculations by Maseras probed two different pathways. Coordination of pyridine would normally lead to easy *ortho*-C—H activation through oxidative addition. However, the $Ru(Cl)_2(IMe)$ (IMe = *N*,*N*′-dimethylimidazol-2-ylidene) fragment does not allow for any σ-CAM transformations, and the Ru(IV) complex resulting from oxidative addition lies at high energy ($\Delta E = 28.2$ kcal mol^{-1}). Coordination of HCO_3^- to Ru stabilizes the system by 22.9 kcal mol^{-1}, and from this intermediate, CMD is possible with an energy barrier of 13.9 kcal mol^{-1} and an exothermic reaction energy of −13.7 kcal mol^{-1}. More aryl and heterocyclic C—H bond functionalizations should be possible with catalysts offering an easy orthometalation pathway via metal/base cooperative proton abstraction.

The direct arylation reaction has been extended to the intramolecular activation of aliphatic C—H bonds (Figure 72).[338] When different aliphatic groups are present that may undergo reaction, high selectivity is observed for reaction at a methyl substituent over a secondary carbon. To further

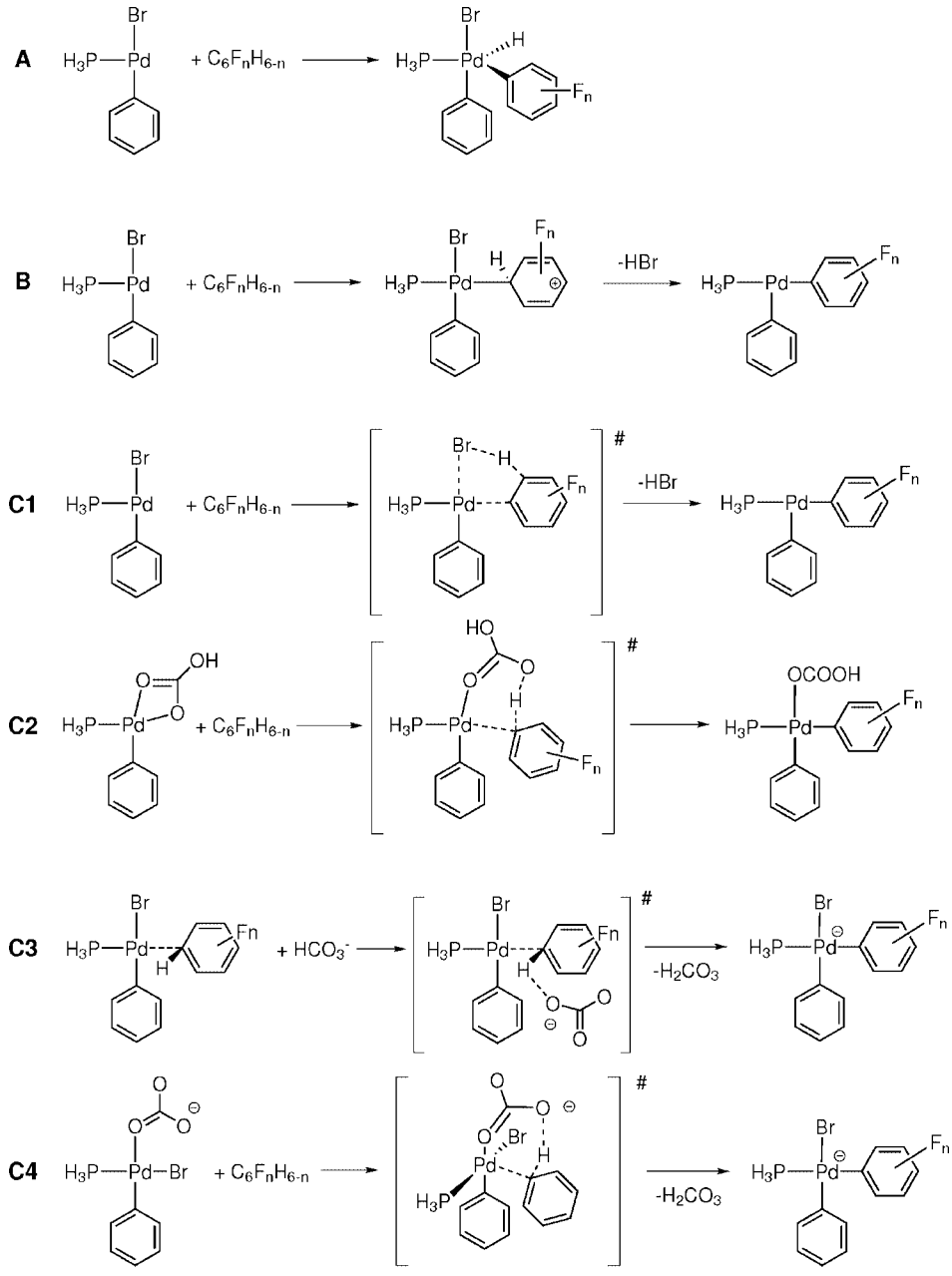

Figure 70. Mechanisms considered for the C—H bond activation of benzene by $Pd(PH_3)(Ph)(Br)$ with added HCO_3^-.

understand the parameters leading to this selectivity, B3LYP calculations examined the mechanism of C—H cleavage. Here again a Pd(IV) pathway involving an oxidative addition was ruled out. In the calculations, the base was modeled by AcO^- and the phosphine by PMe_3. Within the framework of the CMD mechanism, three different TS structures were located corresponding to C—H activation at various positions ($C\mathbf{H}_3$, $C\mathbf{H}_3CH_2$, and $CH_3C\mathbf{H}_2$, see Figure 72). At the TS, agostic interaction occurs between the σ(C—H) bond and the Pd(II) atom, resulting in significant weakening of the C—H bond. This interaction and the formation of the O···H—C bond compensate for the loss of C—H bonding and explain the relatively low activation barriers. The lowest value is obtained for the activation at the methyl group forming the six-membered palladacycle, in agreement with the experimental observations.

The CMD mechanism was also shown to operate in the synthesis of benzocyclobutene by palladium-catalyzed C—H activation of methyl groups (Figure 73).[339] For the reaction

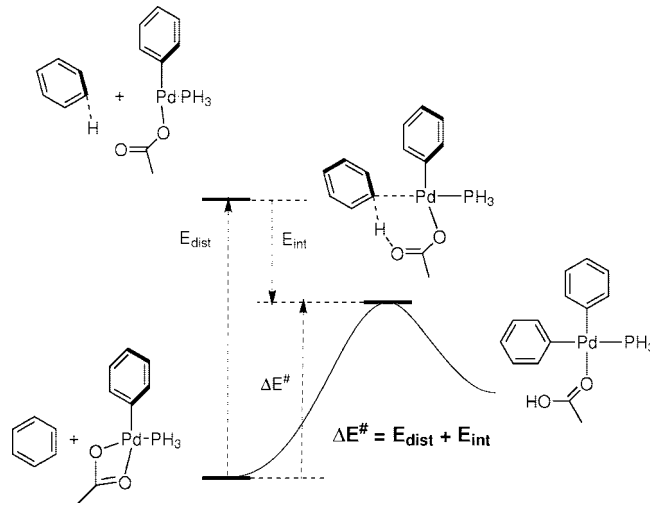

Figure 71. Scheme for the activation-strain analysis with definition of E_{dist} and E_{int} and their relation to $\Delta E^{\ddagger}$.

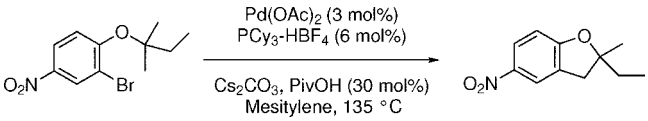

Figure 72. Palladium-catalyzed intramolecular alkane arylation.

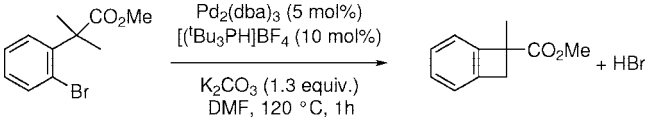

Figure 73. Optimized conditions for the synthesis of benzocyclobutenes.

of 2-^{t}Bu-bromobenzene, the complete catalytic cycle with Pd(P^tBu_3) as the model for catalyst was computed at the B3PW91 level with inclusion of the influence of the solvent DMF (PCM single point calculations). The influence of the base was also tested by considering three different cases (acetate, bicarbonate, and carbonate). Of the three different steps (C−Br oxidative addition, C−H activation, and C−C coupling), the intramolecular C−H activation by Pd(II) complexes presents the highest energy barrier ($\Delta E^{\ddagger} = 4.7$ kcal mol^{-1}, C−Br oxidative addition; $\Delta E^{\ddagger} = 27.6$ kcal mol^{-1}, C−H oxidative addition with CO_3^{2-}; $\Delta E^{\ddagger} = 22.5$ kcal mol^{-1}, C−C coupling reaction). Experimentally, the nature of the base is shown to influence drastically the yield of the reaction with quantitative transformation with carbonate, 80% yield with bicarbonate, and only 10% yield with acetate. In the square planar geometry traditionally proposed for CMD transition states at Pd(II), the aryl and the phosphine are cis, thus leading to a cis relative position for the base and the C−H bond to be cleaved. Such a geometry in the TS failed to reproduce the experimental result since the energy barriers were calculated to vary as acetate < bicarbonate < carbonate. The high barrier for CO_3^{2-} is due to the necessary $\kappa^2-\kappa^1$ isomerization of the base before actual proton abstraction. In another geometry for the TS, where aryl and phosphine are trans, only κ^1 coordination of the base trans to the agostic C−H bond allows proton transfer. In that case, the relative values for the energy barriers, carbonate < bicarbonate < acetate, are in agreement with the relative yields observed experimentally. Moreover, this TS structure also allows proton transfer to the aromatic ring, thus providing an explanation for the formal 1,4 migration observed with some substituted aromatic rings.

Heteroatom-assisted C−H activation by carboxylate or carbonate bases are particularly prominent in the development of new catalysts where C−H activation can be exploited in synthesis. The common features of such processes appear to be the simultaneous ambiphilic activation by a Lewis acidic metal center and an intramolecular base. Macgregor and Davies have suggested using the acronym AMLA (ambiphilic metal−ligand activation) for such reactions.[38]

4. Catalytic Alkane and Arene Functionalization

Catalytic reactions based on C−H activation are not yet frequent, and computational studies of the full cycle are even rarer. Very often, computational studies of catalytic reactions have focused on some selected parts of the cycle. This is the case of many reactions involving chelation-assisted C−H activation (section 3.2) or base-assisted C−H activation (section 3.4). Several reactions based on C−H σ-bond metathesis are catalytic and described in section 2.2. In the following section, we describe three groups of reactions where the computational studies help to understand the catalytic nature of the reaction. The first subsection on dehydrogenation of alkanes has been complemented by studies on stoichiometric dehydrogenation of alkanes where computational results help to understand better the crucial step of dehydrogenation.

4.1. Alkane Dehydrogenation

Alkane dehydrogenation is highly demanding thermodynamically and kinetically because of the strength of the C−H bond (BDE(C−H) $\simeq$ 105 kcal mol^{-1} in methane) and also because it is the reverse of a $2\pi + 2\sigma$ addition typically forbidden by symmetry rules. A transition metal fragment can mediate an alternative path to the forbidden direct reaction. The endothermic aspect of the reaction can be dealt with by a sacrificial hydrogen acceptor. Therefore alkane dehydrogenation can be achieved if it becomes an alkane transfer dehydrogenation using an olefin as a sacrificial hydrogen acceptor. Several transition metal complexes have been found to be able to catalyze such reaction. The first catalysts were made by Felkin with Re, Ru, and Ir polyhydrides[340,341] and also by Crabtree for Ir polyhydride.[342,343] The next generation of catalysts were Rh catalysts.[344,345] Jensen and Kaska discovered that iridium pincer complexes ($^{R'}$PCP)IrH_2 where $^{R'}$PCP = κ^3-2,6-(R′$_2$PCH_2)$_2C_6H_3$Ir were active catalysts.[19,346,347] Acceptorless dehydrogenation is a reaction that is even more attractive because it does not require the sacrificial olefin, and the loss of H_2 expelled from solution makes the reaction thermodynamically possible. The proof of principal of this reaction (reflux-driven removal of H_2 was first shown by Saito[348] and by Crabtree,[349] and efficiency was greatly increased with the Ir pincer complexes.[40,350] This reaction led to the remarkable discovery of the catalytic alkane metathesis by tandem alkane dehydrogenation/olefin metathesis.[42] It should be noted that the reaction in the presence of sacrificial olefin occurs at relatively low temperature ($T < 100$ °C), while the acceptorless reaction requires higher temperature ($T > 150$ °C).

The catalytic dehydrogenation of an alkane R−H by a metal fragment ML_n is mechanistically a simple reaction made of two successive C−H bond cleavages: (1) in the first step, the C−H bond of the alkane RH is oxidatively added to the metal fragment L_nM to form the hydrido alkyl complex, $L_nM(H)(R)$; (2) in the second step, a β-H elimination from the alkyl complex forms the olefin and leaves an additional hydride on the metal to form L_nMH_2. L_nMH_2 has to return to L_nM by losing the two hydrogen atoms. Computational studies were carried out on the reaction of the pincer dihydrido Ir(III) complex, ($^{R'}$PCP)IrH_2, with various alkanes to determine how the reaction occurs in presence of sacrificial olefin and in the acceptorless conditions.[351−358] The studies focused on the nature of the mechanism, which can be either dissociative or associative with or without the sacrificial olefin (Figure 74).

The reaction with sacrificial olefin was studied by Hall et al. with DFT(B3LYP) calculations for the iridium pincer complex with κ^3-2,6-(H_2PCH_2)$_2C_6H_3$) as the PCP ligand, ethylene as the hydrogen acceptor, and ethane as the substrate.[352] The calculations show that the transfer dehydrogenation of ethane by (PCP)IrH_2 occurs with two distinct stages. First, (PCP)IrH_2 is dehydrogenated by the hydrogen acceptor (coordination of C_2H_4 cis to the PCP ligand, followed by insertion of ethylene into the Ir−H bond and

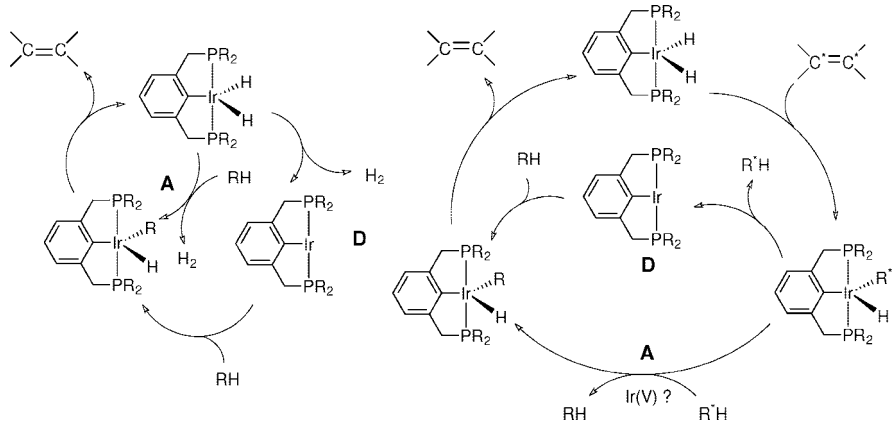

Figure 74. (PCP)Ir-catalyzed acceptorless alkane dehydrogenation (left) possible associative (**A**) and dissociative (**D**) pathways and (PCP)Ir-catalyzed alkane transfer-dehydrogenation (right) possible associative (**A**) and dissociative (**D**) pathways.

by the reductive elimination of ethane). This yields the 14-electron (PCP)Ir complex that reacts with ethane by way of oxidative addition into the C—H bond, β-H elimination, and dissociation of ethylene cis to the PCP ligand with regeneration of the catalyst. The formation of the unsaturated intermediate (PCP)Ir is an endothermic reaction by 12.7 kcal mol^{-1} and proceeds by a cis-pathway. The critical steps of the reaction are the hydride transfer to ethylene, ethane oxidative addition, and dissociation of the coordinated ethylene with energy barriers of 14, 11.6, and 23.4 kcal mol^{-1}, respectively. The acceptorless reaction with the same model is strongly energetically disfavored.[351,356] Calculations with the anthraphos ligand, which renders the catalyst thermodynamically stable have shown that the dissociative (by way of an Ir(I) intermediate) and the associative pathway (by way of an Ir(V) intermediate), as well as a concerted pathway where H_2 leaves as the alkane adds, have similar activation barriers at 298 K.[354]

Krogh-Jespersen and Goldman have carried out a series of computational studies on the reaction mechanism with a particular emphasis on the role of the temperature in the acceptorless process.[353,355,357,358] In their first study,[353] they used DFT(B3LYP) calculations to examine the C—H bond cleavage in alkanes (R—H = CH_3—H, C_2H_5—H, C_3H_7—H) and arenes (R—H = C_6H_5—H) by both (PCP)Ir and (PCP)IrH_2. The conclusions are different using the electronic energy barriers ($\Delta E^{\ddagger}$, no ZPE corrections) and the Gibbs free energy barriers ($\Delta G^{\ddagger}$). Using the electronic energy values, the associative mechanism is preferred over the dissociative mechanism. However the two pathways have comparable Gibbs free energy barriers with a marginal preference for the dissociative pathway. This preference will increase at higher temperature and with both bulkier phosphine and alkane substrates. The dissociative pathway is therefore also preferred for the hydrocarbon/hydrocarbon exchange, which is required in the case of transfer dehydrogenation because the coordination energy of alkanes is very small.

The acceptorless reaction occurs only at high temperature. The lowest temperature at which the reaction was found to be possible is 150 °C for the easily dehydrogenated substrate cyclooctane. Combining computational chemistry with classical thermodynamic considerations led Krogh-Jespersen and Goldman to show that the dissociative pathway was significantly preferred at the temperatures used experimentally.[355] The dissociative pathway for the reaction of (^{Me}PCP)IrH_2 with cyclohexane and propane is calculated to have an energy barrier of ca. 36 kcal mol^{-1}; the highest transition state corresponds to the oxidative addition of the alkane to the 14-electron (^{Me}PCP)Ir fragment obtained after loss of H_2. This energy barrier transforms into a free energy barrier of 36 kcal mol^{-1} at standard thermodynamic conditions (P_{H_2} = 1 atm and T = 298 K). However, a free energy barrier of only 18 kcal mol^{-1} for the C—H activation step is calculated for conditions under which the dehydrogenation is thermodynamically possible (T = 423 K and $P_{H_2} = 10^{-7}$ atm with concentration of hydrocarbon C—H bonds equal to those in neat solution). The rate-determining step of the catalytic cycle is now the loss of H_2 from (^{Me}PCP)IrH_2 with an activation energy barrier of 27.2 kcal mol^{-1}. The associative pathway has an energy barrier for the C—H activation step of $\Delta E^{\ddagger}$ = 20.1 kcal mol^{-1} and for the whole reaction of $\Delta E^{\ddagger}$ = 28.4 kcal mol^{-1} (loss of H_2). The energy barriers translate into Gibbs free energy barriers of $\Delta G^{\ddagger}$ = 32.2 kcal mol^{-1} for the C—H bond activation step and $\Delta G^{\ddagger}$ = 37.4 kcal mol^{-1} for subsequent loss of H_2 at standard thermodynamic conditions. In the simulation of the experimental conditions, the respective values for the Gibbs free energy barriers for the C—H addition and H_2 loss are 31.3 and 36.0 kcal mol^{-1}. The preference for the dissociative pathway is thus nonambiguous. The dissociative pathway is shown to account also for the lack of H for D exchange in cyclohexane-d_{12}. Substitution of the pincer ligand at the para position by a π donor such as methoxy groups gives catalytic activity higher than unsubstituted analogues.[358] However, DFT calculations do not provide a clear interpretation of the substituent effects because the methoxy group stabilizes the transition state as much as the resting state. A computational and experimental study of the effect on catalytic activity resulting from systematically varying steric crowding by the substitution of one methyl group for one of the phosphine *tert*-butyl groups of the ^{tBu_4}PCP ligand has been recently published.[359] The electronic structure calculations show that a single Me-for-^{t}Bu substitution has a favorable energetic effect on the β-H elimination step. However, the stabilizing effect on the overall barrier is shown to be partially offset by the stronger binding of the 1-alkene to the $^{Me\,tBu_3}$PCPIr catalyst.

The relation between alkane dehydrogenation and alkene H for D exchange was considered computationally by Eisenstein and Crabtree for $IrH_2(O_2CCF_3)_2(PAr_3)_2$ (Ar = p-FC_6H_4).[88] It is shown that the H/D scrambling involves the insertion of the olefin to give an alkyl hydride complex that reductively eliminates to lead to a transition state that contains an η^3-bound alkane. The relatively large binding

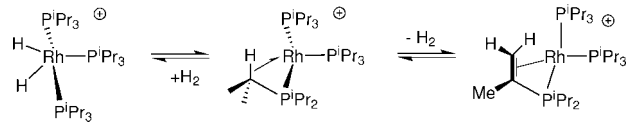

Figure 75. Alkane dehydrogenation in a Rh(I) complex via an isolated agostic intermediate.

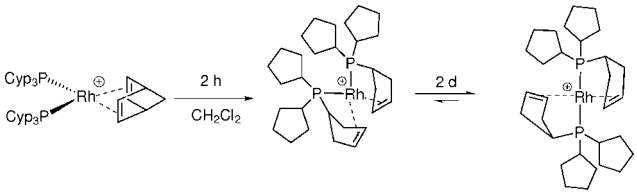

Figure 76. Intramolecular alkyl phosphine dehydrogenation in cationic rhodium complexes of $P(Cyp)_3$ (Cyp = cyclopentyl).

energy of the alkane, which is ascribed to the poor electron donating power of O_2CCF_3, allows the H for D exchange to occur.

Alkyl dehydrogenation in a Rh(I) complex via an isolated agostic intermediate was studied by a combined experimental and computational approach by Macgregor and Weller.[360] The T-shaped 14-electron rhodium phosphine complex $[Rh(P^iPr_3)_3][BAr^F_4]$ (Ar^F = 3,5-$(CF_3)_2C_6H_3$ was shown to contain an unusual β-C—H agostic interaction from the isopropyl phosphine ligand and undergoes intramolecular dehydrogenation (Figure 75). DFT calculations on the cationic system $Rh(PH_2{}^iPr)(PH_3)_2{}^+$ show that several structures are possible. The most stable is a γ-agostic system, while the β-agostic complex is 5.6 kcal mol^{-1} higher in energy. C—H activation in the β- and γ-agostic complexes yield three- and four-membered metallacycles, respectively. The latter is more stable. The calculations show that only the metallacyclophosphapropane can achieve full dehydrogenation, as observed experimentally. This shows that only the product of C—H activation at the β-position can lead to productive dehydrogenation.

Weller and Macgregor have carried out an experimental and computational study of $Rh(nbd)(PCyp_3)_2$ (nbd = norbornadiene, $PCyp_3$ = tri(cyclopentylphosphine)), which spontaneously undergoes dehydrogenation of each $PCyp_3$ ligand in CH_2Cl_2 solution to form an equilibrium mixture of *cis*- and *trans*-$[Rh(PCyp_2(\eta^2\text{-}C_5H_7)]_2[BAr^F_4]$ (Figure 76).[361] Furthermore competition experiments using mixed cyclohexyl cyclopentyl phosphine ligand $PCy_2(Cyp)$ show that $RhCl(nbd)(PCy_2(Cyp))_2{}^+$ undergoes dehydrogenation at the cyclopentyl group. The DFT(BP86) calculations were carried out on the neutral complexes $Rh(dppe)PCyp_3$ and $Rh(dppe)PCy_3$. The C—H activation in the cyclopentylphosphine complex forms directly the rhodium hydride complex with an energy barrier of 9.9 kcal mol^{-1}. The corresponding reaction in the cyclohexylphosphine complex has a slightly higher energy barrier of 13.6 kcal mol^{-1} and a conformational change in the chairlike cyclohexyl substituent is required to yield the final hydrido product. The lower energy barriers for the C—H activation in the cyclopentyl case are related to the presence of agostic interactions in the reactant. Interestingly, an additional agostic C—H interaction appears at the transition state in the cyclopentyl case (Rh···C = 2.47 Å, C—H = 1.11 Å), while the corresponding Rh···H distance is over 3 Å in the cyclohexyl species. The final dehydrogenation requires β-H transfer and H_2 elimination. The potential energy surfaces for the two systems are parallel for this stage of the reaction, but that for cyclohexyl is 5 kcal mol^{-1} higher in energy than that for the cyclopentyl case. The results are in good agreement with the experimental results of this paper and the known greater propensity for cyclopentylphosphine to dehydrogenate further. This property led to interesting complexes with reversible H_2 uptake[362] or formation of Ru(0) complexes.[363,364]

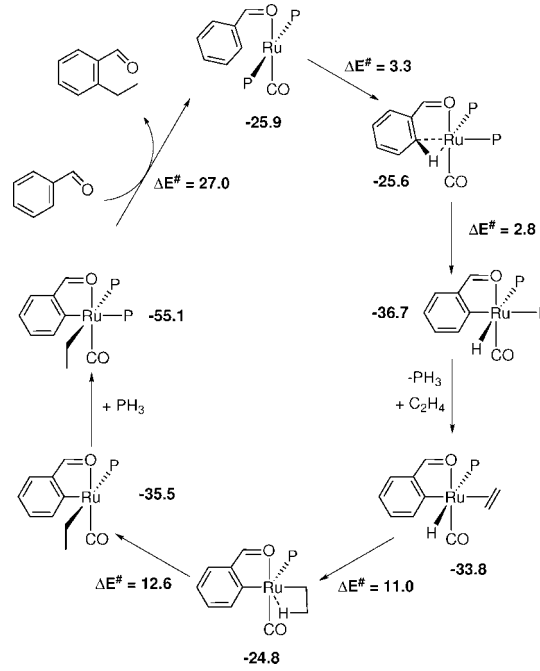

Figure 77. Computed catalytic cycle (B3LYP) for the insertion of ethylene in the *ortho*-C—H bond of benzaldehyde. The energies (kcal mol^{-1}) of the various intermediates are expressed relative to the separated reactants, benzaldehyde and $Ru(PH_3)_2(CO)$, and the energy barriers are given for each elementary step. P stands for PH_3.

4.2. Hydroarylation of Olefins

The Murai reaction is one of the early examples of catalytic functionalization of an aromatic C—H bond.[16] The reaction consists of the selective insertion of an olefin into an aromatic C—H bond ortho to an orientating group. Even though Jordan has shown catalytic insertion of propene into the *ortho*-C—H bond of α-picoline in 1989,[281] the reaction was shown to be limited to α-picoline and propene. The Murai reaction, in contrast, shows a larger scope of substrates that are able to insert a great variety of alkenes. A typical catalyst for this reaction is $Ru(H)_2(CO)(PPh_3)_3$, and the transformation is usually carried out in refluxing toluene. The active species is assumed to be a Ru(0) complex after hydrogen abstraction by the alkene in excess under the catalytic conditions.

A computational study at the B3LYP level was carried out by Morokuma to characterize the entire catalytic cycle.[365] Two different active species were considered in the model, $Ru(CO)(PH_3)_2$ and $Ru(CO)(PH_3)_3$. The substrate was benzaldehyde and ethylene was the inserting alkene.

The most favorable pathway starts with O-coordination of benzaldehyde trans to the carbonyl group of $Ru(CO)(PH_3)_2$ with a stabilization of $\Delta E = -25.9$ kcal mol^{-1} (Figure 77). The C—H activation is a two-step process with the formation of an agostic interaction ($\Delta E^{\ddagger} = 3.3$ kcal mol^{-1}) followed by the actual cleavage of the C—H bond ($\Delta E^{\ddagger} = 2.8$ kcal mol^{-1}). These two energy barriers are very low and show the critical influence of the coordination of the carbonyl

group to ease the activation of the *ortho*-C—H bond. From the C—H activation product, substitution of the labile phosphine trans to the Ru—C bond by ethylene affords the required cis-geometry for alkene and H to facilitate the alkene insertion into the Ru—H bond. The latter is endothermic by $\Delta E = 9$ kcal mol^{-1} with a low energy barrier ($\Delta E^{\ddagger} = 11.0$ kcal mol^{-1}). The high energy of the insertion product is a result of creating the new Ru—C bond trans to the already existing Ru—C bond with the aromatic ring. Loss of the agostic interaction trans to phosphine, associated with the rotation of the ethyl ligand around the Ru—C bond ($\Delta E^{\ddagger} =$ 12.6 kcal mol^{-1}), allows the latter to be cis to the aryl group. This isomer is 1.7 kcal mol^{-1} more stable than the hydrido-alkene complex. Further stabilization is achieved through PH_3 coordination at the vacant site. The complex obtained presents the ideal geometry for C—C reductive reaction. Despite the favorable geometrical features, the C—C coupling is the rate-determining step with a calculated energy barrier $\Delta E^{\ddagger}$ of 27.0 kcal mol^{-1}, in agreement with the experimental observations.

An interesting feature of homogeneous catalysis is to provide synthetic strategies that allow formation of products traditionally difficult to obtain. Periana has shown that bis-(acac-O,O)-Ir(III) complexes (acac-O,O = κ^2-O,O-acetylacetonate) are active catalysts in the anti-Markovnikov arylation of olefins with benzene to produce straight-chain alkylbenzenes with higher selectivity than the branched ones.[43,366,367] The experimental observation indicated that the catalysis proceeds by arene C—H bond activation by way of a thermally stable homogeneous mononuclear (acac-O,O)$_2$Ir(py)(Ph) species (py = pyridine).[43]

In a series of papers, Goddard and Periana studied the catalytic cycle of homogeneous Ir(III) catalyzed regioselective arylation of alkenes,[200,368,369] even though these reactions have limited use (high temperatures, extended reaction times, limited activity). In the first contribution, the mechanism of hydroarylation of olefins by a homogeneous (acac-O,O)$_2$Ir(H$_2$O)(Ph) catalyst is elucidated by B3LYP calculations (Figure 78).[200]

After dissociation of the water ligand, a vacant site is generated and ethylene coordination is possible. However, coordination of ethylene to the empty coordination site following departure of water would lead to a complex with the phenyl and ethylene ligands in trans coordination, hence preventing the insertion of ethylene in the metal−phenyl bond. The bis-acac complex has to isomerize to bring the two acac ligands in cis coordination, which opens the empty coordination site cis to the phenyl ligand. This isomerization was shown to proceed on the ML$_5$ (acac-O,O)$_2$Ir(Ph) complex with an activation barrier $\Delta G^{\ddagger} = 25.9$ kcal mol^{-1} in good agreement with the experimental value of 28.7 kcal mol^{-1} at 413−473 K. Coordination of ethylene leads to the *cis*-(acac-O,O)$_2$Ir(Ph)(C$_2$H$_4$) intermediate lying slightly above the starting reactants *trans*-(acac-O,O)$_2$Ir(Ph)(H$_2$O) and ethylene ($\Delta G = 4.5$ kcal mol^{-1}). Insertion of ethylene into the Ir—Ph bond has an activation barrier of $\Delta G^{\ddagger} = 24.8$ kcal mol^{-1} and produces the ethylbenzene complex with coordination of one *ortho*-C—H bond of benzene. Coordination of a new benzene molecule instead of the *ortho*-C—H bond is not favored entropically but sets the system for further C—H activation. The latter proceeds along an OHM transfer (see section 2.4) with $\Delta G^{\ddagger} = 12.9$ kcal mol^{-1} and $\Delta G = 0.2$ kcal mol^{-1}. Finally, substitution of the η^2-(C—H) bond of

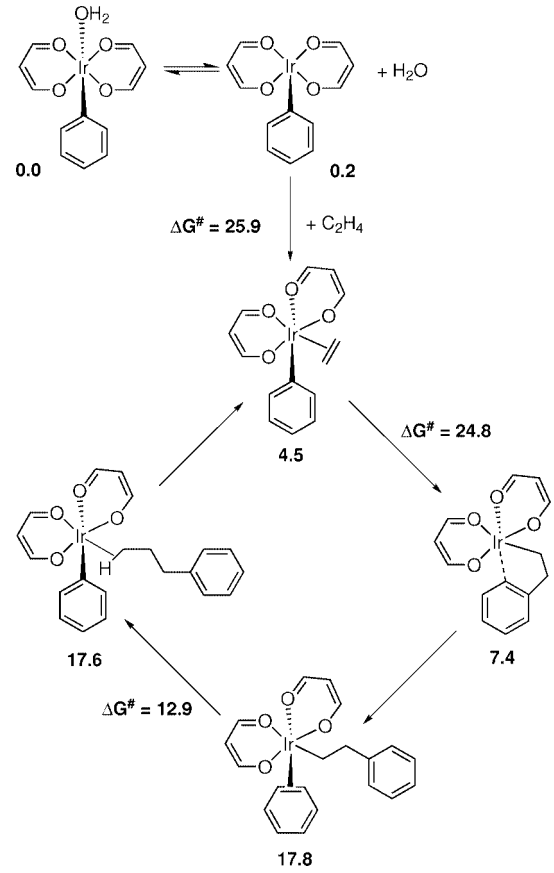

Figure 78. Computed catalytic cycle for the formation of ethylbenzene by insertion of ethylene into the C—H bond of benzene in presence of (acac-O,O)$_2$Ir(Ph)(H$_2$O). Gibbs free energies (kcal mol^{-1}) are expressed relative to ethylene and the water complex. The activation barriers are given for each elementary step.

the ethylbenzene produced by a new ethylene molecule closes the catalytic cycle.

The authors find that the rate-determining step is olefin insertion into the Ir—Ph bond. Calculations of the transition states of olefin insertion for various alkenes (propene, styrene, and isobutene) probed at the regioselectivity between 1,2 and 2,1 insertion. The experimental ratios between the branched and the linear alkylbenzene allow the determination of $\Delta\Delta G^{\ddagger}$ for the rate-determining step. These experimental values can be directly compared with the calculated values from the energies of the two transition states for insertion. The agreement is excellent, and the preference for the linear isomer is shown to be preferentially due to the electron-donating character of the substituent of the alkene. The steric influence of the substituent has a lower influence to prevent insertion leading to a branched isomer.

From the ethylbenzene product of ethylene insertion (Figure 78), a β-hydride elimination is possible generating a hydrido-styrene complex. This process is calculated to be easier than benzene coordination because the β-H elimination is an intramolecular reaction. This pathway constitutes a potential deactivation route. However, the dissociation energy of styrene is computed to be larger than the activation barrier for insertion of styrene into Ir—H (the reverse of β-elimination). Therefore, if formed, the hydrido-styrene would preferentially revert to the ethylbenzene, and the catalytic cycle could eventually be closed.

Inhibition of the catalyst by ethylene was also studied computationally. Again, from the ethylbenzene product of

the ethylene insertion into the Ir—Ph bond, coordination of ethylene at the vacant site leads to an adduct more stable than benzene coordination. The ethylene complex can follow two different paths, insertion in the Ir—C bond to give a butylbenzene intermediate or C—H activation through an OHM process to release the product (ethylbenzene) and a vinyl complex. These two routes are associated with transition states with similar Gibbs free energies. One pathway is productive, while the other leads to multi-insertion products. Calculations indicate that both are likely to occur. This explains the experimental results of diminution of the TOF upon increase of the ethylene/benzene ratio.

A detailed analysis of the C—H bond activation of benzene was carried out experimentally and computationally on (acac-O,O)$_2$Ir(R)(py) (py = pyridine; R = CH_3, C_2H_5, Ph, CH_2CHPh).[368] Pyridine dissociation easily generates *trans*-(acac-O,O)$_2$Ir(R), and the C—H activation reaction necessitates further isomerization to produce the *cis*-acac intermediate. This reaction constitutes the bulk of the barrier for the C—H activation. Overall the C—H activation reaction has been shown to proceed in four key steps: (i) a pre-equilibrium loss of pyridine, (ii) a rate-determining unimolecular isomerization of the *trans*-(acac-O,O)$_2$Ir(R) to the *cis*-(acac-O,O)$_2$Ir(R) complex, (iii) coordination of benzene to the cis-isomer, and (iv) rapid C—H cleavage. With the ultimate goal of designing more active catalysts for the hydroarylation of unactivated olefins, Periana synthesized (trop-O,O)$_2$Ir(Ph)(py) (trop-O,O = κ^2-O,O-troponolate).[369] The catalytic activity of this new system is comparable to that of (acac-O,O)$_2$Ir(Ph)(py). The computed reaction pathway for the transformation was very similar to that computed with the acetylacetonate complex.

In an interesting variation, Periana showed that (acac-O,O)$_2$Ir(py)(vy) (vy = HC═CH_2) is a catalyst for the hydrovinylation of olefins.[370] The products of the reaction are 1-butene and *cis*- and *trans*-2-butene in a 1:2:1 ratio. Calculations by Goddard showed that a mechanism similar to that for the hydroarylation of olefin is operative.[371] After dissociation of pyridine and trans−cis isomerization, a coordinated ethylene inserts into the Ir—vy bond to generate an Ir—CH_2—CH_2—CH═CH_2 complex. The latter isomerizes to an Ir(η^3-allyl) complex through a series of β-hydride transfer reactions. This η^3-allyl intermediate is the most stable species and constitutes the resting state of the catalyst. The $\eta^3-\eta^1$ isomerization of the allyl opens a coordination site for ethylene followed by C—H activation through an OHM process, which generates the product 2-butene and reforms the vinyl complex. The C—H activation is computed to be rate-determining with $\Delta H^{\ddagger}$ = 31.6 kcal mol^{-1} and $\Delta G^{\ddagger}$ = 32.1 kcal mol^{-1}. Formation of 1-butene is not favorable from the η^3-allyl complex, and the experimental observation of 1-butene is explained by isomerization of 2-butene after release of the latter from Ir.

Another system, TpRu(CO)(NCMe)(Ph), was shown by Gunnoe to catalyze the addition of arene to ethylene and propene.[44] The catalyst system is mildly selective for the linear alkylbenzene with an observed ratio of 1.6:1 in favor of propylbenzene with respect to isopropylbenzene. The catalytic cycle for this transformation has been determined computationally by Goddard (Figure 79).[201] The calculations were carried out using the experimental system and ethylene. The reaction starts with dissociation of acetonitrile and coordination of ethylene. The Tp ligand imposes a fac geometry for the three other ligands, which drives the phenyl and ethylene ligands in cis coordination. The next step is ethylene insertion to produce an ethylbenzene, which interacts weakly with the metal by the benzene ring. This intramolecular benzene coordination is easily converted into an intermolecular coordination of an additional benzene molecule. C—H activation directly transfers the hydrogen atom from benzene to the ethyl group, generating the product without explicit formation of a Ru(IV) intermediate. The TS of C—H cleavage features the short Ru···H distance typical of OHM transition states (see section 2.4).

The mechanism calculated for the present Ru(II) system has been contrasted with the mechanism calculated for Ir(III).[201] In both cases, the rate-determining step is ethylene insertion into M—Ph. For this step, the activation barrier for Ru is 3.8 kcal mol^{-1} lower than that for Ir, thus rationalizing the rate enhancement of 200 at 90 °C observed experimentally between the Ru and Ir catalysts. The C—H bond activation step, on the other hand, is higher in energy in the Ru system. The opposite trends in the two key steps will influence the outcome and yield of the catalytic hydroarylation. Improving C—H activation would most likely impede insertion and thus overall rate, while improving insertion and impeding C—H activation would most likely lead to faster rates but extensive polymerization.

A detailed mechanistic analysis of hydroarylation catalysts has been carried out by Periana and Goddard for a large number of metal fragments.[372] There are two key steps in the process: (i) insertion of ethylene into the M—Ph and (ii) C—H activation of an unactivated benzene. These two key steps were computed for TpRu(CO)(Ph) and *cis*-(acac-O,O)$_2$Ir(Ph), the two complexes shown to be active catalysts, but also for Rh, Pd, Os, and Pt with similar ligand sets. From the extended set of data, it appears that the activation barrier for the two key steps are inversely correlated, complicating optimization of the overall process. The accessibility of the M^{n+2} oxidation state is at the heart of this behavior. The C—H activation, as an OHM transfer, develops a M^{n+2} oxidized character in the TS, which makes it easier for more easily oxidized metal (Ir(III) vs Ru(II)). An easily energetically accessible M^{n+2} state implies that a low-lying unoccupied d orbital is available. The metal is acidic, and coordination of an olefin is stronger, thus making the olefin insertion more difficult through a ground-state stabilization effect.

A long-standing collaboration between the experimental group of Gunnoe and the computational group of Cundari led to a detailled study of the catalytic properties of the TpRu system.[202,373–378] An account of this collaboration has been recently published.[379] The first calculations were carried out on the model (Tab)Ru(CO)(Ph) (Tab = HB(—N═NH)$_3$) and ethylene.[373] The computational study particularly addressed the nature of the C—H activation step and showed that no Ru(IV) intermediate was implied.

The complex TpRu(CO)(NCMe)(Me) was shown to initiate C—H bond activation at the 2-position of furan and thiophene to produce TpRu(CO)(NCMe)(Ar) (Ar = 2-furyl, 2-thienyl).[374] The 2-furyl complex serves as a catalyst for the formation of 2-ethylfuran from ethylene and furan. DFT calculations specifically studied the nature of the C—H activation process.

Substituting CO with PMe_3 in TpRu(CO)(NCMe)(Ph) gave a system that exhibited lower catalytic activity in the hydrophenylation of ethylene.[376] For TpRu(PMe_3)(NCMe)(Ph), C—H activation of ethylene to ultimately

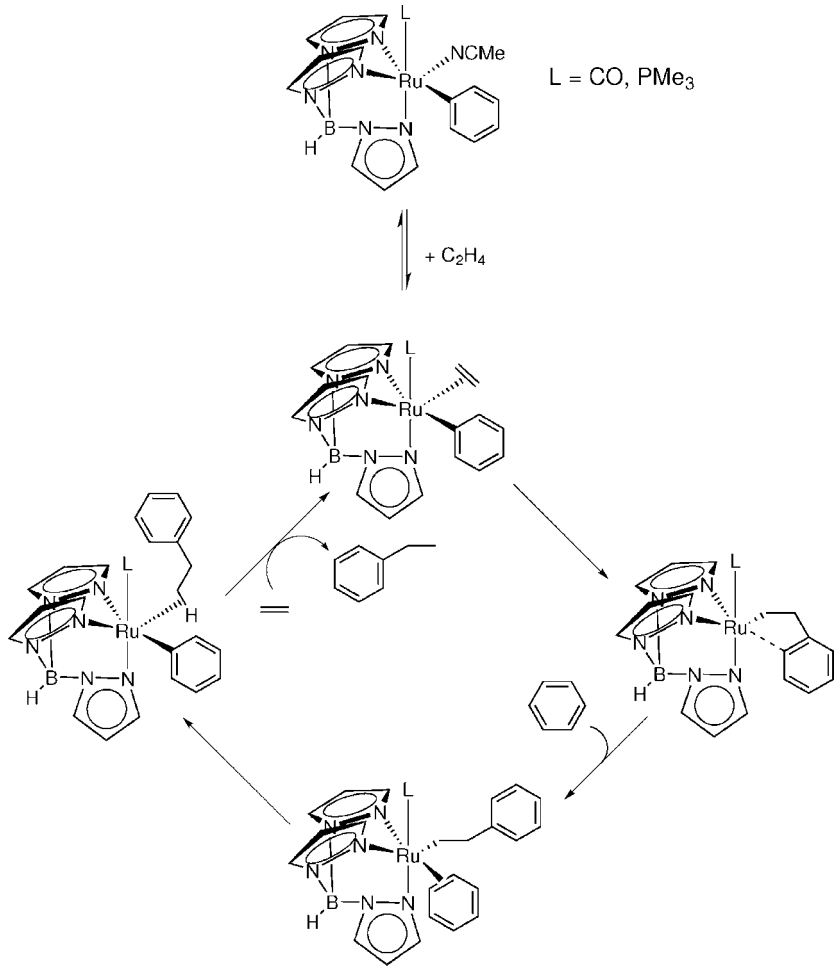

Figure 79. Computed catalytic cycle for the formation of ethylbenzene by insertion of ethylene into the C—H bond of benzene in the presence of TpRu(L)(CNMe)(Ph) (L = CO, PMe_3).

produce TpRu(PMe_3)(η^3-C_4H_7) is found to kinetically compete with catalytic ethylene hydrophenylation. The DFT(B3LYP) calculations were carried out with the experimental ligands Tp, CO, and PMe_3. The entire catalytic cycle was computed for TpRu(L)Ph (L = CO and PMe_3), and in both cases, the highest point on the PES is the TS for C—H activation of benzene generating the ethylbenzene product. The lower activity in the case of L = PMe_3 is due to easy C—H activation of ethylene by TpRu(PMe_3)Ph to form the vinyl complex TpRu(PMe_3)(vy). The latter converts to an η^3-allyl complex in the presence of excess ethylene. The calculations show that ethylene insertion into Ru—Ph is much easier than ethylene C—H activation for L = CO ($\Delta\Delta G^{\ddagger}$ = 8.6 kcal mol^{-1}), whereas the difference between the two pathways is less pronounced for L = PMe_3 ($\Delta\Delta G^{\ddagger}$ = 3.1 kcal mol^{-1} in favor of ethylene insertion).

Combined experimental and computational study of hydroarylation of olefins by TpRu{P(pyr)$_3$}(NCMe)Ph (pyr = *N*-pyrrolyl) tested the impact of sterics on the catalytic activity.[377] The steric bulk of the tris-*N*-pyrrolyl phosphine ligand inhibits coordination of ethylene and thus prevents C—C bond formation, rendering the catalyst inefficient.

In an effort to more precisely delineate the effect of the ancillary ligand L on Ru-mediated olefin hydroarylation activity, Gunnoe prepared and studied the reactivity of TpRu{P(OCH$_2$)$_3$CEt}(NCMe)Ph (P(OCH$_2$)$_3$CEt = 4-ethyl-2,6,7-trioxa-1-phosphabicyclo[2.2.2]octane). The reduced cone angle (101°) of the P(OCH$_2$)$_3$CEt ligand was anticipated to allow olefin coordination, while the moderate π-acidity of the phosphite was expected to potentially bias the kinetics toward olefin insertion over olefin C—H activation as observed with CO and contrary to the situation with PMe_3. A maximum activity of 10 TONs was achieved at 90 °C and 10 psi of ethylene. As in the other cases, the rate-determining step for the entire catalytic cycle to form the ethylbenzene product is computed to be the C—H bond activation of benzene. However, a crucial step for the deactivation of the catalyst is the competition between ethylene insertion into Ru—Ph and C—H activation of ethylene to produce a vinyl complex that eventually evolves to an η^3-allyl complex. In the present case, the $\Delta\Delta G^{\ddagger}$ value of 7.4 kcal mol^{-1} is intermediate between that for CO (8.6 kcal mol^{-1}) and that for PMe_3 (3.1 kcal mol^{-1}), in agreement with a catalytic activity for the phosphite complex intermediate between that of the carbonyl and that of the phosphine complexes.

4.3. Borylation of Alkanes

Metal-catalyzed borylation of arenes[380] and alkanes[46] is a powerful way to functionalize a C—H bond in a selective manner.[45] For instance, with Cp*W(CO)$_3$Bcat′ (cat′ = 1,2-$O_2C_6H_2$-3,5-$(CH_3)_2$), the alkane functionalization resulted in remarkably high yields (Figure 80).

The mechanism for the borylation of alkanes was first addressed by Wan et al. using BH_3 as a model for H-Bpin (pin = pinacolate) used in the experiments. B3LYP, B3PW91, and MP2 calculations of the reaction of CpRhH(BH_2) with

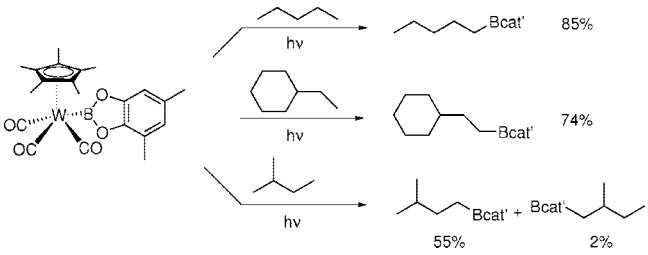

Figure 80. Selective functionalization of alkanes by transition metal boryl complexes.

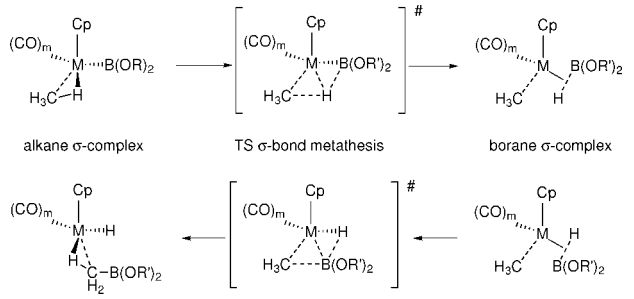

Figure 81. Proposed general reaction pathway for $CpM(CO)_m(B(OCH_2)_2)$ (M = Fe, $m = 2$; M = W, $m = 3$) reacting with CH_4.

CH_4 were carried out.[381] The formation of the reactive $CpRhH(BH_2)$ species by reaction of $CpRhH_2$ with BH_3 was also considered, and it was shown that eliminating H_2 from $CpRh(H)_3BH_2$ is a high-energy process. However, the unsaturated $CpRhH(BH_2)$ forms first a complex with CH_4 before cleaving the C—H bond. The B—C bond is formed afterward from the isomer where the CH_3 and BH_2 are in a cis position. The authors mentioned a significant influence of the method of calculation. Both the DFT(B3PW91) and MP2 methods propose a preference for an oxidative addition/reductive elimination process over a σ-CAM transformation, but the B3LYP method gives different results for no clear reasons.

The reaction pathway was studied by Hall using a model for the boryl ligand closer to the experimental systems.[382] DFT(B3LYP) calculations on the reaction of $CpM(CO)_m(B(OCH_2)_2)$ (M = Fe, $m = 2$; M = W, $m = 3$) with CH_4 were carried out (Figure 81). After formation of a CH_4 complex ($\Delta H = -6.1$ kcal mol^{-1}, Fe; $\Delta H = -3.7$ kcal mol^{-1}, W), the C—H activation occurs by σ-bond methatesis ($\Delta H^{\ddagger} = 1.3$ kcal mol^{-1}, Fe; $\Delta H^{\ddagger} = 4.3$ kcal mol^{-1}, W; relative to separated reactants) to form a borane σ-complex as an intermediate ($\Delta H = -5.4$ kcal mol^{-1}, Fe; $\Delta H = -3.1$ kcal mol^{-1}, W). This borane σ-complex rotates from a conformer where H is closer to the CH_3 group to one where the $B(OR)_2$ group is closer (cis) to the CH_3 group. The next step is a transfer of the $B(OR)_2$ group toward CH_3 through a four-center transition state with $B(OR)_2$ at the β-position of the ring. The overall reaction, which is described as a boron-assisted σ-bond metathesis is a nice example of a σ-CAM mechanism where the facile rotation of the borane σ-complex (energy barriers of 6.2 kcal mol^{-1} for Fe and 4 kcal mol^{-1} for W) is indispensable for the formation of the B—C bond. The analysis of the electron density shows that the electropositive nature of the boron causes the electron pair in the M—B bond to attack the H; this attack is supported by (i) transfer of the electron pair from R—H to the new M—C bond and (ii) back-donation of electrons on the metal to the boron p orbital.

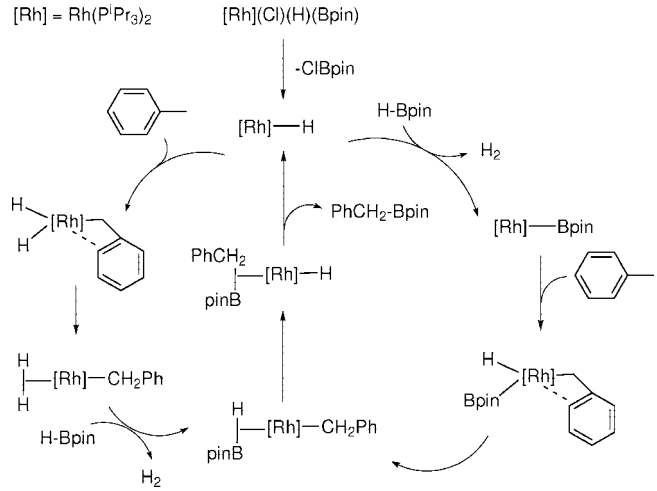

Figure 82. Reaction pathway for the rhodium−phosphine-catalyzed borylation of C—H bonds with pinacolborane.

This work was followed by a combined experimental/computational study on the rhodium boryl complexes where monoboryl and bisboryl complexes were compared.[383] The DFT(B3LYP) studies show that the ancillary boryl ligand on the metal tunes the shape of the potential energy surface without changing the global picture. In all cases, the C—H bond cleavage process occurs by a boron-assisted σ-bond metathesis mechanism to generate a borane complex that isomerizes, if necessary, to place the alkyl group cis to the boryl group. This complex with cis boryl and alkyl groups undergoes B—C bond formation by a second σ-bond metathesis to generate the product. The calculations show that the presence of an ancillary boryl in place of a hydride lowers the energy of all intermediates and transition states but notably that of the final product. This contributes to drive thermodynamically the reaction to completion. It is also shown that the substituents on the boron influence the potential energy surface and that the experimental OR substituent should not be replaced by hydrogen.

Methane and benzene borylation by $CpFe(CO)(BO_2C_2H_2)$ and $CpW(CO)_2(BO_2C_2H_2)$ were compared with B3LYP calculations.[384] The calculations show that the C—H bond cleavage and B—C bond formation occurs in a concerted manner in a one-step mechanism for the Fe complex because Fe does not favor a high oxidation state. In contrast, a two-step reaction with intermediate formation of a hydrido alkyl boryl complex with a W(IV) oxidation state is observed in the case of W. The reaction with benzene is found to have significantly lower barrier with the Fe complex ($\Delta E^{\ddagger} = 20.3$ kcal mol^{-1}, CH_4; $\Delta E^{\ddagger} = 11.7$ kcal mol^{-1}, benzene) in agreement with experiment. This is attributed to a significantly stabilizing interaction between the boron p orbital of the boryl group and the π orbitals of benzene at the transition state. These interactions are negligible for the tungsten complex because the functionalization occurs in a two-step process. Additional calculations on $CpRu(CO)(BO_2C_2H_2)$ predict that the reactivity difference toward alkanes and arenes should be smaller than that of the iron−boryl complexes.

The reaction mechanism of the rhodium−phosphine catalyzed borylation of methyl-substituted arenes using pinacolborane (HBin) has been investigated using DFT(B3PW91) calculations with additional single point calculations at the CCSD(T) level (Figure 82).[385] Factors affecting selectivity for benzylic vs aromatic C—H bond activation were

examined. The study compares the pathway in which $RhH(PMe_3)_2$, model for $RhH(P^iPr_3)_2$, reacts first with toluene and next with H-Bpin with the pathway where the two substrates react in the reverse order. If the reaction starts with the formation of the boryl derivative, the C—H addition to toluene becomes very unfavorable (highest TS on the PES, 31.8 kcal mol^{-1} above reactants) due to the exceedingly large trans influence of the boryl group.[386] This is especially important in this reaction where the reactive metal fragment has a mer-type coordination at Rh, which maximizes trans influence. It is interesting to note that this is not the case with the cyclopentadienyl derivatives described previously, which have a fac-type geometry where boryl is never trans to the incoming ligand. The preference for the benzylic regioselectivity observed experimentally is attributed to the formation of a stable η^3-benzyl intermediate. The potential energy surfaces for the reactions at the benzylic and aromatic CH differ only slightly (difference of 2.3 kcal mol^{-1} between the highest points of the two pathways), but the trend is predicted correctly. It agrees with the 4:1 product ratio of $PhCH_2Bpin$ and $Me\text{-}C_6H_4Bpin$ in the borylation of toluene.

The catalytic hydroborylation of arenes was studied with DFT calculations by Sakaki et al.[387] Following the report of hydroborylation of benzene by Smith et al.,[380] who used $CpIr(H)(Bpin)(PMe_3)$ (pin = pinacolato ($-OCMe_2-CMe_2O-$)), $[IrCl(cod)]_2$/phosphine, and [Ir(ind)(cod)]/phosphine (ind = indenyl) as catalysts, Hartwig et al. used a mixture of bis(pinacolato)diboron with $[IrCl(cod)]_2$/bpy (bpy = 2,2′-bipyridine or 4,4′-di-*tert*-butyl-2,2′-bypridine) as precatalyst.[388,389] The reaction forms C_6H_5-Bpin and releases dihydrogen. Calculations were carried out at the B3LYP level using a diimine model of the bipyridine ligand for exploratory calculations and the full ligand for the rest of the study. The pinacolate group is modeled by a bis(ethylene glycol) (Beg) group. To model a reaction in solution, the authors consider that it is better not to include the translational and rotational contributions to the entropy.

The key steps of the reaction are the oxidative addition of the C—H bond of benzene to the Ir complex, initiated by π-coordination of the arene, and the reductive elimination of the phenylborane. One interesting aspect of this study is that benzene as well as diborane can be oxidized by the various Ir complexes and intermediates. However diborane is more easily oxidized than benzene, which rationalizes the excess of diborane used in the experiment. Therefore, diborane but not benzene reacts with the Ir(I) precatalyst, which leads to the proposal of $Ir^{III}(Beg)_3(bpy)$ as the reactive form of the catalyst. This trisboryl Ir(III) complex promotes the oxidative addition of the C—H bond of benzene, yielding the $Ir^{V}(Beg)_3(H)(Ph)(bpy)$ complex. The reductive elimination of phenylborane takes place from this species with the concomitant formation of the $Ir^{III}(H)(Beg)_2(bpy)$ complex. The C—H oxidative addition has an activation barrier of 24.2 kcal mol^{-1}, and the reductive elimination of phenyl borane has a low activation barrier of 4.9 kcal mol^{-1}. The complex $Ir^{III}(H)(Beg)_2(bpy)$ reacts preferably with Beg—Beg with a low activation barrier of 8 kcal mol^{-1} to form an $Ir^{V}(Beg)_3(bpy)$ complex, which eliminates H-Beg with a very low activation barrier of 2.6 kcal mol^{-1} and regenerates the catalyst, $Ir^{III}(Beg)_3(bpy)$. After consumption of the diborane, the catalyst is regenerated by reaction of $Ir^{III}(H)(Beg)_2(bpy)$ with H-Beg while H_2 is eliminated. The charge analysis shows that the Beg group stabilizes the Ir^{V} oxidation state, in agreement with the large electron-donating effect of the boryl group.[386] This study is confirmed by the reaction of square based diphosphine trisboryl Ir^{III} complex with the $C(sp^2)$—H bond of arene and thiophene derivatives.[390]

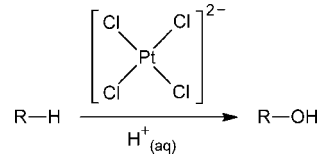

Figure 83. The Shilov reaction.

5. C—H Oxidation

5.1. Shilov Chemistry: Methane Oxidation

Garnett and Hodges originally discovered that $[Pt(Cl)_4]^{2-}$ promotes H/D isotope exchange in arenes.[391] Following this work, Shilov showed that the inert C—H bonds of several alkanes were activated by $[Pt(Cl)_4]^{2-}$ in acidic aqueous conditions (Figure 83).[1,392] This transformation, known as the Shilov reaction and developed in the period 1970—1985, revolutionized the field of alkane functionalization because, at that time, it was believed that inert C—H bonds could be only activated by metal surfaces, strong oxidants, or radical reagents. In addition, the Shilov reaction obeyed the following selectivity pattern: primary C—H > secondary C—H > tertiary C—H. This pattern was unexpected and opposite to that given by electrophilic and radical reagents. The selectivity suggested that the C—H bond is cleaved through oxidative addition, but this was felt at the time to be unlikely since it would involve the oxidation of Pt(II) to Pt(IV). Another puzzling feature of the Shilov reaction is the fact that it works under aqueous conditions, in which water competes strongly with the alkane substrates for coordination to the metal. Several theoretical studies have focused on the reaction mechanism of the Shilov reaction in order to rationalize its puzzling features and facilitate its further development and optimization. Despite all experimental efforts, the exact identity of the active species is not fully clear yet, and the theoretical studies are indeed based on different models of these species. These studies have shown that the nature of the ligands and their spatial arrangement around the metal center have a strong influence on the reaction mechanism. The review by Lersch and Tilset summarizes the mechanistic studies on C—H activation by platinum complexes up to 2005.[57]

The Shilov reaction was theoretically studied by Siegbahn and Crabtree, using DFT and *ab initio* methods.[393] The C—H activation of methane by *trans*-$[Pt(Cl)_2(H_2O)_2]$ was considered as a model reaction (Figure 84). The mechanism starts with the substitution of one aqua ligand by methane, which has an energy cost of 10 kcal mol^{-1}. The next step has been described by Crabtree as a σ-bond metathesis in which one H of methane is transferred to a Cl ligand yielding HCl and a $Pt-CH_3$ bond. However, it can be alternatively described as an ambiphilic metal—ligand activation (AMLA) since the lone pair of the Cl ligand assists the deprotonation of methane. This reaction has an energy barrier of 16.5 kcal mol^{-1}. Considering the initial substitution step, the overall activation energy of ca. 27 kcal mol^{-1} is in remarkable agreement with the experimental value of 28 kcal mol^{-1}. In the final step, an intramolecular proton transfer from HCl to one of the water molecules stabilizes the system by ca. 12 kcal mol^{-1}. The σ-bond metathesis or AMLA mechanism avoids the formation of Pt(IV). The participation of water

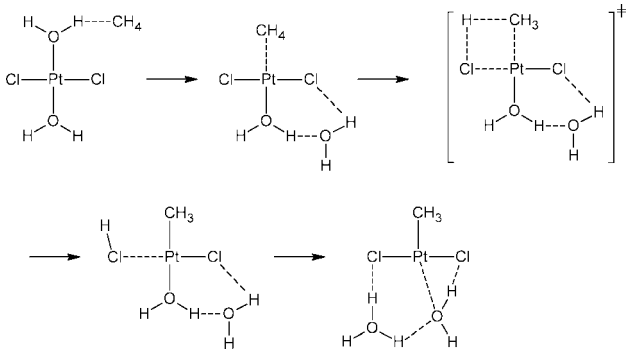

Figure 84. The mechanism proposed by Siegbahn and Crabtree for the Shilov reaction.

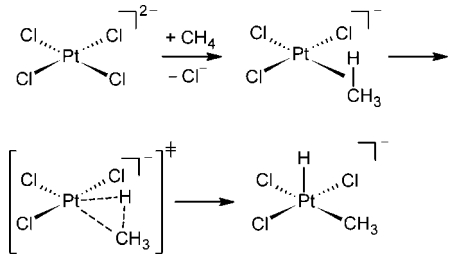

Figure 85. The methane uptake/oxidative addition mechanism proposed by Zhu and Ziegler for the Shilov reaction.

in the first and third steps highlights the critical role played by the solvent. The origin of the unusual selectivity, primary C—H > secondary C—H, was traced to the higher polarity and strength of the Pt—(*n*-alkyl) bond with respect to the Pt—(isoalkyl) bond. An alternative oxidative addition mechanism for C—H activation is also possible and may compete with σ-bond metathesis. The predominant trans-influence of the Pt—R bond over the other ligands prevents the formation of a vacant site cis to the alkyl R ligand.[394] When R contains more than one C atom, this prevents β-elimination, which would erode the selectivity of the reaction by yielding the corresponding alkene.

The mechanism of the Shilov reaction has been also explored by Zhu and Ziegler, in a series of theoretical studies.[395–398] In the first study, the isotope H/D exchange in methane promoted by $[Pt(Cl)_4]^{2-}$ was investigated using a DFT method.[395] This reaction involves the following four steps: (1) methane uptake, in which one of the ligands bound to Pt is replaced by methane, (2) C—H oxidative addition, yielding a Pt(IV) hydride intermediate, (3) H/D exchange, and (4) extrusion of the deuterated product, CH_3D, by reductive elimination. The reactions leading to C—H activation (Figure 85) were analyzed in detail, and the calculations indicated that methane uptake is the rate-determining step. However, the mechanistic nature of this step, which can be either associative or dissociative, could not be established due to the limitations of the theoretical method in predicting accurate free energies. In order to solve this problem, an alternative kinetic approach was used by deriving a H/D exchange rate expression for each mechanism. When $[Pt(Cl)_4]^{2-}$ is used as catalyst in acidic aqueous solutions, a mixture of $[Pt(Cl)_4]^{2-}$, $[Pt(Cl)_3(H_2O)]^-$, and $[Pt(Cl)_2(H_2O)_2]$ is formed by Cl^-/H_2O ligand substitution. Each one of these species contributes to the overall rate of the reaction, depending on their concentration and energy barrier for methane uptake. For the dissociative mechanism, the largest contribution to the overall rate comes from $[Pt(Cl)_4]^{2-}$, whereas for the associative mechanism, it comes from

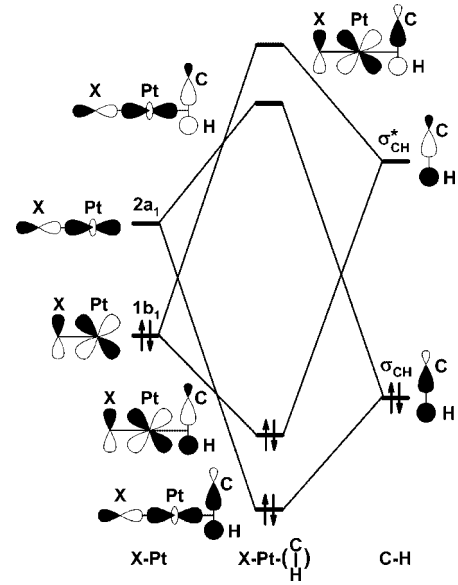

Figure 86. Schematic diagram with the key molecular orbitals of the trans X—Pt—(CH) fragment.

$[Pt(Cl)_3(H_2O)]^-$. For both mechanisms, the contribution of $[Pt(Cl)_2(H_2O)_2]$ is negligible due to the extremely low concentration of this species. $[Pt(Cl)_2(H_2O)_2]$ becomes the dominant active species only when it is directly used as catalyst. The calculations support the associative mechanism because it gives the best agreement between the experimental and theoretical rates.

In a subsequent study by the same authors, the activation of methane by 1:2 mixtures of $[Pt(Cl)_2(H_2O)_2]$ and X (X = F^-, Cl^-, Br^-, I^-, NO_2^-, and CN^-) was investigated, by considering the possible Cl^-/X and H_2O/X ligand substitutions in aqueous solution.[396] In all cases, methane uptake is the rate-determining step, rather than the cleavage of the C—H bond. The ligand pattern around the square planar Pt center of the active species depends on the nature of X. For the weak coordinating X ligands, Cl^-, Br^-, and I^-, the active species are *cis*-$[Pt(Cl)(H_2O)(X)_2]^-$ and *trans*-$[Pt(Cl)_2(X)(H_2O)]^-$, whereas the dominant $[Pt(Cl)_2(X)_2]^{2-}$ complex has no noticeable activity. For the strong coordinating X ligands, F^-, NO_2^-, and CN^-, a complex mixture of Pt species, including $[Pt(Cl)_2(H_2O)_2]$, $[Pt(Cl)_2(X)(H_2O)]^-$, $[Pt(Cl)(X)_2(H_2O)]^-$, $[Pt(Cl)(X)_3]^{2-}$, and $[Pt(Cl)_4]^{2-}$, is formed. Of all these complexes, only *cis*-$[Pt(Cl)_2(H_2O)_2]$ and *cis*-$[Pt(Cl)_2(X)(H_2O)]^-$ are efficient catalysts. This study showed that catalytic activity requires the presence of an aqua ligand acting as leaving group in the rate-determining methane uptake. In the absence of aqua ligands, the X ligands, which are much poorer leaving groups than water, yield high energy barriers.

The calculations by Zhu and Ziegler revealed that the cis/trans isomerism in the active Pt aqua species plays a key role, because methane uptake is facilitated by strong labilizing ligands trans to the H_2O ligand. Nevertheless, as the trans-labilizing strength of the ligand increases, the energy barrier associated with C—H cleavage becomes higher. This undesired effect was found in a study of the C—H activation of methane by *trans*-$[Pt(Cl)_2(X)(CH_4)]^-$, in which the X ligand (F^-, Cl^-, Br^-, I^-, NO_2^-, or CN^-) lies trans to CH_4.[397] The bonding in the X—Pt—CH_4 fragment involves both donation from the CH_4 σ_{CH} orbital to the Pt—X $2a_1$ orbital and back-donation from the Pt—X $1b_1$ orbital to the CH_4 σ_{CH}* orbital (Figure 86). As the electronegativity of X

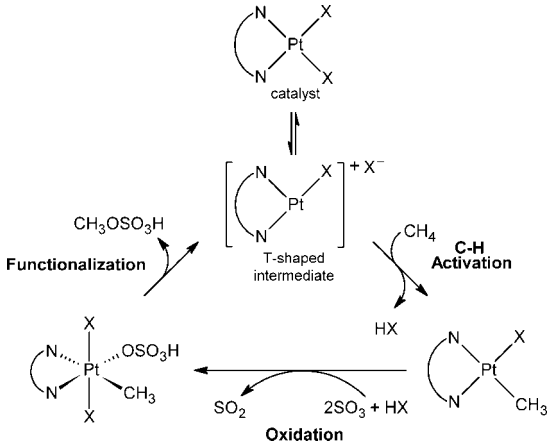

Figure 87. Reaction mechanism for the catalytic oxidation of methane proposed by Periana. The chelating N,N ligand is bipyrimidine and X = Cl or OSO_3H.

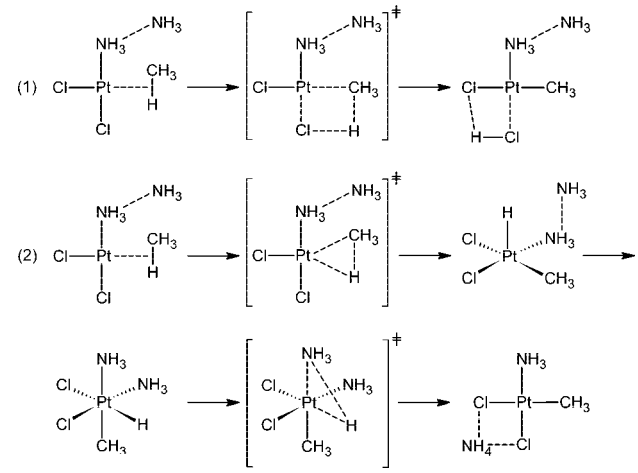

Figure 88. The (1) σ-bond metathesis and (2) oxidative addition mechanisms for the C—H activation of methane by *cis*-$[Pt(NH_3)_2(Cl)_2]$.

decreases, $F^- > Cl^- > Br^- > I^- > NO_2^- > CN^-$, the contribution of X into the $2a_1$ and $1b_1$ orbitals increases, whereas the contribution of Pt to the same orbitals becomes smaller. As a consequence, the $\langle\sigma_{CH}|2a_1\rangle$ and $\langle\sigma_{CH}^*|1b_1\rangle$ overlaps decrease, and the Pt—CH_4 bond is weakened. This effect is stronger in the transition state than in the reactant adduct, and therefore, the C—H cleavage energy barrier increases following the order $F^- < Cl^- < Br^- < I^- < NO_2^- < CN^-$. These calculations showed that the trans-labilizing effect of the X ligand needs to be finely tuned to achieve the optimal balance between the energy costs associated with C—H cleavage and H_2O/CH_4 ligand substitution. This principle was further confirmed in a recent study by considering many other ligands, including phosphines, amines, and imines.[398]

The Shilov chemistry was further developed by Periana, who reported the Catalytica process for the oxidation of methane to methanol.[4,399–401] In this process, methane is catalytically oxidized by a Pt(II) complex, $[Pt(Cl)_2(bpym)]$ (bpym = bipyrimidine), under moderate conditions using concentrated sufuric acid as solvent and oxidant.[49] The product of the reaction is a mixture of methyl bisulfate (CH_3OSO_3H), protonated methanol, and methanol, depending on the concentration of sulfuric acid. Both the methyl bisulfate and protonated methanol subproducts are easily converted to methanol by hydrolysis. Periana proposed a mechanism for this reaction (Figure 87), which consists of four steps: (1) dissociation of one of the X ligands, which can be either Cl^- or OSO_3H^-, yielding a T-shaped Pt(II) complex, $[Pt(X)(bpym)]^+$, (2) formation of a Pt(II)—CH_3 intermediate, $[Pt(X)(CH_3)(bpym)]$, by C—H activation, (3) oxidation by SO_3 to a Pt(IV) octahedral complex, $[Pt(X)_2(CH_3)(OSO_3H)(bpym)]$, and (4) functionalization by reductive elimination of CH_3OSO_3H, in which the catalyst is recovered. A theoretical study by Hush using cisplatin, $[Pt(Cl)_2(NH_3)_2]$, as model catalyst, showed that this reaction mechanism is thermodynamically feasible.[402] The calculations suggested that a H_2SO_4-solvated form of the postulated T-shaped intermediate, $[Pt(OSO_3H)(OSO_3H_2)(NH_3)_2]^+$, is likely to be the active catalytic species. In this complex, the anionic OSO_3H^- ligand is bound to Pt through the deprotonated O, whereas the neutral OSO_3H_2 ligand is bound to Pt through one oxygen of the S=O groups. An alternative mechanism, involving the formation of a Pt—H species by oxidative addition of the C—H bond, is excluded.

These studies were further extended by the same authors.[403] Thermodynamic and kinetic aspects of the mechanism of methane oxidation by cis- and transplatin were studied. The reaction is initiated by the substitution of an NH_3 ligand by CH_4. This step, with an energy barrier of ca. 34 kcal mol^{-1} for the cis isomer and ca. 44 kcal mol^{-1} for the trans isomer, is effectively rate-determining. The large energy needed for the NH_3/CH_4 substitution is associated with the high strength of the Pt—NH_3 bond. The following steps, in which methane is activated, involve similar but slightly lower energy barriers. The C—H bond of methane can be cleaved by either σ-bond metathesis or oxidative addition (Figure 88). The metathesis mechanism (or AMLA), which preserves the Pt(II) oxidation state, involves a proton transfer from methane to a Cl^- ligand. The oxidative addition mechanism yields an octahedral Pt(IV) hydride intermediate. Following this step, the reaction is completed by reductive elimination of NH_4^+. The Pt—CH_3 and Pt—H bonds obtained by oxidative addition are always cis to each other due to trans influence. In addition, the nature of the mechanism depends on the cis/trans isomerism of the catalyst. For cisplatin, the metathesis and oxidative addition mechanisms have similar energy profiles and may compete. In contrast, for transplatin, the oxidative addition mechanism is favored over the σ-bond metathesis mechanism.

A theoretical study by Gilbert and Ziegler, with a DFT method including solvation, suggested that the active species in the Catalytica process is either $[Pt(bipym)(Cl)]^+$ or $[Pt(bipym)(OSO_3H)]^+$.[404] The inclusion of the full bipym ligand in the model revealed that the system does not undergo the dissociation of the Pt—N bond, due to the bidentate nature of the real ligand. In addition, the axial attack of methane to the square planar $[Pt(bipym)(Cl)_2]$ catalyst was excluded. Interestingly, the C—H activation mechanism depends on the nature of the catalyst: it is an oxidative addition for $[Pt(bipym)(Cl)]^+$ but a σ-bond metathesis for $[Pt(bipym)(OSO_3H)]^+$. The protonation of the bipym ligand is unfavorable but promotes σ-bond metathesis by lowering the associated energy barriers. The calculations showed that the need for high temperatures, 180—220 °C, is due to the high energy needed to substitute a Cl^- or a OSO_3H^- ligand by methane.

The reaction mechanism of methane oxidation catalyzed by *cis*-$[Pt(NH_3)_2(Cl)_2]$ and $[Pt(bpym)(Cl)_2]$ was theoretically investigated by Periana and Goddard.[405] The potential substitution of a Cl^- ligand by OSO_3H^- was considered for each step of the original mechanistic proposal (Figure 87).

The initial coordination and C—H activation of methane involve $[Pt(L_2)(Cl)_2]$ (L_2 = bpym or $(NH_3)_2$), in which one of the Cl^- ligands is replaced by CH_3. The Pt(IV) octahedral intermediate formed in the oxidation step has $X = OSO_3H^-$ ligands in the trans apical positions. The final functionalization step yields $[Pt(L_2)(Cl)(OSO_3H)]$, which by OSO_3H^-/CH_4 ligand exchange closes the catalytic cycle. In the C—H activation step, the σ-bond metathesis mechanism, referred to as electrophilic substitution by Periana and Goddard, is preferred for the $[Pt(bpym)(Cl)_2]$ catalyst. In contrast, when the catalyst is *cis*-$[Pt(NH_3)_2(Cl)_2]$, the most favored mechanism is oxidative addition.

The oxidation of Pt(II) to Pt(IV) by SO_3 (Figure 87) has been studied in detail theoretically. DFT calculations by Hristov and Ziegler showed that this reaction involves the coordination of SO_3 to the Pt—CH_3 intermediate.[406] After protonation of the SO_3 ligand, Pt(II) is oxidized to Pt(IV) by S—OH bond cleavage in the resulting SO_3H ligand, which leads to a *cis*-$Pt(SO_2)(OH)$ species. Final dissociation of SO_2 and OH^-/OSO_3H^- ligand exchange yields the *cis*-$Pt(OSO_3H)(CH_3)$ intermediate, which leads to the final reaction product by reductive elimination. Other calculations by Goddard[405,407] and Musgrave[408] showed that the oxidation step is more favorable for $[Pt(NH_3)_2(Cl)_2]$ than for $[Pt(bpym)(Cl)_2]$, thus suggesting that the former complex has a higher catalytic activity. Nevertheless, $[Pt(bpym)(Cl)_2]$ was found to be the most robust catalyst, in good agreement with the experiments, because it is more resistant to the strong acidic media associated with the concentrated sulfuric acid reagent.[405] The protonation of the bipyrimidine ligand weakens the Pt—N bonds, but the ligand remains coordinated to Pt.[407] In addition, the L/OSO_3H^- ligand exchange is exoergic for $L = NH_3$, with $\Delta G = -23$ kcal mol^{-1}, but endoergic for L = bipym, with $\Delta G = 16$ kcal mol^{-1}. All these results indicate that NH_3 is easily dissociated from $[Pt(NH_3)_2(Cl)_2]$ in hot concentrated H_2SO_4, leading to $PtCl_2$, which will induce catalyst deactivation by the formation of a $[PtCl_2]_n$ precipitate.

The influence of the pH on the oxidation of methane by $[Pt(bpym)(Cl)_2]/H_2SO_4$ was further explored in a subsequent study.[409] Two different prototropic forms of the Pt(II) active species, $[Pt(Hbpym)(Cl)(OSO_3H)]^+$ (Hbpym = protonated bipyrimidine) and $[Pt(Hbpym)(Cl)(OSO_3H_2)]^{2+}$, were studied. In Hbpym, a nitrogen not bound to Pt is protonated, so chelation is preserved. Both OSO_3H^- and OSO_3H_2 act as η^1 ligands bound to Pt through O. The dicationic complex, which is generated by the protonation of the OSO_3H^- ligand, will predominate under the strong acidic conditions of the reaction. The most difficult step in the C—H activation process is methane uptake, in which CH_4 coordinates to Pt by displacing the S-containing ligand. The calculations showed that the energy barrier associated with this step is significantly reduced by protonation, from 39.0 kcal mol^{-1} for $[Pt(Hbpym)(Cl)(OSO_3H)]^+$ to 27.9 kcal mol^{-1} for $[Pt(Hbpym)(Cl)(OSO_3H_2)]^{2+}$. These results suggest that sulfuric acid acts not only as an oxidant but also as a cocatalyst.

Periana and Goddard improved the efficiency of the Catalytica sytem by exploiting the interplay between experiments and theory.[410] The calculations showed that the C—H activation of methane involves an overall energy barrier of ~32 kcal mol^{-1}, which is too high to make the process commercially viable. This energy barrier can be separated into 27 kcal mol^{-1} for methane coordination and 5 kcal mol^{-1} for C—H cleavage. Hence, the efficiency of the catalyst would be improved by promoting methane coordination without proportionally increasing the barrier associated with C—H cleavage. The calculations predicted that these requirements would be fulfilled by the $[Pt(pic)(TFA)_2]^-$ (pic^- = η^2-*N*,*O*-picolinate, TFA^- = trifluoroacetate) catalyst. In contrast with the neutral bpym ligand, the monoanionic character of the pic^- ligand should facilitate methane coordination by making the metal center more electron-rich. In addition, the TFA^- ligand has the ability to assist the C—H cleavage step. These hypotheses were confirmed by comparing the catalytic properties of $[Pt(bpym)(TFA)_2]$ and $[Pt(pic)(TFA)_2]^-$ in the oxidation of benzene with H_2SO_4. The experiments showed that the $[Pt(pic)(TFA)_2]^-$ catalyst is 300 times more active than $[Pt(bpym)(TFA)_2]$. With the bpym ligand, the coordination of benzene involves an energy barrier of 14 kcal mol^{-1}, which is reduced to 5 kcal mol^{-1} with the pic^- ligand. In contrast, the barrier for C—H cleavage is increased by 3 kcal mol^{-1} when the pic^- ligand is used. Nevertheless, the overall C—H energy barrier is reduced from 27 kcal mol^{-1} for $[Pt(bpym)(TFA)_2]$ to 21 kcal mol^{-1} for $[Pt(pic)(TFA)_2]^-$, which is not only lower but also in good agreement with the experimental value, 23 kcal mol^{-1}. The C—H cleavage is assisted by the TFA^- ligand, which takes a proton from the activated bond yielding a cyclic six-membered transition state (Figure 89).

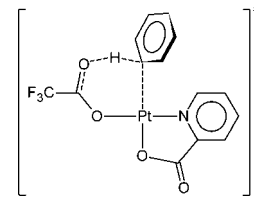

Figure 89. Cyclic six-membered transition state for the C—H activation of benzene catalyzed by $[Pt(pic)(TFA)_2]^-$.

One of the main drawbacks of the Catalytica process is deactivation by water. However, Cheng et al. reported that tolerance to water is increased by adding pyrazolium-based ionic liquids.[411] A theoretical study by Oxgaard and Goddard showed that in the presence of these additives, the solid $PtCl_2$ catalyst is dissolved in concentrated H_2SO_4 due to the formation of a strong ion pair, $[PtCl_4][HPzm]_2$ (HPzm = protonated pyrazolium).[412] The formation of this ion pair, in which the $[PtCl_4]^{2-}$ and $HPzm^+$ ions are bound by electrostatic forces and H···Cl H-bonds, is exothermic by 68.3 kcal mol^{-1}. Interestingly, the substitution of a Cl^- ligand of the ion pair by either HSO_4^- or H_2O is energy-uphill, in contrast with the original Catalytica catalyst, $[Pt(bpym)(Cl)_2]$, in which it is exothermic. This indicates that the ionic liquid prevents the poisoning by water. The C—H activation of methane by $[PtCl_4][HPzm]_2$ follows a two-step mechanism: (1) coordination of CH_4 to Pt by an associative reaction, in which a Cl^- ligand is displaced toward the second coordination sphere with the assistance of the HPzm counterions, and (2) C—H bond cleavage by oxidative addition yielding a *cis*-$Pt(CH_3)(H)$ intermediate. The transition states associated with these reactions are 26.5 kcal mol^{-1} for methane-coordination and 21.1 kcal mol^{-1} for C—H cleavage above the energy of reactants. This study showed that the introduction of ionic liquids in the Catalytica process not only reduces the deactivation of the catalyst by water, but also facilitates methane activation and changes the nature of the C—H cleavage mechanism from ambiphilic metal—ligand activation (AMLA) to oxidative addition.

The tolerance of the Shilov reaction to water has been also enhanced by Vedernikov, who reported the synthesis and reactivity of $[Pt(X)(CH_3)_2]^-$.[413,414] These complexes, in which the Pt(II) center is chelated by a bidentate anionic dipyridine ligand (X), promote the C—H activation of benzene in biphasic water—benzene systems.[414] DFT calculations suggest that the protonation of $[Pt(X)(CH_3)_2]^-$ in the water phase generates a lipophilic $[Pt(X)(CH_3)_2H]$ species, which is efficiently extracted into the benzene phase. This complex generates $[Pt(X)(CH_3)(CH_4)]$ in a facile reductive elimination step, with $\Delta H^{\ddagger} = 9.2$ kcal mol^{-1} and $\Delta H = 5.2$ kcal mol^{-1}. Since the organic phase is ~100% benzene, the methane ligand is easily replaced by benzene, which yields $[Pt(X)(CH_3)(C_6H_6)]$. In a subsequent step, one of the C—H bonds of the C_6H_6 ligand is cleaved by oxidative addition, leading to a Pt(IV) hydride intermediate, $[Pt(X)(CH_3)(C_6H_5)(H)]$, which completes the C—H activation process. This study shows that $[Pt(X)(CH_3)_2H]$ is an active species in arene C—H activation. The abstraction of this complex into the reactant phase allows for high efficiency even in the presence of water, which remains in the other phase of the system.

A new computational approach to the discovery of new catalysts, known as quantum mechanical rapid prototyping (QM-RP), was developed by Goddard.[415] The QM-RP approach profits from the excellent accuracy/cost relationship offered by modern QM calculations, thanks to the DFT methods, and follows a five-step flow diagram: (1) complete and detailed description of the reaction mechanism for a well-known experimental system, in which all intermediates and transition states involved in the mechanism are computed; (2) characterization of the catalytic bottlenecks, in which the critical steps involving the largest activation or reaction energies are identified; (3) discovery of new catalysts by screening, in which a variety of modifications in the nature of metal, ligand, cocatalyst, or solvent are applied in order to test how they affect the catalytic bottlenecks and other critical factors like catalyst stability and poisoning; (4) catalyst refinement, in which the leads found in the previous step are further improved by fine-tuning their electronic and steric properties; (5) experimental tests, in which the leads are finally synthetized and tested in the laboratory.

The QM-RP approach was applied to the oxidation of methane by the Catalytica system in the quest for new and more efficient catalysts.[415] The calculations on the nature of the reaction mechanism revealed the strong influence of the pH on the reactivity of the $[Pt(bpym)(Cl)_2]$ catalyst. The cleavage of the C—H bond is thermodynamically and kinetically favored by the protonation of the bpym ligand. In addition, it was found that water inhibits the reaction by solvating the ground state of the reactants, which is more stabilized than the subsequent intermediates and transition states. By application of the QM-RP protocol, other metals, including Ir, Os, and Au, and ligands, including tridentate NNN, NNC, and NON and bidentate NN and OO ligands, were tested. One of the new catalysts found in this study was an Ir(III) complex with a pincer NNC ligand, which was predicted to promote C—H activation through energy barriers lower than 30 kcal mol^{-1}, without being poisoned by water. Six years later, Periana and Goddard reported the synthesis of this complex, which turned out to be an excellent catalyst for methane oxidation in trifluoroacetic acid.[416]

A variation of the original Catalytica process, based on a new gold catalyst, was developed by Periana.[417] In the presence of Au(0), methane is oxidized to methanol with selectivities higher than 90%. The reaction is performed in a 3 M solution of H_2SeO_4, which is needed to oxidize and solubilize Au(0), in 96% H_2SO_4 at 180 °C. Under these conditions, the catalyst is formed *in situ* and can be either a Au(III) or a Au(I) species. DFT calculations considering solvent effects showed that the most stable complexes are the square planar $[Au(SO_4)_2]^-$ for Au(III) and the linear $[Au(OSO_3H)_2]^-$ for Au(I). In the case of $[Au(SO_4)_2]^-$, one of the SO_4^{2-} ligands needs to be protonated to facilitate the coordination of methane, which undergoes ambiphilic metal—ligand C—H activation. This step has an energy barrier of 28.1 kcal mol^{-1} and involves a proton transfer from methane to the OSO_3H^- ligand. The final functionalization step, which has a much lower energy barrier, consists of an S_N2-like reaction in which a free bisulfate anion attacks the CH_3 ligand. The alternative Au(I) catalyst, $[Au(OSO_3H)_2]^-$, promotes C—H cleavage by oxidative addition with an energy barrier of 21.1 kcal mol^{-1}, lower than that associated with the Au(III) catalyst. These results suggest that $[Au(OSO_3H)_2]^-$ is catalytically more efficient than $[Au(SO_4)_2]^-$. Nevertheless, the small energy difference, 7 kcal mol^{-1}, between the highest energy barriers found in each case and the concentration of Au(I), which is unlikely to be much higher than that of Au(III), suggest that both complexes may act as active species.

Periana also reported that Pd^{2+} dissolved in concentrated H_2SO_4 catalyzes the direct oxidation of methane to acetic acid in the presence of O_2 and CO at 453 K.[418] This reaction was computationally studied by Bell.[419] Interestingly, the model used in this study was built by assuming that Pd(II) is totally solvated by H_2SO_4, so all the ligands in the first coordination sphere are either OSO_3H^- or OSO_3H_2. The calculations indicated that the dominant species in the Pd(II)/H_2SO_4 mixture is $[Pd(\eta^2\text{-}OSO_3H)(OSO_3H)(OSO_3H_2)]$. In this square planar Pd(II) complex, one of the hydrogen sulfate ligands, η^2-OSO_3H^-, is bound to Pd through two of its oxygen atoms, whereas in the other ligands only one oxygen is bound to the metal. This species undergoes a concerted metalation deprotonation (CMD) of methane, in which the formation of the Pd—CH_3 bond is concomitant with a proton transfer to the η^2-OSO_3H^- ligand. This step has the highest activation barrier, $\Delta G^{\ddagger} = 41.5$ kcal mol^{-1}, and leads to the formation of $[Pd(CH_3)(OSO_3H)(OSO_3H_2)_2]$. In the following step, CO adds and inserts into the Pd—CH_3 bond, involving a much lower activation barrier of 14.7 kcal mol^{-1}. The final reductive elimination of CH_3COOSO_3H, which yields the final acetic acid product by hydrolysis, requires the previous oxidation of Pd(II) to Pd(IV) by H_2SO_4 and O_2. The oxidation and reductive elimination steps are exothermic and involve very low energy barriers. These results indicated that Pd(II) is capable of promoting methane oxidation in the absence of chloride, amine, and aqua ligands. The calculations also suggested that Pd(II) is reduced to Pd(0) by CO, which causes the death of the catalyst due the formation of a Pd-black precipitate.

Another alternative to the Shilov and Periana catalysts is $[Rh(CO)_2(I)_2]^-$. Sen found that this complex, which is also used in the Monsanto process, catalyzes the oxidation of methane to methanol and acetic acid by oxygen and carbon monooxide under high pressure.[420,421] The mechanism of this reaction was determined in a theoretical study by Hristov and Ziegler (Figure 90).[422] In the first step, one I^- ligand is substituted by CH_4 through a two-step dissociative ligand

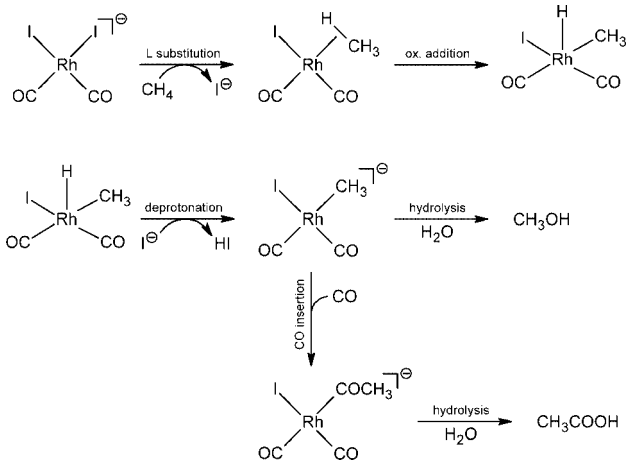

Figure 90. Key steps in the oxidation of methane by $[Rh(CO)_2(I)_2]^-$.

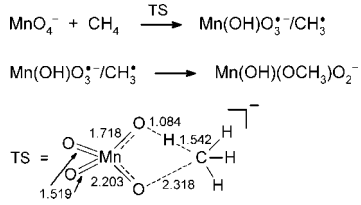

Figure 91. Methane oxidation by permanganate.

exchange mechanism, with an energy cost of only 7.8 kcal mol^{-1}. In the subsequent C—H cleavage step, the oxidative addition mechanism, $\Delta G^{\ddagger}_{sol} = 24.8$ kcal mol^{-1}, is favored over σ-bond metathesis, $\Delta G^{\ddagger}_{sol} = 29.8$ kcal mol^{-1}. The complex obtained in this step, $[Rh(CO)_2(I)(CH_3)(H)]$, eliminates the hydride ligand as a proton by reacting with I^-, which leads to the formation of $[Rh(CO)_2(I)(CH_3)]^-$. This species can undergo either hydrolysis, which yields the methanol product, or CO addition and subsequent insertion into the Rh—CH_3 bond. The latter process, which yields the acetic acid product after hydrolysis, is the most favorable one, involving an energy barrier of 14.7 kcal mol^{-1}. This is in good agreement with the experiments, which show that acetic acid is the major product. The calculations also suggest that the selectivity is switched to methanol in more acidic conditions because the solubility of CO is reduced at low pH.

5.2. Metal—Oxo Species

5.2.1. Inorganic Reagents

The reaction mechanism for the oxidation of methane by permanganate was explored by Strassner and Houk using a DFT method[423] (Figure 91). C—H activation starts with a H abstraction step leading to the formation of a radical ion pair intermediate, $Mn(OH)O_3^{\bullet-}/CH_3^{\bullet}$. This species collapses into the final reaction product, $Mn(OH)(OCH_3)O_2^-$, with no energy barrier. In the transition state, two oxygen atoms of permanganate interact with methane, one with the H being transferred and the other one with the carbon. The final step differs from the classical rebound mechanism, because the methyl radical is trapped by a Mn═O group yielding Mn—OCH_3, rather than forming CH_3OH by OH rebound. The reaction has a significant energy barrier and is clearly endothermic, with $\Delta H^{\ddagger} = 32.3$ kcal mol^{-1} and $\Delta H = 24.3$ kcal mol^{-1}. The same mechanism was characterized for the oxidation of the benzyl carbon of toluene by MnO_4^-. In this

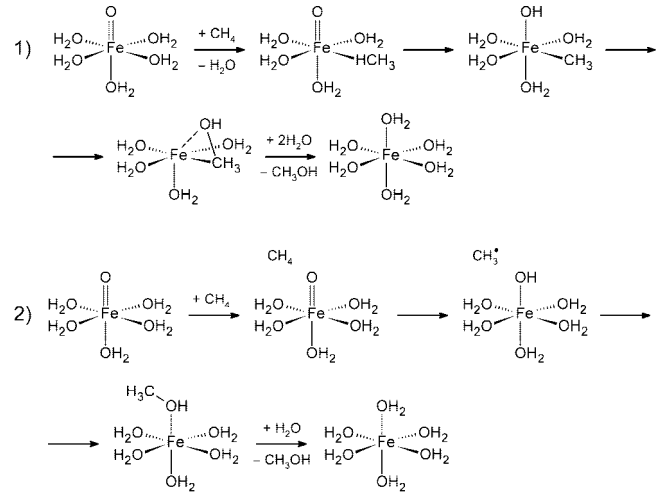

Figure 92. Coordination (1) and rebound (2) mechanisms in methane-to-methanol oxidation by the Fenton reagent.

case, the energy barrier was lower than that of methane by 10.5 kcal mol^{-1}. It was also shown that radical character is present in this reaction.

Alkanes and arylalkanes can also be oxidized using $KMnO_4$ in acetonitrile. The rate of this process becomes faster by over 7 orders of magnitude if a few equivalents of BF_3 are added to the reaction mixture. Experimental and computational data[424] indicate that BF_3 reacts with MnO_4^- yielding an adduct, $[(BF_3)_xMnO_4]^-$ ($x = 1, 2$), which is the active species in C—H oxidation. The kinetic isotope effects, $k_H/k_D \approx 7$ for toluene and ethylbenzene, and the correlation between log(k) and the bond strength, D(C—H), suggest that the rate-determining step of the reaction is a H atom transfer from the substrate to the Mn═O moiety. DFT calculations show that BF_3 accelerates the reaction by lowering the energy barrier associated with this process, from 32.1 kcal mol^{-1} for MnO_4^- to 26.2 kcal mol^{-1} for $[BF_3MnO_4]^-$ and to 20.5 kcal mol^{-1} for $[(BF_3)_2MnO_4]^-$. The analysis of the electronic structure showed that BF_3 lowers the energy barrier by helping the metal to reach a Mn(VI) d^1 configuration in the transition state.

The oxidation of methane to methanol by the Fenton reagent was theoretically studied by Baerends.[425] In previous studies,[426,427] it was demonstrated that the solvated ferryl ion, $[Fe(O)(H_2O)_5]^{2+}$, is easily formed from the Fenton reagent, which is an aqueous mixture of Fe^{2+} and H_2O_2 used as oxidant. Two different mechanisms were explored *in vacuo* by means of static DFT calculations: the oxygen rebound mechanism postulated for cytochrome P450 and the coordination mechanism postulated for bare metal oxo ions, which requires a free coordination site at the metal center (Figure 92). In both mechanisms, the cleavage of the C—H bond is associated with the highest energy barrier: 3.4 kcal mol^{-1} for the rebound mechanism and 22.8 kcal mol^{-1} for the coordination mechanism. Significant preference was thus found for the rebound mechanism. In the presence of the solvent, water, which was modeled by means of CPMD calculations, the energy barrier for H abstraction in the rebound mechanism is increased to 21.8 kcal mol^{-1}. The barrier in solution is much higher than that in vacuo due to the decreased hydration of the reacting oxo/hydroxo ligand and the higher energy of solvation of the $Fe^{IV}O$ ion with respect to the $Fe^{III}OH$ ion. This study strongly supports the $[Fe(O)(H_2O)_5]^{2+}$ complex as the active species in the oxidation of organic compounds by the Fenton's reagent.

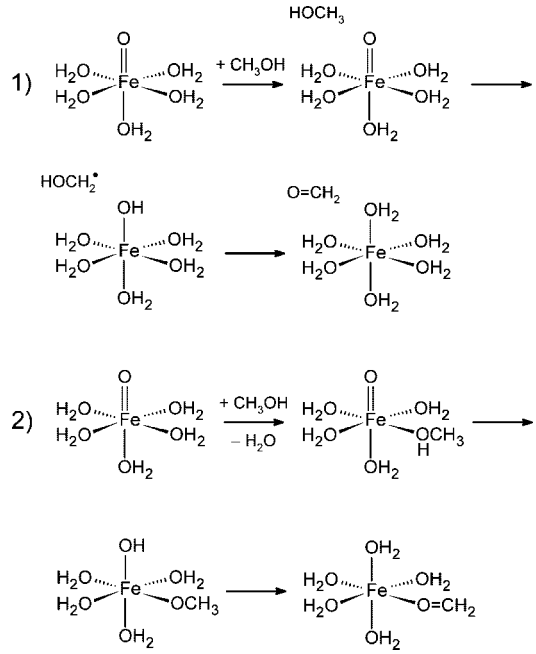

Figure 93. Direct (1) and coordination (2) mechanisms in methanol-to-formaldehyde oxidation by the Fenton reagent.

The product of the first oxidation reaction, methanol, can be further oxidized by the Fenton reagent to formaldehyde. The mechanism of this reaction was also studied by Baerends at the DFT level.[428] The reaction was modeled both in the gas phase, by considering microsolvated clusters, and in aqueous solution by means of CPMD calculations. Two different mechanisms with variants were investigated (Figure 93): a direct mechanism, in which methanol is directly attacked by the $Fe^{IV}O^{2+}$ moiety, and a coordination mechanism, in which the OH group of methanol coordinates previously to the metal. The reaction does not follow the oxygen rebound mechanism; after the first step, the radical intermediate undergoes a second H abstraction yielding an $Fe^{II}(OH_2)^{2+}$ species, rather than OH rebound. In the direct mechanism, the first H abstraction involves the C—H bond, whereas in the coordination mechanism, it involves the O—H bond. The energy barrier associated with the homolytic C—H cleavage in the direct mechanism is dramatically increased from less than ca. 1 kcal mol^{-1} in gas phase to ca. 12 kcal mol^{-1} in solution, as in the case of methane-to-methanol oxidation.[425] The subsequent H abstraction from the O—H bond proceeds spontaneously without energy barrier. In the coordination mechanism, the first H abstraction involves an energy barrier of more than 25 kcal mol^{-1} in the gas phase. This barrier is lowered to 8−12 kcal mol^{-1} by the participation of bridging molecules of water, which assist the transfer of the H from the O of methanol to the O of the $Fe^{IV}O^{2+}$ moiety. Both mechanisms are thus possible. Nevertheless, the coordination mechanism requires a previous ligand substitution reaction, in which one aqua ligand is replaced by methanol. The calculations also showed that the deprotonation of $[Fe(O)(H_2O)_5]^{2+}$ to form $[Fe(O)(H_2O)_4(OH)]^{+}$ decreases the oxidizing power of the Fenton reagent by increasing the associated energy barriers. These results suggest that optimal reactivity is achieved under acidic conditions, in total agreement with experiments.

C—H oxidation is promoted by several metal−oxo moieties, but $[Fe^{IV}O]^{2+}$ is by far the most widespread. $[Fe^{IV}O]^{2+}$ is the reactive core in the Fenton reagent, in biomimetic iron complexes, in heme and non-heme enzymes, and in iron-containing zeolites. In general, metal−oxo complexes act as potent electrophiles capable of accepting electrons from very poor donors, like aliphatic C—H bonds. Theoretical studies by Baerends[429–431] showed that in the case of $[Fe^{IV}O]^{2+}$, both the energy and the shape of the lowest acceptor orbital depend on the spin state and the nature of the ligands and the solvent. The role of the metal was also clarified by Baerends with a systematic study on the oxidation of methane to methanol in the gas phase by $[MO(H_2O)_x]^{2+}$ (M = V, Cr, Mn, Fe, or Co, $x = 5$, and M = Ni, Cu, $x = 4$).[432] For all metals, the reaction follows the oxygen rebound mechanism, with the H abstraction step having the highest energy barrier. The calculations show that the energy of the lowest acceptor orbital is crucial; the barrier associated with the H abstraction step is lowered as this energy decreases. In addition, the nature of the orbital plays also a key role; at a given energy level, a σ^* acceptor is much more efficient than a π^* acceptor. $[Fe^{IV}O]^{2+}$ is thus specially efficient in promoting C—H oxidation because it has a low-lying σ^* acceptor ligand. Nevertheless, the calculations suggest that the abundance of iron is likely to be a relevant factor, because $[Fe^{IV}O]^{2+}$ is particularly efficient but $[Mn^{IV}O]^{2+}$ and $[Co^{IV}O]^{2+}$ are also potent oxidants.

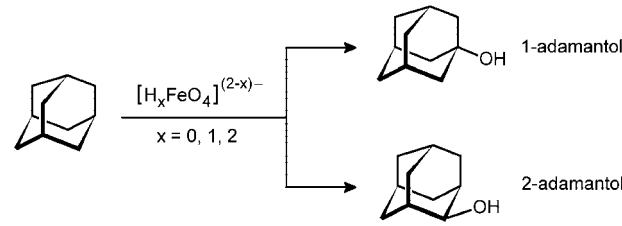

Figure 94. The oxidation of adamantane can yield either 1- or 2-adamantol.

The competitive oxidation of adamantane to 1- and 2-adamantol by ferrate(VI) was studied at the DFT level by Yoshizawa,[433] considering the different protonation states of the oxidant, FeO_4^{2-}, $HFeO_4^{-}$, and H_2FeO_4 (Figure 94). Diprotonated ferrate, H_2FeO_4, is the best oxidant, promoting hydroxylation by the classical rebound mechanism. The energy barrier of H abstraction was found to be lower for the formation of 1-adamantol ($\Delta E^{\ddagger} = 6.9$ kcal mol^{-1}) than for the formation of 2-adamantol ($\Delta E^{\ddagger} = 8.4$ kcal mol^{-1}), showing a preference for the cleavage of a tertiary over a secondary C—H bond. Transition state theory was applied successfully to assess the temperature dependence of the C—H bond oxidation rates and the ratio of 1- versus 2-adamantol products. The selectivity of C—H oxidation by the rebound mechanism is controlled by the relative stability of the involved radicals; the reaction pathway involving a tertiary radical (1-adamantol) is favored over that involving a secondary radical (2-adamantol).

5.2.2. Non-heme Iron Biomimetics

Several non-heme enzymes, including methane monooxygenase and ribonucleotide reductase, catalyze the oxidation of C—H bonds. The active centers of these enzymes, which contain the oxoferryl group, Fe^{IV}═O, have been modeled by means of the synthesis of biomimetic complexes.[226,227] These complexes also play a crucial role in the quest for efficient synthetic catalysts active in alkane oxidation.[434] In the iron non-heme complexes, the $[Fe^{IV}O]^{2+}$ cation is stabilized by a polydentate chelating ligand in an octahedral coordination environment. Some of the most relevant ligands used in the synthesis of these complexes are represented in

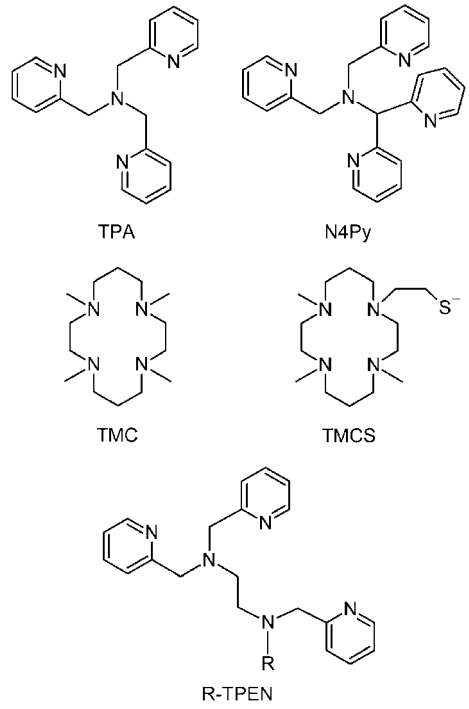

Figure 95. Polydentate chelating ligands used in the synthesis of iron non-heme biomimetic complexes.

Figure 95. When the ligand is tetradentate, TPA and TMC, the remaining vacant site is occupied by a molecule of solvent, that is, MeCN, or a counteranion, in most cases coordinated trans to the oxo group. These species have been studied by a combination of spectroscopic and theoretical methods. The calculations have shown that reactivity depends strongly on the nature of the spin states of the active Fe^{IV}=O complexes.

Alkene hydroxylation catalyzed by [Fe(TPA)] (TPA = tris(2-pyridyl-methyl)amine) was studied by Bassan with a DFT method.[435] In the presence of H_2O_2, this biomimetic non-heme complex generates [Fe(O)(TPA)(OH)], which is believed to be the active species. In [Fe(O)(TPA)(OH)], an oxo and a hydroxo ligand are coordinated in cis to the Fe(V) center in an octahedral environment. The quartet state is more stable than the doublet, but the calculations suggested that quartet to doublet spin crossover may be involved in the reaction. The calculations showed that methane and propane are hydroxylated by [Fe(O)(TPA)(OH)] following the classical rebound mechanism. In both cases, the barrier for radical H abstraction is clearly higher than that of OH rebound. The barrier in the case of methane, 17.0 kcal mol^{-1}, which involves the cleavage of a primary C—H bond, is higher than that for propane, 7.0 kcal mol^{-1}, involving a secondary C—H. The rebound barrier is extremely low, and in the case of propane, the relaxation of the H abstraction transition state led directly to the final 2-propanol product. This suggests that the radical intermediate has a very short lifetime, which agrees with the stereospecificity of the reaction observed experimentally. An oxo-hydroxo tautomerism mechanism was also computed. The tautomerism involves a water-assisted concerted proton transfer from the oxo group to the hydroxo, with an energy barrier of 14.2 kcal mol^{-1}. This mechanism accounts for the incorporation of oxygen coming from the solvent, water, into the final reaction product observed experimentally. The oxidation of acetonitrile, which is a common solvent in this reaction, was also explored. This process is exothermic but involves a relatively high energy barrier, 18.3 kcal mol^{-1}, which makes this process unlikely, in good agreement with experiments.

In a DFT study on methane oxidation by $[Fe(O)(TPA)(OH)]^{2+}$, Balbuena demonstrated that the catalytic activity of this compound can be tuned by introducing different substituents in the TPA ligand.[436] Within the framework of the rebound mechanism, the calculations show that the energy barrier to H abstraction for TPA, 15.7 kcal mol^{-1}, is lowered to 13.4 kcal mol^{-1} by introducing nitro groups in the pyridine rings and is increased to 18.0 kcal mol^{-1} by introducing methoxy groups in the same position. These results indicate that the critical barrier of the reaction is lowered by electron-withdrawing groups whereas it is increased by electron-donating groups. This is consistent with a reactivity model in which the catalyst, acting as the electrophile, undergoes nucleophilic attack of the C—H bond.

C—H hydroxylation by the biomimetic non-heme $[Fe(O)(N4Py)]^{2+}$ (N4Py = *N*,*N*-bis(2-pyridylmethyl)-*N*-bis(2-pyridyl)methylamine) complex was studied by Shaik with a DFT method including solvent effects.[437] This compound acts as a potent oxidant capable of activating inert C—H bonds, with dissociation energies higher than 95 kcal mol^{-1}. The ground state of $[Fe(O)(N4Py)]^{2+}$ is a triplet, in agreement with experiments, followed by a quintet state and an open-shell singlet. The rebound mechanism for the hydroxylation of cyclohexane, which has a strong C—H bond (D(C—H) = 99 kcal mol^{-1}), was explored in detail. The calculations showed that the H abstraction barrier is 9.6 kcal mol^{-1} in vacuo, which is increased to 11.9 kcal mol^{-1} by solvation and to 26−27 kcal mol^{-1} by entropic effects. These results suggested that $[Fe(O)(N4Py)]^{2+}$ is intrinsically a more potent oxidant than the compound I species of CYP450 due to the double positive charge of the system, which stabilizes the three-center three-electron (3c/3e) O···H···C moiety of the transition state.

These studies were subsequently extended by exploring the mechanism of alkane hydroxylation by several iron oxo complexes. Three substrates, toluene, cyclohexane, and acetonitrile, and three $Fe^{IV}O$ oxidants with different N-bound chelating ligands, TMC (1,4,8,11-tetramethyl-1,4,8,11-tetraazacyclotetradecane), N4Py, and Bn-TPEN (*N*-benzyl-*N*,*N*′,*N*′-tris(2-pyridylmethyl)-1,2-diaminoethane), were considered.[438] The calculations provide a rationalization of the experimental reactivity trends by means of a two-state reactivity (TSR) model. In this model, two spin states, which must be close in energy, interplay giving rise to the overall reactivity observed experimentally. The $Fe^{IV}O$ biomimetics have a triplet ground state and a low-lying quintet state, within an energy range of 1−10 kcal mol^{-1}. Both spin states are able to promote C—H oxidation but involve different reaction mechanisms. In the triplet state, the reaction follows the classical stepwise oxygen rebound mechanism, in which H abstraction is followed by the rebound of the carbon radical to the OH group. In the quintet state, the reaction is effectively concerted because the OH rebound step is barrier free. Another key feature is the fact that the quintet is less stable but more reactive than the triplet, because in the quintet state the energy barrier associated with the rate-determining H abstraction step is lower. Depending on the energy difference between the spin states, $\Delta E_{T/Q}$, which is determined by the nature of the ligands bound to Fe, two main TSR scenarios are possible (Figure 96): (1) when $\Delta E_{T/Q}$ is small, the two states undergo pre-equilibration and the subsequent reaction takes place in the quintet state, which

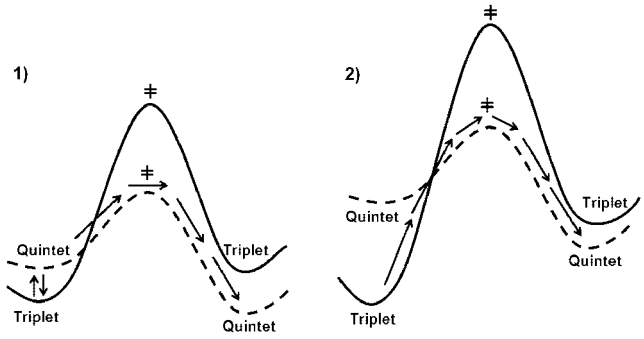

Figure 96. The TSR model can involve either triplet/quintet pre-equilibration (case 1) or triplet to quintet spin crossover en route to the transition state (case 2).

is associated with the lowest energy path, or (2) when $\Delta E_{T/Q}$ is large, spin-crossover from triplet to quintet may happen en route to the H abstraction transition state. Between these extremes, several intermediate cases are possible. In addition, in case 2, if the triplet and quintet transition states are close in energy or the spin-crossover is ineffective, the reaction may take place entirely on the triplet surface. This will have a dramatic effect on the selectivity of the reaction; in the triplet state, the generation of radicals will lower the selectivity due to the formation of side products or the loss of stereochemistry.

The TSR model, previously proposed by Shaik for cytochrome P450 on the basis of calculations,[439–441] has allowed rationalization of several intriguing aspects of the chemistry of the non-heme iron biomimetics.[442–445] Surprisingly, experiments show that the oxidation of phosphines and alkanes by the series of complexes $[TMC(L)FeO]^{2+}$ (L = CH_3CN, $CF_3CO_2^-$, N_3^-, SR^-) follows opposite trends. The rate of phosphine oxidation increases as the electrophilicity of the oxidant becomes higher, following the order $CH_3CN > CF_3CO_2^- > N_3^- > SR^-$, whereas alkane hydroxylation follows the counterintuitive opposite trend. The TSR model provides a simple explanation for this unexpected observation.[442,443] As the electron donor character of L decreases, the $Fe^{IV}O$ complex becomes more electrophilic and thus more oxidating, but the quintet state is shifted up in energy. Therefore, the participation of the triplet state, which involves higher energy barriers, increases, and the overall reactivity is diminished. This counterintuitive trend is not observed for the $Ru^{IV}O$ analogues, which show lower reactivities. In the framework of the TSR model, these experimental results are explained by the high energy of the quintet state, obtained when Fe is replaced by Ru.[444] Due to this high energy, the quintet is not accessible, and the system follows a single state reactivity model, which involves only the triplet state. Without the interplay between the different spin states, the relationship between the electrophilicity and the reactivity of the $Ru^{IV}O$ complexes follows the expected trend for both phosphine and C—H oxidation. In addition, the high energy barriers associated with the triplet state account for the sluggish reactivity of these Ru species.

Another intriguing feature is the unusual kinetic isotope effect pattern measured for $[Fe(O)(N4Py)]^{2+}$ and $[Fe(O)(Bn\text{-}TPEN)]^{2+}$. For some substrates, like acetonitrile and cyclohexane, the KIE falls within the semiclassical region, with $k_H/k_D < 7$. Conversely, other substrates, like ethylbenzene and dihydroanthracene, show large nonclassical KIE, with $k_H/k_D > 7$, in some cases ≥ 30. In the latter case, the large KIEs are typical of tunneling and support the homolytic C—H cleavage as the rate-determining step. Nevertheless, if only the triplet participates in the reaction, the k_H/k_D values are too large, considering the high energy barriers associated with this spin state. In contrast, in the TSR framework, the system may cross the high triplet barrier by hoping to the lower energy quintet surface, opening a tunneling-like pathway.[445] If the zero-point energy stored in the C—H bond that undergoes activation is equal to or higher than the quintet energy barrier, the vibration of this bond may propagate the reactant directly to the products. This phenomenon depends strongly on the strength of the C—H bond, D(C—H). As D(C—H) increases, the quintet energy barrier becomes higher thus hampering the tunneling-like pathway. Therefore, the large KIEs are only possible for a narrow range of substrates with weak C—H bonds, D(C—H) < 93 kcal mol^{-1}, as observed experimentally for ethylbenzene and dihydroanthracene. With stronger C—H bonds, the KIEs follow the semiclassical regime.

The effect of external electric fields (EF) on C—H oxidation by non-heme iron—oxo complexes was studied by Shaik at the DFT level.[446] The application of an EF changes the potential energy surface of the system, which has a great impact on the mechanism, the selectivity, and the rate of the reaction. The largest effects are observed when the EF is aligned with the axis of the Fe═O bond, in which the electrons flow from the substrate to the Fe center during the reaction. This electron flow is stimulated by the EF yielding lower energy barriers. Two different spin states were studied, the triplet and the quintet, and the effect of the EF was found to be larger in the quintet state. The influence of the EF on the reaction mechanism was explored considering two different ligands bound to Fe, N4Py and TMC(SR), and two different substrates, cyclohexane and toluene. When the iron complex is a good acceptor, $[Fe(O)(N4Py)]^{2+}$, the reaction did not follow the classical OH rebound pathway. If the substrate is a good acceptor, toluene, the H abstraction step is replaced by electron transfer, whereas if it is a poor acceptor, cyclohexane, the EF promotes hydride transfer yielding a carbocation. When both the acceptor and donor characters are poor, like in the reaction of $[Fe(O)(TMC(SR))]^+$ with cyclohexane, the rebound mechanism prevails and the EF lowers the energy barriers of the H abstraction and the OH rebound steps.

The $[Fe(O)(TMCS)]^+$ (TMCS = 1-mercaptoethyl-4,8,11-trimethyl-1,4,8,11-tetraazacyclotetradecane) complex is an interesting biomimetic of the cytochrome P450 enzyme. This complex promotes the C—H oxidation of several alkanes in a chemoselective fashion. For instance, when $[Fe(O)(TMCS)]^+$ is used to oxidize propene, which can easily undergo epoxidation of the C═C bond, only the CH_3-hydroxylation product is obtained. This selective reaction was theoretically studied by de Visser.[447] The calculations showed that the reaction follows a single-state reactivity regime, since both the hydroxylation and the epoxidation take place fully in the quintet state. The hydroxylation process follows the rebound mechanism with the highest energy barrier, 15.0 kcal mol^{-1}, being associated with the H abstraction step. This barrier is 3 kcal mol^{-1} lower than the highest energy barrier associated with the epoxidation reaction, suggesting that hydroxylation takes place preferentially, in total agreement with the experiments. The selectivity is due to the steric hindrance between the catalyst and the substrate in the transition state, which is larger in the epoxidation reaction. The comparison of [Fe(O)(T-

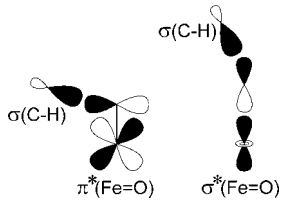

Figure 97. The π−FMO (left) and the σ−FMO (right) pathways in C−H oxidation by non-heme Fe^{IV}=O biomimetic complexes.

MCS)]$^+$ with the natural enzymatic systems revealed that the biomimetic complex involves higher energy barriers, but is less sensitive to external perturbations like the H bonds or the dielectric constant associated with the solvent.

The series of non-heme Fe^{IV}=O complexes [Fe(O)(TMC)-(NCMe)]$^{2+}$, [Fe(O)(TMC)(OCOCF$_3$)]$^+$ and [Fe(O)(N4Py)]$^{2+}$ were studied by means of spectroscopic and DFT techniques by Que and Solomon.[448] The ground state of these complexes is a low-spin triplet, in contrast with the Fe enzyme intermediates, which are high-spin quintet species. The Fe=O bonds are strong and have high covalent character. The complex with the strongest Fe=O bond, [Fe(O)(N4Py)]$^{2+}$, has also the highest reactivity in C−H oxidation. Due to the strength and covalency of the iron−oxo bond, the frontier molecular orbitals (FMOs) that govern the reactivity have strong oxygen character. These FMOs, which are the antibonding $\pi^*_{xz/yz}$(Fe=O) orbitals, $d_{xz}-p_x$ and $d_{yz}-p_y$, activate the iron complex for an electrophilic attack. In the transition state of the key H abstraction step, the σ(C−H) orbital of the oxidized C−H bond interacts with one of the $\pi^*_{xz/yz}$(Fe=O) orbitals (Figure 97). In this reaction pathway, labeled as π−FMO, there is a lateral approach of the substrate perpendicular to the Fe=O direction, with an Fe−O−H angle of ∼120° for an optimal overlap between the σ(C−H) and $\pi^*_{xz/yz}$(Fe=O) orbitals. This π−FMO pathway is also followed by the Fe enzyme intermediates. In these systems, the σ^*_z(Fe=O) orbital, $d_{z^2}-p_z$, is also low in energy and has high oxygen character, due to the spin polarization associated with the high-spin quintet ground state. This orbital opens an alternative σ−FMO pathway in which the substrate approaches the iron complex in a vertical orientation along the Fe=O direction.

Two different Fe^{IV}=O complexes, one heme ([Fe(O)(por)-(NCMe)]$^{2+}$ (por = porphyrin)) and one non-heme ([Fe(O)-(TMC)(NCMe)]$^{2+}$), were studied and compared by Solomon.[449] The electronic structure and the iron−oxo bonding are essentially the same in both complexes, as indicated by the very similar FMOs and Fe−O distances and vibrational frequencies. Thus, both the porphyrin and the TMC ligands do not interact to a great extent with the π Fe=O bond. This is normal for the TMC ligand, which is a pure σ-donor, but it is not expected for the π-donor/acceptor porphyrin ligand. The calculations show that this is due to the strong and covalent character of the iron−oxo bond, which decouples the π system of the Fe=O group from the π system of the porphyrin. Nevertheless, in C−H oxidation reactions, the product of the key H abstraction step, which is an Fe^{III}OH intermediate, has different electronic structure and Fe−O bonding in the heme and non-heme environments. The weakening of the iron−oxygen bond along the reaction pathway from Fe=O to Fe−OH promotes the mixing of the π systems of the reactive center and the ligand in the product, which is only possible with the porphyrin ligand of the heme complex. As a consequence, the Fe^{III}OH intermediate is more stable with the porphyrin ligand than with TMC, and therefore, H abstraction is thermodynamically more favorable in the heme case.

The non-heme iron(II) [Fe(Tp^{Ph2})BF] (Tp^{Ph2} = hydrotris-(3,5-diphenylpyrazol-1-yl)borate; BF = benzoylformate) complex promotes the hydroxylation of phenyl rings, using O_2 as oxidant. This complex reproduces the activity of the α-ketoglutarate-dependent enzymes. A DFT study reported by Borowski and Siegbahn showed that this reaction does not follow the classical oxygen rebound mechanism.[450] The oxidation of [Fe(Tp^{Ph2})BF] by O_2 yields a high-valent Fe^{IV}O species (Figure 98). The oxo group makes an electrophilic attack to a C−H bond of the phenyl ring, generating a new C(H)−O bond. In the next step, the hydrogen is transferred to O with the assistance of the BF ligand, yielding the C−OH group of the phenol product. A single electron is transferred in each step; the formation of the C−O bond leads to a phenyl radical, and the H transfer is indeed a proton-coupled electron transfer. As in the multistate reactivity models proposed by Shaik, three different spin states may participate in the reaction, a triplet, a quintet, and a septet.

This reaction mechanism is also followed in aromatic hydroxylation of arenes by the $Fe^{IV}O^{2+}$ complexes [Fe(O)-(Bn-tpen)]$^{2+}$ and [Fe(O)(N4Py)]$^{2+}$. This reaction was analyzed in a combined experimental/theoretical study by Nam and de Visser.[451] Isotope labeling experiments proved that the oxygen of the product comes from the [Fe^{IV}O]$^{2+}$ moiety, thus confirming the iron−oxo complexes as active species. The large and negative value of the Hammet ρ parameter, −3.9, and the inverse KIE value of 0.9, were consistent with an electrophilic pathway. This was further confirmed by the calculations, which indicated that the reaction follows an electrophilic substitution mechanism. The reaction starts with an electrophilic attack of the oxidant to a carbon of the aromatic ring, leading to an Fe−O−Ph intermediate, in which the phenyl ring can have either radical or cationic character. This step is followed by a proton-shuttle mechanism in which the hydrogen at the *ipso* position is transferred to the oxygen with the help of a N of the ligand, yielding the final phenol product. This mechanism is more efficient than H abstraction followed by OH rebound. The calculations show that the TSR model also applies to this reaction, which involves both the triplet and quintet states.

The non-heme biomimetic complex [Fe(O)(R-TPEN)]$^{2+}$ has three different isomers, labeled A, B, and C. In isomers A and B, the three pyridine rings of the R-TPEN ligand are cis to the oxo group, whereas in isomer C one pyridine is in trans position. Isomers A and B differ in the orientation of the pyridine rings with respect to the Fe=O axis; one pyridine is perpendicular to this axis in A and two in B. The hydroxylation of cyclohexane by the three isomers of [Fe(O)(R-TPEN)]$^{2+}$ was studied by Han[452] The calculations showed that isomers A, B, and C have triplet ground states and low-lying quintet states. The three isomers promote C−H oxidation. The reaction follows the oxygen rebound mechanism and involves both the triplet and quintet states, within a TSR framework. The relative stability of the isomers follows the order A > B > C, in good agreement with previous studies by Klinker et al.[453] Conversely, the reactivity follows a different trend, B > A > C. The higher reactivity of isomer B with respect to A, is due to the presence of one more pyridine ring perpendicular to the Fe=O axis, which stimulates the reactivity of the iron−oxo

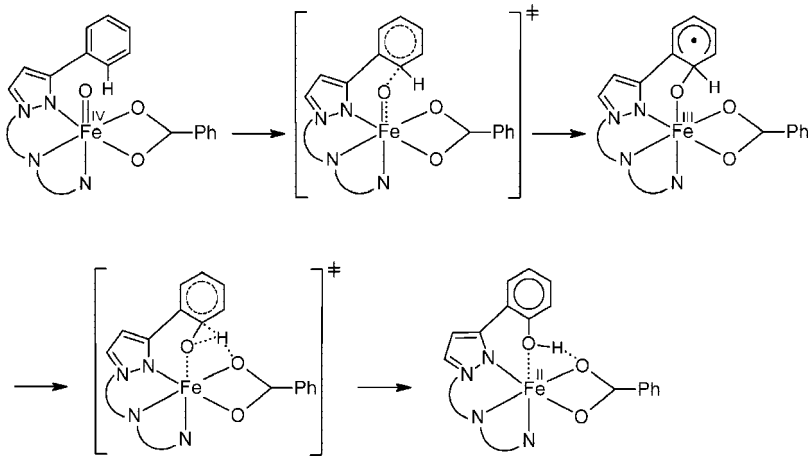

Figure 98. The reaction mechanism of phenyl hydroxylation by $Fe^{IV}O$.

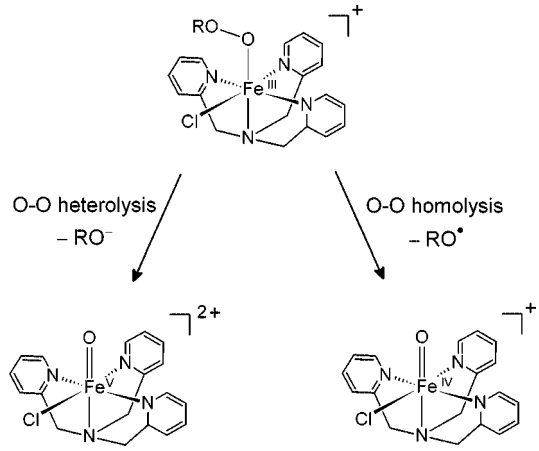

Figure 99. Halogenase biomimetics: the two possible non-heme iron-oxo active species.

group. The presence of a pyridine trans to the oxo ligand in C diminishes both the stability and the reactivity of the system.

The mechanism of oxidative chlorination catalyzed by $[Fe(TPA)(Cl)_2]^+$ was theoretically studied by Siegbahn.[454] The reaction of this compound with a peroxide yields $[Fe(OOR)(TPA)(Cl)]^+$, which generates either $[Fe^V(O)(TPA)(Cl)]^{2+}$ by O—O heterolysis or $[Fe^{IV}(O)(TPA)(Cl)]^+$, by O—O homolysis (Figure 99). These iron−oxo species are biomimetic complexes of the non-heme halogenase enzymes. The oxidative chlorination of cyclohexane by $[Fe^V(O)(TPA)(Cl)]^{2+}$ and $[Fe^{IV}(O)(TPA)(Cl)]^+$ was studied considering different spin states. In the case of $[Fe^V(O)(TPA)(Cl)]^{2+}$, cyclohexane is initially oxidized yielding a cyclohexyl radical cation. In the subsequent step, the transition state for H abstraction has an unusually long O···H distance (1.88 Å) and involves an energy barrier of 12.8 kcal mol^{-1}. The relaxation of this transition state leads directly to the formation of the chlorinated product, by transfer of a Cl^- ion. This prevents hydroxylation and explains the exclusive and stereospecific chlorination reaction observed experimentally. In contrast, the $[Fe^{IV}(O)(TPA)(Cl)]^+$ species follows the classical two-step rebound mechanism, in which the energy barrier for OH rebound is very similar to that of Cl transfer. Hence, for this particular complex, the calculations did not account for the experimental observations.

Fe^{IV}═O is generally accepted as the reactive group in C—H oxidation by non-heme iron biomimetics. Nevertheless, the nature of the active species has been debated. The hydroxylation of cyclohexane by high-valent iron−oxo bispidine complexes was studied by Comba using a combined experimental/theoretical approach.[455] The calculations show that the active species may be either an Fe^{IV}═O or an Fe^V═O complex, since both groups promote C—H oxidation by an oxygen rebound mechanism. The Fe^{IV}═O species is thermodynamically favored by ca. 12 kcal mol^{-1}, whereas the Fe^V═O species involves energy barriers that are lower than those associated with Fe^{IV}═O by ca. 6 kcal mol^{-1}. These results suggest that the hydroxylation of cyclohexane is promoted by both Fe^{IV}═O and Fe^V═O species in competing parallel reaction pathways. This scenario gives indeed the best fit with the experiments.

Some biomimetic Fe^{IV}═O complexes are able to promote oxidative C—H addition not only by hydroxylation but also by dehydrogenation. For instance, dihydroanthracene is oxidized to anthracene by $[Fe(O)(TMC)]^{2+}$. This reaction was theoretically studied at the DFT level by Johansson and Siegbahn.[456] Previous NMR studies by Rhode and Que[457] revealed that several isomers of the active species are present in the reaction mixture, which contains the counteranion, $CF_3CO_2^-$, and the solvent, acetonitrile. The coordination environment of iron is different in each of these isomers. The axial ligand trans to the oxo group can be either acetonitrile or the counteranion. In addition, the complex may be cationic or neutral depending on whether an ion pair is formed in solution. This issue was considered in the theoretical study by using five models with different axial ligands and counteranion arrangements. The results show that neither the nature of the axial ligand nor the number of counteranions in the ion pairs have a great effect on the reactivity of $[Fe(O)(TMC)]^{2+}$. The reaction follows a two-step mechanism consisting of two H abstraction steps (Figure 100). The first step is rate-limiting, with an energy barrier of ca. 16 kcal mol^{-1}, in good agreement with the experimental value of ca. 19 kcal mol^{-1}. The second H abstraction has a much lower energy barrier, mainly of entropic origin. As for C—H hydroxylation, the reaction obeys a TSR regime by starting in the triplet ground state and ending in the quintet state, after spin crossover during the first step. The overall reaction is strongly exothermic, by more than 60 kcal mol^{-1}, due to the formation of the aromatic anthracene product.

5.2.3. Non-heme Iron Enzymes

The oxidation of propene by the non-heme taurine/α-ketoglutarate dioxygenase (TauD) enzyme was theoretically

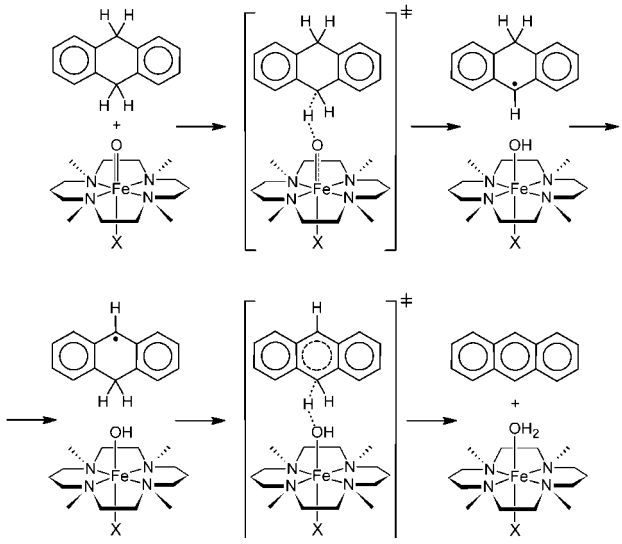

Figure 100. Dihydroanthracene oxidation by $[Fe(O)(TMC)(X)]^{2+}$ (X = MeCN or $CF_3CO_2^-$).

studied by de Visser.[458,459] The Fe^{IV}═O center of this enzyme is capable of oxidizing both the CH_3 (hydroxylation) and the CH═CH_2 (epoxidation) groups of the substrate. Three different spin states, triplet, quintet, and septet, are able to promote the hydroxylation and epoxidation of propene, but the reactivity is controlled by the quintet, which provides the lowest energy pathways. The hydroxylation reaction, with a highest energy barrier of 5.4 kcal mol^{-1}, follows the classical oxygen rebound mechanism and competes with the epoxidation reaction, which has almost the same maximum barrier, 4.8 kcal mol^{-1}.

Heme enzymes, such as cytochrome P450 (CP450), were compared with the non-heme TauD enzyme, which is fundamentally different in many ways: Fe is five-coordinated in TauD and six-coordinated in the heme enzymes; the reactivity follows a single-state reactivity (SSR) model in TauD and a two-state reactivity (TSR) model in the heme enzymes; in TauD, both electrons of the oxidized substrate are absorbed by Fe, whereas in the heme enzymes, one electron is taken by Fe and the other by the porphyrin ligand; and finally, the valence molecular orbitals are different in each case. In addition to these differences, the calculations showed that the oxidative power of TauD is much higher than that of the heme enzymes, due to lower energy barriers. The higher reactivity of TauD is assigned to the higher radical character of the reactive Fe center, the stronger FeO—H bond formed in the rate-determining H abstraction step, and the higher exchange stabilization of the key metal FMOs. In a subsequent study, the whole TauD enzyme was modeled at the QM/MM level.[460] These calculations showed that despite the many H-bond and salt-bridge interactions between the reactive center and the protein environment, the structure and reactivity are essentially the same as those found in the previous DFT models.[458,459]

Aromatic hydroxylation by tetrahydrobiopterin-dependent hydroxylases was modeled by Bassan at the DFT(B3LYP) level.[461] In a previous theoretical study, the authors had demonstrated that the active species, an Fe^{IV}═O complex, is generated from molecular oxygen with the assistance of the tetrahydrobiopterin cofactor.[462] The oxidation of the aromatic ring of phenylalanine, modeled as benzene, and tryptophan, modeled as indole, was explored considering two different protonation states of the catalytic core: $[HO—Fe^{IV}═O]$ and $[H_2O—Fe^{IV}═O]^+$ (Figure 101). The oxo and the OH/H_2O ligands are bound to the iron(IV) center in a cis position within an octahedral environment. The other four coordination sites are occupied by a monodentate glutamate and an aqua ligand in cis and by two cis histidine molecules. The solvent is explicitly considered in the model by introducing two molecules of water; one to stabilize the octahedral coordination of iron and the other to better model the proton transfers involved in the reaction.

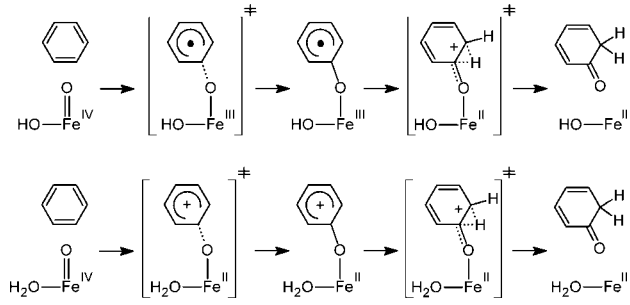

Figure 101. Reaction mechanism for the oxidation of benzene by $[HO—Fe^{IV}═O]$ and $[H_2O—Fe^{IV}═O]^+$ species.

With the neutral model, $[HO—Fe^{IV}═O]$, the oxidation of the aromatic substrate, in which the FeO—Ph bond is formed, involves a phenyl radical. A subsequent 1,2-hydride shift leads to the formation of a keto intermediate, which by keto−enol tautomerization yields the final hydroxylated product. An alternative final step with a higher energy profile, involving the formation of an epoxide, was discarded. With the cationic model, $[H_2O—Fe^{IV}═O]^+$, the formation of the FeO—Ph bond involves a $2e^-$ oxidation yielding an arenium cation. For both catalysts and substrates, the higher energy barrier corresponds to the oxidative formation of the FeO—Ph bond. In the case of benzene, this step involves an energy barrier of 16.2 kcal mol^{-1} for the radical mechanism ($[HO—Fe^{IV}═O]$) and of 10.0 kcal mol^{-1} for the cationic mechanism ($[H_2O—Fe^{IV}═O]^+$). Similar barriers were found for indole. The critical energy barrier is lowered by the protonation of the OH ligand. The reaction occurs on the quintet surface, which is also the ground state of the isolated catalyst. The hydroxylation of the benzylic carbon of the substrates was also investigated, considering the oxidation of toluene by the rebound mechanism. In this case, H abstraction has the highest energy barrier, 11.1 kcal mol^{-1}. The results obtained in this study showed that an Fe^{IV}═O center in the catalytic core of hydroxylases is capable not only of aromatic hydroxylation but also of benzylic hydroxylation, in good agreement with experiments.

A similar catalytic system in which L-phenylalanine is oxidized to L-tyrosine by a non-heme iron hydroxylase was studied by Yoshizawa with QM and QM/MM methods.[463] The hydroxylation of the substrate by the active site of the enzyme, which contains an $Fe^{IV}O$ active species, may involve two different mechanisms: (1) the classical oxygen rebound mechanism, with C—H cleavage by H abstraction followed by OH rebound or (2) oxygen insertion by electrophilic aromatic addition, followed by 1,2-hydride shift, which yields the keto tautomer of the reaction product, as in Figure 101. The rebound mechanism was explored by considering the triplet, quintet, and septet states of the system. The calculations show that the energy barriers associated with the H abstraction and OH rebound steps amount to 24.6 and 9.2 kcal mol^{-1}, respectively. In contrast, in the oxygen insertion mechanism, the electrophilic addition is barrier-free and the

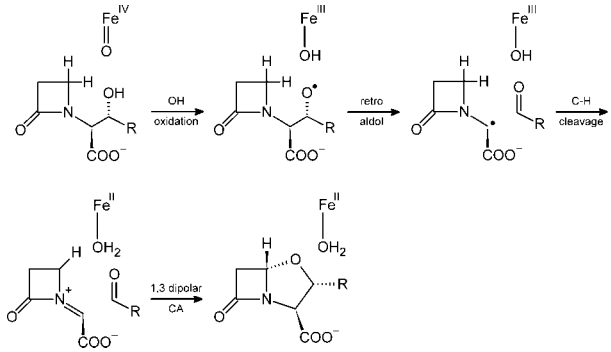

Figure 102. Reaction mechanism for the oxidative cyclization of proclavaminic acid (R = $CH_2CH_2NH_3^+$).

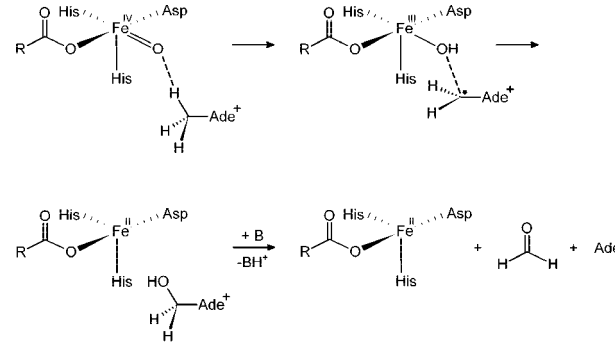

Figure 103. Reaction mechanism for the oxidative dealkylation of 1-methyladenine ($AdeCH_3^+$) by the AlkB family of enzymes.

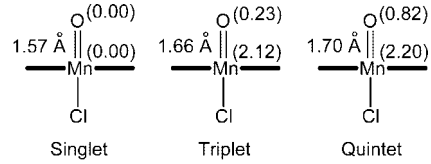

Figure 104. Manganese−oxo bond lengths and spin densities (in parentheses) for [Mn(O)(Cl)(por)].

$\Delta E^{\ddagger}$ for the 1,2-hydride shift is only 9.0 kcal mol^{-1}. This study thus showed that the insertion mechanism is favored over the rebound one.

The oxidative cyclization of proclavaminic acid catalyzed by clavamic acid synthase was theoretically studied by Borowski and Siegbahn.[464] A realistic structure of the enzyme−substrate complex was obtained by molecular dynamics simulations. The reaction mechanism was explored by means of DFT(B3LYP) calculations on a large model of the reactive center, which contains an $Fe^{IV}O$ active species. A new reaction mechanism was proposed on the basis of the calculations (Figure 102): (1) oxidation of the hydroxyl group by reduction of the metal center to $Fe^{III}OH$, (2) retro-aldol-like decomposition of the O radical intermediate, (3) C—H cleavage by H abstraction, in which the metal center is further reduced to $Fe^{II}OH_2$, and (4) 1,3-dipolar cycloaddition yielding the final reaction product. The C—H cleavage step involves an energy barrier of 20.6 kcal mol^{-1}. Interestingly, the calculations show that this mechanism involves a reaction pathway lower in energy, and thus more favorable, than the mechanism originally proposed for this reaction,[465] which consists of radical H abstraction followed by transfer of one electron and one proton. In addition, the new mechanism is consistent with experimental isotope kinetics data.[466]

Another cyclization reaction of high relevance is the biosynthesis of four-membered β-lactam rings, which are present in several antibiotic drugs, by isopenicillin N synthase. This reaction has been studied by Siegbahn at the DFT level.[467,468] The calculations showed that the mechanism involves two key steps: (1) cysteine C—H activation by a radical Fe(III) superoxo species, which has an energy barrier of 14.6 kcal mol^{-1}, and (2) valine C—H activation by a ferryl Fe(IV) oxo species, which has an energy barrier of 15.3 kcal mol^{-1}. These energy barriers are the highest found along the reaction pathway, which suggests that both steps are partially rate-determining, in good agreement with the experiments. Interestingly, the order in which the C—H bonds are cleaved is determined by the oxidative strength of the active species, since the strong C—H bond of valine can only be cleaved by the ferryl−oxo species.

The α-ketoglutarate Fe(II)-dependent AlkB family of enzymes remove the alkylation damage from DNA nucleobases by oxidative dealkylation. The regeneration of 1-methyladenine ($AdeCH_3^+$) by the Fe^{IV}═O reactive center of these enzymes was theoretically studied by Gauld at the DFT(B3LYP) level.[469] The damaging methyl group is oxidized by the Fe^{IV}═O moiety yielding $AdeCH_2OH^+$. This process involves radical H abstraction, followed by OH rebound (Figure 103). In the next step, the hydroxyl group of $AdeCH_2OH^+$ is deprotonated by a Bronsted base, which leads to formaldehyde and the repaired base, adenine, by C—N cleavage. This reaction mechanism was studied by exploring the potential energy surfaces associated with the triplet, quintet, and septet states. The calculations showed that H abstraction is the rate-determining step, with an energy barrier of ca. 22 kcal mol^{-1}, in good agreement with the experimental value, ca. 21 kcal mol^{-1}.

5.2.4. Manganese Porphyrin Biomimetics

The oxidation of toluene to benzyl alcohol by [Mn(O)(por)(Cl)] (por = porphyrin) was studied by Eisenstein et al. at the DFT(BP86) level.[320] Manganese porphyrins are efficient synthetic catalysts and biomimetic models of the heme cofactors of the cytochrome enzymes. The calculations showed that [Mn(O)(por)(Cl)] has three accessible spin states: a singlet, a triplet, and a quintet, all within an energy range of ∼10 kcal mol^{-1}. As the total spin of the system increases, the Mn═O distance elongates and the radical character on oxygen ($O^{\bullet}$ character) becomes higher, due to the occupation of antibonding π^*(Mn═O) orbitals (Figure 104). The singlet, which is the ground state, lacks $O^{\bullet}$ character and does not promote C—H oxidation. In contrast, both the triplet and quintet states, having $O^{\bullet}$ character, promote C—H oxidation. In the triplet state, the highest energy barrier, 2.6 kcal mol^{-1}, corresponds to the H abstraction step. The resulting hydroxo intermediate, [Mn(OH)(por)(Cl)], undergoes OH rebound with almost no barrier. The quintet surface is higher in energy in the H abstraction step but lower in the OH rebound, which suggested that triplet → quintet spin-crossover may happen during the reaction. This study showed that the rebound mechanism for Mn(porphyrin)-catalyzed C—H hydroxylation is only favored for spin states with radical character on oxygen.

In a subsequent study by the same authors, the influence of the axial ligand, X, on C—H oxidation by $[Mn(O)(por)(X)]^+$ (X = OH_2, OH^-, O^{2-}) was rationalized by means of DFT(BP86) calculations.[321] The relative concentration of these three prototropic species is determined by the pH. At low pH, $[Mn(O)(por)(OH_2)]^+$ is the dominant species, whereas at high pH, $[Mn(O)_2(por)]^-$ is the dominant species.

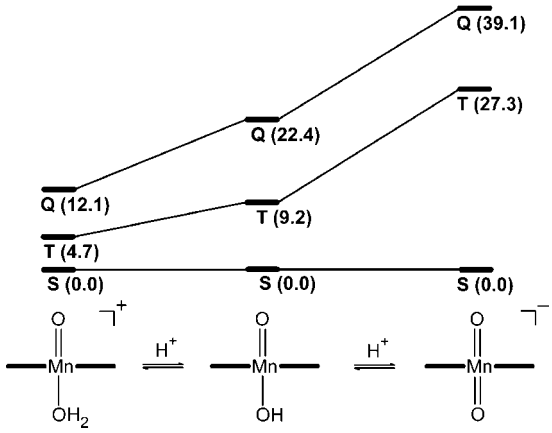

Figure 105. Energy differences, in kcal mol^{-1}, between the singlet (S), triplet (T), and quintet (Q) states of [Mn(O)(X)(por)]$^+$ (X = OH_2, OH^-, O^{2-}).

Although the trans influence of X increases from X = OH_2 to X = O^{2-}, causing the elongation of the Mn=O bond, the reactivity in C−H oxidation decreases. The theoretical study showed that the O$^\bullet$ character is essential for efficient reaction, as previously shown for [Mn(O)(por)(Cl)].[320] For all X, the singlet ground state, lacking O$^\bullet$ character, is nonreactive, whereas the high-spin states, triplet and quintet, having O$^\bullet$ character, promote C−H oxidation. The low-spin/high-spin energy difference, $\Delta E_{LS/HS}$, is determined by the nature of the axial ligand.[470] As the trans influence of X is reduced by making the pH more acidic, $\Delta E_{LS/HS}$ decreases, and the reactive high-spin states become thus more accessible, which promotes the reaction (Figure 105). This is due to the energy of the singly occupied π^*(Mn=O) orbitals in the high-spin states, which becomes lower as the π-donor character and trans influence of the axial ligand decreases. This study showed that C−H oxidation by [MnO(por)(X)]$^+$ is promoted by changing the pH from high, X = O^{2-}, to low, X = OH_2, in total agreement with experiments.

5.2.5. Copper Biomimetics

Cu^I α-ketocarboxylate complexes with supporting N-donor ligands are biomimetics of copper-containing oxygenase enzymes. The reactivity of these complexes was studied at the DFT and CASSCF/CASPT2 levels by Gagliardi, Tolman, and Cramer.[471] The oxidation of the Cu^I complex by O_2 may yield a mixture of Cu−peracid and Cu−oxo species, which are both capable of hydroxylating a phenyl ring of the supporting ligand. The calculations show that the oxo species are more reactive than the peracid species. Formally, the most reactive complex contains the Cu^{III}=O oxo group. Nevertheless, the study revealed that this group is better described as a Cu^{II}—O$^\bullet$ oxyl. The introduction of different substituents at several positions of the metal backbone showed that an electron-donating ligand increases the Cu−O bond strength. This makes the Cu−oxyl species more stable than the peracid species but also reduces its reactivity. The triplet state of the Cu−oxyl species promotes aromatic hydroxylation, with the following two-step reaction mechanism: (1) O-attack to the ortho C of the phenyl ring and (2) H transfer from the ipso carbon to the oxygen. This mechanism is analogous to that described by Borowski and Siegbahn for [Fe(Tp^{Ph2})BF] (Figure 98).[450] The highest activation barrier associated with this process is only 10.1 kcal mol^{-1}. Interestingly, the reaction may also follow the oxygen rebound mechanism. Nevertheless, this mechanism involves higher activation barriers: 15.6 kcal mol^{-1} for the H abstraction step and 13.3 kcal mol^{-1} for the OH rebound step.

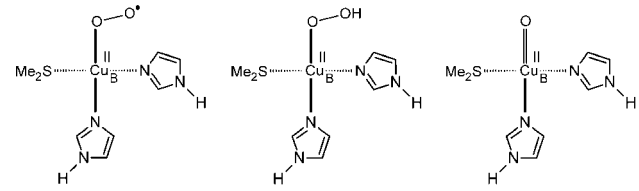

Figure 106. Superoxo (left), hydroperoxo (center), and oxo (right) forms of the CuB site in DBM.

5.2.6. Copper Monooxygenases

The catalytic mechanism of dopamine β-monooxygenase (DBM) was explored computationally by Yoshizawa in order to identify the active species and reveal the function of the surrounding amino acid residues.[472] DBM contains two reactive copper sites, CuA and CuB, which promote the stereoselective hydroxylation of dopamine. A 3D structure of the whole enzyme was constructed by homology modeling from the crystal structure of a closely related enzyme, peptidylglycine α-hydroxylating monooxygenase. This structure, containing about 4700 atoms, was optimized at the QM(B3LYP)/MM(Amber96) level. The calculations showed that copper is coordinated to three histidine residues in the CuA site and to two histidines and one methionine in the CuB site. Three other residues, two glutamates and one tyrosine, play a key role in orienting the substrate through H bonds to promote H abstraction in a stereospecific fashion. The reactivity of the active center was modeled with DFT(B3LYP) calculations on small models extracted from the QM part of the QM/MM geometries. Three active species, with different charges and spin states, were investigated: Cu−superoxo, Cu−hydroperoxo, and Cu−oxo (Figure 106). The Cu−superoxo species is able to promote H abstraction with an energy barrier of 16.9 kcal mol^{-1} but is less reactive than the Cu−oxo, which involves a barrier of only 3.8 kcal mol^{-1}. The Cu−hydroperoxo species was ruled out because it is associated with an energy barrier of ∼40 kcal mol^{-1}, which is too high in physiological conditions.

In a subsequent study by the same authors, the reactivity of the copper center is studied on the whole enzymatic system by QM/MM calculations.[473] In this extended model, the energy barrier for the H abstraction step was 23.1 kcal mol^{-1} for the Cu−superoxo species and 5.4 kcal mol^{-1} for the Cu−oxo. The energy of the hydroxo radical intermediate was found to be 18.4 kcal mol^{-1} in the Cu−superoxo pathway and −14.2 kcal mol^{-1} in the Cu−oxo. These results indicate that the active species is likely to contain a Cu=O oxo group, which according to the calculations is better described as a Cu—O$^\bullet$ oxyl group. The protein environment favors the hydroxylation reaction both kinetically and thermodynamically. All steps are clearly exothermic and involve low energy barriers, supporting the oxygen rebound mechanism.

The catalytic mechanism of peptidylglycine α-hydroxylating monooxygenase was studied by Amzel and Estrin.[474] This copper-containing enzyme catalyzes the α-hydroxylation of terminal glycine residues of proteins (Figure 107). The full enzymatic system solvated by water, with a total of 23 441 atoms, was modeled with a QM/MM approach. The reactive CuB site, included in the QM part, contains a copper atom coordinated to the oxidant, O_2, the substrate, formyl glycine, and the residues of the protein side chains, two histidines and one methionine. The calculations show that

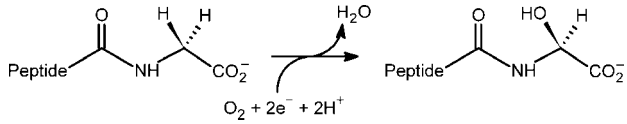

Figure 107. Oxidation of terminal glycine residues of proteins by α-hydroxylating monooxygenase.

O_2 binds to the CuB site yielding a $Cu^{II}—O_2^{\bullet -}$ species. The binding of O_2 is promoted by previous coordination of the substrate. The reduction of this compound to $Cu^{I}—O_2^{\bullet -}$ by electron transfer from the CuA site increases the stability of the system due to higher π-back-donation. Neither of these two species is capable of H abstraction. Spontaneous proton transfer from the solvent generates a $Cu^{II}—OOH^{+}$ compound, which is not active in H abstraction either. Nevertheless, a second proton transfer yields a $Cu{=}O^{2+}$ complex by water release. In the quartet ground state of this species, two unpaired electrons localized in a $Cu^{III}{=}O^{+}$ moiety, are ferromagnetically coupled with a radical cation delocalized over the protein residues coordinated to the metal. The $Cu{=}O^{2+}$ complex promotes the hydroxylation of the substrate in a concerted manner with almost no energy barrier. The reduction of $Cu{=}O^{2+}$ by ascorbate yields $Cu{=}O^{+}$, which is also active in H abstraction but with a classical two-step rebound mechanism involving higher energy barriers. Both species undergo spin inversion during the reaction. In view of the results obtained, the $Cu{=}O^{2+}$ complex was proposed as the active species. This study revealed that the catalytic mechanism of peptidylglycine α-hydroxylating monooxygenase is analogous to that of cytochrome P450.

5.2.7. Dehydrogenases

The mechanism of hydrocarbon oxidation by ethylbenzene dehydrogenase was studied by Szaleniec at a DFT level.[475] This enzyme, which contains a molybdenum oxo group in its reactive center, catalyzes the stereoselective oxidation of ethylbenzene to (*S*)-1-phenylethanol. Three different mechanisms were considered, depending on the cationic or radical character of the intermediates (Figure 108). In mechanism I, the substrate undergoes homolytic C—H cleavage yielding a carbocation and a Mo(IV)—OH intermediate. In a subsequent step, the carbocation attacks the hydroxo ligand yielding the final reaction product. Mechanism II is the classical oxygen rebound mechanism. Mechanism III is a combination of mechanisms I and II, in which homolytic C—H cleavage is followed by electron transfer leading to the carbocation and the Mo(IV)—OH intermediate. A simple quantitative structure−activity relationship (QSAR) model was developed in order to determine the nature of the reaction mechanism. This model suggested that the transition state has a predominant carbocationic character. Mechanism I is thus preferred, but if the rate is controlled by the OH-rebound step, mechanism III cannot be discarded.

5.3. Metal−Hydroxo Species

5.3.1. Lipoxygenases

The role of nuclear quantum mechanical (NQM) effects in enzyme catalysis was explored in the case of lipoxygenases by Siegbahn and Warshel.[476] In biological systems, lipids are catalytically oxidized by lipoxygenases. The reaction involves radical H abstraction from the aliphatic chain of the lipid by an $Fe^{III}—OH$ active species, yielding a carbon radical (Figure 109). This is the critical step of the mechanism, as indicated by the extremely large kinetic isotopic effects (KIE) observed experimentally. The reaction was studied by applying the quantum classical path (QCP) approach in order to model the NQM effects, which due to the H transfer nature of the reaction include large tunneling effects. The experimental KIE was well reproduced, as well as the temperature dependence of the H abstraction rate constants. In the case of D abstraction, the simulation was less successful. The calculations showed that the influence of the media, either the enzyme or a solution, is essentially irrelevant. The outer-sphere reorganization energies were found to be extremely low, due to the very small charge

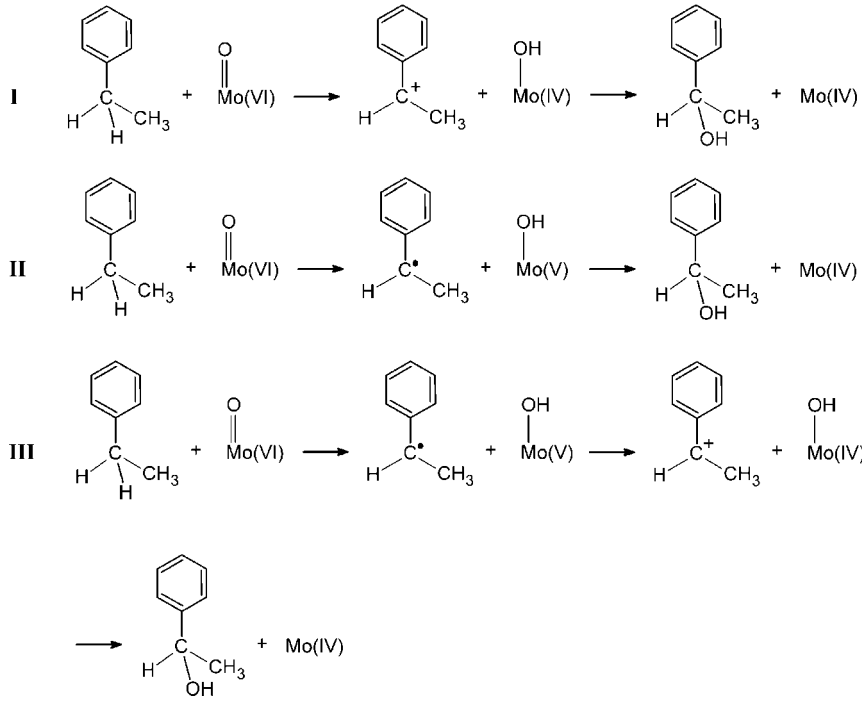

Figure 108. Oxidation reaction mechanisms proposed for ethylbenzene dehydrogenase.

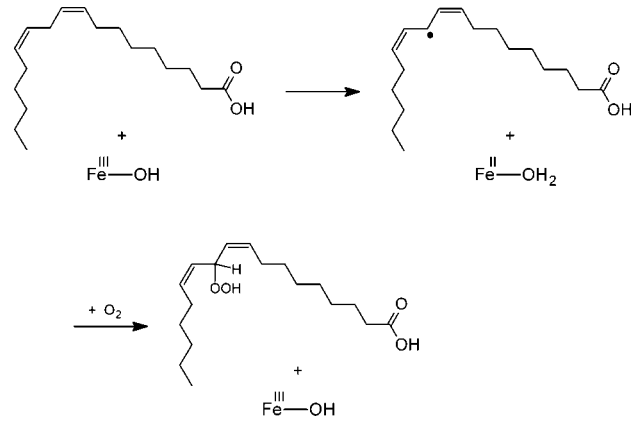

Figure 109. Reaction mechanism for the oxidation of fatty acids by the $Fe^{III}(OH)$ center of lypoxygenases.

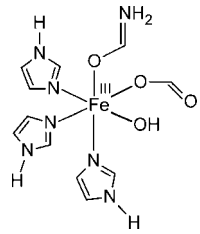

Figure 110. Model of the lipoxygenases reactive center.

transfer associated with the reaction. Interestingly, the NQM effects were found to be the same in the enzyme and in solution, which suggests that they do not contribute to the catalysis. This study proved that the QCP approach can be successfully applied to model the contribution of NQM effects to activation free energies in the framework of enzymatic catalysis, even when large tunneling effects are involved.

Proton-coupled electron transfer (PCET) in soybean lipoxygenases was theoretically studied by Hammes-Schiffer.[477] The first step in lipid oxidation by lipoxygenases (Figure 109) can be regarded as a PCET, a process in which one proton and one electron, that is, a $H^{\bullet}$, are transferred simultaneously. The reaction was studied by applying the multistate continuum theory, in which the transferred hydrogen is modeled with a quantum mechanical wave function. The reorganization energy associated with the reaction was evaluated with DFT calculations for the iron cofactor (Figure 110) and with a frequency-resolved cavity model for conformations obtained with docking calculations. The values computed for these energies were ~19 and ~2 kcal mol^{-1}, respectively. The precited dependence of the rate constant and KIE on the temperature was in good agreement with experiments, which supported the PCET mechanism. The dependence of the rate constants on the temperature is low due to the small $\Delta G^{\ddagger}$ of the reaction, which results from the balance between the total reorganization energy and the ΔG. The high deuterium KIE observed for this reaction, 81, is due to the following factors: (1) the small overlap between the proton vibrational wave functions of the reactant and the product and (2) the dominance of the lowest vibronic states of the reactant and the product for the tunneling process. This study reveals that the proton donor−acceptor vibrational motion plays a key role in reducing the donor−acceptor distance relative to its equilibrium value, which facilitates the PCET process.

In a subsequent study, the dynamics of this enzymatic reaction was explored by the same authors.[478] The reaction

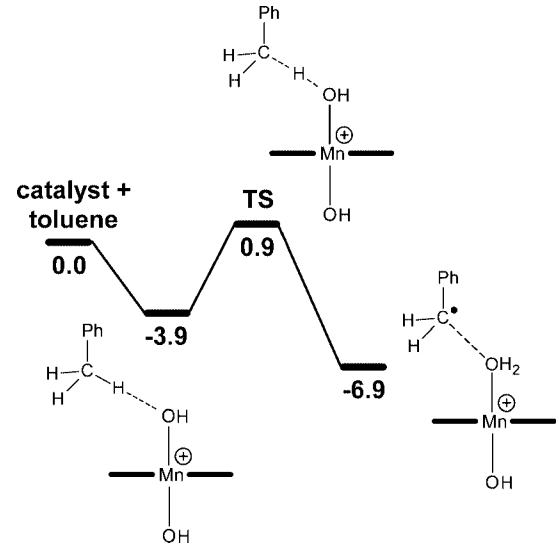

Figure 111. Energy profile, in kcal mol^{-1}, for H abstraction from toluene by $[Mn(OH)_2(por)]^+$ in the triplet state.

was investigated with a vibronically nonadiabatic approach, in which the active electrons and the transferred proton were treated at a quantum mechanical level. The motion of all atoms in the full solvated enzyme system was also included in the model. The calculations showed that the dynamic behavior of the system is dominated by the motion of the protein and the solvent and not by the proton donor−acceptor motion. The rate constant was calculated as the time integral of a probability flux correlation function. The magnitude of the overall rate is strongly influenced by three different factors: (1) the proton donor−acceptor frequency, (2) the vibronic coupling, and (3) the protein/solvent reorganization energy, which was estimated to be ~39 kcal mol^{-1}.

5.3.2. Manganese Porphyrin Biomimetics

C−H oxidation by hydroxo manganese(V) porphyrins was studied by Eisenstein at the DFT(BP86) level.[322] These complexes mimic the catalytic properties of cytochrome P450 enzymes. The rebound mechanism was explored considering toluene as model substrate and porphin as model porphyrin. In the classical rebound mechanism, radical H abstraction is promoted by the $Mn^{V}O$ group, but in this study, the authors postulate $Mn^{V}OH$ as the active group. In the acidic conditions required for reaction, two different prototropic species can be present: [Mn(O)(por)(OH)] and $[Mn(OH)_2(por)]^+$ (por = porphyrin); both species contain the $Mn^{V}OH$ group. The ground state of $[Mn(OH)_2(por)]^+$ is the triplet, followed by the quintet, 0.3 kcal mol^{-1} above, and the singlet, 16.2 kcal mol^{-1} above. The triplet and quintet states promote toluene hydroxylation by the rebound mechanism, involving exothermic steps with low energy barriers. The highest energy point along the reaction pathway is only 0.9 kcal mol^{-1} above reactants (Figure 111). The aqua tautomer of the dihydroxo complex, $[Mn(O)(por)(OH_2)]^+$, which can only react with the $Mn^{V}O$ group, requires a maximum energy gain of 4.8 kcal mol^{-1}. These results suggested that $Mn^{V}OH$ is capable of promoting C−H oxidation. In contrast, in the neutral [Mn(O)(por)(OH)] complex, C−H oxidation can be promoted by both axial ligands, but preferentially by $Mn^{V}O$. This study showed that more acidic conditions not only make the Mn(por) catalysts more reactive but also change the nature of the reactive center from $Mn^{V}O$ to $Mn^{V}OH$. C−H

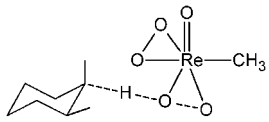

Figure 112. Transition state for the C—H oxidation of *cis*-1,2-dimethylcyclohexane by $[Re(O)(\eta^2\text{-}O_2)_2(CH_3)]$.

oxidation is promoted by $Mn^{V}O$ and $Mn^{V}OH$ because in both cases there are singly occupied $\pi^*(Mn{=}O)$ orbitals. The relevant contribution of oxygen to these orbitals has a double consequence: (1) it increases the electrophilic character of oxygen, which promotes the nucleophilic attack of the C—H bond, and (2) it introduces the oxyl character, which promotes the radical H abstraction from the substrate.

5.4. Metal—Peroxo Species

5.4.1. Methyltrioxorhenium

The catalytic C—H oxidation of several substrates, including *cis*-1,2-dimethylcyclohexane, toluene, 1-phenylethanol, and 1-phenylethyl methyl ether, by methyltrioxorhenium (MTO), $[Re(O)_3(CH_3)]$, was studied by Privalov at the DFT level.[479] In the presence of hydrogen peroxide, MTO yields a mixture of two peroxo complexes: the dioxo peroxo complex $[Re(O)_2(\eta^2\text{-}O_2)(CH_3)]$, and the oxo diperoxo complex $[Re(O)(\eta^2\text{-}O_2)_2(CH_3)]$. Both complexes are active in C—H oxidation, but the diperoxo is much more reactive. The calculations showed that the reaction follows a single-step concerted mechanism without the formation of ionic intermediates, even in polar solvents. The oxidation process promoted by the diperoxo complex involves the concomitant cleavage of the C—H bond of the substrate and the O—O bond of the catalyst. In the transition state (Figure 112), the C···H···O moiety is aligned in a linear manner, resembling the H abstraction step of the oxygen rebound mechanism. The relaxation of this TS, followed by IRC calculations, showed that once the hydride is transferred to the peroxo ligand, the Re—OH bond rotates to undergo oxygen rebound with the resulting carbocation, without the formation of any intermediate. This mechanism has energy barriers of 20—23 kcal mol^{-1} for the different tested substrates, which are much more reasonable than those of the classical oxidation mechanisms involving metal alkoxide and metal carbonyl intermediates. The predicted KIE, $k_H/k_D = 2.9$, was in very good agreement with the experimental value, 3.2. The butterfly transition states associated with a side-on approach of MTO to the C—H bond, previously suggested by analogy with the oxidation mechanisms of dimethyldioxirane,[480,481] were discarded.

5.5. Metal—Hydroperoxo Species

5.5.1. Activated Bleomycin

Bleomycin, BLM, is a glycopeptide used as an antibiotic chemotherapy agent. In its active form, ABLM, it is coordinated to a low-spin Fe^{III}—OOH center. ABLM induces single- and double-strand DNA damage by H abstraction from the C-4′ deoxyribose sugar moiety. The mechanism of this C—H bond cleavage has been debated. Two alternative mechanisms (Figure 113) are possible: (1) a two-step mechanism, starting with the homolysis of the O—O bond, like in the heme chemistry, followed by H abstraction by the OH radical, which leads to a carbon radical and a molecule of water and (2) a direct mechanism, in which the

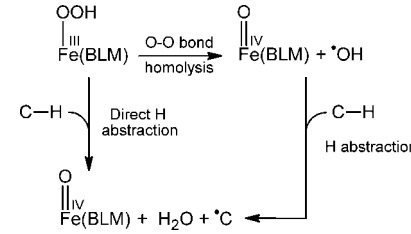

Figure 113. Stepwise and concerted mechanisms for C—H activation by activated bleomycin.

same reaction products are obtained in a single concerted step from the Fe^{III}—OOH species. A mixed spectroscopic/computational (DFT) study by Que and Solomon[482] showed that O—O bond homolysis in ABLM is feasible, with a free energy gain of 12 kcal mol^{-1} and no energy barrier, like in the non-heme Fe^{III} complexes $[Fe(OOH)(N4Py)]^{2+}$ and $[Fe(OOH)(TPA)(OH_2)]^{2+}$. Other theoretical studies by Shaik pointed out that the O—O bond may also undergo heterolytic cleavage after protonation.[483] Nevertheless, previous experiments revealed the presence of prominent KIEs, $k_H/k_D \approx 2-7$,[484] which are too large for H abstraction by OH•, thus supporting the direct H abstraction mechanism.

The structure and reactivity of ABLM was studied by Solomon using a combination of spectroscopic and computational (DFT) techniques.[485,486] The calculations showed that ABLM promotes H abstraction without requiring the previous cleavage of the O—O bond, thus following the direct reaction mechanism. In the concerted transition state, the cleavage of the sugar C—H bond is concomitant with the formation of an O—H bond and the cleavage of the Fe^{III}O—OH bond. The reaction is favorable at the thermodynamic and kinetic levels, with a ΔG of −10 kcal mol^{-1} and an activation barrier in solution of 17 kcal mol^{-1}. This energy pathway is below those associated with the homolytic and heterolytic cleavage of the O—O bond. Interestingly, the $Fe^{IV}{=}O$ product of the reaction is a reactive species able to promote a second H abstraction, which may explain why a single molecule of ABLM is capable of cleaving both DNA strands. The direct H abstraction mechanism was further supported in a recent study in which the kinetics of the ABLM + DNA reaction was compared with that of the ABLM decay.[487] The spectroscopic and DFT results show that the decay reaction, in which ABLM undergoes the intramolecular cleavage of a N—H bond, is slower than the reaction with DNA.

5.6. Bimetallic μ-Oxo Species

5.6.1. Copper Biomimetics

The mechanism of intramolecular C—H activation in $[(LCu)_2(\mu\text{-}O)_2]^{2+}$, L = 1,4,7-trialkyl-1,4,7-triazacyclononane, was theoretically studied by Cramer with a QM/MM approach.[488] $[(LCu)_2(\mu\text{-}O)_2]^{2+}$ is a biomimetic complex of copper-containing metalloenzymes. Experiments had shown that this compound undergoes N-dealkylation yielding benzaldehyde. The calculations showed that this reaction involves intramolecular C—H activation by a classical rebound mechanism. In the initial rate-determining step, a benzylic H is transferred to a bridging oxo group. The transferred H is on the equatorial plane defined by the diamond Cu_2O_2 core. The reaction yields a copper hydroxo intermediate, by breaking the Cu—O—Cu bridge. This intermediate has a mixed radical/ionic character. In a subsequent almost barrierless rebound step, the hydroxo group is transferred

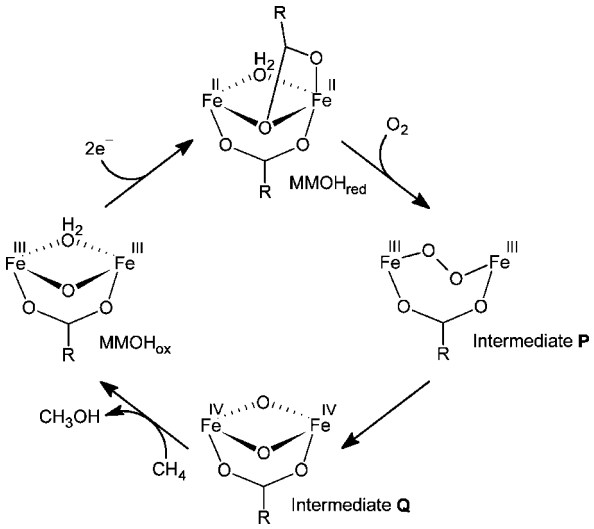

Figure 114. Reaction mechanism proposed for methane hydroxylation by MMO.

from copper to the oxidized benzylic carbon, leading to the formation of an aminal intermediate, which yields the final benzaldehyde product by hydrolysis. The reaction is weakly sensitive to aromatic substitution in the ligand, due to some polar character in the H abstraction transition state. The calculations also reveal that at 233 K, tunneling plays a significant role in the kinetics of the reaction. This study suggested that this type of copper biomimetic may be potentially active not only in the intramolecular but also in the intermolecular C—H activation.

5.6.2. Methane Monooxygenase

Methane monooxygenase (MMO), an enzyme found in methanotroph bacteria, catalyzes the oxidation of methane to methanol, by using O_2 as oxidant.[216,217] This enzyme has two different forms: cytoplasmic soluble MMO (sMMO) and membrane-bound particulate (pMMO). The sMMO form contains iron in the active site, whereas the pMMO form, which is much more difficult to isolate, purify, and characterize, contains copper. The sMMO form contains three components: hydroxylase (MMOH), B component (MMOB), and reductase (MMOR). The MMOH component binds oxygen and catalyzes the oxidation of methane. The resting state of MMOH is the oxidized form, $MMOH_{ox}$, which contains a diferric Fe^{III}—Fe^{III} core (Figure 114). After a $2e^-$ reduction by NAD(P)H and oxidation by O_2 a metastable intermediate with a bridging peroxo ligand, known as intermediate P, is formed. This species leads to an Fe^{IV}—$(\mu\text{-O})_2$—Fe^{IV} diamond core species, known as intermediate Q, which is the active species in methane oxidation. In intermediate Q, the iron atoms are bridged by two oxo ligands and one bidentate glutamate ligand. In addition, each Fe is bound to other glutamate and histidine residues in terminal positions and a molecule of water may be also present within the first coordination sphere.

The exact structure of the active site of intermediate Q is not fully clear, and different computational models have been proposed in order to study the mechanism of methane hydroxylation by MMO. In a first approach, the enzyme was modeled by means of DFT(B3LYP) calculations on small model complexes of the reactive site. Four different models were proposed by the research groups of Yoshizawa,[489–491] Morokuma—Basch,[492] Siegbahn,[493–497] and Friesner—Lippard.[498–501] These models differ in their size, spin state, charge, and Fe coordination number. Different basis sets were used in each case to optimize the geometries and refine the energies, and the calculations were carried out using different computational programs. In a second generation of more sophisticated studies, the whole enzyme and surrounding molecules of solvent were included in the model, by means of hybrid QM/MM calculations. Remarkably, despite the diversity of models and methods, all theoretical studies indicated that H abstraction from methane by the bridging μ-oxo ligand is the rate-determining step of the process.

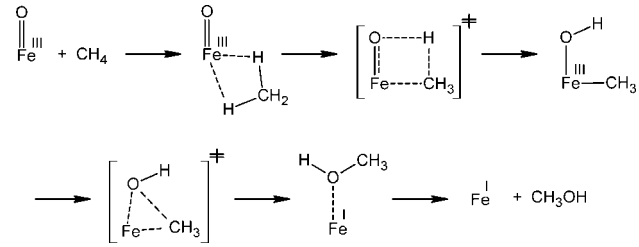

Figure 115. Nonradical mechanism proposed for methane oxidation by FeO^+.

The reaction mechanism of C—H activation by bare metal—oxo species in the gas phase has been extensively studied by means of spectroscopic and computational techniques by Schröder, Schwarz, and Shaik.[502–505] In line with these studies, FeO^+ was initially considered by Yoshizawa as the simplest possible model of sMMO. In this model, the formal oxidation state of Fe is not IV, as it is in intermediate Q, but III instead, and the reaction is not catalytic. Nevertheless, experiments have shown that this bare metal—oxo cation oxidizes methane to methanol under ion cyclotron resonance conditions.[506,507] The hydroxylation mechanism proposed by Yoshizawa[508–515] is represented in Figure 115. In the starting intermediate, methane is bound to FeO^+ through two weak Fe···H bonds. From this species, the activation of the C—H bond involves a four-center transition state leading to a hydroxo methyl iron intermediate. In a final reductive elimination step, referred to as "methyl migration", the concerted cleavage of the Fe—C bond and formation of the C—O bond, yields a molecule of methanol and an Fe^I cation.

This model of intermediate Q was subsequently extended by Yoshizawa considering two different diiron complexes, one with aqua terminal ligands[516,517] and the other with hydroxo terminal ligands,[518] and in both cases with one glutamate and two oxo bridging ligands. The complex electronic structure of the system was initially modeled assuming a closed shell singlet configuration with all spins paired. The rate-determining step of the mechanism is the migration of one hydrogen from methane, which is initially coordinated to the unsaturated Fe atom, to one of the bridging oxo moieties (Figure 116). The relaxation of the transition state, 31 kcal mol^{-1} above reactants, leads to an intermediate with a μ-hydroxo bridge, in which the resulting methyl fragment is bound to the metal. In the next step, the methyl ligand migrates from the metal to the μ-hydroxo bridge yielding a methanol complex, 39 kcal mol^{-1} below reactants. In this mechanism, which does not have radical character, the formal oxidation state of the metal does not change in the H abstraction step. The two-electron oxidation of methane is associated with the methyl migration step. A subsequent study[519] on the antiferromagnetic state by broken-symmetry DFT calculations[520] showed that the magnetic coupling

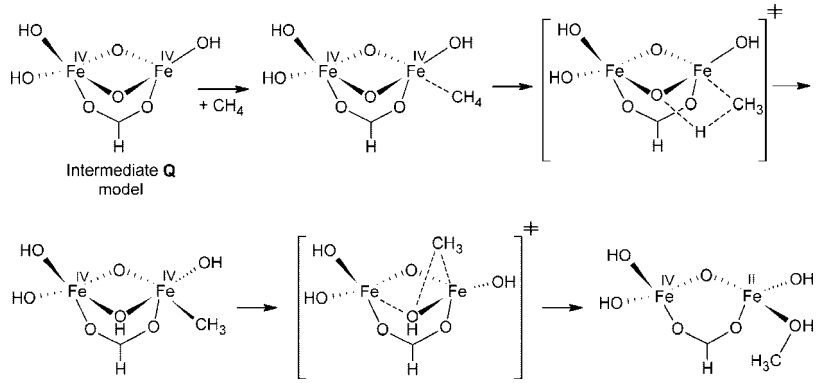

Figure 116. Nonradical mechanism proposed in the Yoshizawa model of sMMO.

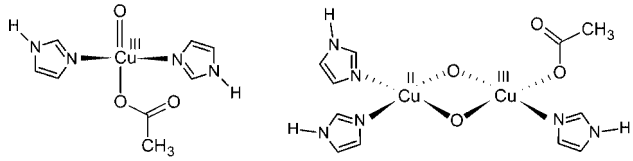

Figure 117. Mononuclear and dinuclear models of the copper active sites of pMMO.

between the two metal centers may shift the whole pathway down in energy, leading to lower energy barriers in better agreement with experiments.

The mechanism of methane hydroxylation by sMMO was recently further explored by Yoshizawa using a more sophisticated model.[521] In this model, the two metal centers are bridged by two μ-oxo ligands and a bidentate glutamate carboxylate, modeled as formate. One of the iron atoms is coordinatively saturated with three extra ligands: two monodentate formates and one imidazole ring, used as a model of histidine. The other iron atom is coordinated with two extra ligands, one formate and one imidazole, and has thus a vacant coordination site, as supported by experimental EXAFS data.[522] The calculations were carried out for the broken-symmetry singlet state, which involves two high-spin Fe^{IV} centers antiferromagnetically coupled.

The iron vacant site is occupied by methane, which undergoes heterolytic C—H cleavage promoted by one of the μ-oxo ligands. In the subsequent step, the methyl ligand is transferred from the metal to the μ-hydroxo ligand through a three-centered transition state. The C—H cleavage is the most difficult step of the mechanism, with a high energy barrier of 36.5 kcal mol^{-1}. In the context of the classical oxygen rebound mechanism, a transition state for radical H abstraction by the μ-oxo ligand, without the direct participation of Fe, was also optimized. Nevertheless, this stationary point could only be located in the high-spin nonet and undecet states and not in the antiferromagnetic singlet ground state. Changing the electronic nature of the C—H cleavage from heterolytic to homolytic does not alter to a great extent the kinetic isotopic effects associated with this step. This study supported a two-step mechanism, in which the substrate does not generate any radical or ionic species. This mechanism is essentially identical to that of the simpler FeO^+ and diiron systems.

The oxidation of methane by the particulate form of methane monooxygenase (pMMO) was also explored by Yoshizawa, combining DFT and QM/MM methods.[523] Both the monocopper and dicopper active sites of the enzyme were modeled (Figure 117). The oxidation of the mononuclear site by O_2, leading to an oxo Cu^{III} species, is endothermic. In contrast, the oxidation of the dinuclear site, leading to a bis(μ-oxo) $Cu^{II}Cu^{III}$ species, is exothermic. Both active species promote the oxidation of methane under physiological conditions. The reaction mechanism is analogous to that of sMMO and involves H abstraction by the terminal (mononuclear site) or bridging (dinuclear site) oxo ligand, yielding a methyl fragment that is stabilized by coordination to copper. The intermediate undergoes methyl migration from the metal to the hydroxo group, giving rise to methanol. The overall process is strongly exothermic by more than 45 kcal mol^{-1}. Interestingly, the identity of the rate-determining step depends on the nature of the active site. In the mononuclear model, the H abstraction step has the highest energy barrier and may involve two different spin states, singlet and triplet, with similar energies. In the dinuclear model, the methyl migration step has the highest energy barrier and the reactive state is a doublet. In both cases, the σ^* orbital of the Cu—O bond is singly occupied and plays a crucial role in the cleavage of the C—H bond. The predicted kinetic isotope effect at 300 K was in reasonable agreement with experiments.

In a very recent study, the nature of the active site of pMMO was further studied by comparing the reactivity of two bis(μ-oxo) complexes with different oxidation states in the bimetallic core, $Cu^{II}Cu^{III}$ and $Cu^{III}Cu^{III}$.[524] The calculations showed that the bis(μ-oxo) $Cu^{II}Cu^{III}$ complex promotes the C—H bond activation of methane, whereas the bis(μ-oxo) $Cu^{III}Cu^{III}$ complex is nonreactive. Nevertheless, this complex can undergo an intramolecular isomerization process, in which one of the Cu—O bonds is cleaved with an energy cost of 23.6 kcal mol^{-1}, yielding a Cu^{III}—O—Cu^{III}—O species. Interestingly, the terminal oxygen of this species promotes the oxidation of methane to methanol, through the same two-step nonradical mechanism previously proposed by Yoshizawa for the Fe and Cu models of sMMO and pMMO. The bis(μ-oxo) $Cu^{II}Cu^{III}$ complex follows the same mechanism without requiring the previous cleavage of a Cu—O bond. For both complexes, the methyl migration step, in which methanol is formed, is predicted to be slower than the H abstraction step, in which the C—H bond is cleaved. The energy of the migration transition state relative to reactants is 35.8 kcal mol^{-1} for the bis(μ-oxo) $Cu^{II}Cu^{III}$ complex and 53.5 kcal mol^{-1} for the bis(μ-oxo) $Cu^{III}Cu^{III}$ complex, indicating that the bimetallic $Cu^{II}Cu^{III}$ core is more efficient in the hydroxylation of methane than the $Cu^{III}Cu^{III}$ core. The oxygen rebound mechanism was excluded due to the high energy barrier associated with the radical H abstraction step.

The reactivity of pMMO has been also explored by Chan,[525] by means of DFT calculations on small models of

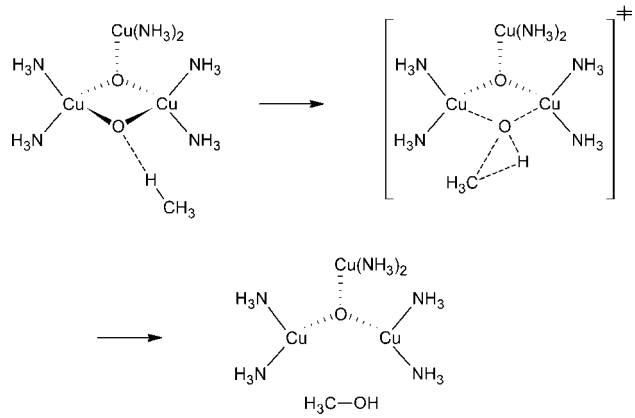

Figure 118. The oxo-transfer concerted mechanism proposed by Chan for pMMO.

the reactive site. Three different models were considered: a dinuclear bis(μ-oxo) $Cu^{III}Cu^{III}$ complex, a dinuclear bis(μ-oxo) $Cu^{II}Cu^{III}$ complex, and a trinuclear bis(μ_3-oxo) Cu^{II}-$Cu^{II}Cu^{III}$ complex proposed by the same authors in a previous study.[526] The calculations show that the trinuclear species promotes methane oxidation more efficiently than the dinuclear, with a reaction rate higher by 5−6 orders of magnitude. The kinetic isotope effect predicted for the trinuclear species, 5.2 at 300 K, is in good agreement with experiments. The reaction mechanism, which consists of a direct oxo-transfer process, is different from that proposed by Yoshizawa. Methane is hydroxylated by the insertion of one of the bridging oxo ligands yielding methanol in a single concerted step (Figure 118), with an energy barrier of 15 kcal mol^{-1}. This mechanism is consistent with the predominant retention of configuration observed experimentally, which suggests the absence of radical intermediates.

The mechanism of methane oxidation by sMMO was also investigated by Morokuma and Basch.[527−531] In order to avoid computational complications, a high-spin configuration with two ferromagnetically coupled Fe^{IV} centers was assumed. The model complex has neutral charge, in contrast with the cationic models proposed by Yoshizawa. In the original Morokuma−Basch model, the histidine ligands were modeled as NH_2^-, the terminal glutamates as H_2O, and the bridging glutamates as $HCOO^-$. The main drawback of this simple model is that the charges of the real system, neutral for histidine and anionic for the terminal glutamate are reversed in the model. This was improved in a subsequent extended model,[531] in which the histidine residues were modeled as imidazole rings and all the glutamates, both terminal and bridging, as formates. In this model, each iron is coordinatively saturated with a total of six ligands in a nearly octahedral arrangement. This is indeed the main difference with respect to the Yoshizawa models, in which the iron promoting C−H oxidation has a vacant site. The absence of a vacant site causes a major change in the reaction mechanism, which in the Morokuma−Basch model becomes the classical oxygen rebound mechanism (Figure 119). In contrast with the nonradical mechanism proposed by Yoshiwaza, in the rebound mechanism one electron is transferred from methane to the diiron core at each step.

The bridging oxo group in the side of the complex occupied by the terminal formate ligands, which has radical character, promotes H abstraction from methane.[531] This step involves the transfer of a H radical and can be thus viewed as a proton-coupled electron transfer.[532] The transition state has a linear O···H···C arrangement and leads to a μ-hydroxo intermediate bound to a methyl radical, which due to the absence of vacant sites does not coordinate to iron. In the next step, the carbon radical undergoes OH rebound with the μ-hydroxo ligand, yielding a methanol-bound product intermediate. This species contains an $Fe^{III}Fe^{III}$ core, which in the ferromagnetic configuration approach is an ^{11}A state, whereas the starting $Fe^{IV}Fe^{IV}$ species is associated with a ^9A state. Both spin surfaces were modeled, and the calculations indicated that the reaction starts on the ^9A surface and finishes on the ^{11}A one after spin crossover in the OH rebound transition state region. These results should be taken

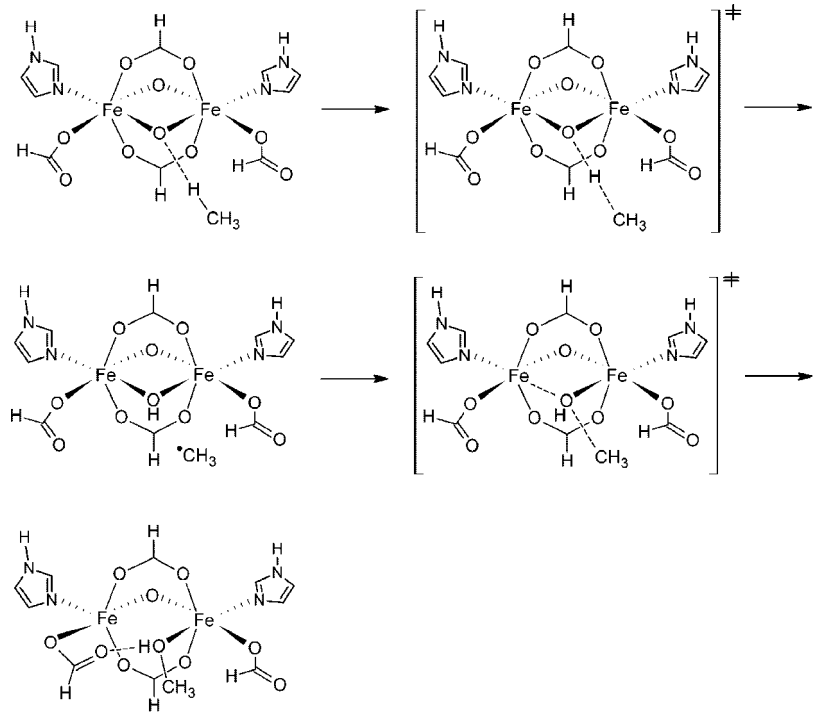

Figure 119. The radical oxygen rebound mechanism in the Morokuma−Basch model of sMMO.

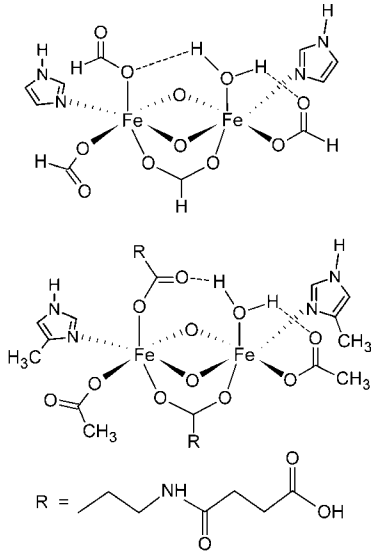

Figure 120. The Siegbahn (top) and Friesner (bottom) models of sMMO, with one of the bridging carboxylate ligands shifted.

with much care though, due to the unrealistic nature of the ^{9}A and ^{11}A states; Mössbauer and EPR experiments[533–535] showed that both intermediate Q and the final methanol product are singlet species.

The radical H abstraction step is rate-determining, with an associated energy barrier of 13 kcal mol^{-1}, ca. twice the height of the OH rebound barrier, 7 kcal mol^{-1}. The calculations showed that the energy barrier associated with the radical H abstraction step decreases as the cleaved C—H bond becomes weaker,[531] from H—CH_3 to H—CH_2F and H—CH_2CH_3, as expected. Interestingly, the reaction pathway associated with the radical oxygen rebound mechanism of the Morokuma−Basch model is clearly lower in energy than that associated with the nonradical mechanism of the Yoshizawa model.

The reactivity of sMMO was also investigated by Siegbahn.[536–539] As in the Morokuma−Basch approach, a neutral complex was used to model the reactive center of intermediate Q. In the original model,[536] all ligands other than the two μ-oxo bridges were represented with water and hydroxo ligands. It was then found that two bridging complexes should be introduced in the model to reproduce properly the experimental Fe···Fe distances.[537] The model was further refined by including imidazole and formate ligands to account for the histidine and glutamate residues, respectively, present in the real enzymatic system. In the last and more sophisticated study,[539] the model was modified to include the carboxylate shift proposed by Friesner and Lippard,[540] in which one of the formate bridging ligands rearranges from the bridging coordination mode to the terminal mode (Figure 120), with an energy loss of 10 kcal mol^{-1}. The resulting vacant site is occupied by a molecule of water. Both the ferromagnetic and the antiferromagnetic broken-symmetry configurations were considered.

Siegbahn proposed a new key intermediate for the hydroxylation of methane, labeled as Q′, which is a mixed valence $Fe^{III}Fe^{IV}$ species with an unpaired electron in one of the bridging oxygens. This species has a ferromagnetic μ-O(↑)Fe(↑↑↑↑)Fe(↑↓↑↑) ^{9}A configuration and is generated from intermediate Q by an intramolecular electron transfer from the μ-O ligand to the diiron core. The Q′ intermediate, which is only 2 kcal mol^{-1} above intermediate Q, promotes the oxidation of methane. The radical H abstraction step has the highest energy barrier, 14 kcal mol^{-1}, and yields a μ-OH intermediate bound to a $^{\bullet}CH_3$ radical. This species undergoes OH rebound giving rise to the final methanol product. Despite the carboxylate shift difference between the Morokuma−Basch and Siegbahn models, in both cases the calculations suggested essentially the same oxygen rebound mechanism.

Noodleman and co-workers studied the structure of methane monooxygenase, taking into account the electrostatic interactions between the active site and the protein environment.[541–543] The results showed that the protein has a relevant impact on the structure and energetics of the active site, suggesting that minimum-sized DFT models are not appropriate. In line with this, Friesner, Lippard, and co-workers developed a new computational model by systematically increasing its size,[540] with the final aim of reproducing the X-ray crystal structure of $MMOH_{red}$.[544] The best results were obtained with a large-scale model of about 100 atoms (Figure 120), which succeeded in reproducing the most distinctive features of the active site in $MMOH_{red}$, including the Fe···Fe distance. As the Morokuma−Basch and Siegbahn models, the Friesner−Lippard model is fully saturated, with two six-coordinated Fe centers in a pseudo-octahedral environment. The system has a low-spin antiferromagnetic configuration, as supported by experiments,[533–535] which is computed by means of the DFT broken-symmetry approach.

The mechanism of methane hydroxylation by sMMO was studied using the Friesner−Lippard model.[545] The reaction follows a particular oxygen rebound mechanism, involving two parallel reaction pathways. The nucleophilic attack of methane to the μ-oxo ligand in the carboxylate side of the active species, promotes the homolytic cleavage of one of the C—H bonds, with an energy barrier of 18 kcal mol^{-1}. Right after the H abstraction step, the reaction pathway bifurcates and two different intermediates can be formed, depending on how the methyl radical binds to the μ-hydroxo ligand. In the pathway labeled as "bound-radical", $^{\bullet}CH_3$ binds to μ-OH with an unusually short C···O distance of 1.97 Å. In the other pathway, labeled as "nonsynchronous concerted", this distance is even shorter. These species have similar energies and undergo OH rebound through very low energy barriers, yielding the same methanol complex product in a strongly exothermic fashion. In this mechanistic framework, the authors suggest that $^{\bullet}CH_3$ is indeed a bound radical with a very short lifetime. In addition, the lifetime depends on the pathway followed by the system and is predicted to be significantly shorter in the "nonsynchronous concerted" path, which has an associated rebound barrier of only 1.3 kcal mol^{-1}, than in the "bound-radical" path, which has a higher rebound barrier of 3.9 kcal mol^{-1}. All these results have an intuitive connection with the experiments done on the racemization of CH_3CHDT, which revealed that retention of configuration dominates over inversion.[546,547]

The CH_3CHDT racemization experiments were modeled by means of semiclassical molecular dynamics calculations.[548] In the "nonsynchronous concerted" pathway, the substrate is oxidized with total retention of configuration. In the parallel "bound-radical" pathway, inversion takes place preferentially due to the lifetime of the ethyl radical, 320 fs, which is significantly longer than the time required to rotate the C—C bond of the substrate. The inversion/retention ratio is indeed determined by the radical lifetime and the rate of the C—C bond rotation. Interestingly, this rate depends strongly on the C···O distance between the carbon radical

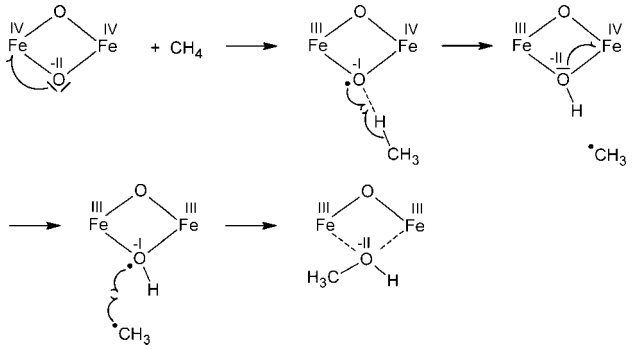

Figure 121. Electron flow in the oxygen rebound mechanism for the hydroxylation of methane by sMMO.

and the oxygen of the μ-OH ligand; the closer is the radical to the diiron core, the slower is the C—C bond rotation, favoring retention of configuration over inversion. On the basis of the results obtained, the authors predicted a retention of configuration of 69−84%, in agreement with the experimental result, 72%.

The rearrangement of the electronic structure along the reaction pathway was analyzed in the Friesner−Lippard model (Figure 121).[549] The binding of methane induces a single electron transfer from a lone pair of a bridging oxygen to one of the Fe^{IV} centers, which is reduced to Fe^{III}. This process involves the promotion of one electron from the occupied $\pi(Fe_2O_2)$ bonding orbitals, consisting of in-phase combinations of the Fe $d_{x^2-y^2}$ and the O $p_{x/y}$ orbitals to the corresponding $\pi^*(Fe_2O_2)$ antibonding orbitals. Such electron transfer makes the μ-O ligand radicaloid and more electrophilic, thus promoting H abstraction at this site by absorption of one electron from the σ orbital of the C—H bond. The resulting intermediate undergoes a second electron transfer from a lone pair of the μ-OH ligand to the remaining Fe^{IV} center, which is also reduced to Fe^{III}. This yields a radicaloid and electrophilic μ-$OH^{\bullet\delta+}$ moiety, which readily reacts with the $^{\bullet}CH_3$ radical collapsing into the final methanol $Fe^{III}Fe^{III}$ product complex. The singlet antiferromagnetic configuration of the system is kept all along the reaction pathway, and no spin crossover is thus needed.

The Friesner−Lippard model was further refined including the protein environment surrounding the active site, by means of mixed QM/MM calculations.[550] The oxidation of several CH_3X (X = H, CH_3, OH, CN, and NO_2) substrates by sMMO was explored. The calculations were used to rationalize the kinetic data obtained in a previous experimental study.[551] Two steps were analyzed in detail, the initial binding of the substrate to the enzyme, which has a nonnegligible diffusion barrier, and the subsequent H abstraction.

For X = CN and NO_2, the oxidation reactions were run under saturating conditions, and therefore the activation barrier associated with H abstraction was computed for comparison with experiments. In this case, an excellent agreement with the empirical values was obtained, with deviations of 1−2 kcal mol^{-1}. For the other substrates, X = H, CH_3, and OH, the activation barrier associated with the substrate binding has to be included in the model. For methane, the predicted activation barrier was ~3 kcal mol^{-1} higher than the experimental measure. This deviation was also obtained for X = CH_3 and OH, and it is probably due to an inadequate sampling of the configurational space or the harmonic approaches used to compute the entropy or both. The consideration of the protein environment effects (van der Waals and electrostatic interactions) is essential for the accurate calculation of the absolute free energies. The van der Waals interactions stabilize the transition state, and the inclusion of the electrostatic interactions is needed for a proper modeling of the reaction with the more polar substrates.

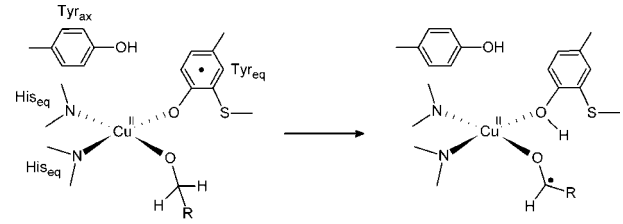

Figure 122. The key hydrogen atom transfer step in the oxidation of alcohols by galactose oxidase.

5.7. Metal−Alkoxo Species

5.7.1. Galactose Oxidase

Galactose oxidase catalyzes the oxidation of primary alcohols to aldehydes by O_2. The active site of this enzyme contains a Cu(II) center, which binds to the substrate and four amino acid residues in a square pyramidal geometry.[552] The equatorial plane is occupied by two histidines in cis, one tyrosine, and the substrate. The axial position is occupied by a tyrosine. The mechanism postulated for the reaction[553] involves the following four steps: (1) proton transfer from the hydroxyl group of the alcohol to the axial tyrosine, (2) H atom transfer from the substrate to the equatorial tyrosine, (3) electron transfer from the substrate to the metal center, which yields the aldehyde product by Cu(II) → Cu(I) reduction, and (4) catalyst recovery by reoxidation of the metal center with O_2. The experiments suggest that the H atom transfer (Figure 122), in which a C—H bond of the substrate is cleaved, plays a central role, being the rate-determining step of the process. This reaction mechanism has been also studied theoretically.[554–558] The oxidation of methanol to formaldehyde by galactose oxidase was explored by Himo and co-workers employing two different computational models: a small model, computed at the DFT(B3LYP) level, and a more relatistic model, computed at the IMOMM(B3LYP/MM3) level.[559] The calculations show that after the proton transfer step, the substrate undergoes radical H abstraction by the Cu-bound O of the equatorial tyrosine, which has a π-radical in the phenyl ring. Interestingly, the location of this π-radical is displaced from the axial tyrosine to the equatorial tyrosine during the initial proton transfer step. The transition state associated with the H atom transfer is the highest energy point along the reaction pathway, which suggests that this step is rate-determining, in total agreement with the experiments. The radical product readily undergoes electron transfer to the metal center, which suggests that this intermediate is very unstable and thus very difficult to detect. The energy barrier computed for H atom transfer is 11.1 kcal mol^{-1} at the DFT(B3LYP) level and 13.6 kcal mol^{-1} at the IMOMM(B3LYP/MM3) level. These low energy barriers give further support to the reaction mechanism postulated for this enzymatic system.

The complexes [M(L)] (M = Zn(II), Cu(II); L = *N*,*N*′-bis(3,5-di-*tert*-butyl-2-hydroxyphenyl)-1,2-diiminoquinone) are functional models of galactose oxidase. The oxidation of primary alcohols with O_2 catalyzed by these two complexes was studied by Wu at the DFT(B3LYP) level, including solvent effects.[560] The quinone acts as a tetradentate

ONNO chelating ligand and its oxygen atoms have radical phenoxyl character. In the first step of the mechanism, one of these oxygen atoms abstracts a proton from the alcohol substrate by breaking the O—H bond. In the following step, the other oxygen abstracts a radical hydrogen from the substrate by homolytic C—H cleavage. These two reactions weaken the metal−oxygen bonds involving the ligand. The calculations revealed a more favorable alternative pathway for the initial protonation step, in which an external base, triethylamine, takes the proton from the alcohol. H abstraction by the phenoxyl radical is the rate-determining step. The energy barriers computed for this step, 16.7 kcal mol^{-1} for Cu and 23.0 kcal mol^{-1} for Zn, are in good agreement with the experimental values, 19.5 and 21.1 kcal mol^{-1}, respectively, and confirmed that the Zn catalyst is less efficient than the Cu one.

6. Conclusions

Computational studies have considerably improved the perspective that chemists have on C—H bond activation by transition metal complexes. The past few years have seen significant advances in the field. In the past, where the theoretical methodologies and the computer speed imposed severe limitations on the size of the systems to calculate, computations were carried out on species that were heavily simplified relative to the real systems. Despite these limitations, computational studies had been very successful to quantify the role played by the metal centers on the barrier heights and energy of reactions. They also accounted successfully for the way electron-donating and electron-withdrawing ligands modify the electronic properties of the metal. As a result, calculations provided good insights in the fundamental aspects of the oxidative addition, σ bond metathesis and 1,2 addition. This resulted in an increasing role of computational studies devoted to reactivity and in particular to C—H activation as evidenced by the key reviews published in *Chemical Reviews* at the dawn of the 21st century.[23–25] The ability to compute systems with a large number of atoms and thus species closer to the real systems did much more than just improve further the understanding of the well-established mechanisms. New mechanisms were discovered. For instance, σ-bond metathesis, which was originally considered almost exclusively for early transition metal complexes, was found to be also possible for late transition metal complexes, with the appropriate choice of ligands. However, only late metal complexes can form stable σ(C—H) bond complexes. To highlight the differences between early and late transition metal systems, the name σ-CAM was coined and computational studies have contributed to revealing the situations where this mechanism applies. The ability to calculate systems with large number of atoms has been of great importance to reveal the active role that ligands or various additives (base, counteranion) play in the C—H bond activation by assisting the C—H cleavage usually by way of a proton transfer. These mechanisms have been named CMD and AMLA. The calculations have shown that the assistance for the C—H activation can be achieved by a wide variety of ligands and that heterolytic cleavage of C—H is frequent. It is interesting to note that these new mechanisms, σ-CAM, CMD, and AMLA, lead to C—H activation occurring without change of oxidation state at the metal center and with low or moderate energy barriers. This is clearly an important direction to explore further for discovering new efficient ways to activate the C—H bond.

The computational studies of C—H oxidation are also relatively recent because experimental systems engaging in C—H oxidation are often large, charged, or complex. The metal has often open-shell configurations, and several electronic states of the metal species can participate in the reaction. In a number of cases, the reactive species contain more than one metal, which makes the computational studies even more challenging. Even though DFT calculations of open shell systems need to be carried out with caution, there is no doubt that these calculations were able to suggest mechanisms and rationalize a considerable amount of experimental information. We refer the reader to the accompanying paper by Shaik, Thiel, et al. in this issue for the specific case of cytochrome P450 chemistry.[50]

It is rewarding that C—H activation is now the step of efficient catalytic processes. Computations have been and will be crucial to determine the rate-determining step in further catalytic processes. This information is required for improving the catalytic efficiency.

The computational modeling of a reaction necessitates representing in an appropriate manner the experimental conditions (solvent, temperature, pressure). For instance, the modeling of the pressure of H_2 gas was crucial to understand the acceptorless catalytic dehydrogenation of alkanes. The representation of experimental conditions is still a challenge for computational chemists but is required for future studies and especially for design of catalytic reactions.

This review did not address the influence of the level of calculation on the energy profiles and mechanistic issues presented here because most of the studies have been carried out with a single method. Most of the authors have used a DFT method, which has proven its validity and solidity. Furthermore, most of the authors have used traditional functionals, which do not perform well to represent weak interactions. In a paradoxical manner, this may lead to a decrease of the quality of the calculations when considering complexes with the large real ligands because of the lack of representation of the weak interactions present in this case. This may not modify the essential features of the mechanism but may influence selectivity issues where interactions between ligands or between ligands and substrate could play a role. New functionals with the ability to represent weak interactions are being explored, and they will probably be more widely used in the future. Finally large systems could introduce conformational complexity, which may need also to be considered. In other words, it is very appealing to carry out computational studies of C—H bond activation with models similar to the experimental systems if the computational power is available, but the additional associated difficulties should not be forgotten.

Finally, while there is still much more work to do to fully understand the selectivity of the C—H bond activation, it is clear that computational chemistry will be even more tightly associated with the experimental quest for new and more efficient transition metal catalysts.

7. Acknowledgments

Our interest in C—H activation originates from many years of collaboration with experimental chemists. We would like to thank in particular Richard A. Andersen, Kenneth G. Caulton, Bruno Chaudret, Robert H. Crabtree, William D. Jones, Eduardo Peris, Robin N. Perutz, and Sylviane Sabo-Etienne for having shared their most exciting results with us and having educated us on the topic. Some of our own

results are presented, and we are very grateful to Maria Besora, Marta Feliz, Hélène Gérard, Ulrike Helmstedt, Laurent Maron, Claire Mégret, Lionel Perrin, and Christophe Raynaud for their contributions. D.B. thanks Sanofi-Aventis for a postdoctoral fellowship. O.E. thanks University of California, Berkeley, for its hospitality during the preparation of the review.

8. References

(1) Shilov, A. E.; Shul'pin, G. B. *Chem. Rev.* **1997**, *97*, 2879.
(2) Bergman, R. G. *Science* **1984**, *223*, 902.
(3) Jones, W. D.; Feher, F. J. *Acc. Chem. Res.* **1989**, *22*, 91.
(4) Crabtree, R. H. *Chem. Rev.* **1985**, *85*, 245.
(5) Crabtree, R. H. *Chem. Rev.* **1995**, *95*, 987.
(6) Arndtsen, B. A.; Bergman, R. G.; Mobley, T. A.; Peterson, T. H. *Acc. Chem. Res.* **1995**, *28*, 154.
(7) Jones, W. D. *Top. Organomet. Chem.* **1999**, *3*, 9.
(8) Crabtree, R. H. *J. Chem. Soc., Dalton Trans.* **2001**, 2437.
(9) Labinger, J. A.; Bercaw, J. E. *Nature* **2002**, *417*, 507.
(10) Labinger, J. A. *J. Mol. Catal. A* **2004**, *220*, 27.
(11) Etienne, M.; McGrady, J. E.; Maseras, F. *Coord. Chem. Rev.* **2009**, *253*, 635.
(12) Dyker, G. *Angew. Chem., Int. Ed.* **1999**, *38*, 1698.
(13) Sen, A. *Acc. Chem. Res.* **1998**, *31*, 550.
(14) Guari, Y.; Sabo-Etienne, S.; Chaudret, B. *Eur. J. Inorg. Chem.* **1999**, 1047.
(15) Jia, C.; Kitamura, T.; Fujiwara, Y. *Acc. Chem. Res.* **2001**, *34*, 633.
(16) Kakiuchi, F.; Murai, S. *Acc. Chem. Res.* **2002**, *35*, 826.
(17) Ritleng, V.; Sirlin, C.; Pfeffer, M. *Chem. Rev.* **2002**, *102*, 1731.
(18) Kakiuchi, F.; Chatani, N. *Adv. Synth. Catal.* **2003**, *345*, 1077.
(19) Jensen, C. M. *Chem. Commun.* **1999**, 2443.
(20) Lewis, J. C.; Bergman, R. G.; Ellman, J. A. *Acc. Chem. Res.* **2008**, *41*, 1013.
(21) Godula, K.; Sames, D. *Science* **2006**, *312*, 67.
(22) Dedieu, A. *Top. Organomet. Chem.* **1999**, *4*, 69.
(23) Niu, S.; Hall, M. B. *Chem. Rev.* **2000**, *100*, 353.
(24) Torrent, M.; Solà, M.; Frenking, G. *Chem. Rev.* **2000**, *100*, 439.
(25) Dedieu, A. *Chem. Rev.* **2000**, *100*, 543.
(26) Sakaki, S. *Top. Organomet. Chem.* **2005**, *12*, 31.
(27) Siegbahn, P. E. M. *Adv. Chem. Phys.* **1996**, *93*, 333.
(28) Görling, A.; Trickey, S. B.; Gisdakis, P.; Rösch, N. *Top. Organomet. Chem.* **1999**, *4*, 109.
(29) Authors report their results in terms of various energies: electronic energy (E), electronic energy corrected with zero-point energy (E + ZPE), enthalpy (H), and Gibbs free energy (G). Energy differences between a transition state and its associated reactant are referred to as energy barriers for $\Delta E^{\ddagger}$, $\Delta(E + \mathrm{ZPE})^{\ddagger}$, and $\Delta H^{\ddagger}$ and as activation barriers for $\Delta G^{\ddagger}$. The term activation energy refers to experimental values.
(30) Blomberg, M. R. A.; Siegbahn, P. E. M.; Nagashima, U.; Wennerberg, J. *J. Am. Chem. Soc.* **1991**, *113*, 424.
(31) Blomberg, M. R. A.; Siegbahn, P. E. M.; Svensson, M. *J. Am. Chem. Soc.* **1992**, *114*, 6095.
(32) Sautet, P.; Delbecq, F. *Chem. Rev.* **2010**, *110*, doi: 10.1021/cr900295b.
(33) The electrophilic substitution mechanism is described in the section about Shilov chemistry.
(34) Groves, J. T. *J. Chem. Educ.* **1985**, *62*, 928.
(35) Murai, S.; Kakiuchi, F.; Sekine, S.; Tanaka, Y.; Kamatani, A.; Sonoda, M.; Chatani, N. *Nature* **1993**, *366*, 529.
(36) Das, S.; Brudvig, G. W.; Crabtree, R. H. *Chem. Commun.* **2008**, 413.
(37) Gorelsky, S. I.; Lapointe, D.; Fagnou, K. *J. Am. Chem. Soc.* **2008**, *130*, 10848.
(38) Boutadla, Y.; Davies, D. L.; Macgregor, S. A.; Poblador-Bahamonde, A. L. *Dalton Trans.* **2009**, 5820.
(39) Crabtree, R. H.; Mellea, M. F.; Mihelcic, J. M.; Quirk, J. M. *J. Am. Chem. Soc.* **1982**, *104*, 107.
(40) Xu, W. W.; Rosini, G. P.; Gupta, M.; Jensen, C. M.; Kaska, W. C.; Krogh-Jespersen, K.; Goldman, A. S. *Chem. Commun.* **1997**, 2273.
(41) Liu, F. C.; Pak, E. B.; Singh, B.; Jensen, C. M.; Goldman, A. S. *J. Am. Chem. Soc.* **1999**, *121*, 4086.
(42) Goldman, A. S.; Roy, A. H.; Huang, Z.; Ahuja, R.; Schinski, W.; Brookhart, M. *Science* **2006**, *312*, 257.
(43) Periana, R. A.; Liu, X. Y.; Bhalla, G. *Chem. Commun.* **2002**, 3000.
(44) Lail, M.; Arrowood, B. N.; Gunnoe, T. B. *J. Am. Chem. Soc.* **2003**, *125*, 7506.
(45) Waltz, K. M.; Hartwig, J. F. *Science* **1997**, *277*, 211.
(46) Chen, H. Y.; Schlecht, S.; Semple, T. C.; Hartwig, J. F. *Science* **2000**, *287*, 1995.
(47) Goldshle, N. F.; Shteinmaa, A. A.; Shilov, A. E.; Eskova, V. V. *Zh. Fiz. Khim.* **1972**, *46*, 1353.
(48) Periana, R. A.; Taube, D. J.; Evitt, E. R.; Loffler, D. G.; Wentrcek, P. R.; Voss, G.; Masuda, T. *Science* **1993**, *259*, 340.
(49) Periana, R. A.; Taube, D. J.; Gamble, S.; Taube, H.; Satoh, T.; Fujii, H. *Science* **1998**, *280*, 560.
(50) Shaik, S.; Cohen, S.; Wang, Y.; Chen, H.; Kumar, D.; Thiel, W. *Chem. Rev.* **2010**, *110*, doi: 10.1021/cr900121s.
(51) Ortiz de Montellano, P. R. *Chem. Rev.* **2010**, *110*, doi: 10.1021/cr9002193.
(52) Wasserman, E. P.; Moore, C. B.; Bergman, R. G. *Science* **1992**, *255*, 315.
(53) Hall, C.; Perutz, R. N. *Chem. Rev.* **1996**, *96*, 3125.
(54) Geftakis, S.; Ball, G. E. *J. Am. Chem. Soc.* **1998**, *120*, 9953.
(55) Cowan, A. J.; Portius, P.; Kawanami, H. K.; Jina, O. S.; Grills, D. C.; Sun, X.-Z.; McMaster, J.; George, M. W. *Proc. Natl. Acad. Sci. U.S.A.* **2007**, *104*, 6933.
(56) Bernskoetter, W. H.; Schauer, C. K.; Goldberg, K. I.; Brookhart, M. *Science* **2009**, *326*, 553.
(57) Lersch, M.; Tilset, M. *Chem. Rev.* **2005**, *105*, 2471.
(58) Ziegler, T.; Tschinke, V.; Fan, V.-Y.; Becke, A. D. *J. Am. Chem. Soc.* **1989**, *111*, 9177.
(59) Song, J.; Hall, M. B. *Organometallics* **1993**, *12*, 3118.
(60) Musaev, D. G.; Morokuma, K. *J. Am. Chem. Soc.* **1995**, *117*, 799.
(61) Siegbahn, P. E. M. *J. Am. Chem. Soc.* **1996**, *118*, 1487.
(62) Su, M.-D.; Chu, S.-Y. *Organometallics* **1997**, *16*, 1621.
(63) Jiménez-Cataño, R.; Hall, M. B. *Organometallics* **1996**, *15*, 1889.
(64) Su, M.-D.; Chu, S.-Y. *J. Phys. Chem. A* **1997**, *101*, 6798.
(65) Su, M.-D.; Chu, S.-Y. *Int. J. Quantum Chem.* **1999**, *72*, 405.
(66) Xavier, E. S.; De Alemeida, W. B.; da Silva, J. C. S.; Rocha, W. R. *Organometallics* **2005**, *24*, 2262.
(67) Su, M.-D.; Chu, S.-Y. *Chem.—Eur. J.* **1999**, *5*, 198.
(68) Bi, S.; Zhang, Z.; Zhu, S. *Chem. Phys. Lett.* **2006**, *431*, 385.
(69) Selmeczy, A. D.; Jones, W. D.; Partridge, M. G.; Perutz, R. N. *Organometallics* **1994**, *12*, 522.
(70) Bosque, R.; Clot, E.; Fantacci, S.; Maseras, F.; Eisenstein, O.; Perutz, R. N.; Renkema, K. B.; Caulton, K. G. *J. Am. Chem. Soc.* **1998**, *120*, 12634.
(71) Gérard, H.; Davidson, E. R.; Eisenstein, O. *Mol. Phys.* **2002**, *100*, 533.
(72) Reinhold, M.; McGrady, J. E.; Perutz, R. N. *J. Am. Chem. Soc.* **2004**, *126*, 5268.
(73) Nova, A.; Erhardt, S.; Jasim, N. A.; Perutz, R. N.; Macgregor, S. A.; McGrady, J. E.; Whitwood, A. C. *J. Am. Chem. Soc.* **2008**, *130*, 15499.
(74) Erhardt, S.; Macgregor, S. A. *J. Am. Chem. Soc.* **2008**, *130*, 15490.
(75) Stoutland, P. O.; Bergman, R. G. *J. Am. Chem. Soc.* **1985**, *107*, 4581.
(76) Smith, K. M.; Poli, R.; Harvey, J. N. *Chem.—Eur. J.* **2001**, *7*, 1679.
(77) Harvey, J. N.; Aschi, M.; Schwarz, H.; Koch, W. *Theor. Chem. Acc.* **1998**, *99*, 95.
(78) Harvey, J. N.; Aschi, M. *Phys. Chem. Chem. Phys.* **1999**, *1*, 5555.
(79) Petit, A.; Richard, P.; Cacelli, I.; Poli, R. *Chem.—Eur. J.* **2006**, *12*, 813.
(80) Asplund, M. C.; Snee, P. T.; Yeston, J. S.; Wilkens, M. J.; Payne, C. K.; Yang, H.; Kotz, K. T.; Frei, H.; Bergman, R. G.; Harris, C. B. *J. Am. Chem. Soc.* **2002**, *124*, 10605.
(81) Asbury, J. B.; Ghosh, H. N.; Yeston, J. S.; Bergman, R. G.; Lian, T. *Organometallics* **1998**, *17*, 3417.
(82) Bromberg, S. E.; Yang, H.; Asplund, M. C.; Lian, T.; McNamara, B. K.; Kotz, K. T.; Yeston, J. S.; Wilkens, M.; Frei, H.; Bergman, R. G.; Harris, C. B. *Science* **1997**, *278*, 260.
(83) Zarić, S.; Hall, M. B. *J. Phys. Chem. A* **1998**, *102*, 1963.
(84) Blake, A. J.; Georges, M. W.; Hall, M. B.; McMaster, J.; Portius, P.; Sun, X. Z.; Towrie, M.; Webster, C. E.; Wilson, C.; Zarić, S. *Organometallics* **2008**, *27*, 189.
(85) Clot, E.; Eisenstein, O.; Jones, W. D. *Proc. Natl. Acad. Sci. U.S.A.* **2007**, *104*, 6939.
(86) Northcutt, T. O.; Wick, D. D.; Vetter, A. J.; Jones, W. D. *J. Am. Chem. Soc.* **2001**, *123*, 7257.
(87) Jones, W. D. *Acc. Chem. Res.* **2003**, *36*, 140.
(88) Gérard, H.; Eisenstein, O.; Lee, D.-H.; Chen, J.; Crabtree, R. H. *New J. Chem.* **2001**, *25*, 1121.
(89) Iron, M. A.; Lo, H. C.; Martin, J. M. L.; Keinan, E. *J. Am. Chem. Soc.* **2002**, *124*, 7041.
(90) Jensen, M. P.; Wick, D. D.; Reinartz, S.; White, P. S.; Templeton, J. L.; Goldberg, K. I. *J. Am. Chem. Soc.* **2003**, *125*, 8614.
(91) Vastine, B. A.; Webster, C. E.; Hall, M. B. *J. Chem. Theory Comput.* **2007**, *3*, 2268.
(92) Holtcamp, M. W.; Labinger, J. A.; Bercaw, J. E. *J. Am. Chem. Soc.* **1997**, *119*, 848.
(93) Heiberg, H.; Johansson, L.; Gropen, O.; Ryan, O. B.; Swang, O.; Tilset, M. *J. Am. Chem. Soc.* **2000**, *122*, 10831.

(94) Johansson, L.; Tilset, M.; Labinger, J. A.; Bercaw, J. E. *J. Am. Chem. Soc.* **2000**, *122*, 10846.
(95) Heiberg, H.; Swang, O.; Ryan, O. B.; Gropen, O. *J. Phys. Chem. A* **1999**, *103*, 10004.
(96) Heiberg, H.; Gropen, O.; Swang, O. *Int. J. Quantum Chem.* **2003**, *92*, 391.
(97) Li, J.-L.; Geng, C.-Y.; Huang, X.-R.; Zhang, X.; Sun, C.-C. *Organometallics* **2007**, *26*, 2203.
(98) Nückel, S.; Bürger, P. *Angew. Chem., Int. Ed.* **2003**, *42*, 1632.
(99) Burger, P.; Bergman, R. G. *J. Am. Chem. Soc.* **1993**, *115*, 10462.
(100) Tellers, D. M.; Yung, C. M.; Arndtsen, B. A.; Adamson, D. R.; Bergman, R. G. *J. Am. Chem. Soc.* **2002**, *124*, 1400.
(101) Hinderling, C.; Feichtinger, D.; Plattner, D. A.; Chen, P. *J. Am. Chem. Soc.* **1997**, *119*, 10793.
(102) Luecke, H. F.; Bergman, R. G. *J. Am. Chem. Soc.* **1997**, *119*, 11538.
(103) Strout, D. L.; Zarić, S.; Niu, S.; Hall, M. B. *J. Am. Chem. Soc.* **1996**, *118*, 6068.
(104) Niu, S.; Hall, M. B. *J. Am. Chem. Soc.* **1998**, *120*, 6169.
(105) Webster, C. E.; Hall, M. B. *Organometallics* **2001**, *20*, 5606.
(106) Webster, C. E.; Hall, M. B. *J. Organomet. Chem.* **2003**, *238*−*239*, 315.
(107) Viciano, M.; Feliz, M.; Corberán, R.; Mata, J. A.; Clot, E.; Peris, E. *Organometallics* **2007**, *26*, 5304.
(108) Bergman, R. G.; Cundari, T. R.; Gillespie, A. M.; Gunnoe, T. B.; Harman, W. D.; Klinckman, T. R.; Temple, M. D.; White, D. P. *Organometallics* **2003**, *22*, 2331.
(109) Clot, E.; Oelckers, B.; Klahn, A. H.; Eisenstein, O.; Perutz, R. N. *Dalton Trans.* **2003**, 4065.
(110) Carbó, J. J.; Eisenstein, O.; Higgit, C. L.; Klahn, A. H.; Maseras, F.; Oelckers, B.; Perutz, R. N. *Dalton Trans.* **2001**, 1452.
(111) Lee, K.; Legzdins, P.; Pamplin, C. B.; Patrick, B. O.; Wada, K. *Organometallics* **2005**, *24*, 638.
(112) Grebnik, P.; Downs, A. J.; Green, M. L. H.; Perutz, R. N. *J. Chem. Soc., Chem. Commun.* **1979**, 742.
(113) Chetwynd-Talbot, J.; Grebnik, P.; Perutz, R. N. *Inorg. Chem.* **1982**, *21*, 3647.
(114) Gianotti, C.; Green, M. L. H. *J. Chem. Soc., Chem. Commun.* **1972**, 1114.
(115) Cooper, N. J.; Green, M. L. H.; Mahtab, R. *J. Chem. Soc., Dalton Trans.* **1979**, 1557.
(116) Berry, M.; Elmitt, K.; Green, M. L. H. *J. Chem. Soc., Dalton Trans.* **1979**, 1950.
(117) Bullock, R. M.; Headford, C. E. L.; Kegley, S. E.; Norton, J. R. *J. Am. Chem. Soc.* **1985**, *107*, 727.
(118) Bullock, R. M.; Headford, C. E. L.; Hennessy, K. M.; Kegley, S. E.; Norton, J. R. *J. Am. Chem. Soc.* **1989**, *111*, 3897.
(119) Parkin, G.; Bercaw, J. E. *Organometallics* **1989**, *8*, 1172.
(120) Labella, L.; Chernega, A.; Green, M. L. H. *J. Chem. Soc., Dalton Trans.* **1995**, 395.
(121) Green, J. C.; Jardine, C. N. *J. Chem. Soc., Dalton Trans.* **1998**, 1057.
(122) Su, M.-D.; Chu, S.-Y. *J. Phys. Chem. A* **2001**, *105*, 3591.
(123) Green, J. C.; Harvey, J. N.; Poli, R. *J. Chem. Soc., Dalton Trans.* **2002**, 1861.
(124) Green, J. C. *Polyhedron* **2005**, *24*, 1382.
(125) Carreón-Macedo, J.-L.; Harvey, J. N.; Poli, R. *Eur. J. Inorg. Chem.* **2005**, 2999.
(126) Cox, P. A.; Grebenik, P.; Perutz, R. N.; Robinson, M. D.; Grinter, R.; Stern, D. *Inorg. Chem.* **1983**, *22*, 3614.
(127) Grebenik, P.; Grinter, R.; Perutz, R. N. *Chem. Soc. Rev.* **1988**, 453.
(128) Shaik, S. *J. Am. Chem. Soc.* **1981**, *103*, 3692.
(129) Churchill, D. G.; Janak, K. E.; Wittenberg, J. S.; Parkin, G. *J. Am. Chem. Soc.* **2003**, *125*, 1403.
(130) Janak, K. E.; Parkin, G. *J. Am. Chem. Soc.* **2003**, *125*, 6889.
(131) Parkin, G. *Acc. Chem. Res.* **2009**, *42*, 315.
(132) Lin, Z. *Coord. Chem. Rev.* **2007**, *251*, 2280.
(133) Ephritikhine, M. *Chem. Rev.* **1997**, *97*, 2193.
(134) Kaminsky, W.; Arndt, M. *Adv. Polym. Sci.* **1997**, *127*, 143.
(135) Burger, B. J.; Thompson, M. E.; Cotter, W. D.; Bercaw, J. E. *J. Am. Chem. Soc.* **1990**, *112*, 1566.
(136) Thompson, M. E.; Buxter, S. M.; Bulls, A. R.; Burger, B. J.; Nolan, M. C.; Santarsiero, B. D.; Schaefer, W. P.; Bercaw, J. E. *J. Am. Chem. Soc.* **1987**, *109*, 203.
(137) Margl, P.; Deng, L.; Ziegler, T. *J. Am. Chem. Soc.* **1999**, *121*, 154.
(138) Watson, P. L.; Parshall, G. W. *Acc. Chem. Res.* **1985**, *18*, 51.
(139) Davies, J. A.; Watson, P. L.; Liebman, J. F.; Greenberg, A. *Selective Hydrocarbon Activation:Principles and Progress*; VCH Publishers: New York, 1990.
(140) Werkema, E. L.; Messines, E.; Perrin, L.; Maron, L.; Eisenstein, O.; Andersen, R. A. *J. Am. Chem. Soc.* **2005**, *127*, 7781.
(141) Werkema, E. L.; Andersen, R. A.; Yahia, A.; Maron, L.; Eisenstein, O. *Organometallics* **2009**, *28*, 3173.
(142) Maron, L.; Werkema, E. L.; Perrin, L.; Eisenstein, O.; Andersen, R. A. *J. Am. Chem. Soc.* **2005**, *127*, 279.
(143) Werkema, E. L.; Andersen, R. A. *J. Am. Chem. Soc.* **2008**, *130*, 7153.
(144) Ma, K.; Piers, W. E.; Parvez, M. J. *J. Am. Chem. Soc.* **2006**, *128*, 3303.
(145) Yang, X.; Hall, M. B. *J. Phys. Chem. A* **2009**, *113*, 2152.
(146) Sadow, A. D.; Tilley, T. D. *J. Am. Chem. Soc.* **2003**, *125*, 7971.
(147) Fontaine, F. G.; Tilley, T. D. *Organometallics* **2005**, *24*, 4340.
(148) Steigerwald, M. L.; Goddard III, W. A. *J. Am. Chem. Soc.* **1984**, *106*, 308.
(149) Rappé, A. K. *Organometallics* **1990**, *9*, 466.
(150) Ziegler, T.; Folga, E.; Berces, A. *J. Am. Chem. Soc.* **1993**, *155*, 636.
(151) Maron, L.; Eisenstein, O. *J. Am. Chem. Soc.* **2001**, *123*, 1036.
(152) Maron, L.; Eisenstein, O.; Alary, F.; Poteau, R. *J. Phys. Chem. A* **2002**, *106*, 1797.
(153) Perrin, L.; Maron, L.; Eisenstein, O. *New J. Chem.* **2004**, *28*, 1255.
(154) Maron, L.; Eisenstein, O. *J. Phys. Chem. A* **2000**, *104*, 7140.
(155) Perrin, L.; Maron, L.; Eisenstein, O. *Activation and Functionalization of C-H Bonds*; Goldberg, K. I.; Goldman, A. S., Eds.; ACS Symposium Series 885; American Chemical Society: Washington, DC, 2004; p 116.
(156) Folga, E.; Ziegler, T. *Can. J. Chem.* **1992**, *70*, 333.
(157) Maron, L.; Perrin, L.; Eisenstein, O. *J. Chem. Soc., Dalton Trans.* **2002**, 534.
(158) Barros, N.; Eisentein, O.; Maron, L. *Dalton Trans.* **2006**, 3052.
(159) Ziegler, T.; Folga, E. *J. Organomet. Chem.* **1994**, *478*, 57.
(160) Perrin, L.; Maron, L.; Eisenstein, O. *Inorg. Chem.* **2002**, *41*, 4355.
(161) Perrin, L.; Eisenstein, O.; Maron, L. *New J. Chem.* **2007**, *31*, 549.
(162) Perrin, L.; Maron, L.; Eisenstein, O.; Tilley, T. D. *Organometallics* **2009**, *28*, 3767.
(163) Copéret, C.; Grouiller, A.; Basset, J.-M.; Chermette, H. *ChemPhysChem* **2003**, *4*, 608.
(164) Sherer, E. C.; Cramer, C. J. *Organometallics* **2003**, *22*, 1682.
(165) Woodrum, N. L.; Cramer, C. J. *Organometallics* **2006**, *25*, 68.
(166) Lewin, J. L.; Woodrum, N. L.; Cramer, C. J. *Organometallics* **2006**, *25*, 5906.
(167) Barros, N.; Eisenstein, O.; Maron, L.; Tilley, T. D. *Organometallics* **2006**, *25*, 5699.
(168) Barros, N.; Eisenstein, O.; Maron, L.; Tilley, T. D. *Organometallics* **2008**, *27*, 2252.
(169) Following this publication, the structure proposed by Hall could not be identified as a transition state. Maron, L. Private communication.
(170) Perrin, L.; Maron, L.; Eisenstein, O. *Dalton Trans.* **2003**, 4313.
(171) Werkema, E. L.; Maron, L.; Eisenstein, O.; Andersen, R. A. *J. Am. Chem. Soc.* **2007**, *129*, 2529.
(172) Guerrero-Rios, I.; Novarino, E.; van der Veer, S.; Hessen, B.; Bouwkamp, M. W. *J. Am. Chem. Soc.* **2009**, *131*, 16658.
(173) Bennett, J. L.; Wolczanski, P. T. *J. Am. Chem. Soc.* **1997**, *119*, 10696.
(174) Slaughter, L. M.; Wolczanski, P. T.; Klinckman, T. R.; Cundari, T. R. *J. Am. Chem. Soc.* **2000**, *122*, 7953.
(175) Cundari, T. R.; Klinckman, T. R.; Wolczanski, P. T. *J. Am. Chem. Soc.* **2002**, *124*, 1481.
(176) Ochi, N.; Nakao, Y.; Sato, H.; Sakaki, S. *J. Am. Chem. Soc.* **2007**, *129*, 8615.
(177) Nakai, H.; Suzuki, J.; Kikuchi, Y. *Chem. Phys. Lett.* **2008**, *460*, 347.
(178) Bailey, B. C.; Fan, H.; Baum, E. W.; Huffman, J. C.; Baik, M.-H.; Mindiola, D. J. *J. Am. Chem. Soc.* **2005**, *127*, 16016.
(179) Bailey, B. C.; Fan, H.; Huffman, J. C.; Baik, M.-H.; Mindiola, D. J. *J. Am. Chem. Soc.* **2007**, *129*, 8781.
(180) He, G.; Zhu, J.; Hung, W. Y.; Wen, T. B.; Sung, H. H.-Y.; Williams, I. D.; Lin, Z.; Jia, G. *Angew. Chem., Int. Ed.* **2007**, *46*, 9065.
(181) Pamplin, C. B.; Legzdins, P. *Acc. Chem. Res.* **2003**, *36*, 223.
(182) Poli, R.; Smith, K. M. *Organometallics* **2000**, *19*, 2858.
(183) Adams, C. S.; Legzdins, P.; McNeil, W. S. *Organometallics* **2001**, *20*, 4939.
(184) Fan, Y.; Hall, M. B. *J. Chem. Soc., Dalton Trans.* **2002**, 713.
(185) Wada, K.; Pamplin, C. B.; Legzdins, P. *J. Am. Chem. Soc.* **2002**, *124*, 9680.
(186) Wada, K.; Pamplin, C. B.; Legzdins, P.; Patrick, B. O.; Tsyba, I.; Bau, R. *J. Am. Chem. Soc.* **2003**, *125*, 7035.
(187) Fulton, J. R.; Holland, A. W.; Fox, D. J.; Bergman, R. G. *Acc. Chem. Res.* **2002**, *35*, 44.
(188) Conner, D.; Jayaprakash, K. N.; Cundari, T. R.; Gunnoe, T. B. *Organometallics* **2004**, *23*, 2724.
(189) Feng, Y.; Lail, M.; Barakat, K. A.; Cundari, T. R.; Gunnoe, T. B.; Petersen, J. L. *J. Am. Chem. Soc.* **2005**, *127*, 14174.
(190) Feng, Y.; Gunnoe, T. B.; Grimes, T. V.; Cundari, T. R. *Organometallics* **2006**, *25*, 5456.
(191) Feng, Y.; Lail, M.; Foley, N. A.; Gunnoe, T. B.; Barakat, K. A.; Cundari, T. R.; Petersen, J. L. *J. Am. Chem. Soc.* **2006**, *128*, 7982.
(192) Cundari, T. R.; Grimes, T. V.; Gunnoe, T. B. *J. Am. Chem. Soc.* **2007**, *129*, 13172.
(193) Tenn, W. J., III; Young, K. J. H.; Bhalla, G.; Oxgaard, J.; Goddard, W. A., III; Periana, R. A. *J. Am. Chem. Soc.* **2005**, *127*, 14172.

(194) Tenn, W. J., III; Young, K. J. H.; Oxgaard, J.; Nielsen, R. J.; Goddard, W. A., III; Periana, R. A. *Organometallics* **2006**, *25*, 5173.
(195) Oxgaard, J.; Tenn, W. J., III; Nielsen, R. J.; Periana, R. A.; Goddard, W. A., III *Organometallics* **2007**, *26*, 1565.
(196) Perutz, R. N.; Sabo-Etienne, S. *Angew. Chem., Int. Ed.* **2007**, *46*, 2578.
(197) Toner, A. J.; Gründemann, S.; Clot, E.; Limbach, H.-H.; Donnadieu, B.; Sabo-Etienne, S.; Chaudret, B. *J. Am. Chem. Soc.* **2000**, *122*, 6777.
(198) Ng, S. M.; Lam, W. H.; Mak, C. C.; Tsang, C. W.; Jia, G.; Lin, Z.; Lau, C. P. *Organometallics* **2003**, *22*, 641.
(199) Lam, W. H.; Jia, G.; Lin, Z.; Lau, C. P.; Eisenstein, O. *Chem.—Eur. J.* **2003**, *9*, 2775.
(200) Oxgaard, J.; Muller, R. P.; Goddard, W. A., III; Periana, R. A. *J. Am. Chem. Soc.* **2004**, *126*, 352.
(201) Oxgaard, J.; Goddard, W. A., III *J. Am. Chem. Soc.* **2004**, *126*, 442.
(202) DeYonker, N. J.; Foley, N. J.; Cundari, T. R.; Gunnoe, T. B.; Petersen, J. L. *Organometallics* **2007**, *26*, 6604.
(203) Foley, N. A.; Gunnoe, T. B.; Cundari, T. R.; Boyle, P. D.; Petersen, J. L. *Angew. Chem., Int. Ed.* **2008**, *47*, 726.
(204) Butschke, B.; Schröder, D.; Schwarz, H. *Organometallics* **2009**, *28*, 4340.
(205) Lin, B.-L.; Bhattachryya, K. X.; Labinger, J. A.; Bercaw, J. E. *Organometallics* **2009**, *28*, 4400.
(206) Bader, R. W. F. *Atoms in Molecules, a Quantum Theory*; Oxford University Press: Ithaca, NY, 1989.
(207) Vastine, B. A.; Hall, M. B. *J. Am. Chem. Soc.* **2007**, *129*, 12068.
(208) Vastine, B. A.; Hall, M. B. *Coord. Chem. Rev.* **2009**, *253*, 1202.
(209) Fan, Y.; Hall, M. B. *Organometallics* **2005**, *24*, 3827.
(210) Ess, D. H.; Nielsen, R. J.; Goddard, W. A., III; Periana, R. A. *J. Am. Chem. Soc.* **2009**, *131*, 11686.
(211) Khaliullin, R. Z.; Cobar, E. A.; Lochan, R. C.; Bell, A. T.; Head-Gordon, M. *J. Phys. Chem. A* **2007**, *111*, 8753.
(212) *Metal-Oxo and Metal-Peroxo Species in Catalytic Oxidations (Structure and Bonding)*; Meunier, B., Ed.; Springer-Verlag: Berlin, 2000.
(213) *Catalytic Activation and Functionalisation of Light Alkanes- Advances and Challenges*; Derouane, E. G., Haber, J., Lemos, F., Ribeiro, F. R., Guisnet, M., Eds.; Springer: Dordrecht, The Netherlands, 1998.
(214) *Biomimetic Oxidations Catalyzed by Transition Metal Complexes*; Meunier, B., Ed.; Imperial College Press: London, 2000.
(215) *Modern Biooxidation: Enzymes, Reactions and Applications*; Schmid, R. D., Urlacher, V., Eds.; Wiley-VCH: Weinheim, Germany, 2007.
(216) Solomon, E. I.; Sundaram, U. M.; Machonkin, T. E. *Chem. Rev.* **1996**, *96*, 2563.
(217) Que, L.; Dong, Y. H. *Acc. Chem. Res.* **1996**, *29*, 190.
(218) *Cytochrome P450: Structure, Mechanism, and Biochemistry*; de Montellano, P. R. O., Ed.; Springer: New York, 2005.
(219) Groves, J. T.; McClusky, G. A. *J. Am. Chem. Soc.* **1976**, *98*, 859.
(220) Das, S.; Incarvito, C. D.; Crabtree, R. H.; Brudvig, G. W. *Science* **2006**, *312*, 1941.
(221) Denisov, I. G.; Makris, T. M.; Sligar, S. G.; Schlichting, I. *Chem. Rev.* **2005**, *105*, 2253.
(222) Loew, G. H.; Harris, D. L. *Chem. Rev.* **2000**, *100*, 407.
(223) Dawson, J. H.; Sono, M. *Chem. Rev.* **1987**, *87*, 1255.
(224) Meunier, B.; de Visser, S. P.; Shaik, S. *Chem. Rev.* **2004**, *104*, 3947.
(225) Shaik, S.; Kumar, D.; de Visser, S. P.; Altun, A.; Thiel, W. *Chem. Rev.* **2005**, *105*, 2279.
(226) Costas, M.; Mehn, M. P.; Jensen, M. P.; Que, L. *Chem. Rev.* **2004**, *104*, 939.
(227) Que, L. *Acc. Chem. Res.* **2007**, *40*, 493.
(228) Que, L.; Ho, R. Y. N. *Chem. Rev.* **1996**, *96*, 2607.
(229) Carlsen, C. U.; Moller, J. K. S.; Skibsted, L. H. *Coord. Chem. Rev.* **2005**, *249*, 485.
(230) Hammes-Schiffer, S. *Acc. Chem. Res.* **2006**, *39*, 93.
(231) Fenton, H. J. H. *J. Chem. Soc. Trans.* **1894**, *65*, 899.
(232) Koch, W.; Holthausen, M. C. *A Chemist's Guide to Density Functional Theory*; Wiley-VCH: Weinheim, Germany, 2000.
(233) Maseras, F.; Morokuma, K. *J. Comput. Chem.* **1995**, *16*, 1170.
(234) Uddin, J.; Morales, C. M.; Maynard, J. H.; Landis, C. R. *Organometallics* **2006**, *25*, 5566.
(235) Shilov, A. E. *Alkane Activation Complexes of Rhodium, Iridium and Related Species*; Wiley: New York, 1989; p 372.
(236) Hong, S.; Marks, T. J. *Acc. Chem. Res.* **2004**, *37*, 673.
(237) Martinho-Simões, J. A.; Beauchamp, J. L. *Chem. Rev.* **1990**, *90*, 629.
(238) Hoff, C. D. *Prog. Inorg. Chem.* **1992**, *40*, 503.
(239) King, W. A.; DiBella, S.; Gulino, A.; Lanza, G.; Fragalá, I. L.; Stern, C. L.; Marks, T. J. *J. Am. Chem. Soc.* **1999**, *121*, 355.
(240) Bryndza, H. E.; Fong, L. K.; Paciello, R. A.; Tam, W.; Bercaw, J. E. *J. Am. Chem. Soc.* **1987**, *109*, 1444.
(241) Jones, W. D.; Hessell, E. T. *J. Am. Chem. Soc.* **1993**, *115*, 554.
(242) Wick, D. D.; Jones, W. D. *Organometallics* **1999**, *18*, 495.
(243) Bennett, J. L.; Wolczanski, P. T. *J. Am. Chem. Soc.* **1994**, *116*, 2179.
(244) Holland, P. L.; Andersen, R. A.; Bergman, R. G.; Huang, J.; Nolan, S. P. *J. Am. Chem. Soc.* **1997**, *119*, 12800.
(245) Holland, P. L.; Andersen, R. A.; Bergman, R. G. *Comments Inorg. Chem.* **1999**, *21*, 115.
(246) Schock, L. E.; Marks, T. J. *J. Am. Chem. Soc.* **1988**, *110*, 7701.
(247) Yao, X.-Q.; Hou, X.-J.; Jiao, H.; Xiang, H.-W.; Li, Y.-W. *J. Phys. Chem. A* **2003**, *107*, 9991.
(248) Zhao, Y.; Lynch, B. J.; Truhlar, D. G. *J. Phys. Chem. A* **2004**, *108*, 2715.
(249) Zhao, Y.; Lynch, B. J.; Truhlar, D. G. *J. Phys. Chem. A* **2004**, *108*, 4786.
(250) Izgorodina, E. I.; Coote, M. L.; Radom, L. *J. Phys. Chem. A* **2005**, *109*, 7558.
(251) Gillies, M. B.; Matyjaszewski, K.; Norrby, P. O.; Pintauer, T.; Poli, R.; Richard, P. *Macromolecules* **2003**, *36*, 8551.
(252) Henry, D. J.; Parkinson, C. J.; Mayer, P. M.; Radom, L. *J. Phys. Chem. A* **2001**, *105*, 6750.
(253) Zhao, Y.; Truhlar, D. G. *Acc. Chem. Res.* **2008**, *41*, 157.
(254) Schwabe, T.; Grimme, S. *Acc. Chem. Res.* **2008**, *41*, 569.
(255) Ziegler, T.; Tschinke, V.; Becke, A. *J. Am. Chem. Soc.* **1987**, *109*, 1351.
(256) Folga, E.; Ziegler, T. *J. Am. Chem. Soc.* **1993**, *115*, 5169.
(257) Ziegler, T.; Cheng, W.; Baerends, E. J.; Ravanek, W. *Inorg. Chem.* **1988**, *27*, 3458.
(258) Harvey, J. N. *Organometallics* **2001**, *20*, 4887.
(259) Clot, E.; Mégret, C.; Eisenstein, O.; Perutz, R. N. *J. Am. Chem. Soc.* **2006**, *128*, 8350.
(260) Mitoraj, M.; Zhu, H.; Michalak, A.; Ziegler, T. *Organometallics* **2007**, *26*, 1627.
(261) Clot, E.; Besora, M.; Maseras, F.; Mégret, C.; Eisenstein, O.; Oelckers, B.; Perutz, R. N. *Chem. Commun.* **2003**, 490.
(262) Clot, E.; Mégret, C.; Eisenstein, O.; Perutz, R. N. *J. Am. Chem. Soc.* **2009**, *131*, 7817.
(263) Evans, M. E.; Burke, C. L.; Yaibuathes, S.; Clot, E.; Eisenstein, O.; Jones, W. D. *J. Am. Chem. Soc.* **2009**, *131*, 13464.
(264) Diggle, R. A.; Kennedy, A. A.; Macgregor, S. A.; Whittlesey, M. K. *Organometallics* **2008**, *27*, 938.
(265) Matsubara, T.; Koga, N.; Musaev, D.; Morokuma, K. *J. Am. Chem. Soc.* **1998**, *120*, 12692.
(266) Guari, Y.; Sabo-Etienne, S.; Chaudret, B. *J. Am. Chem. Soc.* **1998**, *120*, 4228.
(267) Toner, A.; Matthes, J.; Gründemann, S.; Limbach, H.-H.; Chaudret, B.; Clot, E.; Sabo-Etienne, S. *Proc. Natl. Acad. Sci. U.S.A.* **2007**, *104*, 6945.
(268) Barrio, P.; Castarlenas, R.; Esteruelas, M. A.; Lledós, A.; Maseras, F.; Oñate, E.; Tomàs, J. *Organometallics* **2001**, *20*, 442.
(269) Esteruelas, M. A.; Lledós, A.; Oliván, M.; Oñate, E.; Tajada, M. A.; Ujaque, G. *Organometallics* **2003**, *22*, 3753.
(270) Ben-Ari, E.; Gandelman, M.; Rozenberg, H.; Shimon, L. J. W.; Milstein, D. *J. Am. Chem. Soc.* **2003**, *125*, 4714.
(271) Ben-Ari, E.; Cohen, R.; Gandelman, M.; Shimon, L. J. W.; Martin, J. M. L.; Milstein, D. *Organometallics* **2006**, *25*, 3190.
(272) Fan, L.; Parkin, S.; Ozerov, O. V. *J. Am. Chem. Soc.* **2005**, *127*, 16772.
(273) Wu, H.; Hall, M. B. *Dalton Trans.* **2009**, 5933.
(274) Wu, H.; Hall, M. B. *J. Phys. Chem. A* **2009**, *113*, 11706.
(275) Zhang, X.; Kanzelberger, M.; Emge, T. J.; Goldman, A. S. *J. Am. Chem. Soc.* **2004**, *126*, 13192.
(276) Zhang, X.; Emge, T. J.; Ghosh, R.; Krogh-Jespersen, K.; Goldman, A. S. *Organometallics* **2006**, *25*, 1303.
(277) Feller, M.; Karton, A.; Leitus, G.; Martin, J. M. L.; Milstein, D. *J. Am. Chem. Soc.* **2006**, *128*, 12400.
(278) Paneque, M.; Poveda, M. L.; Santos, L. L.; Carmona, E.; Lledós, A.; Ujaque, G.; Mereiter, K. *Angew. Chem., Int. Ed.* **2004**, *43*, 3708.
(279) Lara, P.; Paneque, M.; Poveda, M. L.; Santos, L. L.; Valpuesta, J. E. V.; Carmona, E.; Moncho, S.; Ujaque, G.; Lledós, A.; Álvarez, E.; Mereiter, K. *Chem.—Eur. J.* **2009**, *15*, 9034.
(280) Lara, P.; Paneque, M.; Poveda, M. L.; Santos, L. L.; Valpuesta, J. E. V.; Salazar, V.; Carmona, E.; Moncho, S.; Ujaque, G.; Lledós, A.; Maya, C.; Mereiter, K. *Chem.—Eur. J.* **2009**, *15*, 9046.
(281) Jordan, R. F.; Taylor, D. F. *J. Am. Chem. Soc.* **1989**, *111*, 778.
(282) Bi, S.; Lin, Z.; Jordan, R. F. *Organometallics* **2004**, *23*, 4882.
(283) Pool, J. A.; Scott, B. L.; Kiplinger, J. L. *J. Alloys Compd.* **2006**, *418*, 178.
(284) Kiplinger, J. L.; Scott, B. L.; Schelter, E. J.; Pool, J. A. *J. Alloys Compd.* **2007**, *444−445*, 477.
(285) Yang, P.; Warnke, I.; Martin, R. L.; Hay, P. J. *Organometallics* **2008**, *27*, 1384.
(286) Tan, K. L.; Bergman, R. G.; Ellman, J. A. *J. Am. Chem. Soc.* **2002**, *124*, 3202.
(287) Wiedemann, S. H.; Lewis, J. C.; Ellman, J. A.; Bergman, R. G. *J. Am. Chem. Soc.* **2006**, *128*, 2452.

(288) Yao, W. B.; Eisenstein, O.; Crabtree, R. H. *Inorg. Chem. Acta* **1997**, *254*, 105.
(289) Baya, M.; Eguillor, B.; Esteruelas, M. A.; Lledós, A.; Oliván, M.; Oñate, E. *Organometallics* **2007**, *26*, 5140.
(290) Esteruelas, M. A.; Fernández-Alvarez, F. J.; Oñate, E. *J. Am. Chem. Soc.* **2006**, *128*, 13044.
(291) Esteruelas, M. A.; Forcén, E.; Oliván, M.; Oñate, E. *Organometallics* **2008**, *27*, 6188.
(292) Esteruelas, M. A.; Fernández-Alverez, F. J.; Oñate, E. *Organometallics* **2008**, *27*, 6236.
(293) Eguillor, B.; Esteruelas, M. A.; García-Raboso, J.; Oliván, M.; Oñate, E. *Organometallics* **2009**, *28*, 3700.
(294) Clot, E.; Chen, J.; Lee, D.-H.; Sung, S. Y.; Appelhans, L. N.; Faller, J. W.; Crabtree, R. H.; Eisenstein, O. *J. Am. Chem. Soc.* **2004**, *126*, 8795.
(295) van der Boom, M.; Milstein, D. *Chem. Rev.* **2003**, *103*, 1759.
(296) Diez-González, S.; Marion, N.; Nolan, S. P. *Chem. Rev.* **2009**, *109*, 3612.
(297) Vigalok, A.; Uzan, O.; Shimon, L. J. W.; Ben-David, Y.; Martin, J. M. L.; Milstein, D. *J. Am. Chem. Soc.* **1998**, *120*, 12539.
(298) Montag, M.; Schwartsburd, L.; Cohen, R.; Leitus, G.; Ben-David, Y.; Martin, J. M. L.; Milstein, D. *Angew. Chem., Int. Ed.* **2007**, *46*, 1901.
(299) Rybtchinski, B.; Cohen, R.; Ben-David, Y.; Martin, J. M. L.; Milstein, D. *J. Am. Chem. Soc.* **2003**, *125*, 11041.
(300) Rybtchinski, B.; Konstantinovsky, L.; Shimon, L. J. W.; Vigalok, A.; Milstein, D. *Chem.—Eur. J.* **2000**, *6*, 3287.
(301) Blug, M.; Heuclin, H.; Cantat, T.; Le Goff, X.-F.; Mézailles, N.; Le Floch, P. *Organometallics* **2009**, *28*, 1969.
(302) Cantat, T.; Demange, M.; Mézailles, N.; Ricard, L.; Jean, Y.; Le Floch, P. *Organometallics* **2005**, *24*, 4838.
(303) Jazzar, R. F. R.; Macgregor, S. A.; Mahon, M. F.; Richards, S. P.; Whittlesey, M. K. *J. Am. Chem. Soc.* **2002**, *124*, 4944.
(304) Diggle, R. A.; Macgregor, S. A.; Whittlesey, M. K. *Organometallics* **2008**, *27*, 617.
(305) Mathew, J.; Koga, N.; Suresh, C. H. *Organometallics* **2008**, *27*, 4666.
(306) Diggle, R. A.; Macgregor, S. A.; Whittlesey, M. K. *Organometallics* **2004**, *23*, 1857.
(307) Poyatos, M.; Mata, J. A.; Peris, E. *Chem. Rev.* **2009**, *109*, 3677.
(308) Viciano, M.; Poyatos, M.; Sanaú, M.; Peris, E.; Rossin, A.; Ujaque, G.; Lledós, A. *Organometallics* **2006**, *25*, 1120.
(309) Kovacevic, A.; Gründemann, S.; Miecznikowski, J. R.; Clot, E.; Eisenstein, O.; Crabtree, R. H. *Chem. Commun.* **2002**, 2580.
(310) Appelhans, L. N.; Zuccaccia, D.; Kovacevic, A.; Chianese, A. R.; Miecznikowski, J. R.; Macchioni, A.; Clot, E.; Eisenstein, O.; Crabtree, R. H. *J. Am. Chem. Soc.* **2005**, *127*, 16299.
(311) Clot, E. *Eur. J. Inorg. Chem.* **2009**, 2319.
(312) Häller, L. J. L.; Page, M. J.; Macgregor, S. A.; Mahon, M. F.; Whittlesey, M. K. *J. Am. Chem. Soc.* **2009**, *131*, 4604.
(313) Marrone, A.; Re, N.; Romeo, R. *Organometallics* **2008**, *27*, 2215.
(314) Kuznetsov, V. F.; Abdur-Rashid, K.; Lough, A. J.; Gusev, D. G. *J. Am. Chem. Soc.* **2006**, *128*, 14388.
(315) Ingleson, M. J.; Yang, X.; Pink, M.; Caulton, K. G. *J. Am. Chem. Soc.* **2005**, *127*, 10846.
(316) Walstrom, A.; Pink, M.; Tsvetkov, N. P.; Fan, H.; Ingleson, M. J.; Caulton, K. G. *J. Am. Chem. Soc.* **2005**, *127*, 16780.
(317) Das, S.; Brudvig, G. W.; Crabtree, R. H. *J. Am. Chem. Soc.* **2008**, *130*, 1628.
(318) Balcells, D.; Moles, P.; Blakemore, J.; Raynaud, C.; Brudvig, G. W.; Crabtree, R. H.; Eisenstein, O. *Dalton Trans.* **2009**, 5989.
(319) Lundberg, M.; Blomberg, M. R. A.; Siegbahn, P. E. M. *Inorg. Chem.* **2004**, *43*, 264.
(320) Balcells, D.; Raynaud, C.; Crabtree, R. H.; Eisenstein, O. *Chem. Commun.* **2008**, 744.
(321) Balcells, D.; Raynaud, C.; Crabtree, R. H.; Eisenstein, O. *Inorg. Chem.* **2008**, *47*, 10090.
(322) Balcells, D.; Raynaud, C.; Crabtree, R. H.; Eisenstein, O. *Chem. Commun.* **2009**, 1772.
(323) Biswas, B.; Sugimoto, M.; Sakaki, S. *Organometallics* **2000**, *19*, 3895.
(324) Davies, D. L.; Donald, S. M. A.; Macgregor, S. A. *J. Am. Chem. Soc.* **2005**, *127*, 13754.
(325) Davies, D. L.; Donald, S. M. A.; Al-Duaij, O.; Macgregor, S. A.; Pölleth, M. *J. Am. Chem. Soc.* **2006**, *128*, 4210.
(326) Boutadla, Y.; Davies, D. L.; Macgregor, S. A.; Poblador-Bahamonde, A. I. *Dalton Trans.* **2009**, 5887.
(327) Davies, D. L.; Donald, S. M. A.; Al-Duaij, O.; Fawcett, J.; Little, C.; Macgregor, S. A. *Organometallics* **2006**, *25*, 5976.
(328) Bielsa, R.; Navarro, R.; Urriolabeitia, E. P.; Lledós, A. *Inorg. Chem.* **2007**, *46*, 10133.
(329) Aguilar, D.; Bielsa, R.; Contel, M.; Lledós, A.; Navarro, R.; Soler, T.; Urriolabeitia, E. P. *Organometallics* **2008**, *27*, 2929.
(330) Aullón, G.; Chat, R.; Favier, I.; Font-Bardia, M.; Gómez, M.; Granell, J.; Martínez, M.; Solans, X. *Dalton Trans.* **2009**, 8292.
(331) Ess, D. H.; Bischof, S. M.; Oxgaard, J.; Periana, R. A.; Goddard III, W. A. *Organometallics* **2008**, *27*, 6440.
(332) García-Cuadrado, D.; Braga, A. A. C.; Maseras, F.; Echavarren, A. M. *J. Am. Chem. Soc.* **2006**, *128*, 1066.
(333) García-Cuadrado, D.; de Mendoza, P.; Braga, A. A. C.; Maseras, F.; Echavarren, A. M. *J. Am. Chem. Soc.* **2007**, *129*, 6880.
(334) Pascual, S.; de Mendoza, P.; Braga, A. A. C.; Maseras, F.; Echavarren, A. M. *Tetrahedron* **2008**, *64*, 6021.
(335) Campeau, L.-C.; Fagnou, K. *Chem. Commun.* **2006**, 1253.
(336) Lafrance, M.; Rowley, C. N.; Woo, T. K.; Fagnou, K. *J. Am. Chem. Soc.* **2006**, *128*, 8754.
(337) Özdemir, I.; Demir, S.; Çetinkaya, B.; Gourlaouen, C.; Maseras, F.; Bruneau, C.; Dixneuf, P. H. *J. Am. Chem. Soc.* **2008**, *130*, 1156.
(338) Lafrance, M.; Gorelsky, S. I.; Fagnou, K. *J. Am. Chem. Soc.* **2007**, *129*, 14570.
(339) Chaumontet, M.; Piccardi, R.; Audic, N.; Hitce, J.; Peglion, J.-L.; Clot, E.; Baudoin, O. *J. Am. Chem. Soc.* **2008**, *130*, 15157.
(340) Baudry, D.; Ephritikine, M.; Felkin, H.; Holmes-Smith, R. *J. Chem. Soc., Chem. Commun.* **1983**, 788.
(341) Felkin, H.; Fillebeen-Khan, T.; Gault, Y.; Holmes-Smith, R.; Zakrzewski, J. *Tetrahedron Lett.* **1984**, *25*, 1279.
(342) Burk, M. J.; Crabtree, R. H.; Parnell, C. P.; Uriarte, R. J. *Organometallics* **1984**, *3*, 816.
(343) Burk, M. J.; Crabtree, R. H.; McGrath, D. V. *J. Chem. Soc., Chem Commun.* **1985**, 1829.
(344) Maguire, J. A.; Goldman, A. S. *J. Am. Chem. Soc.* **1991**, *113*, 6706.
(345) Maguire, J. A.; Petrillo, A.; Goldman, A. S. *J. Am. Chem. Soc.* **1992**, *114*, 9492.
(346) Gupta, M.; Hagen, C.; Flesher, R. J.; Kaska, W. C.; Jensen, C. M. *Chem. Commun.* **1996**, 2083.
(347) Gupta, M.; Hagen, C.; Kaska, W. C.; Cramer, R. E.; Jensen, C. M. *J. Am. Chem. Soc.* **1997**, *119*, 840.
(348) Fujii, T.; Saito, Y. *J. Chem. Soc., Chem. Commun.* **1990**, 757.
(349) Aoki, T.; Crabtree, R. H. *Organometallics* **1993**, *12*, 294.
(350) Liu, F.; Goldman, A. S. *Chem. Commun.* **1999**, 655.
(351) Li, S.; Hall, M. B. *Organometallics* **2001**, *20*, 3210.
(352) Li, S.; Hall, M. B. *Organometallics* **2001**, *20*, 2153.
(353) Krogh-Jespersen, K.; Czerw, M.; Kanzelberger, M.; Goldman, A. S. *J. Chem. Inf. Comput. Sci.* **2001**, *41*, 56.
(354) Haenel, M. W.; Oevers, S.; Angermund, K.; Kaska, W. C.; Fan, H.-J.; Hall, M. B. *Angew. Chem., Int. Ed.* **2001**, *40*, 3596.
(355) Krogh-Jespersen, K.; Czerw, M.; Summa, N.; Renkema, K. B.; Achord, P. D.; Goldman, A. S. *J. Am. Chem. Soc.* **2002**, *124*, 11404.
(356) Fan, H.-J.; Hall, M. B. *J. Mol. Catal. A* **2002**, *189*, 111.
(357) Krogh-Jespersen, K.; Czerw, M.; Goldman, A. S. *J. Mol. Catal. A* **2002**, *189*, 95.
(358) Zhu, K.; Achord, P. D.; Zhang, X.; Krogh-Jespersen, K.; Goldman, A. S. *J. Am. Chem. Soc.* **2004**, *126*, 13044.
(359) Kundu, S.; Choliy, Y.; Zhuo, G.; Ahuja, R.; Emge, T. J.; Warmuth, R.; Brookhart, M.; Krogh-Jespersen, K.; Goldman, A. S. *Organometallics* **2009**, *28*, 5432.
(360) Chaplin, A. B.; Poblador-Bahamonde, A. I.; Sparkes, H. A.; Howard, J. A. K.; Macgregor, S. A.; Weller, A. S. *Chem. Commun.* **2009**, 244.
(361) Douglas, T. M.; Brayshaw, S. K.; Dallanegra, R.; Kociok-Köhn, G.; Macgregor, S. A.; Moxham, G. K.; Weller, A. S.; Wondimagegn, T.; Vadivelu, P. *Chem.—Eur. J.* **2008**, *14*, 1004.
(362) Douglas, T. M.; Weller, A. S. *New J. Chem.* **2008**, *32*, 966.
(363) Grellier, M.; Vendier, L.; Sabo-Etienne, S. *Angew. Chem., Int. Ed.* **2007**, *46*, 2613.
(364) Bolton, P. D.; Grellier, M.; Vautravers, N.; Vendier, L.; Sabo-Etienne, S. *Organometallics* **2008**, *27*, 5088.
(365) Matsubara, T.; Koga, N.; Musaev, D. G.; Morokuma, K. *Organometallics* **2000**, *19*, 2318.
(366) Matsumoto, T.; Taube, D. J.; Periana, R. A.; Taube, H.; Yoshida, H. *J. Am. Chem. Soc.* **2000**, *122*, 7414.
(367) Matsumoto, T.; Periana, R. A.; Taube, D. J.; Yoshida, H. *J. Mol. Catal. A* **2002**, *180*, 1.
(368) Bhalla, G.; Liu, X. Y.; Oxgaard, J.; Goddard, W. A., III; Periana, R. A. *J. Am. Chem. Soc.* **2005**, *127*, 11372.
(369) Bhalla, G.; Oxgaard, J.; Goddard, W. A., III; Periana, R. A. *Organometallics* **2005**, *24*, 3229.
(370) Bhalla, G.; Oxgaard, J.; Goddard, W. A., III; Periana, R. A. *Organometallics* **2005**, *24*, 5499.
(371) Oxgaard, J.; Bhalla, G.; Periana, R. A.; Goddard, W. A., III *Organometallics* **2006**, *25*, 1618.
(372) Oxgaard, J.; Periana, R. A.; Goddard, W. A., III *J. Am. Chem. Soc.* **2004**, *126*, 11658.
(373) Lail, M.; Bell, C. M.; Conner, D.; Cundari, T. R.; Gunnoe, T. B.; Petersen, J. L. *Organometallics* **2004**, *23*, 5007.
(374) Pittard, K. A.; Lee, J. P.; Cundari, T. R.; Gunnoe, T. B.; Petersen, J. L. *Organometallics* **2004**, *23*, 5514.

(375) Pittard, K. A.; Cundari, T. R.; Gunnoe, T. B.; Day, C. S.; Petersen, J. L. *Organometallics* **2005**, *24*, 5015.
(376) Foley, N. A.; Lail, M.; Lee, J. P.; Gunnoe, T. B.; Cundari, T. R.; Petersen, J. L. *J. Am. Chem. Soc.* **2007**, *129*, 6765.
(377) Foley, N. A.; Lail, M.; Gunnoe, T. B.; Cundari, T. R.; Boyle, P. D.; Petersen, J. L. *Organometallics* **2007**, *26*, 5507.
(378) Foley, N. A.; Ke, Z.; Gunnoe, T. B.; Cundari, T. R.; Petersen, J. L. *Organometallics* **2008**, *27*, 3007.
(379) Foley, N. A.; Lee, J. P.; Ke, Z.; Gunnoe, T. B.; Cundari, T. R. *Acc. Chem. Res.* **2009**, *42*, 585.
(380) Iverson, C. N.; Smith, M. R., III *J. Am. Chem. Soc.* **1999**, *121*, 7696.
(381) Wan, X.; Wang, X.; Luo, Y.; Takami, S.; Kubo, M.; Miyamoto, A. *Organometallics* **2002**, *21*, 3703.
(382) Webster, C. E.; Fan, Y.; Hall, M. B.; Kunz, D.; Hartwig, J. F. *J. Am. Chem. Soc.* **2003**, *125*, 858.
(383) Hartwig, J. F.; Cook, K. S.; Hapke, M.; Incarvito, C. D.; Fan, Y.; Webster, C. E.; Hall, M. B. *J. Am. Chem. Soc.* **2005**, *127*, 2538.
(384) Lam, W. H.; Lin, Z. *Organometallics* **2003**, *22*, 473.
(385) Lam, W. H.; Lam, K. C.; Lin, Z.; Shimada, S.; Perutz, R. N.; Marder, T. B. *Dalton Trans.* **2004**, 1556.
(386) Dang, L.; Lin, Z.; Marder, T. B. *Chem. Commun.* **2009**, 3987.
(387) Tamura, H.; Yamazaki, H.; Sato, H.; Sakaki, S. *J. Am. Chem. Soc.* **2003**, *125*, 16114.
(388) Ishiyama, T.; Takagi, J.; Ishida, K.; Miyaura, N.; Anastasi, N. R.; Hartwig, J. F. *J. Am. Chem. Soc.* **2002**, *124*, 390.
(389) Ishiyama, T.; Takagi, J.; Hartwig, J. F.; Miyaura, N. *Angew. Chem., Int. Ed.* **2002**, *41*, 3056.
(390) Chotana, G. A.; Vanchura, B. A.; Tse, M. T.; Staples, R. J.; Maleczka, R. E.; Smith, M. R., III *Chem. Commun.* **2009**, 5731.
(391) Garnett, J. L.; Hodges, R. J. *J. Am. Chem. Soc.* **1967**, *89*, 4546.
(392) Shilov, A. E. *Activation of Saturated Hydrocarbons by Transition Metal Complexes*; Springer: Dordrecht, The Netherlands, 1984.
(393) Siegbahn, P. E. M.; Crabtree, R. H. *J. Am. Chem. Soc.* **1996**, *118*, 4442.
(394) Eisenstein, O.; Crabtree, R. H. *New J. Chem.* **2001**, *25*, 665.
(395) Zhu, H.; Ziegler, T. *J. Organomet. Chem.* **2006**, *691*, 4486.
(396) Zhu, H.; Ziegler, T. *Organometallics* **2007**, *26*, 2277.
(397) Zhu, H.; Ziegler, T. *Organometallics* **2008**, *27*, 1743.
(398) Zhu, H.; Ziegler, T. *Organometallics* **2009**, *28*, 2773.
(399) Arakawa, H.; Aresta, M.; Armor, J. N.; Barteau, M. A.; Beckman, E. J.; Bell, A. T.; Bercaw, J. E.; Creutz, C.; Dinjus, E.; Dixon, D. A.; Domen, K.; DuBois, D. L.; Eckert, J.; Fujita, E.; Gibson, D. H.; Goddard, W. A., III; Goodman, D. W.; Keller, J.; Kubas, G. J.; Kung, H. H.; Lyons, J. E.; Manzer, L. E.; Marks, T. J.; Morokuma, K.; Nicholas, K. M.; Periana, R.; Que, L.; Rostrup-Nielson, J.; Sachtler, W. M. H.; Schmidt, L. D.; Sen, A.; Somorjai, G. A.; Stair, P. C.; Stults, B. R.; Tumas, W. *Chem. Rev.* **2001**, *101*, 953.
(400) Periana, R. A.; Bhalla, G.; Tenn, W. J., III; Young, K. J. H.; Liu, X. Y.; Mironov, O.; Jones, C. J.; Ziatdinov, V. R. *J. Mol. Catal. A* **2004**, *220*, 7.
(401) Conley, B. L.; Tenn, W. J., III; Young, K. J. H.; Ganesh, S. K.; Meier, S. K.; Ziatdinov, V. R.; Mironov, O. A.; Oxgaard, J.; Gonzales, J. M.; Goddard, W. A., III; Periana, R. A. *J. Mol. Catal. A* **2006**, *251*, 8.
(402) Mylvaganam, K.; Bacskay, G. B.; Hush, N. S. *J. Am. Chem. Soc.* **1999**, *121*, 4633.
(403) Mylvaganam, K.; Bacskay, G. B.; Hush, N. S. *J. Am. Chem. Soc.* **2000**, *122*, 2041.
(404) Gilbert, T. M.; Hristov, J.; Ziegler, T. *Organometallics* **2001**, *20*, 1183.
(405) Kua, J.; Xu, X.; Periana, R. A.; Goddard, W. A., III *Organometallics* **2002**, *21*, 511.
(406) Hristov, I. H.; Ziegler, T. *Organometallics* **2003**, *22*, 1668.
(407) Xu, X.; Kua, J.; Periana, R. A.; Goddard, W. A., III *Organometallics* **2003**, *22*, 2057.
(408) Paul, A.; Musgrave, C. B. *Organometallics* **2007**, *26*, 793.
(409) Ahlquist, M.; Periana, R. A.; Goddard, W. A., III *Chem. Commun.* **2009**, 2373.
(410) Ziatdinov, V. R.; Oxgaard, J.; Mironov, O. A.; Young, K. J. H.; Goddard, W. A., III; Periana, R. A. *J. Am. Chem. Soc.* **2006**, *128*, 7404.
(411) Cheng, J. H.; Li, Z. W.; Haught, M.; Tang, Y. C. *Chem. Commun.* **2006**, 4617.
(412) Xu, Z.; Oxgaard, J.; Goddard, W. A., III *Organometallics* **2008**, *27*, 3770.
(413) Vedernikov, A. N.; Fettinger, J. C.; Mohr, F. *J. Am. Chem. Soc.* **2004**, *126*, 11160.
(414) Khaskin, E.; Zavalij, P. Y.; Vedernikov, A. N. *J. Am. Chem. Soc.* **2006**, *128*, 13054.
(415) Muller, R. P.; Philipp, D. M.; Goddard, W. A., III *Top. Catal.* **2003**, *23*, 81.
(416) Young, K. J. H.; Oxgaard, J.; Ess, D. H.; Meier, S. K.; Stewart, T.; Goddard, W. A., III; Periana, R. A. *Chem. Commun.* **2009**, 3270.
(417) Jones, C. J.; Taube, D.; Ziatdinov, V. R.; Periana, R. A.; Nielsen, R. J.; Oxgaard, J.; Goddard, W. A., III *Angew. Chem., Int. Ed.* **2004**, *43*, 4626.
(418) Periana, R. A.; Mironov, O.; Taube, D.; Bhalla, G.; Jones, C. J. *Science* **2003**, *301*, 814.
(419) Chempath, S.; Bell, A. T. *J. Am. Chem. Soc.* **2006**, *128*, 4650.
(420) Lin, M.; Sen, A. *Nature* **1994**, *368*, 613.
(421) Lin, M.; Hogan, T. E.; Sen, A. *J. Am. Chem. Soc.* **1996**, *118*, 4574.
(422) Hristov, J. H.; Ziegler, T. *Organometallics* **2003**, *22*, 3513.
(423) Strassner, T.; Houk, K. N. *J. Am. Chem. Soc.* **2000**, *122*, 7821.
(424) Lam, W. W. Y.; Yiu, S.-M.; Lee, J. M. N.; Yau, S. K. Y.; Kwong, H.-K.; Lau, T.-C.; Liu, D.; Lin, Z. *J. Am. Chem. Soc.* **2006**, *128*, 2851.
(425) Ensing, B.; Buda, F.; Gribnau, M. C. M.; Baerends, E. J. *J. Am. Chem. Soc.* **2004**, *126*, 4355.
(426) Buda, F.; Ensing, B.; Gribnau, M. C. M.; Baerends, E. J. *Chem.—Eur. J.* **2001**, *7*, 2775.
(427) Ensing, B.; Buda, F.; Blochl, P. E.; Baerends, E. J. *Phys. Chem. Chem. Phys.* **2002**, *4*, 3619.
(428) Louwerse, M. J.; Vassilev, P.; Baerends, E. J. *J. Phys. Chem. A* **2008**, *112*, 1000.
(429) Bernasconi, L.; Louwerse, M. J.; Baerends, E. J. *Eur. J. Inorg. Chem.* **2007**, 3023.
(430) Bernasconi, L.; Baerends, E. J. *Eur. J. Inorg. Chem.* **2008**, 1672.
(431) Louwerse, M. J.; Baerends, E. J. *Phys. Chem. Chem. Phys.* **2007**, *9*, 156.
(432) Michel, C.; Baerends, E. J. *Inorg. Chem.* **2009**, *48*, 3628.
(433) Shiota, Y.; Kihara, N.; Kamachi, T.; Yoshizawa, K. *J. Org. Chem.* **2003**, *68*, 3958.
(434) Costas, M.; Chen, K.; Que, L. *Coord. Chem. Rev.* **2000**, *200*, 517.
(435) Bassan, A.; Blomberg, M. R. A.; Siegbahn, P. E. M.; Que, L. *Chem.—Eur. J.* **2005**, *11*, 692.
(436) Ma, Y.; Balbuena, P. B. *J. Phys. Chem. B* **2007**, *111*, 2711.
(437) Kumar, D.; Hirao, H.; Que, L.; Shaik, S. *J. Am. Chem. Soc.* **2005**, *127*, 8026.
(438) Hirao, H.; Kumar, D.; Que, L.; Shaik, S. *J. Am. Chem. Soc.* **2006**, *128*, 8590.
(439) Schröder, D.; Shaik, S.; Schwarz, H. *Acc. Chem. Res.* **2000**, *33*, 139.
(440) Shaik, S.; de Visser, S. P.; Ogliaro, F.; Schwarz, H.; Schröder, D. *Curr. Opin. Chem. Biol.* **2002**, *6*, 556.
(441) Shaik, S.; Filatov, M.; Schröder, D.; Schwarz, H. *Chem.—Eur. J.* **1998**, *4*, 193.
(442) Sastri, C. V.; Lee, J.; Oh, K.; Lee, Y. J.; Lee, J.; Jackson, T. A.; Ray, K.; Hirao, H.; Shin, W.; Halfen, J. A.; Kim, J.; Que, L.; Shaik, S.; Nam, W. *Proc. Natl. Acad. Sci. U.S.A.* **2007**, *104*, 19181.
(443) Hirao, H.; Que, L.; Nam, W.; Shaik, S. *Chem.—Eur. J.* **2008**, *14*, 1740.
(444) Dhuri, S. N.; Seo, M. S.; Lee, Y.-M.; Hirao, H.; Wang, Y.; Nam, W.; Shaik, S. *Angew. Chem., Int. Ed.* **2008**, *47*, 3356.
(445) Klinker, E. J.; Shaik, S.; Hirao, H.; Que, L. *Angew. Chem., Int. Ed.* **2009**, *48*, 1291.
(446) Hirao, H.; Chen, H.; Carvajal, M. A.; Wang, Y.; Shaik, S. *J. Am. Chem. Soc.* **2008**, *130*, 3319.
(447) de Visser, S. P. *J. Am. Chem. Soc.* **2006**, *128*, 15809.
(448) Decker, A.; Rohde, J.-U.; Klinker, E. J.; Wong, S. D.; Que, L.; Solomon, E. I. *J. Am. Chem. Soc.* **2007**, *129*, 15983.
(449) Decker, A.; Solomon, E. I. *Angew. Chem., Int. Ed.* **2005**, *44*, 2252.
(450) Borowski, T.; Bassan, A.; Siegbahn, P. E. M. *Inorg. Chem.* **2004**, *43*, 3277.
(451) de Visser, S. P.; Oh, K.; Han, A.-R.; Nam, W. *Inorg. Chem.* **2007**, *46*, 4632.
(452) Wang, Y.; Wang, Y.; Han, K. *J. Biol. Inorg. Chem.* **2009**, *14*, 533.
(453) Klinker, E. J.; Brennessel, W. W.; Woodrum, N. L.; Cramer, C. J.; Que, L. *Angew. Chem., Int. Ed.* **2005**, *44*, 3690.
(454) Noack, H.; Siegbahn, P. E. M. *J. Biol. Inorg. Chem.* **2007**, *12*, 1151.
(455) Comba, P.; Maurer, M.; Vadivelu, P. *J. Phys. Chem. A* **2008**, *112*, 13028.
(456) Johansson, A. J.; Blomberg, M. R. A.; Siegbahn, P. E. M. *J. Phys. Chem. C* **2007**, *111*, 12397.
(457) Rhode, J. U.; Que, L. *Angew. Chem., Int. Ed.* **2005**, *44*, 2255.
(458) de Visser, S. P. *J. Am. Chem. Soc.* **2006**, *128*, 9813.
(459) de Visser, S. P. *Angew. Chem., Int. Ed.* **2006**, *45*, 1790.
(460) Godfrey, E.; Porro, C. S.; de Visser, S. P. *J. Phys. Chem. A* **2008**, *112*, 2464.
(461) Bassan, A.; Blomberg, M. R. A.; Siegbahn, P. E. M. *Chem.—Eur. J.* **2003**, *9*, 4055.
(462) Bassan, A.; Blomberg, M. R. A.; Siegbahn, P. E. M. *Chem.—Eur. J.* **2003**, *9*, 106.
(463) Shiota, Y.; Yoshizawa, K. *J. Phys. Chem. B* **2004**, *108*, 17226.
(464) Borowski, T.; de Marothy, S.; Broclawik, E.; Schofield, C. J.; Siegbahn, P. E. M. *Biochemistry* **2007**, *46*, 3682.
(465) Iwata-Reuyl, D.; Basak, A.; Townsend, C. *J. Am. Chem. Soc.* **1999**, *121*, 11356.

(466) Basak, A.; Salowe, S.; Townsend, C. *J. Am. Chem. Soc.* **1990**, *112*, 1654.
(467) Wirstam, M.; Siegbahn, P. E. M. *J. Am. Chem. Soc.* **2000**, *122*, 8539.
(468) Lundberg, M.; Siegbahn, P. E. M.; Morokuma, K. *Biochemistry* **2008**, *47*, 1031.
(469) Liu, H.; Llano, J.; Gauld, J. W. *J. Phys. Chem. B* **2009**, *113*, 4887.
(470) De Angelis, F.; Jin, N.; Car, R.; Groves, J. T. *Inorg. Chem.* **2006**, *45*, 4268.
(471) Huber, S. M.; Ertem, M. Z.; Aquilante, F.; Gagliardi, L.; Tolman, W. B.; Cramer, C. J. *Chem.—Eur. J.* **2009**, *15*, 4886.
(472) Kamachi, T.; Kihara, N.; Shiota, Y.; Yoshizawa, K. *Inorg. Chem.* **2005**, *44*, 4226.
(473) Yoshizawa, K.; Kihara, N.; Kamachi, T.; Shiota, Y. *Inorg. Chem.* **2006**, *45*, 3034.
(474) Crespo, A.; Marti, M. A.; Roitberg, A. E.; Amzel, L. M.; Estrin, D. A. *J. Am. Chem. Soc.* **2006**, *128*, 12817.
(475) Szaleniec, M.; Witko, M.; Heider, J. *J. Mol. Catal. A: Chem.* **2008**, *286*, 128.
(476) Olsson, M. H. M.; Siegbahn, P. E. M.; Warshel, A. *J. Am. Chem. Soc.* **2004**, *126*, 2820.
(477) Hatcher, E.; Soudackov, A. V.; Hammes-Schiffer, S. *J. Am. Chem. Soc.* **2004**, *126*, 5763.
(478) Hatcher, E.; Soudackov, A. V.; Hammes-Schiffer, S. *J. Am. Chem. Soc.* **2007**, *129*, 187.
(479) Karlsson, E. A.; Privalov, T. *Chem.—Eur. J.* **2009**, *15*, 1862.
(480) Owens, G. S.; Abu-Omar, M. M. *Chem. Commun.* **2000**, 1165.
(481) Bianchini, G.; Crucianelli, M.; De Angelis, F.; Neri, V.; Saladino, R. *Tetrahedron Lett.* **2005**, *46*, 2427.
(482) Lehnert, N.; Neese, F.; Ho, R. Y. N.; Que, L.; Solomon, E. I. *J. Am. Chem. Soc.* **2002**, *124*, 10810.
(483) Kumar, D.; Hirao, H.; Shaik, S.; Kozlowski, P. M. *J. Am. Chem. Soc.* **2006**, *128*, 16148.
(484) Worth, L.; Frank, B. L.; Christner, D. F.; Absalon, M. J.; Stubbe, J.; Kozarich, J. W. *Biochemistry* **1993**, *32*, 2601.
(485) Neese, F.; Zaleski, J. M.; Zaleski, K. L.; Solomon, E. I. *J. Am. Chem. Soc.* **2000**, *122*, 11703.
(486) Decker, A.; Chow, M. S.; Kemsley, J. N.; Lehnert, N.; Solomon, E. I. *J. Am. Chem. Soc.* **2006**, *128*, 4719.
(487) Chow, M. S.; Liu, L. V.; Solomon, E. I. *Proc. Natl. Acad. Sci. U.S.A.* **2008**, *105*, 13241.
(488) Cramer, C. J.; Kinsinger, C. R.; Pak, Y. *J. Mol. Struct. (Theochem)* **2003**, *632*, 111.
(489) Yoshizawa, K. *Acc. Chem. Res.* **2006**, *39*, 375.
(490) Yoshizawa, K. *Coord. Chem. Rev.* **2002**, *226*, 251.
(491) Yoshizawa, K. *J. Biol. Inorg. Chem.* **1998**, *3*, 318.
(492) Torrent, M.; Musaev, D. G.; Basch, H.; Morokuma, K. *J. Comput. Chem.* **2002**, *23*, 59.
(493) Siegbahn, P. E. M.; Blomberg, M. R. A. *Chem. Rev.* **2000**, *100*, 421.
(494) Himo, F.; Siegbahn, P. E. M. *Chem. Rev.* **2003**, *103*, 2421.
(495) Siegbahn, P. E. M.; Borowski, T. *Acc. Chem. Res.* **2006**, *39*, 729.
(496) Siegbahn, P. E. M.; Crabtree, R. H. *Struct. Bonding (Berlin)* **2000**, *97*, 125.
(497) Blomberg, M. R. A.; Siegbahn, P. E. M. *J. Phys. Chem. B* **2001**, *105*, 9375.
(498) Friesner, R. A.; Dunietz, B. D. *Acc. Chem. Res.* **2001**, *34*, 351.
(499) Guallar, V.; Gherman, B. F.; Lippard, S. J.; Friesner, R. A. *Curr. Opin. Chem. Biol.* **2002**, *6*, 236.
(500) Friesner, R. A.; Baik, M. H.; Gherman, B. F.; Guallar, V.; Wirstam, M.; Murphy, R. B.; Lippard, S. J. *Coord. Chem. Rev.* **2003**, *238*, 267.
(501) Baik, M. H.; Newcomb, M.; Friesner, R. A.; Lippard, S. J. *Chem. Rev.* **2003**, *103*, 2385.
(502) Schröder, D.; Schwarz, H. *Angew. Chem., Int. Ed. Engl.* **1995**, *34*, 1973.
(503) Schröder, D.; Schwarz, H.; Shaik, S. *Struct. Bonding (Berlin)* **2000**, *97*, 91.
(504) Schröder, D.; Schwarz, H. *Top Organomet. Chem.* **2007**, *22*, 1.
(505) Schröder, D.; Schwarz, H. *Proc. Natl. Acad. Sci. U.S.A.* **2008**, *105*, 18114.
(506) Fiedler, A.; Schröder, D.; Shaik, S.; Schwarz, H. *J. Am. Chem. Soc.* **1994**, *116*, 10734.
(507) Schröder, D.; Schwarz, H. *Angew. Chem., Int. Ed. Engl.* **1990**, *29*, 1433.
(508) Shiota, Y.; Yoshizawa, K. *J. Am. Chem. Soc.* **2000**, *122*, 12317.
(509) Yoshizawa, K.; Shiota, Y.; Yamabe, T. *Chem.—Eur. J.* **1997**, *3*, 1160.
(510) Yoshizawa, K.; Yamabe, T.; Hoffmann, R. *New J. Chem.* **1997**, *21*, 151.
(511) Yoshizawa, K.; Shiota, Y.; Yamabe, T. *J. Am. Chem. Soc.* **1998**, *120*, 564.
(512) Yoshizawa, K.; Shiota, Y.; Yamabe, T. *Organometallics* **1998**, *17*, 2825.
(513) Yoshizawa, K.; Shiota, Y.; Kagawa, Y.; Yamabe, T. *J. Phys. Chem. A* **2000**, *104*, 2552.
(514) Yoshizawa, K.; Shiota, Y.; Yamabe, T. *J. Chem. Phys.* **1999**, *111*, 538.
(515) Yoshizawa, K.; Ohta, T.; Shiota, Y.; Yamabe, T. *Chem. Lett.* **1997**, 1213.
(516) Yoshizawa, K.; Ohta, T.; Yamabe, T.; Hoffmann, R. *J. Am. Chem. Soc.* **1997**, *119*, 12311.
(517) Yoshizawa, K.; Ohta, T.; Yamabe, T. *Bull. Chem. Soc. Jpn.* **1998**, *71*, 1899.
(518) Yoshizawa, K. *J. Inorg. Biochem.* **2000**, *78*, 23.
(519) Yoshizawa, K.; Suzuki, A.; Shiota, Y.; Yamabe, T. *Bull. Chem. Soc. Jpn.* **2000**, *73*, 815.
(520) Noodleman, L.; Lovell, T.; Han, W.-G.; Li, J.; Himo, F. *Chem. Rev.* **2004**, *104*, 459.
(521) Yoshizawa, K.; Yumura, T. *Chem.—Eur. J.* **2003**, *92*, 347.
(522) Shu, L. J.; Nesheim, J. C.; Kauffmann, K.; Munck, E.; Lipscomb, J. D.; Que, L. *Science* **1997**, *275*, 515.
(523) Yoshizawa, K.; Shiota, Y. *J. Am. Chem. Soc.* **2006**, *128*, 9873.
(524) Shiota, Y.; Yoshizawa, K. *Inorg. Chem.* **2009**, *48*, 838.
(525) Chen, P. P. Y.; Chan, S. I. *J. Inorg. Biochem.* **2006**, *100*, 801.
(526) Chan, S. I.; Chen, K. H. C.; Yu, S. S. F.; Chen, C. L.; Kuo, S. S. J. *Biochemistry* **2004**, *43*, 4421.
(527) Torrent, M.; Vreven, T.; Musaev, D. G.; Morokuma, K.; Farkas, O.; Schlegel, H. B. *J. Am. Chem. Soc.* **2002**, *124*, 192.
(528) Basch, H.; Mogi, K.; Musaev, D. G.; Morokuma, K. *J. Am. Chem. Soc.* **1999**, *121*, 7249.
(529) Basch, H.; Musaev, D. G.; Morokuma, K. *J. Phys. Chem. B* **2001**, *105*, 8452.
(530) Basch, H.; Musaev, D. G.; Mogi, K.; Morokuma, K. *J. Phys. Chem. A* **2001**, *105*, 3615.
(531) Musaev, D. G.; Basch, H.; Morokuma, K. *J. Am. Chem. Soc.* **2002**, *124*, 4135.
(532) Huynh, M. H. V.; Meyer, T. J. *Chem. Rev.* **2007**, *107*, 5004.
(533) DeWitt, J. G.; Bentsen, J. G.; Rosenzweig, A. C.; Hedman, B.; Green, J.; Pilkington, S.; Papaefthymiou, G. C.; Dalton, H.; Hodgson, K. O.; Lippard, S. J. *J. Am. Chem. Soc.* **1991**, *113*, 9219.
(534) Fox, B. G.; Surerus, K. K.; Munck, E.; Lipscomb, J. D. *J. Biol. Chem.* **1988**, *263*, 10553.
(535) Fox, B. G.; Hendrich, M. P.; Surerus, K. K.; Andersson, K. K.; Froland, W. A.; Lipscomb, J. D.; Munck, E. *J. Am. Chem. Soc.* **1993**, *115*, 3688.
(536) Siegbahn, P. E. M.; Crabtree, R. H. *J. Am. Chem. Soc.* **1997**, *119*, 3103.
(537) Siegbahn, P. E. M. *Inorg. Chem.* **1999**, *38*, 2880.
(538) Siegbahn, P. E. M.; Crabtree, R. H.; Nordlund, P. *J. Biol. Inorg. Chem.* **1998**, *3*, 314.
(539) Siegbahn, P. E. M. *J. Biol. Inorg. Chem.* **2001**, *6*, 27.
(540) Dunietz, B. D.; Beachy, M. D.; Cao, Y. X.; Whittington, D. A.; Lippard, S. J.; Friesner, R. A. *J. Am. Chem. Soc.* **2000**, *122*, 2828.
(541) Lovell, T.; Li, J.; Noodleman, L. *Inorg. Chem.* **2001**, *40*, 5251.
(542) Lovell, T.; Li, J.; Noodleman, L. *Inorg. Chem.* **2001**, *40*, 5267.
(543) Lovell, T.; Li, J.; Noodleman, L. *J. Biol. Inorg. Chem.* **2002**, *7*, 799.
(544) Rosenzweig, A. C.; Nordlund, P.; Takahara, P. M.; Frederick, C. A.; Lippard, S. J. *Chem. Biol.* **1995**, *2*, 409.
(545) Gherman, B. F.; Dunietz, B. D.; Whittington, D. A.; Lippard, S. J.; Friesner, R. A. *J. Am. Chem. Soc.* **2001**, *123*, 3836.
(546) Valentine, A. M.; Wilkinson, B.; Liu, K. E.; Komar-Panicucci, S.; Priestley, N. D.; Williams, P. G.; Morimoto, H.; Floss, H. G.; Lippard, S. J. *J. Am. Chem. Soc.* **1997**, *119*, 1818.
(547) Priestley, N. D.; Floss, H. G.; Froland, W. A.; Lipscomb, J. D.; Williams, P. G.; Morimoto, H. *J. Am. Chem. Soc.* **1992**, *114*, 7561.
(548) Guallar, V.; Gherman, B. F.; Miller, W. H.; Lippard, S. J.; Friesner, R. A. *J. Am. Chem. Soc.* **2002**, *124*, 3377.
(549) Baik, M. H.; Gherman, B. F.; Friesner, R. A.; Lippard, S. J. *J. Am. Chem. Soc.* **2002**, *124*, 14608.
(550) Gherman, B. F.; Lippard, S. J.; Friesner, R. A. *J. Am. Chem. Soc.* **2005**, *127*, 1025.
(551) Ambundo, E. A.; Friesner, R. A.; Lippard, S. J. *J. Am. Chem. Soc.* **2002**, *124*, 8770.
(552) Ito, N.; Phillips, S. E. V.; Stevens, C.; Ogel, Z. B.; McPherson, M. J.; Keen, J. N.; Yadav, K. D. S.; Knowles, P. F. *Nature* **1991**, *350*, 87.
(553) Branchaud, B. P.; Montague-Smith, M. P.; Kosman, D. J.; McLaren, F. R. *J. Am. Chem. Soc.* **1993**, *115*, 798.
(554) Rothlisberger, U.; Carloni, P. *Int. J. Quantum Chem.* **1999**, *73*, 209.
(555) Rothlisberger, U.; Carloni, P.; Doclo, K.; Parrinello, M. *J. Biol. Inorg. Chem.* **2000**, *5*, 236.
(556) Guidoni, L.; Spiegel, K.; Zumstein, M.; Rothlisberger, U. *Angew. Chem., Int. Ed.* **2004**, *43*, 3286.
(557) Zueva, E.; Walton, P. H.; McGrady, J. E. *Dalton Trans.* **2006**, 159.
(558) Bachler, V.; Chaudhuri, P.; Wieghardt, K. *Chem.—Eur. J.* **2001**, *7*, 404.
(559) Himo, F.; Eriksson, L. A.; Maseras, F.; Siegbahn, P. E. M. *J. Am. Chem. Soc.* **2000**, *122*, 8031.
(560) Cheng, L.; Wang, J.; Wang, M.; Wu, Z. *Dalton Trans.* **2009**, 3286.

CR900315K